Investigating aberrant DNA methylation patterns in *LOXL2* as a potential predictor of diabetes-induced cardiac dysfunction

by

Melisse Sharné Erasmus

Dissertation presented for the degree of

Doctor of Science (Medical Physiology)

in the

Faculty of Science

at Stellenbosch University

Supervisor: Dr Rabia Johnson

Co-supervisors: Dr Ebrahim Samodien
Dr Gerald Maarman
Dr Carmen Pheiffer

December 2021

Declaration

By submitting this dissertation electronically, I declare that the entirety of the work contained therein is my own, original work, that I am the sole author thereof (save to the extent explicitly otherwise stated), that reproduction and publication thereof by Stellenbosch University will not infringe any third-party rights and that I have not previously in its entirety or in part submitted it for obtaining any qualification.

December 2021

Abstract

Background:

Cardiovascular disease (CVD) remains the leading cause of mortality worldwide, with 17.9 million deaths annually. CVD pathophysiology is often characterized by increased stiffening of the heart muscle due to fibrosis, thus resulting in diminished cardiac function. Fibrosis can be caused by increased oxidative stress and inflammation, which is strongly linked to lifestyle and the environment. Diets rich in fat and sugar have been implicated as one of the prominent risk factors for the occurrence of CVD including associated risk factors such as obesity and insulin resistance. These diets are known to induce an inflammatory response that promotes myocardial stiffening due to increased cardiac fibrosis. Recently, Lysyl oxidase-like 2 (LOXL2), an enzyme required for collagen and elastin cross-linking in the myocardium, has been proposed to have a profound role in cardiac fibrosis and mechanical dysfunction of stressed hearts. Despite acknowledging the crucial role of LOXL2 as an early marker of cardiac fibrosis, there is a paucity of data on LOXL2 regulation and its role in CVD. Additionally, there is a definite need to investigate if LOXL2 regulation may be mediated by epigenetic mechanisms. This would greatly aid in identifying a means to control and manipulate LOXL2, particularly in humans, thereby developing novel therapeutics to combat this worldwide CVD problem. As such, this study aims to gain insight into (1) the mechanisms by which LOXL2 and its downstream effectors are regulated in physiological conditions responsible for CVD development, (2) whether LOXL2 expression in male and female rats is regulated by DNA methylation, and (3) if a pharmaceutical grade of green rooibos (AfriplexGRT^{TM}) can prevent altered gene expression. Furthermore, in search of new therapeutic targets, this study also aimed to investigate the ameliorative effects of AfriplexGRT^{TM} on high glucose and palmitate (HG+PAL)-induced stress in an *in vitro* H9c2 and *in vivo* obesogenic diet-induced cardiac fibrosis using a Wistar rat model.

Methods:

For the *in vitro* model, H9c2 cells were treated with HG+PAL for 24 hours, followed by further 6-hour treatment with AfriplexGRT^{TM}, or its bioactive compound Aspalathin. The effect of stress induction was investigated by studying ATP production, ROS generation, mitochondrial bioenergetics, mitochondrial

membrane potential and apoptosis. Cells were also harvested for mRNA expression analysis. To establish a model of diet-induced fibrosis *in vivo*, Wistar rats were fed different obesogenic diets, including a high-fat, high-sugar (HFHS) diet, and obesogenic 1 (OB1) diet, or an obesogenic 2 diet (OB2), over a set period with or without supplementation with AfriplexGRT™. Bodyweight, food intake and fasting blood glucoses were monitored over the study period, after which blood was collected for serum analysis of lipids, triglycerides, insulin levels as well as serum LOXL2 levels. Heart tissue was collected for DNA methylation profile (HFHS diet only), mRNA, and protein expression analysis.

Results:

Results from the *in vitro* study showed that HG+PAL treatment induced an inflammatory response, increased oxidative stress and reduced mitochondrial membrane potential, increased apoptosis. It, however, could not induce a significant change in gene expression levels of various fibrotic markers including LOXL2. AfriplexGRT™ and Aspalathin treatments were unable to ameliorate the detrimental effects induced by HG+PAL treatment. Results from the *in vivo* studies indicated that the obesogenic diets were able to increase animal bodyweights, serum insulin levels, triglyceride levels and serum LOXL2, with no significant differences were observed at a gene expression or DNA methylation level. However, enhanced protein expression levels correlated with increased serum levels of LOXL2 in male Wistar rats. Therefore, it has been postulated that early events of cardiac fibrosis might have been activated, that require further validation in future studies.

Conclusion:

This study demonstrated that an obesogenic diet can induce alterations in metabolic parameters that are gender-specific. These findings also indicated that LOXL2 regulation may have been driven by a mechanism independent of DNA methylation and that AfriplexGRT™ was unable to mitigate LOXL2-induced fibrosis or cardiac perturbations in these diet-induced obesity Wistar rat models.

Opsomming

Inleiding:

Kardiovaskulêre siektes (KVS) bly die grootste oorsaak van dood wêreldwyd, met 17.9 miljoen sterftes jaarliks. KVS patofisiologie word dikwels gekenmerk deur verhoogde verstywing van die hartspier as gevolg van fibrose, wat lei tot verswakte hartfunksie. Fibrose kan deur verhoogde oksidatiewestres en inflammasie veroorsaak word, wat gekoppel is aan leefstyl en omgewingsfaktore. Diëte met hoë vet- en suikerinhoud was voorheen geïdentifiseer as een van die hoof risikofaktore vir die voorkoms van KVS, insluitend verwante siektes soos vetsug en insulienweerstandigheid. Hierdie diëte kan ook ’n inflammatoriese reaksie veroorsaak, wat lei tot miokardialeverstywing met onderliggende hartfibrose. Onlangs is die idee voorgestel dat lisiel-oksidase (LOXL2), 'n ensiem nodig vir die vorming van kollageen en elastienkruisbindingsin die miokardium, 'n belangrike rol speel in hartfibrose en meganiese disfunksie tydens verhoogde hartspanning. Ten spyte van die noodsaaklike rol van LOXL2 as 'n vroeë merker van hartfibrose, is daar 'n tekort aan data oor die regulering van LOXL2 en die rol daarvan in KVS. Verder, in die soektog na nuwe terapeutiese teikens, het hierdie studie gemik om die verbeteringseffekte van AfriplexGRT™ op hoë glukose en palmitaat (HG+PAL)-geïnduseerde stres in 'n *in vitro* H9c2 selkultuurmodel, en *in vivo* in ‘n dieet-geïnduseerde Wistar rotmodel van hartfibrose te ondersoek. Addisioneel, is daar 'n definitiewe behoefte om LOXL2-regulering te ondersoek deur middle van epigenetiese meganismes. Dit sal beslis help om 'n manier te vind, ten einde LOXL2 te beheer en te manipuleer, veral in mense, en om sodoende nuwe terapeutiese middele te ontwikkel om hierdie wêreldwye KVS-probleem te beveg. Hierdie studie het dus gepoog om insig te verkry in (1) die meganismes waardeur LOXL2 en stroomafwaartse effektors gereguleer word in fisiologiese toestande wat verantwoordelik is vir KVS-ontwikkeling, (2) of LOXL2-uitdrukking by manlike en vroulike rotte gereguleer word deur DNA-metielasie, en (3) as 'n farmaseutiese kwaliteit van groen rooibos (AfriplexGRT™) veranderde geenuitdrukking kan verhoed.

Metodes:

In die *in vitro*-model, is H9c2-selle vir 24 uur lmet HG+PAL behandel, gevolg deur ‘n verdere 6 uur-behandeling met AfriplexGRT™, of die bioaktiewemiddel, Aspalatien. Die effek van stresinduksie was geondersoek deur middel van die assessering van ATP and ROS produksie, mitokondriale bioenergie faktore,

mitokondriale membraanpotensiaal en apoptose. Selle was ook geoes vir mRNA-uitdrukkingsanalises. Vir die *in vivo,* dieet-geïnduseerde fibrose model, is Wistar-rotte van manlike en vroulike geslag verskillende obesogeniese diëte gevoer, insluitend 'n hoë vet, hoë suiker (HFHS) dieet, ‘n obesogeniese 1 (OB1) dieet, of 'n obesogeniese 2 (OB2) dieet, oor 'n vasgestelde periode, met of sonder AfriplexGRT™. liggaamsgewig, voedselinname en bloedglukose was gedurende die studietydperk gemonitor, waarna bloed getrek is vir serumanalise van bloedvette, trigliseriede, insulienvlakke sowel as LOXL2-vlakke. Hartweefsel was ook vesamel vir DNA-metielasie profiele (slegs HFHS-dieet), RNA en proteïenvlak-analises.

Resultate:

Resultate van die *in vitro*-studie het gewys dat die HG+PAL-behandeling gelei het tot inflammasie, verhoogde oksidatiewestres en apoptose, sowel as verlaagde mitokondriale membraanpotensiaal. Dit kon egter nie 'n verandering teweegbring in geenuitdrukkingsvlakke van verskillende fibrosemerkers nie, insluitende LOXL2. AfriplexGRT™- en Aspalatien-behandelings kon nie die nadelige effekte wat deur HG + PAL-behandeling veroorsaak was, teenwerk nie. Resultate van die *in vivo* studies het aangedui dat die obesogeniese diëte wel die liggaamsgewigte van die diere verhoog het, sowel as die seruminsulien, trigliseried en serum LOXL2, maar geen verskille is waargeneem op 'n geenuitdrukking- of DNA-metileringvlak nie. Verhoogde proteïenuitdrukkingsvlakke het ooreengestem met die verhoogde serumvlakke van LOXL2 in manlike Wistar-rotte. Daarom het ons gepostuleer dat vroeë hartfibrose verwante prosesse moontlik geaktiveer was, wat verdere eksperimente en ondersoeke sal vereis.

Gevolgtrekking:

Hierdie studie het getoon dat 'n obesogeniese dieet geslagspesifieke veranderinge in metaboliese prosesse kan veroorsaak. Hierdie resultate het ook aangedui dat LOXL2-regulering moontlik aangedryf word deur 'n meganisme wat onafhanklik is van DNA-metielasie en dat AfriplexGRT™ nie LOXL2-geïnduseerde fibrose of hartversteurings in die dieet-geïnduseerde Wistar rotmodel kon verbeter nie.

Acknowledgements

Funding bodies: The National Research Foundation, for funding (PDP and Extension bursaries) for the duration of this study. The South African Rooibos Council and South African Medical Research Council for project funding.

Supervisors and co-supervisors: Rabia Johnson, thank you for your assistance and guidance throughout the completion of this degree. Ebrahim Samodien, thank you for understanding how I work, and encouraging me to do my best and keep pushing, despite situations. Thank you for your positive view on life, and for your effort to keep me in good spirits throughout the last few years. Carmen Pheiffer and Gerald Maarman, thank you for co-supervising this project.

BRIP staff and students: Nonhlakanipho Sangweni, Tracey Jooste and Jyoti Sharma, thank you for your assistance with the tissue culture experiments. Nonhle, I appreciate the long hours and weekends you spent in TC to help me complete my TC experiments well. Jyoti, your hours spent editing my thesis have not gone unnoticed.

Ruzayda van Aarde, Desmond Linden and Charna Chapman, thank you for your assistance with my western blots, cutting of histology sections and staining, and for training me. I appreciate everything you each did, always being willing to help where you can.

Colleagues, a few of whom have become good friends, thank you for your support and assistance throughout this journey, I am glad our paths crossed.

Friends and family: you have all been most patient (mostly) with me finishing my studies and I appreciate the constant support and checking up on me and my progress, even though I rarely wanted to talk about the latter. To my parents, I may not carry your surname anymore, but I am glad I can make you proud by finally finishing this degree. Thank you for always being there and often seeming more frustrated than me when things did not go to plan with the studies. And Walt, thank you for your unending love and support through everything the last 4 years have thrown at me; probably the highest points of my life, but also the lowest lows. I appreciate that you have taken everything so in your stride and helped to carry me through. Dani, I want to dedicate this thesis to you; I miss you every day.

My Lord and Saviour: you have shown me throughout this period that there is a strength within me that I did not know I had. I have grown in love, patience and strength through this journey, and I look forward to the next path you lead me down.

Table of Contents

Declaration i

Abstract ii

Opsomming iv

Acknowledgements vi

List of Figures and Tables xv

List of Abbreviations xix

Units of measurement xxiii

Symbols xxiii

Chapter 1: Literature review: Linking LOXL2 to Cardiac Interstitial Fibrosis (published) and Nutrigenomics: The effect of polyphenols on cardiac function and disease

1.1 Introduction 2

1.2 The ECM is compromised during the development of fibrosis 4

1.3 The Lysyl Oxidase Gene Family 6

1.4 LOXL2 in disease 9

1.5 The role of LOXL2 in the development of cardiovascular disease 11

1.6 LOXL2 activity and its gene regulatory network 15

1.7 Epigenetic Control of LOXL2 Expression 17

1.7.1 LOXL2 and DNA methylation 18

1.7.2 LOXL2 and histone modification 19

1.8 Future considerations 19

1.9 Polyphenols as nutraceuticals 211

1.10 The role of polyphenols in health and disease 211

1.11 Diet-induced obesity and polyphenol 222

1.12 *Aspalathus linearis* is rich in polyphenols 233

1.13 The effect of *Aspalathus linearis* and its bioactive compounds on obesity 244

1.14 The effect of *Aspalathus linearis* and its bioactive compounds on diabetes 255

1.15 The effect of *Aspalathus linearis* and its bioactive compounds on oxidative stress and inflammation 255

1.16 The effect of *Aspalathus linearis* and its bioactive compounds on CVD 266

1.18 Conclusions 26

1.18 References 29

Chapter 2: An in vitro investigation of LOXL2 as a candidate for cardiovascular dysfunction using H9c2 cardiomyoblasts

2.1. Introduction 49
2.2. Material and Methods 50
2.2.1. Reagents and Kits 50
2.2.2. H9c2 cell maintenance 50
2.2.3. H9c2 stress induction and treatment conditions 50
2.2.4. Palmitate dose response 51
2.2.5. Measuring mitochondrial membrane potential with JC-1 staining 51
2.2.6. Determination of cell proliferation in H9c2 cells in response to HG+PAL stress and treatment 52
2.2.7. Bradford Protein Determination of H9c2 cells 52
2.2.8. Determination of ROS production in H9c2 cells in response to HG+PAL stress and treatment . 52
2.2.9. Mitochondrial bioenergetics in H9c2 cells in response to high glucose stress and treatment ... 53
2.2.10. Quantification of apoptosis in H9c2 cells in response to high glucose stress and treatment 53
2.2.11. mRNA expression analysis 54
2.2.11.1.1. RNA extraction 54
2.2.11.1.2. RNA quantification 54
2.2.11.1.3. DNase treatment 55
2.2.11.1.4. cDNA synthesis 55
2.2.11.1.5. Assessment of genomic DNA contamination 55
2.2.11.1.6. Quantitative Real-Time PCR (qRT-PCR) 56
2.2.12. Statistical analysis 57
2.3. Results 58
2.3.1. Optimization of the palmitate concentration 58
2.3.2. Determining the effect of AfriplexGRT™ and Aspalathin on cell proliferation and viability 58
2.3.3. Determining the effect of AfriplexGRT™ and Aspalathin on markers of stress 59
2.3.4. Determining the effect of AfriplexGRT™ and Aspalathin on mitochondrial bioenergetics 62
2.3.5. Determining the effect of AfriplexGRT™ and Aspalathin on mitochondrial membrane potential 644
2.3.6. Determining the effect of AfriplexGRT™ and Aspalathin on apoptosis 666
2.3.6.1. RNA expression 6969
2.4. Discussion 777
2.5. Conclusion 833
2.6 References 855

Chapter 3: AfriplexGRT™ does not display a cardioprotective effect in males compared to female Wistar rats on a high fat-high sugar diet

3.1. Introduction 922
3.2. Material and Methods 933
3.2.1. Reagents and Kits 933
3.2.2. Wistar rat model 944
3.2.2.1. Ethics 944
3.2.2.2. Preparation of AfriplexGRT™ dosage 944
3.2.2.3. Study design: Grouping, diet and AfriplexGRT™ treatment of rats 944
3.2.3. Biochemical analysis 966
3.2.3.1. Bodyweight 966
3.2.3.2. Food and water intake monitoring 966
3.2.3.3. Fasting blood glucose level 966
3.2.3.4. Oral Glucose Tolerance test 966
3.2.3.5. Blood collection and tissue harvested 977
3.2.3.6. HOMA-IR 977
3.2.3.7. Lipid Profile and liver enzyme analysis 977
3.2.3.8. Enzyme-linked immunosorbent assay (ELISA) analysis 977
3.2.3.8.1. Serum Insulin analysis 977
3.2.3.8.2. Serum LOXL2 analysis 988
3.2.3.9. Histology and microscopy analysis 988
3.2.3.9.1. Haemotoxylin & Eosin staining 988
3.2.3.9.2. Trichrome staining 9999
3.2.3.9.3. Immunohistochemistry – LOXL2 9999
3.2.4. Gene and Protein expression analysis 1000
3.2.4.1. Investigating methylation signatures 1000
3.2.4.1.1. Pyrosequencing primer design 1000
3.2.4.1.2. DNA extraction 1000
3.2.4.1.3. DNA concentration determination 1011
3.2.4.1.4. Bisulfite conversion and clean-up 1011
3.2.4.1.5. PCR 1022
3.2.4.1.6. Pyrosequencing 1022
3.2.4.2. mRNA expression analysis 1033
3.2.4.2.1. RNA extraction 1033
3.2.4.2.2. RNA quantification 1033
3.2.4.2.3. DNase treatment 1033

3.2.4.2.4. cDNA synthesis 1044
3.2.4.2.5. Assessment of genomic DNA contamination 1044
3.2.4.2.6. Quantitative Real-Time PCR (qRT-PCR) 1044
3.2.4.2.7. RT^2 PCR Rat Fibrosis Profiler Array 1055
3.2.4.3. Protein expression analysis 1066
3.2.4.3.1. Protein extraction 1066
3.2.4.3.2. Quantification of proteins 1066
3.2.4.3.3. Western Blot analysis 1077
3.2.5. Statistical Analysis 1077
3.3. Results 1088
3.3.1. Biochemical Analysis 1088
3.3.1.1. Nutritional composition of diets 1088
3.3.1.2. Caloric intake 1088
3.3.2. Morphometric analysis 1100
3.3.2.1. The effect of HFHS diet on the body weight of Wistar rats 1100
3.3.2.2. The effect of HFHS diet on heart weight, abdominal fat weights and liver weights in male and female rats 1122
3.3.2.3. The effect of HFHS diet on fasting blood glucose levels in both male and female rats 1144
3.3.2.4. The effect of HFHS diet on Oral glucose tolerance test (OGTT) in male and female Wistar rats 1166
3.3.2.5. The effect of HFHS diet on serum liver enzymes of male and female Wistar rats 1188
3.3.2.6. The effect of HFHS diet on serum lipid profiles of male and female Wistar rats 1200
3.3.3. Molecular analysis to study the effects of HFHS diet feeding 1222
3.3.3.1. The effect of HFHS diet on serum insulin levels 1222
3.3.3.2. HOMA-IR calculation as a measurement of insulin resistance 1233
3.3.3.3. Serum LOXL2 levels as an early indicator of fibrosis before clinical diagnosis 1255
3.3.4. The effect of effect of HFHS diet on histology for both male and female rats 1266
3.3.4.1. The effect of HFHS diet on Hematoxylin and Eosin-stained (H&E) heart sections of both male and female Wistar rats 1277
3.3.4.2. The effect of HFHS diet on trichrome stained heart sections of both male and female Wistar rats 129
3.3.4.3. The effect of HFHS diet on LOXL2 immunohistochemical heart sections of both male and female Wistar rats 1311
3.3.5. Gene Expression analysis 1333
3.3.5.1. DNA methylation analysis 1333
3.3.5.2. RNA expression 1366
3.3.5.3. RT^2 PCR Rat Fibrosis Profiler Array 1400
3.3.5.4. Protein expression 1422

3.4. Discussion 1444
3.4.1. The effect of caloric intake 1444
3.4.2. The effect of HFHS diet on bodyweight, FBG, and HOMA-IR 1455
3.4.3. Diets and lipids 1488
3.4.4. The effect of diet on markers of fibrosis 14949
3.4.5. LOXL2 mRNA expression and its downstream regulators as early marker of diet-induced fibrosis 1500
3.4.6. LOXL2 and DNA methylation 1522
3.4.7. LOXL2 and pSMAD2 activation correspond to increased serum levels 1522
3.4.8. Additional markers for diet-induced fibrosis 1544
3.5. Conclusion 155
3.6. References 1566

Chapter 4: Impact of an obesogenic diet and AfriplexGRT^{TM} administration on fibrosis in hearts of male Wistar rats

4.1. Introduction 1666
4.2. Material and Methods 1688
4.2.1. Reagents and Kits 1688
4.2.2. Wistar rat model 1688
4.2.2.1. Ethics 1688
4.2.2.2. Study design: Grouping, diet and AfriplexGRT^{TM} treatment of rats 16969
4.2.2.3. Sample collection 1700
4.2.3. Biochemical analysis 1711
4.2.3.1. Fasting Blood glucose 1711
4.2.3.2. Plasma insulin 1711
4.2.3.3. HOMA-IR 1711
4.2.3.4. Oral Glucose Tolerance test (OGTT) 1711
4.2.3.5. Lipid Profile analysis 1711
4.2.3.6. Enzyme-linked immunosorbent assay (ELISA) analysis 1722
4.2.3.6.1. Serum Insulin analysis 1722
4.2.3.6.2. Serum LOXL2 analysis 1722
4.2.3.7. Histology and microscopy analysis of heart tissue sections 1722
4.2.3.7.1. Hematoxylin & Eosin staining 1722
4.2.4. Gene and Protein expression analysis 1722
4.2.4.1. RNA extraction 1733
4.2.4.1.1. RNA quantification 1733

4.2.4.1.2. DNase treatment 1733
4.2.4.1.3. cDNA conversion and assessment of genomic DNA contamination 1733
4.2.4.1.4. Quantitative Real-Time PCR (qRT-PCR) 1744
4.2.4.2. Protein expression analysis 1744
4.2.4.2.1. Protein extraction 1744
4.2.4.2.2. Quantification of proteins 1755
4.2.4.2.3. Western Blot analysis 1755
4.2.5. Statistical Analysis 1755
4.3. Results 1766
4.3.1. Biochemical analysis 1766
4.3.1.1. Nutritional composition of diets 1766
4.3.1.2. Food and caloric intake 1766
4.3.2. Morphometric analysis 178
4.3.2.1. The effect of diet composition on the bodyweights of male Wistar rats 178
4.3.2.2. The effect of diet composition on fasting blood glucose 17979
4.3.2.3. The effect of diet composition on glucose clearance 179
4.3.2.4. The effect of diet composition on serum liver enzymes and serum lipid profiles of male Wistar rats 1811
4.3.3. Molecular analysis 1833
4.3.3.1. The effect of diet composition on serum insulin levels 1833
4.3.3.2. HOMA-IR calculation as a measurement of insulin resistance 1844
4.3.3.3. Serum LOXL2 levels as an indicator of fibrosis 1855
4.3.4. The effect of effect of diet composition on histology 1866
4.3.4.1. The effect of diet composition on Hematoxylin and Eosin-stained heart sections 1866
4.3.4.2. RNA expression 188
4.3.4.3. Protein expression 1911
4.4. Discussion 1922
4.4.1 Diet composition risk on cardiac metabolic injury 1922
4.4.2 Diet-induced obesity as a risk for CVD 1933
4.4.3 Insulin resistance as a risk of CVD 1944
4.4.4 Hyperlipidemia and CVD 1944
4.4.5 Diet effect on cardiac pathology and serum LOXL2 1955
4.4.6 LOXL2 and its downstream effectors 1966
4.5. Conclusion 198
4.6. References 199199

Chapter 5: Discussion. Conclusion and Future Work:

5.1 Discussion 208
5.2 Conclusion 2111
5.3 Future Studies 2122
5.4 References 2133

List of Figures and Tables

Chapter 1:

Figure 1.1: The structure of the LOX and LOXL1–4 proteins..... 7

Figure 1.2: The mechanism of lysyl oxidase collagen cross-linking..... 8

Figure 1.3: LOXL2-induced cardiac fibrosis..... 10

Figure 1.4: A proposed mechanism by which LOXL2 causes fibrosis and cardiac dysfunction..... 16

Figure 1.5: Figure outlining methods to achieve aims..... 27

Chapter 2:

Figure 2.1: Palmitate dose response..... 58

Figure 2.2: ATP assay..... 59

Figure 2.3: The effect of AfriplexGRT™ and Aspalathin on HG+PAL induced oxidative stress..... 60

Figure 2.4: Gene expression analysis..... 61

Figure 2.5: Seahorse analysis of mitochondrial bioenergetics..... 63

Figure 2.6: JC1 analysis of mitochondrial membrane potential..... 65

Figure 2.7: Analysis of flow cytometry data..... 67

Figure 2.8: Representative images of Annexin and Pi flow cytometry graphs..... 68

Figure 2.9: Analysis of gene expression of fibrotic markers..... 70

Figure 2.10: Analysis of gene expression of fibrotic markers..... 74

Chapter 3:

Figure 3.1: Animal study design..... 95

Figure 3.2: Area under the curve (AUC) analysis of the caloric intake..... 109

Figure 3.3: Body weights of Wistar rats after 9 months of treatment..... 111

Figure 3.4: Organ weights of Wistar rats after 9 months of treatment..... 113

Figure 3.5: Fasting blood glucose of (A) male and (B) female Wistar rats..... 115

Figure 3.6: Glucose response observed during oral glucose tolerance test (OGTT)..... 117

Figure 3.7: Serum AST and ALT levels as an indicator of liver damage..... 119

Figure 3.8: Serum triglycerides, total cholesterol, and HDL-cholesterol..... 121

Figure 3.9: Serum insulin levels..... 123

Figure 3.10: HOMA-IR analysis of insulin resistance..... 124

Figure 3.11: Serum ELISA-based LOXL2 expression..... 125

Figure 3.12: Photomicrograph showing hematoxylin and eosin-stained heart sections..... 128

Figure 3.13: Trichrome stained heart sections..... 130

Figure 3.14: LOXL2 immunohistochemical probing of heart sections..... 132

Figure 3.15: LOXL2 promotor alignment and CpG identification..... 133

Figure 3.16: LOXL2 pyrosequencing analysis..... 135

Figure 3.17: RNA expression in male rats..... 137

Figure 3.18: RNA expression of female rats..... 138

Figure 3.19: Western blot analysis of proteins extracted from heart tissue..... 143

Chapter 4:

Figure 4.1: Obesity can lead to increased risk of cardiovascular disease (CVD) development..... 168

Figure 4.2: Animal study design..... 170

Figure 4.3: Food and caloric intake of animals on the obesogenic diets..... 177

Figure 4.4: Body weights of Wistar rats after the 17-week treatment period..... 178

Figure 4.5: Fasting blood glucose of Wistar rats after 16 weeks..... 179

Figure 4.6: Oral glucose tolerance test AUC plots: The effect of AfriplexGRT™ on glucose metabolism..... 180

Figure 4.7: Serum triglycerides, total cholesterol, and HDL-cholesterol and serum AST and ALT levels as an indicator of liver damage..... 182

Figure 4.8: Fasting serum insulin levels at 17 weeks of diet feeding..... 183

Figure 4.9: HOMA-IR calculation analysis..... 184

Figure 4.10: Serum LOXL2 concentrations after 17 weeks of feeding..... 185

Figure 4.11: Hematoxylin and eosin-stained heart sections..... 187

Figure 4.12: RNA expression in male rats..... 190

Figure 4.13: Western blot analysis of proteins extracted from heart tissue..... 191

Chapter 1:

Table 1.1: Summary of articles investigating LOXL2 and fibrosis in cardiovascular disease..... 13

Chapter 2:

Table 2.1: Taqman® Gene Expression assay list..... 56

Chapter 3:

Table 3.1: A list of the methylation sequencing primers used for pyrosequencing..... 100
Table 3.2: Taqman® Gene Expression assay list..... 105
Table 3.3: List of primary antibodies and their dilutions used for Western Blot analysis..... 107
Table 3.4: Diet composition of the standard rodent diet compared to the high fat patty..... 108
Table 3.5: Oral glucose tolerance test, area under the curve (AUC)..... 116
Table 3.6: Summary of metabolic parameters that differ between males and females..... 126
Table 3.7: PCR Fibrosis Profiler Array results..... 141

Chapter 4:

Table 4.1: Taqman® Gene Expression assay list..... 174
Table 4.2: List of primary antibodies and their dilutions used for Western Blot analysis..... 175
Table 4.3: Diet composition..... 176
Table 4.4: Oral glucose tolerance test..... 180
Table 4.5: Summary of metabolic parameters..... 186

Chapter 5:

Table 5.1: Summary of metabolic and molecular parameters..... 210

Appendix 1:

Supplementary Table A1.1: The macronutrient composition of the control and HFHS diet..... 220
Supplementary Table A2.2: The macronutrient composition of OB1 and OB2 diets..... 221

Appendix 2:

Suplementary Table A2.1: PCR Fibrosis profiler array results..... 223

Appendix 3:

Suplementary Figure A3.1: Proton leak results..... 225

List of Abbreviations

α-SMA	Alpha smooth muscle actin
AfriplexGRT™	Aspalathin-rich rooibos extract
AGE	Advanced glycation end product
AKT	Protein kinase B
ALT	Alanine aminotransferase
ASP	Aspalathin
AST	Aspartate transaminase
AUC	Area under the curve
AZA	5-azacytidine
BSA	Bovine serum albumin
cDNA	Complementary DNA
COL1A1	Collagen type I alpha 1
CTGF	Connective tissue growth factor
CTRL	Control
CVD	Cardiovascular disease
db/db mice	Leptin receptor-deficient mouse model of obesity and type II diabetes
DCFH-DA	2',7'-Dichlorofluorescin Diacetate
DMEM	Dulbecco's Modified Eagle's Medium
DNMT	DNA methyltransferase
DPBS	Dulbecco's phosphate-buffered saline
dYY mice	Deutschland, Denken, and Yoken mice
ECAR	Extracellular acidification rate
ECM	Extracellular matrix
FBS	Fetal bovine serum
FGF-2	Fibroblast growth factor 2
GAL3	Galectin-3

H9c2	Rat heart cardiomyoblast cells
H&E	Hematoxylin and Eosin
HDL	High-density lipoprotein
HF	Heart Failure
HFHS	High fat, high sugar
HG	High glucose
HIF1	Hypoxia-inducible factor 1
HOMA-IR	Homeostatic model assessment of insulin resistance
IDF	International Diabetes Federation
IL-10	Interleukin 10
IL-6	Interleukin 6
JC-1	5,5',6,6'-tetrachloro-1,1',3,3-tetraethylbenzimidazolyl-carbocyanine iodide
LDL	Low-density lipoprotein
LOX	Lysyl oxidase
LOXL1-4	Lysyl oxidase-like 1-4
MMP	Mitochondrial membrane potential
mTOR	Mechanistic target of rapamycin
NFκB	Nuclear factor kappa-light-chain-enhancer of activated B cells
NRF2	Nuclear factor erythroid 2-related factor 2
Ob/ob mice	Leptin deficient mouse model of obesity and type II diabetes
OB1	Obesogenic 1
OB2	Obesogenic 2
OCR	Oxygen consumption rate
OGTT	Oral glucose tolerance test
PAL	Palmitate
PenStrep	Penicillin and streptomycin
PI3K	Phosphoinositide 3-kinase
PRR	Proline-rich region

qRT-PCR	Quantitative real-time PCR
RAAS	Renin-angiotensin aldosterone system
RF	Retroperitoneal fat
ROS	Reactive oxygen species
SMAD2	Mothers against decapentaplegic homolog 2
SMAD3	Mothers against decapentaplegic homolog 3
SOD	Superoxide dismutase
SRCR	Scavenger receptor cysteine-rich domain
T2DM	Type 2 diabetes mellitus
TGF-β	Transforming growth factor beta
TNF	Tumor necrosis factor
WHO	World health organization

Units of measurement

%	Percentage
°C	Degrees Celsius
µL	Microliter
µM	Micromolar
G	Gram
L	litre
M	Molar
mL	Millilitre
mM	Millimolar
Mmol	Millimole
nM	Nanomolar
Mg	Microgram

Symbols

Symbols	
α	Alpha
β	Beta

Chapter 1:

Literature Review: Linking LOXL2 to Cardiac Interstitial Fibrosis

Published: Erasmus, M., Samodien, E., Lecour, S., Cour, M., Lorenzo, O., Dludla, P., Pheiffer, C., & Johnson, R. (2020). Linking LOXL2 to Cardiac Interstitial Fibrosis. *International journal of molecular sciences*, *21*(16), 5913. https://doi.org/10.3390/ijms21165913

1.1 Introduction

According to the latest World Health Organization (WHO) report, cardiovascular diseases (CVDs) account for approximately 31% of all global deaths [1]. To curb this high incidence of CVD, a new initiative from the WHO in collaboration with the United Nations was launched with the sole purpose of up-scaling efforts to prevent and control this global threat of cardiovascular deaths and focuses on nutritional interventions to reduce CVD risk factors such as obesity, diabetes and hypertension [2,3]. An estimated 463 million individuals were reported to have diabetes in 2016, which can partially be attributed to the spread of the Western diet and decreased physical demand of the modern-day [4]. According to the latest International Diabetes Federation (IDF) report, the observed increased diabetes prevalence and its associated cardiovascular risk is driven by a complex interplay of socioeconomic, demographic, environmental and genetic factors [5]. Furthermore, diabetes is a known risk factor for cardiovascular dysfunction, with approximately 85% of CVD deaths occurring as a result of heart failure (HF) or stroke [6]. There are certain lifestyle choices, such as smoking, physical inactivity and consumption of foods high in fat, sugar and salt that contribute to the observed increase in metabolic diseases and subsequent cardiovascular risk [7]. Furthermore, it has been argued that this increased cardiovascular risk is associated with chronic low-grade inflammation which is known to promote cardiac fibrosis and stiffening of the heart muscle [8]. Myocardial stiffening results in HF, which is caused by an inability of the heart to pump blood through the body effectively, thereby resulting in decreased myocardial compliance which has been attributed to alterations in cross-linked collagen [9].

A healthy heart is composed of cardiomyocytes enveloped in cross-linked collagen, the main component making up the extracellular matrix (ECM), which is critical for maintaining the structural integrity of the myocardium [10]. In conditions of cardiac damage, such as those induced by obesity or diabetes, an abnormal increase in collagen deposition is observed between the myocytes, which leads to the thickening of the ventricle wall, thus resulting in the stiffening of the heart muscle [11]. Moreover, dysregulation of cardiac tissue structure that results in increased ECM protein deposition is known to cause myocardial stiffness and dysfunction, further raising the risk for HF [12,13]. Kasner and colleagues (2011) showed that patients with diastolic dysfunction, and those with HF with normal ejection fraction exhibited an upregulation in collagen

type I expression that was accompanied by increased collagen deposition and fibrosis [14]. These findings suggest that optimal regulation of the ECM and controlling collagen deposition is critical in maintaining normal cardiac function. The mechanism of action of how ECM dysregulation contributes to fibrotic disease and CVD is not fully elucidated; thus, a better understanding of this process would add value to current knowledge of drivers of CVD and cardiac fibrosis.

Collagen is the most abundant protein in the ECM, and in the human body, types I-III are the most prominent [15]. Type I collagen is a fibrillar collagen known to be associated with an increase in fibrosis [16]. It consists of two α1 and one α2 polypeptide chains, unlike type II and III collagens, which consist of three α1 peptide chains [17]. Once procollagen has been secreted by the fibroblasts [18], the propeptide regions are then truncated to form tropocollagen [19]. The telopeptide regions of the collagen molecules contain lysine and hydroxylysine residues which are responsible for crosslink formation through chemical bonds, once the collagen molecules have self-assembled [19]. Lysyl oxidase (LOX) aids in the crosslinking by oxidative deamination of the lysine and hydroxylysine residues, which then allow them to form the crosslinks [19].

LOX and its linked LOX-like (LOXL) isoforms are known to play a major role in ECM remodelling, and their physiological regulation has become an important mechanism implicated in the development of connective tissue disorders, including cardiac tissue fibrosis. Certainly, evidence has been summarized on the molecular biology of the LOX family proteins in relation to its role in tumour biology [20,21]. Most recently, Rodríguez and Martínez-González [22,23] discussed findings on the role of the LOX family in the pathogenesis and progression of myocardial disorders. Similarly, Yang et al. (2016) and later Zhao et al. (2017) reported on the role that lysyl oxidase-like 2 (LOX2) plays in the development of cardiac fibrosis and subsequent heart failure [24,25]. More importantly, although such information remains of interest, specialized information on the regulation of LOXL2 in relation to the pathophysiology of cardiac fibrosis remains scarce. This is of interest since LOXL2 is a protein that plays an essential role in the biogenesis of collagen deposition and cross-linking and is thus increasingly being explored for its role in the development of cardiac fibrosis [24].

It is a copper-dependent enzyme that catalyses the cross-linking of collagen fibres and thereby regulates collagen homeostasis, consequently conferring ECM stability [24,26]. Basal levels of LOXL2 expression are necessary for normal ECM deposition and structural composition in tissue and is central to the functionality and maintenance of the myocardium [27]. Miner et al. (2006) argued that dysregulation through an augmented expression of LOXL2, increased collagen deposition between myofibroblasts and is a major driver in the development of cardiac fibrosis, causing heart muscle stiffness and reduced cardiac output [11]. Fong et al. (2007) confirmed this and argued that decreasing excessive collagen cross-linking would potentially reduce myocardial stiffness and improve heart function [28]. They reported that LOXL2 expression may be regulated by DNA methylation and histone modification [28]. As such, it suggests that understanding disease pathophysiology and epigenetic changes that are causal drivers of CVD pathology may allow for insight into the mechanistic action of LOXL2 and its potential use as a marker of cardiovascular dysfunction.

As such, the current review will describe the function of LOXL2 in maintaining ECM homeostasis, with the aim of understanding the involvement of LOXL2 in the pathophysiology of cardiac fibrosis. Additionally, the role that epigenetic mechanisms play in the regulation of LOXL2 expression will also be explored.

1.2 The ECM is compromised during the development of fibrosis

In the heart, the ECM forms a scaffold, supporting the myocardial cells and blood vessels and plays a crucial role in cellular structure and repair, as well as angiogenesis [10,11]. When the heart muscle is relaxed, the ventricles expand, allowing blood to enter the ventricular space [29]. During contraction, however, an electric action potential is generated in the sinoatrial node of the right atrium, which in turn, causes a release of calcium from the sarcoplasmic reticulum [30,31]. This increased calcium in the cytosol binds to troponin which triggers muscle contraction by allowing the myosin heads to bind to the actin binding sites. The subsequent conformational change in the myosin results in the contraction of the ventricles and forces blood out of the heart to be pumped throughout the body [32]. Collagen fibres within the ECM store the energy generated during the contraction of the heart and aid in myocardial relaxation, where cardiomyocytes lengthen and return to their original state [33].

Collagen is the most abundant protein in the body and the main component of the ECM; it plays a key role in the maintenance of cardiac tissue strength and structural integrity [34–36]. Indeed, collagen deposition is key to tissue remodelling and wound healing [37]; however, excessive accumulation of collagen and other extracellular matrix components in the heart can be detrimental, leading to scarring and fibrosis of cardiac tissue [35,37–39]. Mechanistically it has been speculated that the abnormal accumulation of the collagen diminishes the myocytes' contractility in the affected area, while the overall heart compliance and diastolic function are reduced. For example, in a study done by Querejeta et al. (2004) it was argued that an increase in collagen type I in the heart resulted in an increase in myocardial fibrosis, which was observed in hypertensive patients with left ventricular hypertrophy [40]. Similarly, in a study done by Martos et al. (2007), it was reported that ventricular stiffness due to increased collagen deposition resulted in diastolic heart failure or severe diastolic dysfunction in hypertensive patients [41].

The latter studies confirm that apart from its role in maintaining the structural integrity and stability of the myocardium [10], the ECM, and so too, enhanced collagen cross-linking plays a major role in the scaring and fibrotic processes which lead to HF [11]. In the instance of excessive collagen and ECM protein deposition between the myofibroblasts, the resultant thickening of the ventricle wall has been shown to cause confinement of the muscle fibres, restricting their movement past each other [11]. This collagen build-up eventually promotes fibrosis causing stiffening of the heart muscle, resulting in suboptimal contractile and pump function [11]. Therefore, a better understanding of the molecular mechanisms that drive this process, specifically collagen homeostasis, may lead to the development of possible novel antifibrotic therapies. According to Horn and Trafford (2016), increased collagen cross linking may occur via two mechanism: (i) through augmented advanced glycation end products (AGEs) formation, and (ii) enhanced lysyl oxidase (LOX)-mediated aldehyde formation [42].

LOXL2 is a key enzyme that catalyses the cross-linking of collagen fibres and is integral for collagen homeostasis. It is thus needed for normal functioning of the myocardium and is pertinent to cardiac remodelling [13]. Dysregulation of its expression is a major driver of muscle stiffness through induced cardiac fibrosis [24,25,43], which reduces cardiac output. In fact, it has been proposed that decreasing excessive

collagen cross-linking would reduce myocardial fibrosis and stiffness and thereby improve heart function [44]. Thus, finding methods for controlling collagen deposition and cross-linking through LOXL2 could be a monumental breakthrough in protecting the heart against fibrosis, and eventually reducing the burden of CVDs.

1.3 The Lysyl Oxidase Gene Family

Lysyl oxidase (LOX) and lysyl oxidase-like 1–4 (LOXL1–4) are a family of proteins that play an essential role in collagen and elastin cross-linking [45]. It is now well established that the LOX protein family is linked to fibrosis, as well as the development of other connective tissue disorders, such as elastolysis and Ehlers-Danlos syndrome [46]. Although differentiation between the various isoforms is still unclear, LOX is known to promote collagen and elastin cross-linking by oxidatively deaminating the lysine and hydroxylysine groups within the peptide chains [46]. In addition, LOX is implicated in the transcriptional regulation of transforming growth factor beta (TGF-β) signalling [47]. Increased TGF-β is known to upregulate alpha smooth muscle actin (α-SMA) leading to excessive cardiac scar formation with enhanced fibrosis [36,48].

TGF-β and α-SMA form an integral part in the fibrotic signalling pathways along with LOX. Although LOX and the LOXL1–4 isoforms are suspected to function similarly due to the conservation of the catalytic domains, the LOX protein family is predominantly expressed in different tissue types with different substrate preferences [26]. It is known that some of the tissue and substrate targets of the different LOX isoforms may overlap, but the exact localizations and functions of these proteins are not yet clearly defined. As illustrated in Figure 1.1, the copper binding, lysine tyrosylquinone cofactor, cytokine receptor-like and C-terminal regions are catalytic domains that are conserved across the LOX protein family [49–51]. These conserved domains are necessary for LOX activity, and due to these conserved domains and high protein similarity, it is predicted that LOXL 1–4 isoforms perform cross-linking in a similar manner. Any variations in the function of the LOX-family isoforms are likely to occur due to differences in the variable N-terminal regions of each protein.

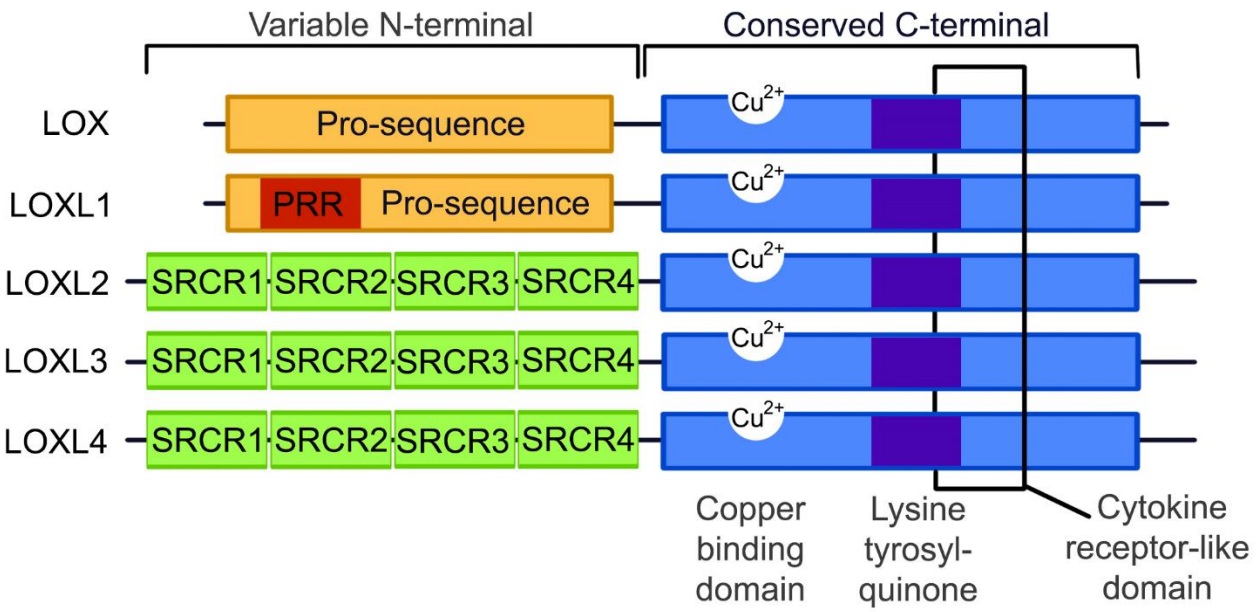

Figure 1.1: The structure of the LOX and LOXL1–4 proteins. The C-terminal is conserved between all the LOX protein family members, containing a copper binding domain, a lysine tyrosylquinone cofactor residue and a cytokine receptor domain. At the N-terminals, LOX and LOXL1 contain pro-sequences, with LOXL1 containing a proline-rich region (PRR), while LOXL2–4 contain scavenger receptor cysteine-rich domains (SRCR) within the *N*-terminal. (Image adapted from Wu 2015 [50]).

LOX exists in an inactive form, which is mainly located in the cytosol, and upon activation, it is translocated to the nucleus and endoplasmic reticulum, and secreted into the extracellular space [52]. The inactive form is associated with the endoplasmic reticulum and receives the copper ion cofactor from Menkes' protein, a copper transporter, to produce the active pro-LOX [26]. Once in the extracellular space, the activated LOX is known to interact with procollagen molecules, and oxidatively deaminates lysine and hydroxylysine residues in the telopeptide portions of the fibres to form lysine aldehyde and hydroxylysine aldehyde, respectively [19]. Once the propeptide fragments of the procollagen molecules are truncated, forming tropocollagen molecules, they self-assemble, and the aldehyde portions form covalent bonds to cross-link the collagen molecules to form fibrils [19]. The mechanisms involved in LOX-dependent cross-linking are depicted in Figure 1.2, with the process thought to be similar for LOXL1-4.

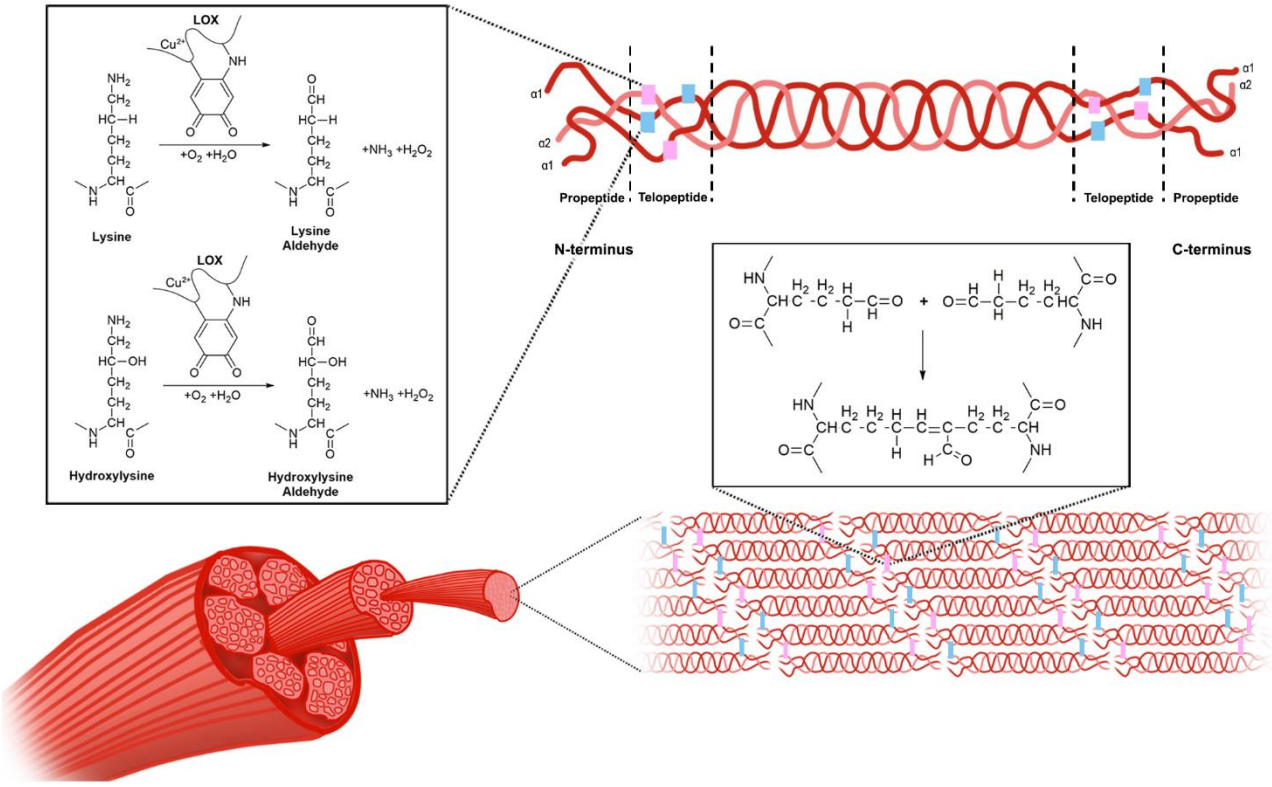

Figure 1.2: The mechanism of lysyl oxidase collagen cross-linking. LOX catalyses the conversion of lysine and hydroxylysine to lysine aldehyde and hydroxylysine aldehyde, respectively. This occurs within the telopeptide region of the procollagen molecules. The propeptide fragments of these molecules are then truncated to form tropocollagen molecules, which self-assemble and form cross-links, thereby forming collagen fibrils.

Apart from collagen and elastin cross-linking, the LOX protein isoforms perform additional functions because of the substrate preference of each enzyme. For example, LOX knock-down studies have shown that it is necessary for the proliferation and differentiation of some cell types, such as osteoblasts [53]. LOX also has the ability to inactivate TGF-β and fibroblast growth factor 2 (FGF-2) by means of oxidation, thus controlling the differentiation of myofibroblasts to fibroblasts [54,55]. Liu et al. (2004) reported that LOXL1 displays substrate preference for elastin and in knockout mouse studies, has been associated with development of abnormal vasculature [56]. In addition, it was shown by Ohmura et al. (2012) that transgenic expression of LOXL1 in mouse hearts induced cardiac hypertrophy [57]. Like LOXL1, Busnadiego et al. (2013) reported that the LOXL4 isoform is involved in vascular remodelling, although it has a preference for collagen as a substrate

[58]. Similarly, LOXL3 has been implicated in vascular remodelling and the development of cartilage and was found to be highly expressed in mesenchymal cells, with an increased substrate affinity for collagen type XI alpha 1 and 2 (COL11A1, COL11A2) and collagen type II alpha 1 (COL2A1), the main structural component of cartilage [59]. A study by Zhang et al. (2015) showed that homozygous LOXL3 knockout mice resulted in perinatal foetal death, and LOXL3 +/− mice were found to have spinal abnormalities and cleft palate [60]. As a result, LOXL3 knockout animals could not be used for studying LOXL3 effect on cardiovascular development or changes. Lastly, LOXL2 uses collagen type IV as its preferred substrate and cross-links it through both enzymatic interactions, by the active protein, and non-enzymatic interactions, by the inactive form of the protein [61]. It is proposed to play a role in a variety of functions such as normal bone development, blood vessel stabilization, and the sprouting of new blood vessels, with LOXL2 often found localized within endothelial cells [61]. In addition, as with LOXL3, studies using LOXL2 knockout mice observed perinatal foetal death as a result of hepatic and cardiovascular defects [62]. This was confirmed by Yang et al. (2016), who demonstrated that LOXL2 secretion increased in stressed mouse hearts, triggering fibrosis [24]. Taken together, the mentioned studies implicated LOXL2 in myocardial function; however, research pertaining to LOXL2 in the heart is lacking, and thus its role in cardiac fibrosis and disease will be further discussed. Given the crucial function of LOXL2, further studies are required to understand what factors govern its regulation and function in cardiac health and disease.

1.4 LOXL2 in disease

Although the *LOXL2* gene has been most widely studied in cancer [50], it has recently attracted interest for its role in fibrotic diseases such as idiopathic pulmonary fibrosis and liver fibrosis during non-alcoholic steatohepatitis [63,64]. As with the previous findings by Yang and Zhao, in a study by Johnson et al. (2020), the results confirm the involvement of LOXL2 in cardiac dysfunction [65]. Nonetheless, evidence on the physiological regulation and data pertaining to the role of LOXL2 in cardiac health has not been reviewed. As such, understanding the mechanism by which LOXL2 is implicated in fibrosis during the pathogenesis of various medical conditions, like CVDs, may pave the way for future therapeutic interventions.

In a healthy state, fibroblasts are present in tissue in an inactive state. After injury, the fibroblasts are activated and differentiate into myofibroblasts in the presence of growth factors and cytokines, such as TGF-β, which stimulate ECM proteins to aid in the healing response [38]. It is known that under conditions of stress, such as inflammation, LOXL2 expression is induced, and its secretion into the extracellular space is increased [66]. Lytle et al. (2017) found, in low-density lipoprotein receptor deficient mice, that consumption of a high-fat, high-sugar diet increased plasma *LOXL2* mRNA levels [67]. This was confirmed by Yang et al. (2016), who showed that augmented LOXL2 expression causes an increase in TGF-β signalling through activation of the phosphoinositide 3-kinase/protein kinase B/mechanistic target of rapamycin (PI3K/AKT/mTOR) pathway [24] (Figure 1.3). Furthermore, they showed that TGF-β induced myofibroblasts formation, subsequently increasing α-SMA [24], which was previously implicated in increased collagen deposition during the fibrotic response and scar tissue formation [38,64]. In this regard, Trackman (2016) concluded that LOXL2 not only plays a role in the collagen cross-linking but can also activate alternative fibrotic pathways through the recruitment of fibroblasts [26]. Since LOXL2 is implicated in fibrosis, it is crucial to understand its role in the pathophysiology of fibrosis-induced cardiac dysfunction.

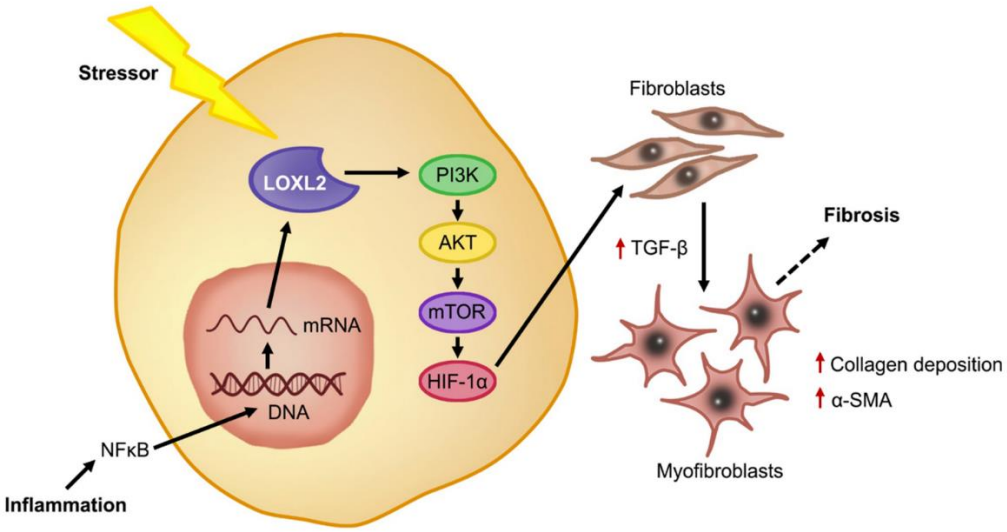

Figure 1.3: LOXL2-induced cardiac fibrosis. Under stress conditions such as inflammation, the activation of NFκB causes increased mRNA expression of *LOXL2* and downstream, LOXL2 activates the PI3K/AKT/mTOR pathway, increasing TGF-β and triggering fibroblasts differentiation, where myofibroblasts secrete α-SMA and increase collagen deposition. Overstimulation of this process results in ECM deposition and fibrosis.

1.5 The role of LOXL2 in the development of cardiovascular disease

Diabetes is a risk factor for cardiac dysfunction and often occurs as a result of increased oxidative stress in the cells [68]. The combination of oxidative stress and the presence of high amounts of glucose in the blood leads to the production of AGEs, which can accumulate in various organs including the kidneys and heart, leading to vascular diseases and endothelial dysfunction [69–71]. AGEs are known to aggregate on proteins involved in fibrotic processes, such as fibronectin and collagen, and can alter the normal degradation of the proteins [72]. When AGEs link with collagen molecules, it has been found to decrease elasticity and increase stiffness within the vasculature and the heart tissue [73]. This leads to myocardial fibrosis by the induction of transcription factor binding, which promotes the expression of genes such as LOXL2 [73].

Cardiac fibrosis is a hallmark of cardiovascular dysfunction, where ventricular wall thickening is a consequence of excessive extracellular matrix deposition, which can reduce cardiac contractility [13]. Literature suggests that LOXL2 expression in the heart needs to be tightly regulated in order to prevent myocardial fibrosis, with these articles summarized in Table 1.1. Briefly, a study confirmed a positive correlation between increased LOXL2 mRNA expression and the development of cardiac dysfunction, in both transgenic mice and humans [24]. In human studies performed by Raghu et al. (2017) and Zhao et al. (2017), Raghu et al. showed that admission of Simtuzumab, which binds to LOXL2 in the treatment of fibrosis, did not improve the health outcomes of the patients with idiopathic pulmonary fibrosis [74]; however, Zhao et al. showed that patients with atrial fibrillation had increased serum LOXL2 levels, which was associated with increased left atrial size; however, there was no effect on left ventricular function [25]. In the same year, Mižíková et al. (2017) found that treating both lung fibroblasts and C57Bl/6J mice with a general inhibitor of the LOX gene family had no effect on the mRNA expression of these genes using both an in vivo and in vitro model [75]. Additionally, Craighead et al. (2018) treated hypertensive patients with the same LOX inhibitor and found an increase in ECM-bound LOXL2 expression in these patients [76]. By means of proteomic analysis, Steppan et al. (2018) confirmed that LOXL2 mediates the stiffening of smooth muscles cells in aging using a LOXL2 knock-out mouse model [77]. This was confirmed by Torregrosa-Carrión et al. (2019), who reported that NOTCH activation led to increased expression of TGF-β2 and collagen, which form part of the

LOXL2 signalling pathway [78]. Lastly, it was shown by Schilter et al. (2019) that administration of a LOXL2 inhibitor for 4-weeks, after left coronary arteries occlusion, resulted in an observed decreased myocardial fibrosis with improved cardiac output in a C57/BL6 mouse model [79]. Although there is data linking LOXL2 to fibrosis, its regulation in the fibrotic cardiac disease pathophysiology remains ill-defined, and as such, more research is required to better define LOXL2's mechanistic role in cardiac tissue fibrosis and subsequent contractile dysfunction.

Table 1.1: Summary of articles investigating LOXL2 and fibrosis in cardiovascular disease.

Species	Study Design	Findings	References
Loxl2+/- knockout mice Human	• Mice: Underwent transaortic constriction followed by LOXL2 expression analysis and histology. • Human: Patients presenting with HFpEF and diastolic dysfunction without symptoms underwent right-ventricular biopsies for evaluation of cardiomyopathy.	• Transgenic mice: cardiac stress results in↑ LOXL2 → myocardial fibrosis & dysfunction. • Inhibition of LOXL2 activity: ↓ cardiac fibrosis and ↑ cardiac function. • LOXL2 acts via the PI3K/AKT pathway to activate TGF-β2. • Diseased human hearts: LOXL2 ↑ in the interstitial space and serum • ↑ LOXL2 expression correlated with ↑ fibrosis and myocardial dysfunction.	Yang et al. (2016) [24]
Human	• Patients (aged 45-85) with idiopathic pulmonary fibrosis were treated with simtuzumab or a placebo once a week and its effects studied.	• Simtuzumab, did not improve survival rates in patients with idiopathic pulmonary fibrosis.	Raghu et al. (2017) [74]
Human	• Patients with atrial fibrillation were assessed in terms of serum LOXL2 levels, left atrial size and left ventricular function.	• Atrial fibrillation patients: ↑ serum LOXL2 • Positively associated with increased left atrial size.	Zhao et al. (2017) [25]
Primary cells isolated from C57Bl/6J mice, macrophages and endothelial cells, and mouse pups	• Primary cells: cultured in the presence of a LOX inhibitor or LOX, LOXL1 and LOXL2 knocked down with siRNA. • Gene expression, amine oxidase activity and microarray analyses were performed. • Mice: a bronchopulmonary dysplasia model was established, and lungs harvested for expression analysis.	• Lox, Loxl1, and Loxl2 are highly expressed in primary mouse lung fibroblasts. • Knockdown of Lox, Loxl1, and Loxl2: associated with Δ in gene expression (primary mouse lung fibroblasts). • BAPN: no impact on mRNA levels of LOX target-genes, in lung fibroblasts or in BAPN-treated mice.	Mižíková et al. (2017) [75]
Human	• Intradermal micro-dialysis fibers were placed in the forearm of young, normotensive and hypertensive individuals. • Fibers treated with β-aminopropionitrile, a LOX inhibitor, or acted as a control. Norepinephrine was used to examine	• LOX inhibition augmented vasoconstrictor sensitivity in young and normotensive but not hypertensive patients. • ECM-bound LOX expression: ↑ in hypertensive subjects vs younger patients.	Craighead et al. (2018) [76]

	the vasoconstrictor function and sodium nitroprusside to study smooth muscle vasodilation.	• Vascular stiffness & microvascular dysfunction in hypertension could be due to ↑ LOX expression.	
Human aortic smooth muscle cells and LOXL2+/- mice	• Human aortic smooth muscle cells were cultured and the secretome analyzed. • Mice: nitric oxide production was assessed in the aortic rings.	• Proteomic analysis: LOXL2: important mediator of age-associated vascular stiffening in smooth muscle cells. • Nitric oxide assessment: it ↓ LOXL2 abundance and activity in the ECM of isolated smooth muscle cells. • Knock out mice: protected from age-associated vascular stiffening. • Isolated aortic rings: LOXL2 mediates vascular stiffening in aging by promoting smooth muscle cell stiffness, contractility, and matrix deposition.	Steppan et al. (2018) [77]
Mouse embryonic endocardial cells, human aortic smooth muscle cells and LOXL2+/- mice	• Mouse embryonic endocardial cells were stimulated with DLL4 and JAG1, with or without NOTCH inhibitors. • Proteomics analysis of the media was conducted to identified proteins that are secreted in response to NOTCH signaling manipulation.	• Secretome analysis identified 129 factors that showed a change in expression when NOTCH was activated or repressed. • NOTCH activation correlated with ↑ expression of TGF-β2 and collagen.	Torregrosa-Carrión et al. (2019) [78]
Wistar rats, Sprague Dawley rats, C57/BL6 mice	• A LOXL2/LOXL3 inhibitor, PXS-5153A, was developed and its effect on LOXL2/3 in relation to collagen cross-linking and fibrosis was assessed.	• PXS-5153A ↓ collagen cross-linking in vitro. • PXS-5153A ↓ collagen expression and cross-linking, thereby ↑ liver function. • In a model of myocardial infarction, addition PXS-5153A, ↑ cardiac output. • This shows that inhibition of LOXL2/LOXL3 activity could be a viable treatment option for liver fibrosis.	Schilter et al. (2019) [79]

1.6 LOXL2 activity and its gene regulatory network

Several mechanisms of LOXL2 regulation have been proposed (Figure 1.4). Interestingly, galectin-3 (GAL3), although not directly related to LOXL2, is also involved in the fibrotic process through its interaction with TGF- β. Although both proinflammatory and anti-inflammatory effects have been suggested for GAL3 [80,81], it has been mostly implicated in the development and progression of HF [82,83]. LOXL2 forms part of the PI3K/AKT/mTOR pathway [24], which is able to upregulate the hypoxia-inducible factor 1 (HIF-1). This protein plays a critical role in cardiac oxygen homeostasis, and its dysregulation results in ischemic heart disease [84,85]. Nevertheless, the PI3K/AKT/mTOR pathway can activate TGF-β signalling, thereby prompting enhanced activity of the fibrotic pathways [24]. A review by Cox and Erler (2014) suggested that tissue fibrosis is caused by specific stressors, which activates TGF-β, cytokines and other inflammatory responses [86]. This in turn could result in the recruitment and subsequent activation of fibroblasts to myofibroblasts, which are then able to produce α-SMA and upregulate proteins such as connective tissue growth factor (CTGF), LOX and LOXL2 [86]. This leads to the promotion of collagen deposition and cross-linking, resulting in the modification of the ECM, tissue stiffening and organ failure [86], making LOXL2 and its gene regulatory network ideal drug targets to protect against cardiac fibrosis and improve heart function.

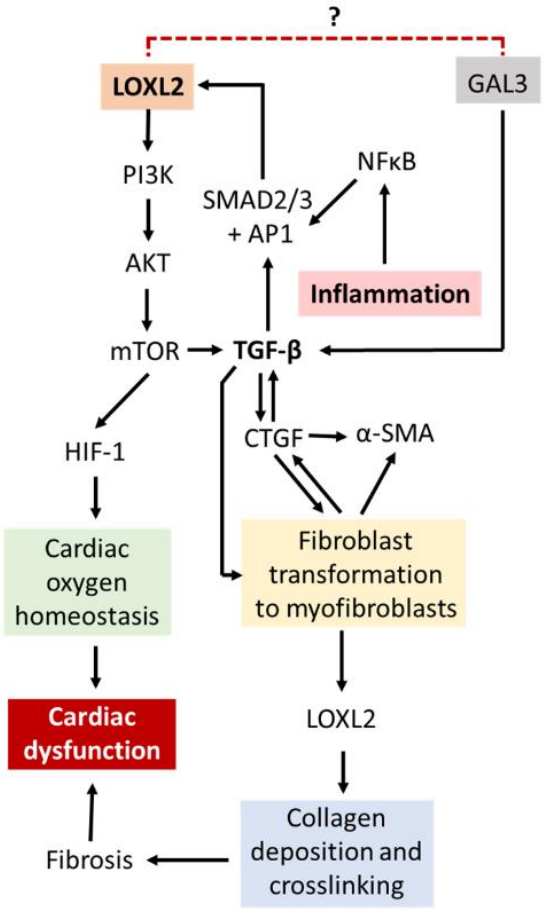

Figure 1.4: A proposed mechanism by which LOXL2 causes fibrosis and cardiac dysfunction. LOXL2 acts via the PI3K/AKT/mTOR pathway to activate TGF-β signalling and HIF-1 protein expression. GAL3 also activates TGF-β signalling, thus with possible similar effects as LOXL2. TGF-β signalling results in an increase in α-SMA, CTGF and LOXL2 expression, which leads to an increase in collagen deposition and cross-linking, resulting in fibrosis, ventricular stiffness and cardiac dysfunction. Inflammation causes an increase in nuclear factor kappa-light-chain-enhancer of activated B cells (NFκB) which interacts with AP1 and Sp-1 proteins, also increasing LOXL2 expression. Dysregulation of HIF-1 protein expression results in the disruption of oxygen homeostasis in the heart, also having pathological effects. Further investigation is needed to find out whether there is a direct interaction between LOXL2 and GAL3.

In addition, Chaudhury reported that signal transducers for TGF-β receptors, mothers against decapentaplegic (SMADs), are important regulators of cellular growth and development through their interaction with TGF-β [87]. Research done by Min Lu et al. (2019) on the regulation of LOX expression

suggested that TGF-β1 plays a pertinent role in the phosphorylation and subsequent activation of SMAD2 and SMAD3 signalling [88], with these molecules subsequently being translocated into the nucleus where they interact with DNA-binding factors such as activating protein 1 (AP-1), specificity protein 1 (Sp-1) and NFκB [89] to have downstream effects on gene expression. *LOXL2* is known to have binding sites for all three the aforementioned DNA-binding factors and thus its expression can be induced through TGF-β1/SMAD2/3 signalling [28]. Interestingly, the SMAD proteins have been found to be present in CVDs or after an ischemic cardiovascular event, where they are involved in the initiation of the fibrotic processes [89]. Moreover, when TGF is inhibited, a decrease in cardiac interstitial fibrosis as well as a suppression of late-stage cardiac remodelling was observed after a myocardial infarction in mice [90]. There is also evidence in a cardiac reperfusion injury model that inhibition of the renin-angiotensin aldosterone system (RAAS) is associated with reduced levels of TGF-h and SMAD activity, together with a decrease in fibrosis [91]. Lu et al. (2019) also showed a decrease in c-Jun, one of the components of the AP-1 DNA-binding factors [88]. This subsequently caused a decrease in LOX expression as well as downstream effectors such as collagen [88]. Taken together, this suggests that TGF-β may act via SMAD and AP-1 to regulate LOX expression, increasing cardiac fibrosis. Although this proposed pathway has not yet been evaluated for LOXL2 by any single research group, it is plausible to assume, that based on the similar structure to LOX, with respect to the regulatory sites for DNA-binding factors, that LOXL2 is regulated in a similar manner to LOX. Nonetheless, in the search to better understand the role that LOXL2 plays in CVD, it is also important to understand the involvement of epigenetic modification.

1.7 Epigenetic Control of LOXL2 Expression

Epigenetic modifications are defined as heritable changes in chromatin structure and DNA expression, with no alteration in the DNA sequence [92]. The major epigenetic modifications are DNA methylation (the addition of methyl groups to cytosine residues of CpG sites), acetylation (the addition of acetyl groups to lysine residues) and histone modification (methylation or acetylation of histones, altering the chromatin structure). These all influence the regulation of gene expression. MicroRNAs (miRNAs) are also a form of epigenetic modification that plays a role in regulating gene expression. Interestingly, however, miRNA

expression has also been shown to be controlled by epigenetic modifications [93,94]. Although epigenetics has been implicated in controlling LOXL2 expression, a paucity of data still exists regarding whether these modifications are key in its regulation.

The *LOXL2* gene is located on chromosome 8p21.3 [95,96] and contains 5 CpG sites within the promotor region and the first exon; these known sites could be influenced by DNA methylation [28,97]. LOXL2 expression is also believed to be controlled through histone modification. Fong et al. (2007) [28] and a later study done by Hollosi et al. (2009) [97] showed that treatment with a histone deacetylase inhibitor resulted in a change in LOXL2 expression, indicating that histone modification influenced LOXL2 expression. Although miRNAs in LOXL2 regulation have not been studied in CVDs, evidence from cancer studies have shown that miRNAs can regulate LOXL2 expression in tumours [98]. Since epigenetic modifications have been linked to the development and progression of various diseases, understanding how these mechanisms regulate LOXL2 could provide new avenues to control its expression, and potentially be advantageous in the treatment of fibrosis induced CVDs.

1.7.1 LOXL2 and DNA methylation

DNA methylation can be affected by environmental factors [99], and is a reversible process, making it an attractive therapeutic approach. The methylation reaction is catalysed by DNA methyltransferases (DNMTs) [100], but its dysregulation in cellular processes by both hyper- and hypomethylation contributes to the development and progression of diseases [100].

Methylation sites within a gene's promotor region are important in the regulation of gene expression [101]. Fong et al. [28] and Zhong et al. [43] both showed that methylation within the *LOXL2* promotor region aids in the regulation of its expression. In addition to this, an in vitro study done on human chondrocytes showed an increase in inflammatory markers resulted in a decrease in LOXL2 expression [102]. Dong et al. (2017) also argued that an inverse relationship exists between DNA methylation and inflammation in healthy African-American teenagers [103]. It is also known that transcription factors, such as NF-κB, and changes in DNA methylation status as well as histone modifications are responsible for the regulation of genes associated

with inflammatory pathways [104]. Inflammatory factors are known to upregulate the expression of LOXL2 and thereby increase fibrosis [105]. In addition, an epigenome-wide association study conducted on Asian and European cohorts showed that genes that are known to be associated with hypertension were differentially methylated, and that there were differences between the methylation statuses of the two cohorts [106]. It was also shown in a mouse model that if DNMT1, an enzyme that catalyses methylation, is silenced, an upregulation is seen in the interleukins and cytokines, thus increasing inflammation [107]. Biological processes of inflammation and high blood pressure, which are both risk factors for the development of CVDs [43], can be controlled by changes in methylation, thus making the discovery of methylation targets important in combating fibrotic diseases.

1.7.2 LOXL2 and histone modification

In addition to methylation, it has been shown that histone modification also plays a role in LOXL2 regulation [28]. Histones are protein structures within chromosomes around which the DNA strands or chromatin are coiled. Histone modification aids in the packaging of DNA with thus influencing gene expression [108]. Although there is little evidence to link histone modification and LOXL2 expression, evaluations in breast cancer cell lines reveal that treatment with a general DNA methylation inhibitor, 5-azacytidine, resulted in a 40-fold upregulation of *LOXL2* mRNA expression, and further co-treatment with a histone deacetylase inhibitor, trichostatin A, resulted in a further 5-fold expression increase [28,97]. It has, however, been shown that an increase in histone acetyltransferase post-myocardial infarction has a positive impact on myocardial remodelling, specifically within the left ventricle [109], and thus, histone modifications could play a key role in the pathogenesis of cardiac fibrosis. More research, however, needs to be conducted surrounding LOXL2 and regulation of its expression by histone modifications.

1.8 Future considerations

The majority of LOXL2 mechanistic studies have been focused on cancer. To date, it is known that the expression of LOXL2 is tightly regulated, with augmented LOXL2 expression being linked to interstitial fibrosis. Nonetheless, to date, there is a paucity of data linking LOXL2 mechanistically to cardiovascular dysfunction. As such, future studies should include functional studies that attempt to inhibit LOXL2 to better understand

its role in the fibrotic process. Although there is no treatment for fibrosis in the myocardium, recently two drugs, pirfenidone and nintedanib have been approved for the treatment of idiopathic pulmonary fibrosis and exert their effects by inhibiting TGF-β, platelet-derived growth factor (PDGF) and FGF receptors, respectively, which are known regulators of LOXL2 expression [110]. What is still unknown however, is how LOXL2, through the ECM, causes changes in TGF-β signalling, and whether LOXL2 has a direct effect on the myofibroblasts to result in their migration. Deeper investigation into the signalling mechanisms driving these processes could be key in identifying other important effectors in the fibrotic process.

Additionally, although some human studies have been conducted [24,25,74,76], characterization of LOXL2 expression and function within the heart is limited. Experimental data need to be validated in humans, in both male and female patients, and non-invasive methods will need to be developed to test these markers by correlations with other risk factors in order to be used as a possible predictor of CVD. A further limitation to current research is that the role of epigenetic effects influencing LOXL2 expression has not been evaluated. Although DNA methylation and histone modification have been implicated in the regulation of LOXL2 expression, it is known that there is an interplay between miRNAs and epigenetic mechanisms [111,112], and thus the effect of miRNAs on LOXL2 gene expression should also be explored.

Epigenetic changes can be regulated by external factors such as smoking, pollution, diet and exercise [113]. Diet, such as the Mediterranean diet, characterized by high polyphenol content is also associated with reduced cardiovascular risk, and as such, should be investigated [114]. Interestingly, polyphenols are also known to have the potential to modulate epigenetic machinery; however, the mechanisms by which polyphenols exert their effects, particularly in affecting *LOXL2* methylation or histone modifications, are yet to be elucidated. Additionally, it is known that polyphenols act as anti-inflammatory agents, reducing the stressors that could activate the fibrotic pathways, and could thus prove to be useful in this regard and warrants further investigation.

1.9 Polyphenols as nutraceuticals

Nutrigenomics can be defined as the interaction between genes, nutrient-diet and nutrition-induced epigenetics and has been the subject of intensive investigation in the last decade. Most studies on nutrigenomics are still in their early primitive stage but is an attractive approach to better understand the impact a nutritious diet has on longevity, immune disorders as well as various non-communicable diseases.

According to Davies et al. (2011), a balanced diet combined with physical activity is an important part of maintaining a healthy lifestyle which will reduce the chances of developing chronic diseases [115]. Indeed, diet plays a central role in pathological consequences of health and disease. Furthermore, the consumption of a balanced diet must include all the daily nutritional requirements of proteins, carbohydrates, fibre, and vitamins without exceeding the recommended intake. Various scientific evidence has shown that overnutrition and an unbalanced diet is the main risk factor for several chronic diseases [116], such as obesity [117], diabetes [118,119] and cardiovascular health [120,121], to name a few.

Lifestyle intervention therapies remain the best method for treatment and coupled with early detection may have positive consequences in the prevention of cardiovascular derangements. Nutrition is a major component of lifestyle interventions with poor diet choices having detrimental effects on health outcomes [122]. In this regard, the Mediterranean diet has become the cornerstone in risk reduction for the prevention of chronic diseases [123]. These diets are comprised of plant-based fruit and leafy vegetables that are rich in phytochemicals named polyphenols [124,125].

1.10 The role of polyphenols in health and disease

Polyphenols are naturally occurring plant-derived phytochemicals that are found in high concentrations in most fruits, vegetables, as well as cereals and herbal medicines and most polyphenols have been widely researched for their health properties [126]. It is well known that polyphenols can be grouped into two main classes, flavonoids and phenolic, where flavonoids can be further classified into flavonones, flavonols, flavanols, flavones and isoflavones, and phenolic acids are classified into hydroxycinnamic and hydroxybenzoic acids [127]. Generally, polyphenols and their secondary metabolites are known to display protective effect against diseases such as cancer, obesity, diabetes and CVD [128]. Indeed, there is

widespread scientific agreement that polyphenols are naturally occurring antioxidants that offer protection through their ability to neutralize free radicals by donating an electron or hydrogen atom, such as the reduction of hydroperoxides and hydrogen peroxide to water and alcohol, actively scavenging free radicals, regulation of gene expression, and the sequestration and chelation of metal ions, thus improving the exogenous antioxidant capacity of a cell [129-132]. As a result, polyphenols and their potential health benefits have gained the interest of both the public and scientific community.

1.11 Diet-induced obesity and polyphenol

Urbanisation and consumption of sugar-sweetened beverages have steadily increased the prevalence of obesity over the past three decades [133]. With pharmacological intervention having various side effects, polyphenols (and their bioactive components) as a functional food supplement, are being considered as an alternative means in the management of various lifestyle diseases. For example, polyphenols such as resveratrol, curcumin and berberine to name a few, are known dietary antioxidants with health benefits aimed at reducing oxidative stress, inflammation and apoptosis, whilst improving β-oxidation in obese individuals [134]. Furthermore, numerous studies have shown that diet-induced obesity is known to alter glucose homeostasis and supplementation with polyphenols are known to lower the risk of CVD [135,136]. As such, the antioxidant properties of plant-derived polyphenols are known to play an important role in preventing diet-induced cardiac dysfunction [137,138].

Hyperglycaemia, inflammation and hyperlipidaemia are three of the major metabolic disturbances associated with the development and progression of CVD [139–141]. These disturbances are said to provoke excessive generation of oxidative stress within the myocardium. Currently, obesity or diabetic drug therapies does not protect the myocardium and as such researchers are investigating the use of plant-derived products, not only to lower circulating blood glucose but also for their antioxidant and anti-inflammatory protective effects. Currently, various studies, including studies done in our laboratory, have shown that plant-derived polyphenols can protect the heart against various metabolic disturbances [137,142–145].

Plant-based diets are known to improve serum lipid profiles, reduce blood pressure, and may contribute to the reversal of structural and functional abnormalities in the setting of coronary heart failure. For example,

in a series of case studies conducted by Najjar and Montgomery (2019), it was observed that lifestyle intervention through a plant-based diet improves the endogenous antioxidant capacity and anti-inflammatory activity, leading to the regression of morphological and functional abnormalities in the heart [146]. Indeed, epidemiological studies report that plant-based diets are becoming increasingly popular as a healthier alternative to a diet laden with meat [147]. Noteworthy, apart from its antioxidant, anti-inflammatory and anti-obesogenic properties, recent scientific evidence suggests that polyphenols may have the ability to reverse diet-induced aberrant DNA methylation signatures involved in pathological conditions, such as obesity, diabetes and CVD [148]. For example, in a study done by Crescenti et al. (2013) DNA methylation was decreased in human leukocytes from cardiovascular disease patients after consumption of polyphenol-rich cocoa beans [149]. In addition, a study by Lee et al. (2005) showed that polyphenols from tea were able to reduce DNA methylation through DNMT1. Indeed, aberrant DNA methylation patterns may lead to pathological consequences including the development of cardiovascular disease [43,150]. Therefore, this section will summarize the current knowledge on dietary polyphenols and cardiovascular health, specifically focussing on the effect of polyphenols found in *Aspalathus linearis*.

1.12 *Aspalathus linearis* is rich in polyphenols

Aspalathus linearis is a species of fynbos that grows in Southern Africa and is best known for its use as a herbal tea, called rooibos tea [151]. The beneficial effect of rooibos as an anti-obesity, anti-diabetic and anti-atherogenic agent comes from both local and international studies. Furthermore, Rooibos is caffeine-free with no reported effects on psychosocial or neurochemical parameters in humans and is therefore viewed as an attractive alternative to prevent diet-induced obesity [152]. Rooibos is found in both a fermented (red) and unfermented (green) form. The fermented form is most commonly extracted and consumed as a tea with health benefits because of its high polyphenolic content and antioxidant levels. To date, numerous studies have demonstrated that fermented rooibos can enhance glucose metabolism and insulin signalling *in vivo* and *in vitro* [15-19] and reduce inflammatory status in both animal models and human subjects. For example, Marnewick et al. (2011) reported that the consumption of fermented rooibos tea for 6 weeks protected the myocardium by reducing oxidative stress, lipid peroxidation and improving the redox status of

adults consuming rooibos tea. Similarly, in a study done by Villano et al. (2010), it was reported that fermented rooibos is a good dietary antioxidant, improving plasma antioxidant capacity in human subjects. Noteworthy, research has recently focused on the unfermented rooibos tea as it presents with a 28% higher *in vitro* antioxidant capacity than the fermented form [151, 153]. Fermentation reduces the total phenolic content to 35% from 41% in unfermented rooibos [153]. Quercetin and Aspalathin are the main active polyphenols in rooibos tea, and although they are present in both fermented and unfermented rooibos tea, Aspalathin has been identified as the major active ingredient present in rooibos tea, however its content is reduced by the fermentation process [154]. This was confirmed by Marnewick et al. (2000) who reported that the polyphenolic content present in rooibos is reduced to 29.7% in fermented rooibos compared to the 41.2% found in unfermented rooibos [155]. For this reason, it is thought that green rooibos has greater health and therapeutic potential. The proof of concept that green rooibos is more effective comes from both local and international studies, for example, Muller et al. (2012) reported on the hypoglycaemic and hyperlipidaemic effect of Aspalathin-rich green rooibos extract *in vitro* and *in vivo* [156]. These findings were independently confirmed by Mazibuko et al (2013; 2015) who reported that green rooibos extract increased glucose uptake via GLUT 4 in both C2C12 muscle and 3T3 fat cells [157,158]. Similarly, Son et al. (2013) demonstrated that green rooibos extracts increasing GLUT4 uptake through AMPK phosphorylation in L6 myotubes [159]. Furthermore, Johnson et al. (2016) reported that Aspalathin prevented augmented advanced glycation end products, reduced fasting blood glucose levels, hypertriglyceridemia and markers of ROS in an *in vitro* H9c2 cell model [142].

1.13 The effect of *Aspalathus linearis* and its bioactive compounds on obesity

Obesity is a risk factor for the development of CVDs. Mahmood et al. (2016) observed that Aspalathin treatment decreased bodyweights of STZ-induced male Wistar rats [160]. Son et al. (2013) demonstrated that Aspalathin could improve glucose clearance without decreasing body weight in a leptin-deficient db/db mouse model [159]. Sanderson et al. (2014) reported on the anti-obesogenic potential of fermented rooibos tea in adipocyte cells, where they observed inhibition of adipogenesis using an *in vitro* 3T3 L1 cell culture model [161]. Confirming Sanderson's findings, Mazibuko et al. (2015) demonstrated that Aspalathin improves

palmitate-induced lipid metabolism in 3T3-L1 adipocytes [158]. Additionally, Layman et al. (2019), reported that a green rooibos extract improved lipid accumulation in the livers in a diet-induced obese Wistar rat model [162].

1.14 The effect of *Aspalathus linearis* and its bioactive compounds on diabetes

Diabetes is classified by elevated blood sugar levels, and a rooibos extract has been shown to have glucose-lowering potential [163]. Marnewick et al (2016), reported that drinking 6 cups of fermented rooibos tea a day reduced blood glucose levels by 14% in the groups who consumed rooibos when compared to their control counterparts [164]. Research conducted by Kawano et al. (2009) confirmed that Aspalathin improves glucose uptake in muscle cells and increases insulin secretion from pancreatic β-cells in an ob/ob diabetic mouse model [165]. Similarly, a study by Kamakura et al. (2015), showed that green rooibos extract had the ability to improve glucose clearance in a mouse model, and it was confirmed *in vitro* that this effect was likely due to the observed increase in glucose uptake induced by the green rooibos extract [166]. Interestingly, the same study observed a greater induction of glucose uptake by the green rooibos extract than by Aspalathin alone, however, a higher concentration of the extract was used for treatment when compared to the Aspalathin concentration. This was confirmed by Mikami et al. (2015) who observed that ddY mice fed a standard chow diet displayed improved glucose clearance, with the effect being more pronounced when treating with the extract than Aspalathin alone [167]. These studies indicate that although Aspalathin is effective as an anti-diabetic agent, other compounds in green rooibos also play a role in this glucose-lowering effect and might work synergistically with Aspalathin to cause the observed effect.

1.15 The effect of *Aspalathus linearis* and its bioactive compounds on oxidative stress and inflammation

Inflammation and oxidative stress are two of the major metabolic disturbances associated with the development of diet-induced diabesity [168]. In a study done by Smith and Swart (2016), it was reported that rooibos tea consumption modulated NF-κB, IL-6 and IL-10 expression, and decreased production of tumour necrosis factor-α (TNF-α) and IL-6 in both an *in vitro* and *in vivo* model [169]. In addition, a study conducted by Baba et al. (2009) reported that consumption of rooibos tea increased SOD activity in a Wistar rat model [170]. Marnewick et al. (2011) also showed a decrease in lipid peroxidation after rooibos tea consumption

[164], whilst Orlando et al. (2019) made use of an Aspalathin-rich rooibos extract (AfriplexGRT^{TM}) and showed that it was able to decrease oxidative stress in diet-induced diabetic vervet monkeys [171]. Aspalathin was also demonstrated to reduce oxidative stress in H9c2 cells and protect against high glucose-induced cell apoptosis [142]. These findings were confirmed in diabetic db/db mice whereby the diabetes-induced oxidative stress was improved by Aspalathin via the downregulation of NRF2, a major regulator of cellular antioxidation [143].

1.16 The effect of *Aspalathus linearis* and its bioactive compounds on CVD

Research by Marnewick et al (2016), showed that the consumption of six cups of fermented rooibos tea a day, for 6 weeks improved the CVD risk profile. The consumption of rooibos tea improved lipid profiles of participants who consumed the tea, causing a reduction in total cholesterol, triglycerides and LDL-cholesterol levels and increasing HDL-cholesterol when compared to the control group [164]. Although research has shown that rooibos or its bioactive compounds can reduce CVD risk factors, studies have also directly investigated its effect on reducing cardiac damage or CVD development. Johnson et al. (2016) showed that Aspalathin was able to decrease ROS formation and caspase 3/7 activity, whilst increasing SOD in a H9c2 cardiomyocyte model treated with 33 mM glucose [142]. Dludla et al. (2017) confirmed this and reported that Aspalathin protects the diabetic heart against glucose-induced oxidative stress and cell damage [172]. Smit et al. (2018), demonstrated that Aspalathin improved glucose uptake of the heart muscle in young and mature obese insulin-resistant rats [173].

1.17 Conclusions

This review presents evidence that, under conditions of stress, increased inflammation activates NFκB, stimulating LOXL2 expression, as well as other factors like TGF-β, COL1A and CTGF, which in turn, lead to elevated collagen deposition and cross-linking, culminating in increased fibrosis. There is, however, a paucity of available literature, thus hindering efforts to fully elucidate not only the exact mechanisms by which LOXL2 signalling occurs in fibrosis, but also the role that epigenetics plays in LOXL2 and cardiovascular disease progression. There is a definite need for further investigating the effects of epigenetics in LOXL2 expression,

which could greatly aid in identifying a means to control and manipulate LOXL2, particularly in humans, thereby developing novel therapeutics to combat this worldwide CVD problem.

Taken together, to the best of our knowledge, no study has investigated the role of AfriplexGRT™ in mitigating enhanced LOXL2 expression induced by an obesogenic diet. Therefore, this study aimed to determine the role that LOXL2 and its downstream effectors play in diet-induced cardiac insults, and to evaluate the therapeutic potential of AfriplexGRT™ in reversing diet-induced stressors (Figure 1.5).

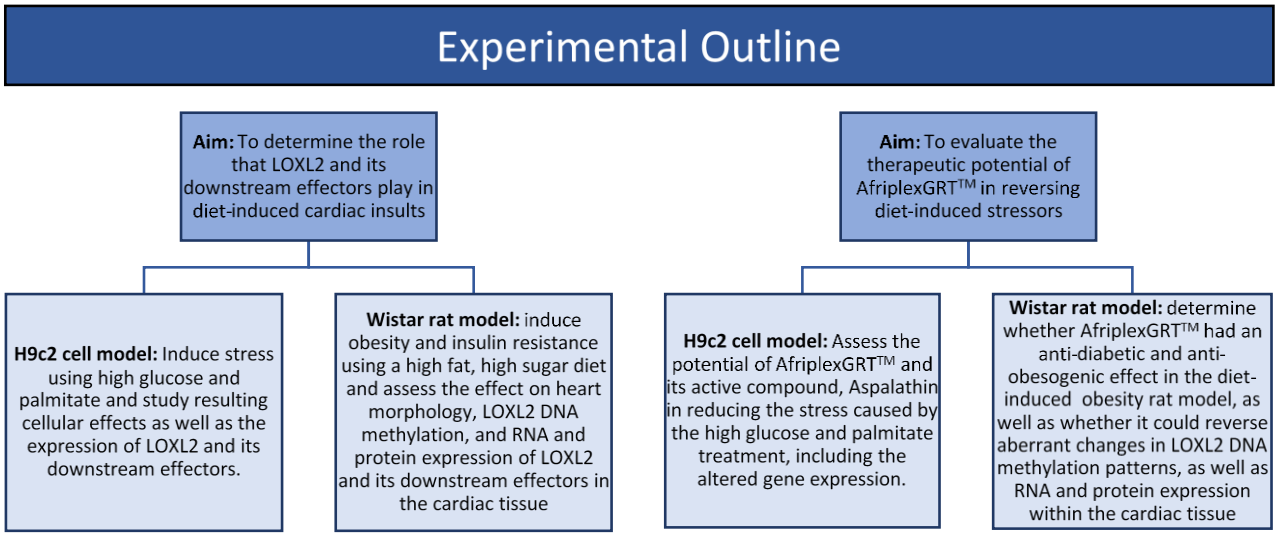

Figure 1.5: Figure outlining methods to achieve aims. An H9c2 cell model and 2 Wistar rat, diet induced obesity models were used to determine the role of LOXL2 and its downstream effectors on diet-induced cardiac insult and evaluate the therapeutic potential of AfriplexGRT™ in reversing these diet-induced stressors.

Of interest in this study was the effect of high fat and glucose exposure on cardiac fibrosis and whether AfriplexGRT™, a polyphenol-rich extract, could mitigate these effects. To this end, firstly, an *in vitro* H9c2 cell model of diabetes and obesity was used where cells were HG+PAL for 24 hours, followed by further 6-hour treatment with AfriplexGRT™, or its bioactive compound Aspalathin. The effect of stress induction and changes in gene expression were investigated in the cell culture model. To study these effects in an *in vivo* model of diet-induced fibrosis, Wistar rats were fed different obesogenic diets, including a high-fat, high-

sugar (HFHS) diet, and obesogenic 1 (OB1) diet, or an obesogenic 2 diet (OB2), over a set period with or without supplementation with AfriplexGRT™. The effects of the different diets and treatments were investigated by studying the animal's food intake, blood glucoses, serum lipids, triglycerides, insulin levels as well as serum LOXL2 levels. Heart tissue was collected for DNA methylation profile (HFHS diet only), mRNA, and protein expression analysis. To our knowledge, this was the first study investigating the role AfriplexGRT™ plays in modulating LOXL2 expression in both male and female Wistar rats.

1.18 References

1. World Health Statistics (WHO). Monitoring health for the SDGs; *WHO:* Geneva, Switzerland, **2019**.

2. World Health Statistics (WHO). New initiative launched to tackle cardiovascular disease, the world's number one killer; *WHO:* Geneva, Switzerland, **2016**.

3. World Health Statistics (WHO). Global Hearts Initiative, working together to promote cardiovascular health. *WHO:* Geneva, Switzerland, **2018**.

4. World Health Statistics (WHO). Obesity and overweight fact sheet Available online: https://www.who.int/news-room/fact-sheets/detail/obesity-and-overweight (accessed on Nov 12, 2018).

5. International Diabetes Federation (IDF). IDF Diabetes Atlas, 9th ed.; *IDF*: Brussels, Belgium, **2019**.

6. World Health Statistics (WHO). Cardiovascular diseases (CVDs) fact sheet Available online: https://www.who.int/news-room/fact-sheets/detail/cardiovascular-diseases-(cvds) (accessed on Sep 12, 2019).

7. CDC. Heart Failure Fact Sheet. Available online: https://www.cdc.gov/dhdsp/data_statistics/fact_sheets/fs_heart_failure.htm (accessed on Jul 13, 2019).

8. Steven, S.; Frenis, K.; Oelze, M.; Kalinovic, S.; Kuntic, M.; Bayo Jimenez, M.T.; Vujacic-Mirski, K.; Helmstädter, J.; Kröller-Schön, S.; Münzel, T.; et al. Vascular Inflammation and Oxidative Stress: Major Triggers for Cardiovascular Disease. *Oxid. Med. Cell. Longev.* **2019**, *2019*, 7092151, doi:10.1155/2019/7092151.

9. López, B.; Querejeta, R.; González, A.; Beaumont, J.; Larman, M.; Díez, J. Impact of treatment on myocardial lysyl oxidase expression and collagen cross-linking in patients with heart failure. *Hypertens.* **2009**, *53*, 236–42, doi:10.1161/HYPERTENSIONAHA.108.125278.

10. Segura, A.M.; Frazier, O.H.; Buja, L.M. Fibrosis and heart failure. *Heart Fail. Rev.* **2014**, *19*, 173–185,

doi:10.1007/s10741-012-9365-4.

11. Miner, E.C.; Miller, W.L. A Look Between the Cardiomyocytes: The Extracellular Matrix in Heart Failure. *Mayo Clin. Proc.* **2006**, *81*, 71–76, doi:10.4065/81.1.71.

12. Schaper, J.; Froede, R.; Hein, S.; Buck, A.; Hashizume, H.; Speiser, B.; Friedl, A.; Bleese, N. Impairment of the myocardial ultrastructure and changes of the cytoskeleton in dilated cardiomyopathy. *Circulation* **1991**, *83*, 504–14, doi:10.1161/01.cir.83.2.504.

13. Frangogiannis, N.G. The extracellular matrix in ischemic and nonischemic heart failure. *Circ. Res.* 2019, *125*, 117–146.

14. Kasner, M.; Westermann, D.; Lopez, B.; Gaub, R.; Escher, F.; Kühl, U.; Schultheiss, H.-P.; Tschöpe, C. Diastolic Tissue Doppler Indexes Correlate With the Degree of Collagen Expression and Cross-Linking in Heart Failure and Normal Ejection Fraction. *J. Am. Coll. Cardiol.* **2011**, *57*, 977–985, doi:10.1016/j.jacc.2010.10.024.

15. Lodish, H.; Berk, A.; Zipursky, S.L.; Matsudaira, P.; Baltimore, D.; Darnell, J. Molecular Cell Biology. 4th edition. Section 22.3, Collagen: The Fibrous Proteins of the Matrix. W. H. Freeman, **2000**.

16. Henriksen, K.; Karsdal, M.A. Type I Collagen. In *Biochemistry of Collagens, Laminins and Elastin: Structure, Function and Biomarkers*; Elsevier Inc., **2016**; pp. 1–11 ISBN 9780128098998.

17. Gao, L.; Orth, P.; Cucchiarini, M.; Madry, H. Effects of solid acellular type-I/III collagen biomaterials on in vitro and in vivo chondrogenesis of mesenchymal stem cells. *Expert Rev. Med. Devices* **2017**, *14*, 717–732.

18. Karsenty, G.; Park, R.W. Regulation of type I collagen genes expression. *Int. Rev. Immunol.* **1995**, *12*, 177–185, doi:10.3109/08830189509056711.

19. Yamauchi, M.; Sricholpech, M. Lysine post-translational modifications of collagen. *Essays Biochem.* **2012**, *52*, 113–33, doi:10.1042/bse0520113.

20. Nishioka, T.; Eustace, A.; West, C. Lysyl oxidase: From basic science to future cancer treatment. *Cell*

Struct. Funct. 2012, *37*, 75–80.

21. Cano, A.; Santamaría, P.G.; Moreno-Bueno, G. LOXL2 in epithelial cell plasticity and tumor progression. *Futur. Oncol.* **2012**, *8*, 1095–1108.

22. Rodríguez, C.; Martínez-González, J. The Role of Lysyl Oxidase Enzymes in Cardiac Function and Remodeling. *Cells* **2019**, *8*, 1483, doi:10.3390/cells8121483.

23. Al-u'datt, D.; Allen, B.G.; Nattel, S. Role of the lysyl oxidase enzyme family in cardiac function and disease. *Cardiovasc. Res.* **2019**, *115*, 1820–1837, doi:10.1093/cvr/cvz176.

24. Yang, J.; Savvatis, K.; Kang, J.S.; Fan, P.; Zhong, H.; Schwartz, K.; Barry, V.; Mikels-Vigdal, A.; Karpinski, S.; Kornyeyev, D.; et al. Targeting LOXL2 for cardiac interstitial fibrosis and heart failure treatment. *Nat. Commun.* **2016**, *7*, 13710, doi:10.1038/ncomms13710.

25. Zhao, Y.; Tang, K.; Tianbao, X.; Wang, J.; Yang, J.; Li, D. Increased serum lysyl oxidase-like 2 levels correlate with the degree of left atrial fibrosis in patients with atrial fibrillation. *Biosci. Rep.* **2017**, *37*, doi:10.1042/BSR20171332.

26. Trackman, P.C. Enzymatic and non-enzymatic functions of the lysyl oxidase family in bone. *Matrix Biol.* **2016**, *52–54*, 7–18, doi:10.1016/j.matbio.2016.01.001.

27. González, A.; López, B.; Ravassa, S.; San José, G.; Díez, J. The complex dynamics of myocardial interstitial fibrosis in heart failure. Focus on collagen cross-linking. *Biochim. Biophys. Acta - Mol. Cell Res.* **2019**, *1866*, 1421–1432, doi:10.1016/J.BBAMCR.2019.06.001.

28. Fong, S.F.T.; Dietzsch, E.; Fong, K.S.K.; Hollosi, P.; Asuncion, L.; He, Q.; Parker, M.I.; Csiszar, K. Lysyl oxidase-like 2 expression is increased in colon and esophageal tumors and associated with less differentiated colon tumors. *Genes, Chromosom. Cancer* **2007**, *46*, 644–655, doi:10.1002/gcc.20444.

29. Saxton, A.; Bordoni, B. *Anatomy, Thorax, Cardiac Muscle*; StatPearls Publishing, 2019;

30. Fabiato, A. Calcium-induced release of calcium from the cardiac sarcoplasmic reticulum. *Am. J. Physiol. Physiol.* **1983**, *245*, C1–C14, doi:10.1152/ajpcell.1983.245.1.C1.

31. Cheng, H.; Lederer, W.; Cannell, M. Calcium sparks: elementary events underlying excitation-contraction coupling in heart muscle. *Science (80).* **1993**, *262*, 740–744, doi:10.1126/science.8235594.

32. Marks, A.R. Calcium and the heart: a question of life and death. *J. Clin. Invest.* **2003**, *111*, 597–600, doi:10.1172/JCI18067.

33. Robinson, T.F.; Factor, S.M.; Sonnenblick, E.H. The Heart as a Suction Pump. *Sci. Am.* **1986**, *254*, 84–91, doi:10.1038/scientificamerican0686-84.

34. Frantz, C.; Stewart, K.M.; Weaver, V.M. The extracellular matrix at a glance. *J. Cell Sci.* **2010**, *123*, 4195–200, doi:10.1242/jcs.023820.

35. Xue, M.; Jackson, C.J. Extracellular Matrix Reorganization During Wound Healing and Its Impact on Abnormal Scarring. *Adv. Wound Care* **2015**, *4*, 119–136, doi:10.1089/wound.2013.0485.

36. Deshmukh, S.; Dive, A.; Moharil, R.; Munde, P. Enigmatic insight into collagen. *J. Oral Maxillofac. Pathol.* **2016**, *20*, 276, doi:10.4103/0973-029X.185932.

37. Eckes, B.; Nischt, R.; Krieg, T. Cell-matrix interactions in dermal repair and scarring. *Fibrogenesis Tissue Repair* **2010**, *3*, 4, doi:10.1186/1755-1536-3-4.

38. Wynn, T.A.; Ramalingam, T.R. Mechanisms of fibrosis: therapeutic translation for fibrotic disease. *Nat. Med.* **2012**, *18*, 1028–1040, doi:10.1038/nm.2807.

39. Campana, L.; Iredale, J.P. Extracellular Matrix Metabolism and Fibrotic Disease. *Curr. Pathobiol. Rep.* **2014**, *2*, 217–224, doi:10.1007/s40139-014-0058-7.

40. Querejeta, R.; López, B.; González, A.; Sánchez, E.; Larman, M.; Martínez Ubago, J.L.; Díez, J. Increased collagen type I synthesis in patients with heart failure of hypertensive origin: Relation to myocardial fibrosis. *Circulation* **2004**, *110*, 1263–1268, doi:10.1161/01.CIR.0000140973.60992.9A.

41. Martos, R.; Baugh, J.; Ledwidge, M.; O'Loughlin, C.; Conlon, C.; Patle, A.; Donnelly, S.C.; McDonald, K. Diastolic heart failure: Evidence of increased myocardial collagen turnover linked to diastolic dysfunction. *Circulation* **2007**, *115*, 888–895, doi:10.1161/CIRCULATIONAHA.106.638569.

42. Horn, M.A.; Trafford, A.W. Aging and the cardiac collagen matrix: Novel mediators of fibrotic remodelling. *J. Mol. Cell. Cardiol.* **2016**, *93*, 175–185.

43. Zhong, J.; Agha, G.; Baccarelli, A.A. The Role of DNA Methylation in Cardiovascular Risk and Disease. *Circ. Res.* **2016**, *118*, 119–131, doi:10.1161/CIRCRESAHA.115.305206.

44. Zibadi, S.; Vazquez, R.; Larson, D.F.; Watson, R.R. T Lymphocyte Regulation of Lysyl Oxidase in Diet-Induced Cardiac Fibrosis. *Cardiovasc. Toxicol.* **2010**, *10*, 190–198, doi:10.1007/s12012-010-9078-7.

45. Lucero, H.A.; Kagan, H.M. Lysyl oxidase: An oxidative enzyme and effector of cell function. *Cell. Mol. Life Sci.* **2006**, *63*, 2304–2316.

46. Moon, H.-J.; Finney, J.; Ronnebaum, T.; Mure, M. Human lysyl oxidase-like 2. *Bioorg. Chem.* **2014**, *57*, 231–41, doi:10.1016/j.bioorg.2014.07.003.

47. Xu, X.-H.; Jia, Y.; Zhou, X.; Xie, D.; Huang, X.; Jia, L.; Zhou, Q.; Zheng, Q.; Zhou, X.; Wang, K.; et al. Downregulation of lysyl oxidase and lysyl oxidase-like protein 2 suppressed the migration and invasion of trophoblasts by activating the TGF-β/collagen pathway in preeclampsia. *Exp. Mol. Med.* **2019**, *51*, 20, doi:10.1038/s12276-019-0211-9.

48. Davidson, J.M.; Zoia, O.; Liu, J.-M. Modulation of transforming growth factor-beta 1 stimulated elastin and collagen production and proliferation in porcine vascular smooth muscle cells and skin fibroblasts by basic fibroblast growth factor, transforming growth factor-α, and insulin-like growth factor-I. *J. Cell. Physiol.* **1993**, *155*, 149–156, doi:10.1002/jcp.1041550119.

49. Rodriguez, C.; Martinez-Gonzalez, J.; Raposo, B.; Alcudia, J.F.; Guadall, A.; Badimon, L. Regulation of lysyl oxidase in vascular cells: lysyl oxidase as a new player in cardiovascular diseases. *Cardiovasc. Res.* **2008**, *79*, 7–13, doi:10.1093/cvr/cvn102.

50. Wu, L.; Zhu, Y. The function and mechanisms of action of LOXL2 in cancer (Review). *Int. J. Mol. Med.* **2015**, *36*, 1200–1204, doi:10.3892/ijmm.2015.2337.

51. Molnar, J.; Fong, K.S.K.; He, Q.P.; Hayashi, K.; Kim, Y.; Fong, S.F.T.; Fogelgren, B.; Szauter, K.M.; Mink,

M.; Csiszar, K. Structural and functional diversity of lysyl oxidase and the LOX-like proteins. *Biochim. Biophys. Acta* **2003**, *1647*, 220–4, doi:10.1016/s1570-9639(03)00053-0.

52. Trackman, P.C. Functional importance of lysyl oxidase family propeptide regions. *J. Cell Commun. Signal.* **2018**, *12*, 45–53, doi:10.1007/s12079-017-0424-4.

53. Khosravi, R.; Sodek, K.L.; Xu, W.-P.; Bais, M. V.; Saxena, D.; Faibish, M.; Trackman, P.C. A Novel Function for Lysyl Oxidase in Pluripotent Mesenchymal Cell Proliferation and Relevance to Inflammation-Associated Osteopenia. *PLoS One* **2014**, *9*, e100669, doi:10.1371/journal.pone.0100669.

54. Liguori, T.T.A.; Liguori, G.R.; Moreira, L.F.P.; Harmsen, M.C. Fibroblast growth factor-2, but not the adipose tissue-derived stromal cells secretome, inhibits TGF-β1-induced differentiation of human cardiac fibroblasts into myofibroblasts. *Sci. Rep.* **2018**, *8*, 1–10, doi:10.1038/s41598-018-34747-3.

55. Itoh, N.; Ohta, H. Pathophysiological roles of FGF signaling in the heart. *Front. Physiol.* **2013**, *4,* 247. doi.org/10.3389/fphys.13.00247.

56. Liu, X.; Zhao, Y.; Gao, J.; Pawlyk, B.; Starcher, B.; Spencer, J.A.; Yanagisawa, H.; Zuo, J.; Li, T. Elastic fiber homeostasis requires lysyl oxidase–like 1 protein. *Nat. Genet.* **2004**, *36*, 178–182, doi:10.1038/ng1297.

57. Ohmura, H.; Yasukawa, H.; Minami, T.; Sugi, Y.; Oba, T.; Nagata, T.; Kyogoku, S.; Ohshima, H.; Aoki, H.; Imaizumi, T. Cardiomyocyte-specific transgenic expression of lysyl oxidase-like protein-1 induces cardiac hypertrophy in mice. *Hypertens. Res.* **2012**, *35*, 1063–1068, doi:10.1038/hr.2012.92.

58. Busnadiego, O.; Gonzalez-Santamaria, J.; Lagares, D.; Guinea-Viniegra, J.; Pichol-Thievend, C.; Muller, L.; Rodriguez-Pascual, F. LOXL4 Is Induced by Transforming Growth Factor 1 through Smad and JunB/Fra2 and Contributes to Vascular Matrix Remodeling. *Mol. Cell. Biol.* **2013**, *33*, 2388–2401, doi:10.1128/mcb.00036-13.

59. Alzahrani, F.; Al Hazzaa, S.A.; Tayeb, H.; Alkuraya, F.S. LOXL3, encoding lysyl oxidase-like 3, is mutated in a family with autosomal recessive Stickler syndrome. *Hum. Genet.* **2015**, *134*, 451–453,

doi:10.1007/s00439-015-1531-z.

60. Zhang, J.; Yang, R.; Liu, Z.; Hou, C.; Zong, W.; Zhang, A.; Sun, X.; Gao, J. Loss of lysyl oxidase-like 3 causes cleft palate and spinal deformity in mice. *Hum. Mol. Genet.* **2015**, *24*, 6174–85, doi:10.1093/hmg/ddv333.

61. Bignon, M.; Pichol-Thievend, C.; Hardouin, J.; Malbouyres, M.; Brechot, N.; Nasciutti, L.; Barret, A.; Teillon, J.; Guillon, E.; Etienne, E.; et al. Lysyl oxidase-like protein-2 regulates sprouting angiogenesis and type IV collagen assembly in the endothelial basement membrane. *Blood* **2011**, *118*, 3979–3989, doi:10.1182/blood-2010-10-313296.

62. Martin, A.; Salvador, F.; Moreno-Bueno, G.; Floristán, A.; Ruiz-Herguido, C.; Cuevas, E.P.; Morales, S.; Santos, V.; Csiszar, K.; Dubus, P.; et al. Lysyl oxidase-like 2 represses Notch1 expression in the skin to promote squamous cell carcinoma progression. *EMBO J.* **2015**, *34*, 1090–1109, doi:10.15252/embj.201489975.

63. Barry-Hamilton, V.; Spangler, R.; Marshall, D.; McCauley, S.; Rodriguez, H.M.; Oyasu, M.; Mikels, A.; Vaysberg, M.; Ghermazien, H.; Wai, C.; et al. Allosteric inhibition of lysyl oxidase–like-2 impedes the development of a pathologic microenvironment. *Nat. Med.* **2010**, *16*, 1009–1017, doi:10.1038/nm.2208.

64. Rockey, D.C.; Bell, P.D.; Hill, J.A. Fibrosis — A Common Pathway to Organ Injury and Failure. *N. Engl. J. Med.* **2015**, *373*, 95–96, doi:10.1056/NEJMc1504848.

65. Johnson, R.; Nxele, X.; Cour, M.; Sangweni, N.; Jooste, T.; Hadebe, N.; Samodien, E.; Benjeddou, M.; Mazino, M.; Louw, J.; et al. Identification of potential biomarkers for predicting the early onset of diabetic cardiomyopathy in a mouse model. *Sci. Rep.* **2020**, *10*, 12352, doi:10.1038/s41598-020-69254-x.

66. Puente, A.; Fortea, J.I.; Cabezas, J.; Arias Loste, M.T.; Iruzubieta, P.; Llerena, S.; Huelin, P.; Fábrega, E.; Crespo, J. LOXL2 - A New Target in Antifibrogenic Therapy? *Int. J. Mol. Sci.* **2019**, *20*, doi:10.3390/ijms20071634.

67. Lytle, K.A.; Wong, C.P.; Jump, D.B. Docosahexaenoic acid blocks progression of western diet-induced nonalcoholic steatohepatitis in obese Ldlr-/- mice. *PLoS One* **2017**, *12*, e0173376, doi:10.1371/journal.pone.0173376.

68. Wright, E.; Scism-Bacon, J.L.; Glass, L.C.; Glass, L. Oxidative stress in type 2 diabetes: the role of fasting and postprandial glycaemia. *Int. J. Clin. Pract.* **2006**, *60*, 308–14, doi:10.1111/j.1368-5031.2006.00825.x.

69. Brownlee, M.D, M. Advanced Protein Glycosylation in Diabetes and Aging. *Annu. Rev. Med.* **1995**, *46*, 223–234, doi:10.1146/annurev.med.46.1.223.

70. Kislinger, T.; Tanji, N.; Wendt, T.; Qu, W.; Lu, Y.; Ferran, L.J.; Taguchi, A.; Olson, K.; Bucciarelli, L.; Goova, M.; et al. Receptor for advanced glycation end products mediates inflammation and enhanced expression of tissue factor in vasculature of diabetic apolipoprotein E-null mice. *Arterioscler. Thromb. Vasc. Biol.* **2001**, *21*, 905–10, doi:10.1161/01.atv.21.6.905.

71. Candido, R.; Forbes, J.M.; Thomas, M.C.; Thallas, V.; Dean, R.G.; Burns, W.C.; Tikellis, C.; Ritchie, R.H.; Twigg, S.M.; Cooper, M.E.; et al. A Breaker of Advanced Glycation End Products Attenuates Diabetes-Induced Myocardial Structural Changes. *Circ. Res.* **2003**, *92*, 785–792, doi:10.1161/01.RES.0000065620.39919.20.

72. Brownlee, M. Biochemistry and molecular cell biology of diabetic complications. *Nature* **2001**, *414*, 813–820, doi:10.1038/414813a.

73. Aronson, D. Cross-linking of glycated collagen in the pathogenesis of arterial and myocardial stiffening of aging and diabetes. *J. Hypertens.* **2003**, *21*, 3–12, doi:10.1097/00004872-200301000-00002.

74. Raghu, G.; Brown, K.K.; Collard, H.R.; Cottin, V.; Gibson, K.F.; Kaner, R.J.; Lederer, D.J.; Martinez, F.J.; Noble, P.W.; Song, J.W.; et al. Efficacy of simtuzumab versus placebo in patients with idiopathic pulmonary fibrosis: a randomised, double-blind, controlled, phase 2 trial. *Lancet Respir. Med.* **2017**, *5*, 22–32, doi:10.1016/S2213-2600(16)30421-0.

75. Mižíková, I.; Palumbo, F.; Tábi, T.; Herold, S.; Vadász, I.; Mayer, K.; Seeger, W.; Morty, R.E.

Perturbations to lysyl oxidase expression broadly influence the transcriptome of lung fibroblasts. *Physiol. Genomics* **2017**, *49*, 416–429, doi:10.1152/physiolgenomics.00026.2017.

76. Craighead, D.H.; Wang, H.; Santhanam, L.; Alexander, L.M. Acute lysyl oxidase inhibition alters microvascular function in normotensive but not hypertensive men and women. *Am. J. Physiol. Heart Circ. Physiol.* **2018**, *314*, H424–H433, doi:10.1152/ajpheart.00521.2017.

77. Steppan, J.; Wang, H.; Bergman, Y.; Rauer, M.J.; Tan, S.; Jandu, S.; Nandakumar, K.; Barreto-Ortiz, S.; Cole, R.N.; Boronina, T.N.; et al. Lysyl oxidase-like 2 depletion is protective in age-associated vascular stiffening. *Am. J. Physiol. Circ. Physiol.* **2019**, *317*, H49–H59, doi:10.1152/ajpheart.00670.2018.

78. Torregrosa-Carrión, R.; Luna-Zurita, L.; García-Marqués, F.; D'Amato, G.; Piñeiro-Sabarís, R.; Bonzón-Kulichenko, E.; Vázquez, J.; de la Pompa, J.L. NOTCH Activation Promotes Valve Formation by Regulating the Endocardial Secretome. *Mol. Cell. Proteomics* **2019**, *18*, 1782–1795, doi:10.1074/mcp.RA119.001492.

79. Schilter, H.; Findlay, A.D.; Perryman, L.; Yow, T.T.; Moses, J.; Zahoor, A.; Turner, C.I.; Deodhar, M.; Foot, J.S.; Zhou, W.; et al. The lysyl oxidase like 2/3 enzymatic inhibitor, PXS-5153A, reduces crosslinks and ameliorates fibrosis. *J. Cell. Mol. Med.* **2018**, *23*, jcmm.14074, doi:10.1111/jcmm.14074.

80. Dragomir, A.-C.D.; Sun, R.; Choi, H.; Laskin, J.D.; Laskin, D.L. Role of Galectin-3 in Classical and Alternative Macrophage Activation in the Liver following Acetaminophen Intoxication. *J. Immunol.* **2012**, *189*, 5934–5941, doi:10.4049/jimmunol.1201851.

81. Li, Y.; Komai-Koma, M.; Gilchrist, D.S.; Hsu, D.K.; Liu, F.-T.; Springall, T.; Xu, D. Galectin-3 Is a Negative Regulator of Lipopolysaccharide-Mediated Inflammation. *J. Immunol.* **2008**, *181*, 2781–2789, doi:10.4049/jimmunol.181.4.2781.

82. McCullough, P.A.; Olobatoke, A.; Vanhecke, T.E. Galectin-3: a novel blood test for the evaluation and management of patients with heart failure. *Rev. Cardiovasc. Med.* **2011**, *12*, 200–10, doi:10.3909/ricm0624.

83. De Boer, R.A.; Voors, A.A.; Muntendam, P.; van Gilst, W.H.; van Veldhuisen, D.J. Galectin-3: a novel

mediator of heart failure development and progression. *Eur. J. Heart Fail.* **2009**, *11*, 811–817, doi:10.1093/eurjhf/hfp097.

84. Pez, F.; Dayan, F.; Durivault, J.; Kaniewski, B.; Aimond, G.; Le Provost, G.S.; Deux, B.; Clézardin, P.; Sommer, P.; Pouysségur, J.; et al. The HIF-1–Inducible Lysyl Oxidase Activates HIF-1 via the Akt Pathway in a Positive Regulation Loop and Synergizes with HIF-1 in Promoting Tumor Cell Growth. *Cancer Res.* **2011**, *71*, 1647–1657, doi:10.1158/0008-5472.CAN-10-1516.

85. Semenza, G.L. HIF-1 mediates metabolic responses to intratumoral hypoxia and oncogenic mutations. *J. Clin. Invest.* **2013**, *123*, 3664–71, doi:10.1172/JCI67230.

86. Cox, T.R.; Erler, J.T. Molecular Pathways: Connecting Fibrosis and Solid Tumor Metastasis. *Clin. Cancer Res.* **2014**, *20*, 3637–3643, doi:10.1158/1078-0432.CCR-13-1059.

87. Chaudhury, A.; Howe, P.H. The tale of transforming growth factor-beta (TGFβ) signaling: a soigné enigma. *IUBMB Life* **2009**, *61*, 929–39, doi:10.1002/iub.239.

88. Lu, M.; Qin, Q.; Yao, J.; Sun, L.; Qin, X. Induction of LOX by TGF-β1/Smad/AP-1 signaling aggravates rat myocardial fibrosis and heart failure. *IUBMB Life* **2019**, iub.2112, doi:10.1002/iub.2112.

89. Eulertaimor, G.; Heger, J. The complex pattern of SMAD signaling in the cardiovascular system. *Cardiovasc. Res.* **2006**, *69*, 15–25, doi:10.1016/j.cardiores.2005.07.007.

90. Ikeuchi, M.; Tsutsui, H.; Shiomi, T.; Matsusaka, H.; Matushima, S.; Wen, J.; Kubota, T.; Takeshita, A. Inhibition of TGF-beta signaling exacerbates early cardiac dysfunction but prevents late remodeling after infarction. *Cardiovasc. Res.* **2004**, *64*, 526–535, doi:10.1016/j.cardiores.2004.07.017.

91. Hao, J.; Wang, B.; Jones, S.C.; Jassal, D.S.; Dixon, I.M.C. Interaction between angiotensin II and Smad proteins in fibroblasts in failing heart and in vitro. *Am. J. Physiol. Circ. Physiol.* **2000**, *279*, H3020–H3030, doi:10.1152/ajpheart.2000.279.6.H3020.

92. Handy, D.E.; Castro, R.; Loscalzo, J. Epigenetic Modifications. *Circulation* **2011**, *123*, 2145–2156, doi:10.1161/CIRCULATIONAHA.110.956839.

93. Chuang, J.C.; Jones, P.A. Epigenetics and microRNAs. *Pediatr. Res.* **2007**, *61*. doi: 10.1203/pdr.0b013e3180457684

94. Morales, S.; Monzo, M.; Navarro, A. Epigenetic regulation mechanisms of microRNA expression. *Biomol. Concepts* **2017**, *8*, 203–212, doi:10.1515/bmc-2017-0024.

95. NCBI - LOXL2 lysyl oxidase like 2 [Homo sapiens (human)] gene Available online: https://www.ncbi.nlm.nih.gov/gene?cmd=Retrieve&dopt=full_report&list_uids=4017 (accessed on May 16, 2019).

96. Ensembl genome browser: LOXL2 (ENSG00000134013) Gene (Homo sapiens) Available online: http://www.ensembl.org/Homo_sapiens/Gene/Summary?g=ENSG00000134013;r=8:23297189-23425328 (accessed on May 16, 2015).

97. Hollosi, P.; Yakushiji, J.K.; Fong, K.S.K.; Csiszar, K.; Fong, S.F.T. Lysyl oxidase-like 2 promotes migration in noninvasive breast cancer cells but not in normal breast epithelial cells. *Int. J. Cancer* **2009**, *125*, 318–327, doi:10.1002/ijc.24308.

98. Nishikawa, R.; Chiyomaru, T.; Enokida, H.; Inoguchi, S.; Ishihara, T.; Matsushita, R.; Goto, Y.; Fukumoto, I.; Nakagawa, M.; Seki, N. Tumour-suppressive microRNA-29s directly regulate LOXL2 expression and inhibit cancer cell migration and invasion in renal cell carcinoma. *FEBS Lett.* **2015**, *589*, 2136–2145, doi:10.1016/j.febslet.2015.06.005.

99. Martin, E.M.; Fry, R.C. Environmental Influences on the Epigenome: Exposure- Associated DNA Methylation in Human Populations. *Annu. Rev. Public Health* **2018**, *39*, 309–333, doi:10.1146/annurev-publhealth-040617-014629.

100. Łuczak, M.W.; Jagodziński, P.P. The role of DNA methylation in cancer development. *Folia Histochem. Cytobiol.* **2006**, *44*, 143–154, doi:10.5603/4561.

101. Moore, L.D.; Le, T.; Fan, G. DNA methylation and its basic function. *Neuropsychopharmacology* **2013**, *38*, 23–38, doi:10.1038/npp.2012.112.

102. Alshenibr, W.; Tashkandi, M.M.; Alsaqer, S.F.; Alkheriji, Y.; Wise, A.; Fulzele, S.; Mehra, P.; Goldring, M.B.; Gerstenfeld, L.C.; Bais, M. V Anabolic role of lysyl oxidase like-2 in cartilage of knee and temporomandibular joints with osteoarthritis. *Arthritis Res. Ther.* **2017**, *19*, 179, doi:10.1186/s13075-017-1388-8.

103. Dong, Y.; Huang, Y.; Gutin, B.; Raed, A.; Dong, Y.; Zhu, H. Associations between Global DNA Methylation and Telomere Length in Healthy Adolescents. *Sci. Rep.* **2017**, *7*, 4210, doi:10.1038/s41598-017-04493-z.

104. Medzhitov, R.; Horng, T. Transcriptional control of the inflammatory response. *Nat. Rev. Immunol.* **2009**, *9*, 692–703, doi:10.1038/nri2634.

105. Gordon, J.W.; Shaw, J.A.; Kirshenbaum, L.A. Multiple facets of NF-κB in the heart: to be or not to NF-κB. *Circ. Res.* **2011**, *108*, 1122–32, doi:10.1161/CIRCRESAHA.110.226928.

106. Nabila Kazmi; Elliott, H.R.; Burrows, K.; Tillin, T.; Hughes, A.D.; Chaturvedi, N.; Gaunt, T.R.; Relton, C.L. Associations between High Blood Pressure and DNA Methylation. *J. Clin. Epigenetics* **2018**, *4*, 16.

107. Makar, K.W.; Wilson, C.B. DNA Methylation Is a Nonredundant Repressor of the Th2 Effector Program. *J. Immunol.* **2004**, *173*, 4402–4406, doi:10.4049/jimmunol.173.7.4402.

108. Bannister, A.J.; Kouzarides, T. Regulation of chromatin by histone modifications. *Cell Res.* **2011**, *21*, 381–395, doi:10.1038/cr.2011.22.

109. Yu, L.-M.; Xu, Y. Epigenetic regulation in cardiac fibrosis. *World J. Cardiol.* **2015**, *7*, 784–91, doi:10.4330/wjc.v7.i11.784.

110. Bargagli, E.; Piccioli, C.; Rosi, E.; Torricelli, E.; Turi, L.; Piccioli, E.; Pistolesi, M.; Ferrari, K.; Voltolini, L. Pirfenidone and Nintedanib in idiopathic pulmonary fibrosis: Real-life experience in an Italian referral centre. *Pulmonology* **2019**, *25*, 149–153, doi:10.1016/j.pulmoe.2018.06.003.

111. Baer, C.; Claus, R.; Plass, C. Genome-wide epigenetic regulation of miRNAs in cancer. *Cancer Res.* **2013**, *73*, 473–477.

112. Saito, Y.; Liang, G.; Egger, G.; Friedman, J.M.; Chuang, J.C.; Coetzee, G.A.; Jones, P.A. Specific activation of microRNA-127 with downregulation of the proto-oncogene BCL6 by chromatin-modifying drugs in human cancer cells. *Cancer Cell* **2006**, *9*, 435–443, doi:10.1016/j.ccr.2006.04.020.

113. Alegría-Torres, J.A.; Baccarelli, A.; Bollati, V. Epigenetics and lifestyle. *Epigenomics* **2011**, *3*, 267–77, doi:10.2217/epi.11.22.

114. Martínez-González, M.A.; Gea, A.; Ruiz-Canela, M. The Mediterranean Diet and Cardiovascular Health: A Critical Review. *Circ. Res.* **2019**, *124*, 779–798, doi:10.1161/CIRCRESAHA.118.313348.

115. Davies, N.J.; Batehup, L.; Thomas, R. The role of diet and physical activity in breast, colorectal, and prostate cancer survivorship: A review of the literature. *Br. J. Cancer* **2011**, *105*, S52–S73, doi:10.1038/bjc.2011.423.

116. Mastorci, F.; Vassalle, C.; Chatzianagnostou, K.; Marabotti, C.; Siddiqui, K.; Eba, A.O.; Mhamed, S.A.S.; Bandopadhyay, A.; Nazzaro, M.S.; Passera, M.; et al. Undernutrition and overnutrition burden for diseases in developing countries: The role of oxidative stress biomarkers to assess disease risk and interventional strategies. *Antioxidants* **2017**, *6, 40*. doi: 10.3390/antiox6020041.

117. Mathur, P.; Pillai, R. Overnutrition: Current scenario & combat strategies. *Indian J. Med. Res.* **2019**, *149*, 695–705. doi.org/10.4103/ijmr.IJMR_1703_18

118. Gupta, D.; B. Krueger, C.; Lastra, G. Over-nutrition, Obesity and Insulin Resistance in the Development of β-Cell Dysfunction. *Curr. Diabetes Rev.* **2012**, *8*, 76–83, doi:10.2174/157339912799424564.

119. Perng, W.; Oken, E.; Dabelea, D. Developmental overnutrition and obesity and type 2 diabetes in offspring. *Diabetologia* **2019**, *62*, 1779–1788. doi: 10.1007/s00125-019-4914-1.

120. Mandavia, C.H.; Pulakat, L.; Demarco, V.; Sowers, J.R. Over-nutrition and metabolic cardiomyopathy. *Metabolism.* **2012**, *61*, 1205–1210. doi.org/10.1016/j.metabol.2012.02.013

121. Jia, G.; Aroor, A.R.; Martinez-Lemus, L.A.; Sowers, J.R. Overnutrition, mTOR signaling, and cardiovascular diseases. *Am. J. Physiol. - Regul. Integr. Comp. Physiol.* 2014, ***307***, R1198–R1206. doi:

10.1152/ajpregu.00262.2014.

122. Khan, A.; Khan, S.U.; Khan, S.; Zia-ul-islam, S.; Baber, N.K.; Khan, M. Nutritional complications and its effects on human health. *J. Food Sci. Nutr.* **2020**, *3*, 17–20, doi:10.35841/food-science.3.5.17-20.

123. Romagnolo, D.F.; Selmin, O.I. Mediterranean Diet and Prevention of Chronic Diseases. *Nutr. Today* **2017**, *52*, 208–222, doi:10.1097/NT.0000000000000228.

124. Castro-Barquero, S.; Lamuela-Raventós, R.M.; Doménech, M.; Estruch, R. Relationship between mediterranean dietary polyphenol intake and obesity. *Nutrients* 2018, *10*. doi.org/10.3390/nu10101523

125. Pernice, R.; Vitaglione, P.; Sacchi, R.; Fogliano, V. Phytochemicals in Mediterranean Diet: The Interaction between Tomato and Olive Oil Bioactive Compounds. In *Handbook of Food Products Manufacturing*; John Wiley & Sons, Inc.: Hoboken, NJ, USA, 2006; Vol. 2, pp. 55–65.

126. Pandey, K.B.; Rizvi, S.I. Plant polyphenols as dietary antioxidants in human health and disease. *Oxid. Med. Cell. Longev.* 2009, *2*, 270–278. doi.org/10.4161/oxim.2.5.9498

127. Dixon, R.A.; Pasinetti, G.M. Flavonoids and isoflavonoids: From plant biology to agriculture and neuroscience. *Plant Physiol.* **2010**, *154*, 453–457, doi:10.1104/pp.110.161430.

128. Lin, D.; Xiao, M.; Zhao, J.; Li, Z.; Xing, B.; Li, X.; Kong, M.; Li, L.; Zhang, Q.; Liu, Y.; et al. An overview of plant phenolic compounds and their importance in human nutrition and management of type 2 diabetes. *Molecules* 2016, *21*, 1374. doi.org/10.3390/molecules21101374

129. Lee, C.Y.; Nanah, C.N.; Held, R.A.; Clark, A.R.; Huynh, U.G.T.; Maraskine, M.C.; Uzarski, R.L.; McCracken, J.; Sharma, A. Effect of electron donating groups on polyphenol-based antioxidant dendrimers. *Biochimie* **2015**, *111*, 125–134, doi:10.1016/j.biochi.2015.02.001.

130. Lobo, V.; Patil, A.; Phatak, A.; Chandra, N. Free radicals, antioxidants and functional foods: Impact on human health. *Pharmacogn. Rev.* **2010**, *4*, 118–126. https://doi.org/10.4103/0973-7847.70902.

131. Brown, J.E.; Rice-Evans, C.A. Luteolin-rich artichoke extract protects low density lipoprotein from

oxidation in vitro. *Free Radic Res*. **1998**, 29:247–255. https://doi.org/10.1080/10715769800300281.

132. Krinsky, N.I. Mechanism of Action of Biological Antioxidants (43429). *Proc Soc Exp Biol Med*, **1992**, 200:248–254. https://doi.org/10.3181/00379727-200-43429.

133. Ng, M.; Fleming, T.; Robinson, M.; Thomson, B.; Graetz, N.; Margono, C.; Mullany, E.C.; Biryukov, S.; Abbafati, C.; Abera, S.F.; et al. Global, regional, and national prevalence of overweight and obesity in children and adults during 1980-2013: A systematic analysis for the Global Burden of Disease Study 2013. *Lancet* **2014**, *384*, 766–781, doi:10.1016/S0140-6736(14)60460-8.

134. Boccellino, M.; D'Angelo, S. Anti-Obesity Effects of Polyphenol Intake: Current Status and Future Possibilities. *Int. J. Mol. Sci.* **2020**, *21*, 5642, doi:10.3390/ijms21165642.

135. Aryaeian, N.; Sedehi, S.K.; Arablou, T. Polyphenols and their effects on diabetes management: A review. *Med. J. Islam. Repub. Iran* **2017**, *31*, 886–892, doi:10.14196/mjiri.31.134.

136. Scalbert, A.; Johnson, I.T.; Saltmarsh, M. Polyphenols: antioxidants and beyond. *Am. J. Clin. Nutr.* **2005**, *81*, 215S-217S, doi:10.1093/ajcn/81.1.215S.

137. Khurana, S.; Venkataraman, K.; Hollingsworth, A.; Piche, M.; Tai, T.C. Polyphenols: Benefits to the cardiovascular system in health and in aging. *Nutrients* **2013**, *5*, 3779–3827. doi.org/10.3390/nu5103779

138. Stromsnes, K.; Mas-Bargues, C.; Gambini, J.; Gimeno-Mallench, L. Protective Effects of Polyphenols Present in Mediterranean Diet on Endothelial Dysfunction. *Oxid. Med. Cell. Longev.* **2020**. doi:10.1155/2020/2097096.

139. Beverly, J.K.; Budoff, M.J. Atherosclerosis: Pathophysiology of insulin resistance, hyperglycemia, hyperlipidemia, and inflammation. *J. Diabetes* **2020**, *12*, 102–104. doi: 10.1111/1753-0407.12970.

140. Ormazabal, V.; Nair, S.; Elfeky, O.; Aguayo, C.; Salomon, C.; Zuñiga, F.A. Association between insulin resistance and the development of cardiovascular disease. *Cardiovasc. Diabetol.* **2018**, *17*, 122.

141. Petrie, J.R.; Guzik, T.J.; Touyz, R.M. Diabetes, Hypertension, and Cardiovascular Disease: Clinical

Insights and Vascular Mechanisms. *Can. J. Cardiol.* **2018**, *34*, 575–584. doi: 10.1016/j.cjca.2017.12.005.

142. Johnson, R.; Dludla, P.; Joubert, E.; February, F.; Mazibuko, S.; Ghoor, S.; Muller, C.; Louw, J. Aspalathin, a dihydrochalcone C-glucoside, protects H9c2 cardiomyocytes against high glucose induced shifts in substrate preference and apoptosis. *Mol. Nutr. Food Res.* **2016**, *60*, 922–934, doi:10.1002/mnfr.201500656.

143. Dludla, P. V.; Muller, C.J.F.; Joubert, E.; Louw, J.; Essop, M.F.; Gabuza, K.B.; Ghoor, S.; Huisamen, B.; Johnson, R. Aspalathin protects the heart against hyperglycemia-induced oxidative damage by up-regulating Nrf2 expression. *Molecules* **2017**, *22*, doi:10.3390/molecules22010129.

144. Cheng, Y.C.; Sheen, J.M.; Hu, W.L.; Hung, Y.C. Polyphenols and Oxidative Stress in Atherosclerosis-Related Ischemic Heart Disease and Stroke. *Oxid. Med. Cell. Longev.* **2017**. doi: 10.1155/2017/8526438.

145. Tangney, C.C.; Rasmussen, H.E. Polyphenols, inflammation, and cardiovascular disease. *Curr. Atheroscler. Rep.* **2013**, *15*, 324, doi:10.1007/s11883-013-0324-x.

146. Najjar, R.S.; Montgomery, B.D. A defined, plant-based diet as a potential therapeutic approach in the treatment of heart failure: A clinical case series. *Complement. Ther. Med.* **2019**, *45*, 211–214, doi:10.1016/j.ctim.2019.06.010.

147. Medawar, E.; Huhn, S.; Villringer, A.; Veronica Witte, A. The effects of plant-based diets on the body and the brain: a systematic review. *Transl. Psychiatry* **2019**, *9*, 1–17.

148. Pan, M.-H.; Lai, C.-S.; Wu, J.-C.; Ho, C.-T. Epigenetic and Disease Targets by Polyphenols. *Curr. Pharm. Des.* **2013**, *19*, 6156–6185, doi:10.2174/1381612811319340010.

149. Crescenti, A.; Solà, R.; Valls, R.M.; Caimari, A.; del Bas, J.M.; Anguera, A.; Anglés, N.; Arola, L. Cocoa Consumption Alters the Global DNA Methylation of Peripheral Leukocytes in Humans with Cardiovascular Disease Risk Factors: A Randomized Controlled Trial. *PLoS One* **2013**, *8*, e65744, doi:10.1371/journal.pone.0065744.

150. Lan, Y. Epigenetic Regulation of Cardiac Development and Disease through DNA Methylation. *JoLS, J. Life Sci.* **2019**, *1*, 1–10, doi:10.36069/jols/20190901.

151. Joubert, E.; de Beer, D. Rooibos (Aspalathus linearis) beyond the farm gate: From herbal tea to potential phytopharmaceutical. *South African J. Bot.* **2011**, *77*, 869–886, doi:10.1016/j.sajb.2011.07.004.

152. Kotzé-Hörstmann, L.M.; Sadie-Van Gijsen, H. Modulation of Glucose Metabolism by Leaf Tea Constituents: A Systematic Review of Recent Clinical and Pre-clinical Findings. *J. Agric. Food Chem.* **2020**, *68*, 2973–3005. doi: 10.1021/acs.jafc.9b07852.

153. Standley, L.; Winterton, P.; Marnewick, J.L.; Gelderblom, W.C.A.; Joubert, E.; Britz, T.J. Influence of processing stages on antimutagenic and antioxidant potentials of rooibos tea. *J. Agric. Food Chem.* **2001**, *49*, 114–117, doi:10.1021/jf000802d.

154. Bramati, L.; Aquilano, F.; Pietta, P. Unfermented Rooibos Tea: Quantitative Characterization of Flavonoids by HPLC-UV and Determination of the Total Antioxidant Activity. *J. Agric. Food Chem.* **2003**, *51*, 7472–7474, doi:10.1021/jf0347721.

155. Marnewick, J.L.; Gelderblom, W.C.A.; Joubert, E. An investigation on the antimutagenic properties of South African herbal teas. *Mutat. Res. - Genet. Toxicol. Environ. Mutagen.* **2000**, *471*, 157–166, doi:10.1016/S1383-5718(00)00128-5.

156. Muller, C.J.F.; Joubert, E.; De Beer, D.; Sanderson, M.; Malherbe, C.J.; Fey, S.J.; Louw, J. Acute assessment of an aspalathin-enriched green rooibos (Aspalathus linearis) extract with hypoglycemic potential. *Phytomedicine* **2012**, *20*, 32–39, doi:10.1016/j.phymed.2012.09.010.

157. Mazibuko, S.E.; Muller, C.J.F.; Joubert, E.; De Beer, D.; Johnson, R.; Opoku, A.R.; Louw, J. Amelioration of palmitate-induced insulin resistance in C2C12 muscle cells by rooibos (Aspalathus linearis). *Phytomedicine* **2013**, *20*, 813–819, doi:10.1016/j.phymed.2013.03.018.

158. Mazibuko, S.E.; Joubert, E.; Johnson, R.; Louw, J.; Opoku, A.R.; Muller, C.J.F. Aspalathin improves glucose and lipid metabolism in 3T3-L1 adipocytes exposed to palmitate. *Mol. Nutr. Food Res.* **2015**,

59, 2199–2208, doi:10.1002/mnfr.201500258.

159. Son, M.J.; Minakawa, M.; Miura, Y.; Yagasaki, K. Aspalathin improves hyperglycemia and glucose intolerance in obese diabetic ob/ob mice. *Eur. J. Nutr.* **2013**, *52*, 1607–1619, doi:10.1007/s00394-012-0466-6.

160. Najafian, M.; Najafian, B.; Najafian, Z. The Effect of Aspalathin on Levels of Sugar and Lipids in Streptozotocin-Induced Diabetic and Normal Rats. *Zahedan J. Res. Med. Sci.* **2016**, *In Press*, doi:10.17795/zjrms-4963.

161. Sanderson, M.; Mazibuko, S.E.; Joubert, E.; De Beer, D.; Johnson, R.; Pheiffer, C.; Louw, J.; Muller, C.J.F. Effects of fermented rooibos (Aspalathus linearis) on adipocyte differentiation. *Phytomedicine* **2014**, *21*, 109–117, doi:10.1016/j.phymed.2013.08.011.

162. Layman, J.I.; Pereira, D.L.; Chellan, N.; Huisamen, B.; Kotzé, S.H. A histomorphometric study on the hepatoprotective effects of a green rooibos extract in a diet-induced obese rat model. *Acta Histochem.* **2019**, *121*, 646–656, doi:10.1016/j.acthis.2019.05.008.

163. Joubert, E.; Louw, J.; Fey, S.J.; Larsen, P.M. An anti-diabetic extract of rooibos **2008**.

164. Marnewick, J.L.; Rautenbach, F.; Venter, I.; Neethling, H.; Blackhurst, D.M.; Wolmarans, P.; MacHaria, M. Effects of rooibos (Aspalathus linearis) on oxidative stress and biochemical parameters in adults at risk for cardiovascular disease. *J. Ethnopharmacol.* **2011**, *133*, 46–52, doi:10.1016/j.jep.2010.08.061.

165. Kawano, A.; Nakamura, H.; Hata, S. ichi; Minakawa, M.; Miura, Y.; Yagasaki, K. Hypoglycemic effect of aspalathin, a rooibos tea component from Aspalathus linearis, in type 2 diabetic model db/db mice. *Phytomedicine* **2009**, *16*, 437–443, doi:10.1016/j.phymed.2008.11.009.

166. Kamakura, R.; Son, M.J.; de Beer, D.; Joubert, E.; Miura, Y.; Yagasaki, K. Antidiabetic effect of green rooibos (Aspalathus linearis) extract in cultured cells and type 2 diabetic model KK-Ay mice. *Cytotechnology* **2015**, *67*, 699–710, doi:10.1007/s10616-014-9816-y.

167. Mikami, N.; Tsujimura, J.; Sato, A.; Narasada, A.; Shigeta, M.; Kato, M.; Hata, S.; Hitomi, E. Green

rooibos extract from Aspalathus linearis, and its component, aspalathin, suppress elevation of blood glucose levels in mice and inhibit α-amylase and α-glucosidase activities in vitro. *Food Sci. Technol. Res.* **2015**, *21*, 231–240, doi:10.3136/fstr.21.231.

168. Pashkow, F.J. Oxidative Stress and Inflammation in Heart Disease: Do Antioxidants Have a Role in Treatment and/or Prevention? *Int. J. Inflam.* **2011**, *2011*, 1–9, doi:10.4061/2011/514623.

169. Smith, C.; Swart, A.C. Rooibos (Aspalathus linearis) facilitates an anti-inflammatory state, modulating IL-6 and IL-10 while not inhibiting the acute glucocorticoid response to a mild novel stressor in vivo. *J. Funct. Foods* **2016**, *27*, 42–54, doi:10.1016/j.jff.2016.08.055.

170. Baba, H.; Ohtsuka, Y.; Haruna, H.; Lee, T.; Nagata, S.; Maeda, M.; Yamashiro, Y.; Shimizu, T. Studies of anti-inflammatory effects of Rooibos tea in rats. *Pediatr. Int.* **2009**, *51*, 700–704, doi:10.1111/j.1442-200X.2009.02835.x.

171. Orlando, P.; Chellan, N.; Louw, J.; Tiano, L.; Cirilli, I.; Dludla, P.; Joubert, E.; Muller, C.J.F. Aspalathin-rich green rooibos extract lowers LDL-cholesterol and oxidative status in high-fat diet-induced diabetic vervet monkeys. *Molecules* **2019**, *24*, 1713, doi:10.3390/molecules24091713.

172. Dludla, P. V.; Muller, C.J.F.; Joubert, E.; Louw, J.; Essop, M.F.; Gabuza, K.B.; Ghoor, S.; Huisamen, B.; Johnson, R. Aspalathin protects the heart against hyperglycemia-induced oxidative damage by up-regulating Nrf2 expression. *Molecules* **2017**, *22*, doi:10.3390/molecules22010129.

173. Smit, S.E.; Johnson, R.; Van Vuuren, M.A.; Huisamen, B. Myocardial Glucose Clearance by Aspalathin Treatment in Young, Mature, and Obese Insulin-Resistant Rats. *Planta Med.* **2018**, *84*, 75–82, doi:10.1055/s-0043-117415.

Chapter 2:

An in vitro investigation of LOXL2 as a candidate for cardiovascular dysfunction using H9c2 cardiomyoblasts

2.1. Introduction

Cardiovascular disease (CVD) is the number one killer worldwide [1], with obesity and type 2 diabetes being some of the main contributors to the development and progression of this non-communicable disease [2]. Diabetes, often occurring in conjunction with an obesogenic state, causes an increase in reactive oxygen species (ROS), which plays a key role in the induction and progression of inflammatory diseases [3]. ROS in turn changes the energy metabolism of the cell and can lead to mitochondrial depolarization which ultimately leads to severe cellular damage or apoptosis. Each of these changes is an indicator of metabolic perturbations and disease progression within the heart.

In addition, fibrosis of the myocardium is one of the major contributors to mortality in CVDs [4]. Fibrosis occurs as the thickening of the heart's septum and ventricular walls, resulting in suboptimal contraction of the muscle fibers, thereby resulting in a reduced ejection fraction [5]. Lysyl oxidase-like 2 (LOXL2) has been implicated in fibrotic diseases, including cardiovascular disease, where upregulated expression of LOXL2 results in an increase in collagen deposition and crosslinking, leading to the accumulation of fibrotic tissue [6]. Although the mechanisms related to LOXL2 signaling are not fully elucidated, it is thought that stressors, such as hyperglycemia, lead to inflammation, which induce LOXL2 upregulation. This in turn activates the TGFβ-induced change of fibroblasts to myofibroblasts through the PI3K/AKT/mTOR pathway [6]. Myofibroblasts produce increased levels of α-smooth muscle actin and collagen, which can induce fibrosis [7].

Diet and nutrition play a critical role in the development or treatment of many ailments because of its effect on the microenvironment and therefore, epigenetics [8]. The regulation of *LOXL2* expression has previously been shown to be regulated by epigenetic modifications, more specifically, DNA methylation [9]. It has also previously been shown that polyphenols are able to attenuate epigenetic changes such as changes in DNA methylation [10–12]. In this study, stress was induced in H9c2 cardiomyoblasts by exposing them to high glucose (HG) and palmitate (PAL) for 24 hours to mimic a hyperglycemic and hyperlipidemic state. The aim was to analyze the hyperglycemic- and hyperlipidemic-induced cardiac dysfunction, metabolic perturbations and disease progression in the H9c2 cell model and to determine the resulting changes in the expression of

LOXL2 and various other downstream effectors involved in the fibrotic pathway. Additionally, cardioprotective potential of polyphenol-rich extract AfriplexGRT™, and its active polyphenol, Aspalathin was also investigated.

2.2. Material and Methods

2.2.1. Reagents and Kits

H9c2 rat cardiomyoblasts were purchased from American Type Culture Collection (ATCC) (Virginia, USA, cat# CRL-1446™) while Dulbecco's Modified Eagle's Medium (DMEM) and penicillin and streptomycin (PenStrep) and the ViaLight Plus Bioassay kit was acquired from Lonza (Basel, Switzerland), fetal bovine serum OptiMEM media, DNA-free kits and cDNA synthesis reverse transcription kit acquired from ThermoFisher Scientific (Massachusetts, United States), and trypsin/EDTA was acquired from Whitehead Scientific (Cape Town, South Africa). Afriplex green rooibos tea (AfriplexGRT™) extract (Batch number BN-730330) and Aspalathin (ASP) (Batch number STZ1D-502-23B) was acquired from Afriplex (Cape Town, South Africa) while bovine serum albumin (BSA), glucose powder, sodium bicarbonate, 3-(4,5-dimethylthiazol-2-yl)−2,5-diphenyltetrazolium bromide (MTT) and dimethyl sulfoxide (DMSO), TRIzol, chloroform, ethanol and isopropanol were purchased from Sigma-Aldrich (Missouri, USA). The RT^2 fibrosis rat PCR profiler array, RT^2 First Strand Kit, RT^2 SYBR Green (ROX), and qPCR Master Mix were purchased from Qiagen (Hilden, Germany). An RC DC™ Protein Assay kit was obtained from Bio-Rad.

2.2.2. H9c2 cell maintenance

H9c2 rat cardiomyoblasts, were cultured in standard culturing medium, DMEM supplemented with 10% fetal bovine serum (FBS) and incubated at 37 °C in a humid atmosphere and 5% CO_2. Media was changed every 2-3 days and cells were split by means of trypsinization upon confluency (70-80%). Depending on the assay performed, cells were seeded into 6-, 24- or 96-well plates at a seeding density of $2x10^4$, $1x10^4$, or $0.8x10^4$, respectively.

2.2.3. H9c2 stress induction and treatment conditions

Once the cells reached a sub-confluence of 80 – 90%, the media was aspirated, and the cells were washed with warm DPBS. Initially, a dose response study was conducted to attain the most appropriate concentration

of palmitate (100 – 500 µM) to use for all subsequent experiments. Cells were then exposed to 33 mM glucose (high glucose) plus palmitate (300 µM) (HG+PAL) for 24 hours to mimic a hyperglycemic and hyperlipidemic state. The 33 mM glucose concentration was decided on, based on literature and previous work from our group [13–15]. The cells were treated with either 10 µg/mL AfriplexGRT™ or 1 µM Aspalathin for an additional 6 hours. Cells exposed to 5.5 mM glucose served as a control (CTRL) for normoglycemic conditions. All treatments were prepared in the high glucose plus palmitate media. For experiments including 5-azacytidine (AZA), either 5 µM or 20 µM AZA was added to the HG+PAL media.

2.2.4. Palmitate dose response

Since the dose of AfriplexGRT™ and Aspalathin were previously reported [13, 16], only the optimal dose of palmitate needed to be determined. H9c2 cells were seeded into black 96-well plates and treated with varying concentrations (100-500 µM) of palmitate in 33 mM glucose media for 24 hours and the mitochondrial potential measured by JC-1 staining to determine the most suitable concentration of palmitate to use for further experiments.

2.2.5. Measuring mitochondrial membrane potential with JC-1 staining

Mitochondrial membrane potential (MMP) was quantified by JC-1 staining as per the manufacturer's instructions. Briefly, H9c2 cells were seeded into black 96-well plates and treated with their relevant treatments for 24 hours. Thereafter, the media was removed, and the cells were stained with 100 µl of 8 µM 5,5',6,6'-tetrachloro-1,1',3,3-tetraethylbenzimidazolyl-carbocyanine iodide (JC-1) (Sigma-Aldrich, St Louis, USA) and incubated for 45 minutes under standard tissue culture conditions. The JC-1 dye was then removed, and the cells washed with 100 µL warm DPBS. Mitochondrial potential was quantified by measuring the fluorescence intensity of J-aggregates (indicating high MMP) and JC-1 monomers (indicating low MMP), using a BioTek® FLx 800 plate reader, and these results were normalized to total protein. The JC-1 dye accumulates in the mitochondria, where green-fluorescent emission (~529 nm) represents JC-1 monomers and red-fluorescent emission (~590 nm) represents J-aggregates within the mitochondria in a concentration dependent manner. Fluorescence imaging was performed using a Nikon inverted fluorescence microscope.

2.2.6. Determination of cell proliferation in H9c2 cells in response to HG+PAL stress and treatment

The amount of ATP produced by a cell can be directly correlated with the viability of the cell as well as the amount of proliferation, and thus the amount of ATP in cells treated with HG+PAL was measured using a ViaLight Plus Cell Proliferation and Cytotoxicity assay kit (LONZA, Basil, Switzerland), as per the manufacturer's instructions. Briefly, cells were seeded into a 96-well clear bottom, white plate, and treated as described in section 2.2.3. Thereafter, all but 60 µL of the treatment media was aspirated and 60 µL ViaLight lysis buffer added and incubated for 10 minutes at room temperature. Thereafter, 10 µL of this mixture was transferred to a new clear plate for Bradford protein determination. To the original assay plate, 100 µL ViaLight ATP reagent was added and incubated at room temperature for 2 minutes after which the luminescence was measured using a Spectramax i3 plate reader (Molecular Devices, California, USA). These values were normalized to the amount of protein in each well.

2.2.7. Bradford Protein Determination of H9c2 cells

A Bradford assay was used to determine protein concentrations compared to known controls by measuring a colorimetric change. To 10 µL of each sample and each BSA protein standard (0.125 – 2 mg/mL), 200 µL Bradford reagent was added. Samples and BSA standards with Bradford reagents were incubated at room temperature for 10 minutes and the absorbance was measured at 595nm using a Spectramax i3 plate reader (Molecular Devices, California, USA). A standard curve method was utilized to determine the concentration of protein in each well. These values were then used to normalize the ATP data.

2.2.8. Determination of ROS production in H9c2 cells in response to HG+PAL stress and treatment

Reactive oxygen species (ROS) is an indicator of cellular stress and thus ROS production was measured as an indicator of adequate stress induction by the HG+PAL treatment. ROS production was quantified using an Oxiselect™ Intracellular ROS Assay Kit (Green Fluorescence) (Cell Biolabs, San Diego, USA) as per the manufacturer's instructions. Briefly, H9c2 cells were seeded into 24-well plates and treated as described above. Thereafter, the media was aspirated, and the cells were washed with pre-warmed HBSS. The cells were stained with 20 µM 2'-7'dichlorofluorescin diacetate (DCFH-DA) prepared in DMEM without FBS. It is a fluorescent dye that measures ROS activity, specifically hydroxyl, peroxyl activity. The cells were incubated

for 30 minutes under standard tissue culture conditions and all steps were conducted in the dark as DCFH-DA is highly light sensitive. The DCFH-DA dye was aspirated and HBSS added to stop the reaction. Thereafter, the stained H9c2 cells were trypsinized for 5 minutes after which serum free pre-warmed media was added to deactivate the trypsin. The cells were then collected into 1.5 mL Eppendorf tubes and centrifuged for 5 minutes at 300 rcf, and the cell pellet re-suspended in 150 uL PBS and placed on ice. DCFH-DA relative fluorescence was assayed using the BD Accuri C6 flow cytometer (BD Biosciences, New Jersey, USA) and measured on FL1 (FITC). At least 10,000 events were used for each measurement and data are presented in relative fluorescence units (RFU). These results were normalized to the total number of cells counted.

2.2.9. Mitochondrial bioenergetics in H9c2 cells in response to high glucose stress and treatment

Seahorse XF96 extracellular flux analyzer (Seahorse Bioscience, Massachusetts, USA) was used to measure the oxygen consumption rate (OCR) and extracellular acidification rate (ECAR) of intact H9c2 cells as per the manufacturer's instructions. Briefly, H9c2 cells were seeded into XF96 cell culture microplates (Seahorse Bioscience) and once sub-confluent, stress was induced, and cells were treated as described in section 2.2.3. After the treatment period, the cells were incubated in base assay medium supplemented with 2 mM glutamine, 25 mM glucose, and 1 mM pyruvate for 60 minutes and OCR and ECAR measured using the XF Cell Mito Stress Kit (Seahorse Bioscience). Mitochondrial OCR was measured over 86 minutes. In this time, the ATP synthase inhibitor, oligomycin (1 mM), mitochondrial uncoupler, FCCP (0.75 mM), and complex I and III inhibitors, rotenone (0.5 mM) and antimycin A (0.5mM) were sequentially added to each well at specified time points.

2.2.10. Quantification of apoptosis in H9c2 cells in response to high glucose stress and treatment

Early/late apoptosis and necrosis was quantified using Annexin V-FITC (Invitrogen, California, USA) and propidium iodide (Pi) (Sigma-Aldrich, Missouri, USA) in H9c2 cells. Briefly, the cells were seeded into 24-well plates and treated as described above. Cells were trypsinized for 5 minutes under standard tissue culture conditions, the trypsin deactivated using 500 µL of DPBS supplemented with 10% FBS and the cells collected in 15 mL centrifuge tubes. The cell suspension was centrifuged at 300 rcf for 5 minutes and the supernatant removed. The cell pellet was re-suspended in 150 µL DPBS with 10% FBS and transferred to 2 mL Eppendorf

tubes. The cardiomyoblasts were then stained with 1.5 µL Annexin V and 1 µL Pi (2 µg/mL) staining solution and incubated in the dark for 10 minutes. Thereafter, cells were processed using a BD Accuri C6 flow cytometer (BD Biosciences) using the BD Accuri C6 Annexin V-FITC/PI template. The live and apoptotic state of the cells was analyzed with the BD Accuri C6 software using the FITC signal detector FL1 (ex/em = 488/530 nm) for Annexin V positive cells and FL3 detector (ex/em = 488/670 nm) for PI positive cells.

2.2.11. mRNA expression analysis

2.2.11.1.1. RNA extraction

H9c2 cells were seeded into 6-well plates and stress induced as described above. The treatment media was then aspirated, and the cells washed with pre-warmed DPBS and the plates stored at -20°C until extraction. Before extraction, the plates were removed from the freezer and allowed to equilibrate to room temperature. Qiazol (300 µL per well) was added to the plates and the cells harvested with cell scrapers and the contents of 3 wells transferred to 2 mL Eppendorf tubes containing a steel bead. Cells were homogenized for 2x 1 minute at 20Hz using a Qiagen 85210 TissueLyser (Hilden, Germany). The homogenate was centrifuged at 4ºC for 10 minutes at 15 000 rcf and the supernatant transferred to a 1.5 mL Eppendorf tube whereafter 200 µL of chloroform was added. This cell suspension was incubated for 3 minutes, shaking occasionally, after which it was centrifuged at 4ºC for 15 minutes at 15 000 rcf and the upper aqueous phase transferred to a new tube and 0.5 mL isopropanol added. The tubes were shaken to mix and then incubated overnight at -20°C. The next morning, tubes were centrifuged at 4°C for 30 minutes at 15000 rcf and the supernatant discarded. The RNA pellet was then washed twice with 1 mL 70% ethanol, centrifuging each time at 4°C for 10 minutes at 15 000 rcf and removing the supernatant. The RNA pellet was then dried on a heating block with the tubes open for 2 minutes at 60°C and the pellet resuspended in 20µL RNase-free water.

2.2.11.1.2. RNA quantification

The mRNA concentrations were then measured using a NanoDrop One system (Thermo Fisher Scientific, Massachusetts, USA), using RNase-free water as a blank and taking readings of 1 µL of each sample in duplicate. The average of each reading was used as the final concentration, and the 260/280 and 260/230 ratios were used as an indicator of RNA integrity and purity.

2.2.11.1.3. DNase treatment

DNase treatment was performed on 20 µg of RNA using an Invitrogen Ambion DNase kit (Thermo Fisher Scientific, Massachusetts, USA) as per the manufacturer's instructions. Briefly, the RNA was incubated with 5µL DNase buffer, 1 µL DNase and water (to a total volume of 49 µL) for 30 minutes at 37°C, followed by the addition of 1 µL DNase and incubation for another 30 minutes. Thereafter, 10 µL DNAse inactivation reagent was added and incubated for 5 minutes at room temperature, after which the tubes were centrifuged at 10000 rcf for 1.5 minutes and the RNA transferred to a clean tube while avoiding the precipitated inactivation reagent.

2.2.11.1.4. cDNA synthesis

Total RNA was reverse transcribed to complementary DNA (cDNA) using a High-Capacity cDNA Reverse transcription kit (Thermo Fisher Scientific, Massachusetts, USA) as per the manufacturer's instructions. Briefly, a RT-positive and RT-negative mixture was made for each sample containing a final concentration of 1 µg RNA, 2x RT buffer, 2x dNTP mix, 2x random primers, 20 U RNase inhibitor (Thermo Fisher Scientific, Massachusetts, USA), 1 µL reverse transcriptase and nuclease free water to a total reaction volume of 20 µL, where the RT negative reactions did not contain the reverse transcriptase. The PCR reaction was run in an Applied Biosystems™ Veriti™ 96-Well Thermal Cycler (Thermo Fisher Scientific, Massachusetts, USA) at 25°C for 10 minutes, 37°C for 120 minutes, 85°C for 5 seconds ending with an infinite hold at 4°C.

2.2.11.1.5. Assessment of genomic DNA contamination

In order to assess whether the synthesized cDNA contains any genomic DNA, 1 µL of the RT-positive and RT-negative reactions was added to a PCR plate and 24 µL of a master mix containing 1x SYBR Green PCR mix, 400 nM each, β-actin forward and reverse primers and RNase-free water. The PCR was run on the Quantstudio 7 Flex Real-Time PCR system (Thermo Fisher Scientific, Massachusetts, USA). Thermocycling conditions were as follows: PCR activation at 95°C for 15 minutes, followed by denaturation at 94°C for 15 seconds, annealing at 60°C for 20 seconds and extension at 95°C for 35 seconds for 40 cycles, followed by an infinite hold at 4°C.

Upon completion of the run, the generated Ct-values obtained for the RT-positive reactions were subtracted from the Ct values obtained from the RT-negative reactions, and a difference of 10 cycles or more was considered to have insignificant genomic DNA contamination. Only the RT-positive reactions were used for further analysis.

2.2.11.1.6. Quantitative Real-Time PCR (qRT-PCR)

cDNA was used for expression analysis by means of qRT-PCR. Briefly, Taqman® Gene Expression assays were purchased from Thermofisher Scientific (Massachusetts, USA). The genes analyzed are found in Table 2.1 and expression was normalized to *ACTβ* and *GAPD.*

Table 2.1: Taqman® Gene Expression assay list

Gene Name	Description	Taqman® Assay ID
LOXL2	Lysyl oxidase-like 2	Rn01466080_m1
COL1A1	Collagen, type I, alpha 1	Rn01463848_m1
α-SMA (ACTA2)	Actin alpha 2 (alpha-smooth muscle actin)	Rn01759928_g1
SMAD2	Mothers against decapentaplegic homolog 2	Rn00569900_m1
SMAD3	Mothers against decapentaplegic homolog 3	Rn00565331_m1
CTGF	Connective tissue growth factor	Rn01537279_g1
TGFβ2	Transforming growth factor beta-2	Rn00676060_m1
HIF1A	Hypoxia-inducible factor 1-alpha	Rn01472831_m1
AKT1	Protein kinase B	Rn00583646_m1
SOD2	Superoxide dismutase 2	Rn00690588_g1
NRF2 (NFE2L2)	Nuclear factor erythroid 2-related factor 2	Rn00582415_m1
ACTβ	Beta-actin	Rn00667869_m1
GAPD	Glyceraldehyde-3-phosphate dehydrogenase	Rn01775763_g1

A standard curve set up to determine the relative expression of each gene; for the standard curve, equal volumes of each of the samples to be run were combined in one tube and a 10-fold dilution series made of this mixture. For qRT-PCR, 10 µL reactions were prepared, containing 1 µL DNA, 5µL Applied Biosystems™ TaqMan™ Fast Advanced Master Mix (Thermo Fisher Scientific, Massachusetts, USA), 0.5 µL probe and 3.5 µL nuclease-free water for a total reaction volume of 10 µL per well.

These samples were run on a Quantstudio 7 Flex Real-Time PCR system (Thermo Fisher Scientific, Massachusetts, USA). Thermocycling conditions were as follows: hold at 95°C for 20 seconds, followed by 95°C for 1 second, 60°C for 20 seconds for 40 cycles.

2.2.12. Statistical analysis

All data were analyzed using GraphPad Prism 5 and expressed as mean ± the standard error of the mean (SEM). Data was tested for normal distribution using a Shapiro-Wilks test, followed by a student's t-test, one-way or a two-way ANOVA with a Tukey's multiple comparison post-test or a Bonferroni post-test, where applicable. $P < 0.05$ was considered statistically significant.

2.3. Results

2.3.1. Optimization of the palmitate concentration

Mitochondrial membrane potential is a marker of mitochondrial activity and ATP production, an indication of cellular activity and health. It was thus used to determine the lowest PAL concentration that would induce stress in the H9c2 cell model. The PAL concentration was optimized for a 24-hour treatment period. The results indicated that there was no significant change in mitochondrial membrane potential at 100-200 µM, however there was a significant reduction in membrane potential at the 300 µM (68.87 ± 1.50) and 500 µM (8.337 ± 0.647) PAL concentration when compared to the normal glucose treated control cells (100 ± 3.59) (Figure 2.1). The exposure of H9c2 cells to a 500 µM PAL treatment was very harsh, therefore, the concentration of 300 µM PAL was selected for further experiments.

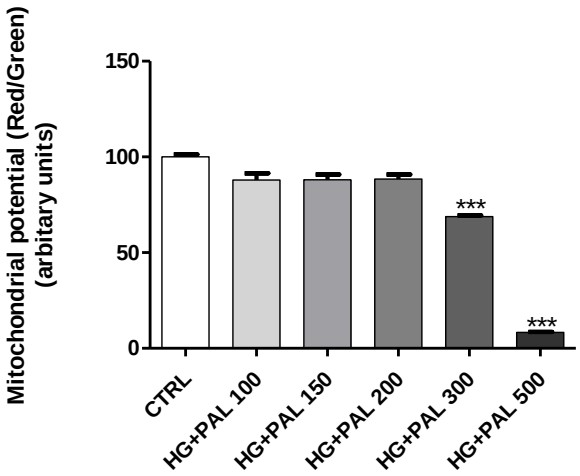

Figure 2.1: Palmitate dose response. Dose response with high glucose (33 mM) and varying concentrations of palmitate measured as a change in mitochondrial potential after a 24-hour treatment period. Three independent experiments were conducted with n=3 biological repeats each. A one-way ANOVA was performed, and statistical significance is depicted as *** p≤0.001 versus the control group.

2.3.2. Determining the effect of AfriplexGRT™ and Aspalathin on cell proliferation and viability

ATP production was measured after the cells were exposed to various treatments to determine the effect of treatment on cell viability and was plotted as a percentage of the controls. The results showed that stress induction with HG+PAL significantly reduced ATP production (49.29 ± 2.65) when compared to the control

treated group (100.8 ± 2.94). There was no significant change in ATP production after co-treatment with either AfriplexGRT™ or Aspalathin (ASP), however, the AfriplexGRT™ treatment slightly further reduced the ATP present in the cells (39.16 ± 1.77), while the ASP treatment (57.30 ± 2.92) slightly improved the effect of the HG+PAL treatment (Figure 2.2).

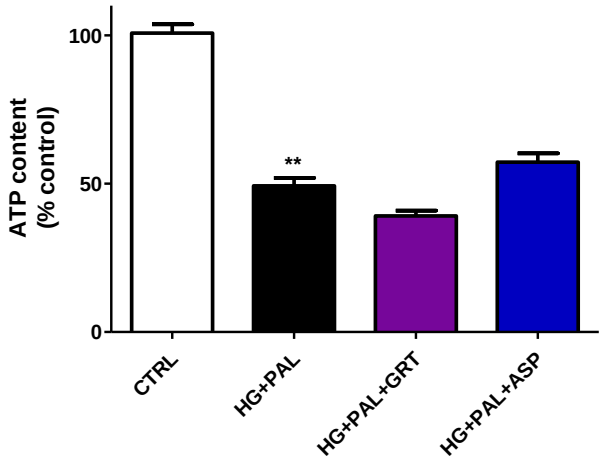

Figure 2.2: ATP assay. Bar graph of the ATP produced by the cells as a representation of cell viability. Cells were treated with normal glucose media (5.5 mM glucose) (CTRL) or high glucose (33 mM) and palmitate (0.3 mM) (HG+PAL) for a 24-hour treatment period media followed by supplemented with AfriplexGRT™ (10 µg/mL) (HG+PAL+GRT) or Aspalathin (1 µM) (ASP) for a further 6 hours. Three independent experiments were conducted with n=3 biological repeats each. A one-way ANOVA was performed, and statistical significance is depicted as ** p≤0.01 versus the control group.

2.3.3. Determining the effect of AfriplexGRT™ and Aspalathin on markers of stress

Since it is evident that the HG+PAL treatment induced stress in the H9c2 cell model, markers of stress were analyzed. ROS is upregulated in cellular stress and was used as a marker of stress induction. Results obtained revealed a significant decrease in ROS levels in the HG+PAL treated cells (108159 ± 5723) when compared to the control treated group (361425 ± 3251), and co-treatment with AfriplexGRT™ (86694 ± 4055) further decreased the ROS levels when compared to the HG+PAL treated cells. ASP (99107 ± 4763) however, had no effect on ROS levels when compared to the HG+PAL treated cells (Figure 2.3).

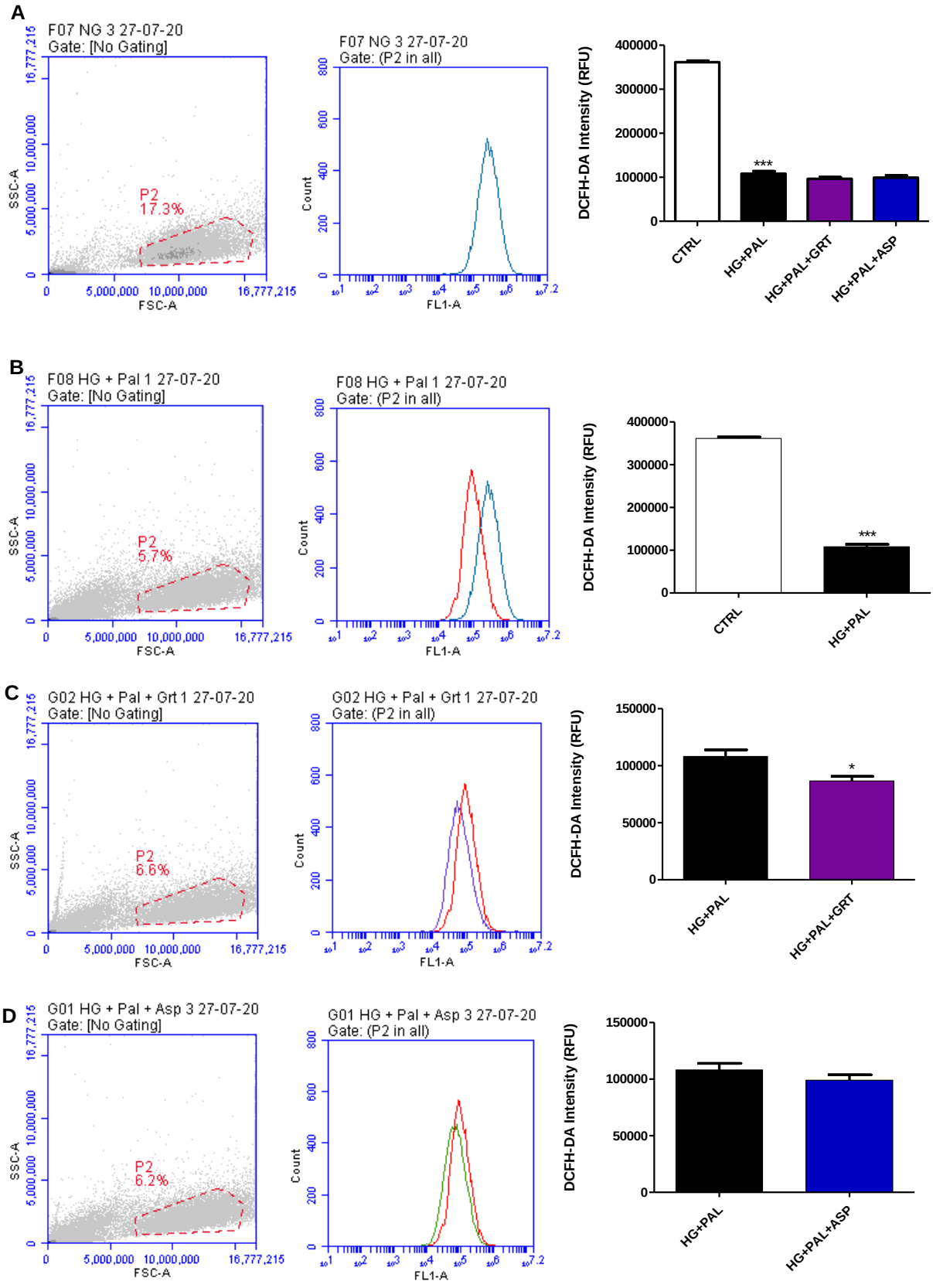

Figure 2.3: The effect of AfriplexGRT™ and Aspalathin on HG+PAL induced oxidative stress. The DCFH-DA (2',7'-Dichlorofluorescin Diacetate) is measured in relative fluorescence units (RFU). Three independent experiments were conducted with n=3 biological repeats each. A one-way ANOVA (A) or t-test (B-D) was performed, and statistical significance is depicted as * p≤0.05 and ** p≤0.01.

Markers of oxidative stress and inflammation, as well as antioxidant levels were also analyzed by means of gene expression analysis to confirm adequate stress induction in the treated cell model. The expression levels of hypoxia inducible factor 1 subunit alpha (*HIF1α*), a marker of oxidative stress, was increased (1.129 ± 0.024) with HG+PAL treatment when compared to their control treated cells (1.00 ± 0.163), although this was not statistically significant (Figure 2.4A). Expression of inflammatory markers, interleukin-6 (*IL-6*) (1.64 ± 0.18) and tumor necrosis factor (*TNF*) (4.72 ± 0.08), were significantly upregulated in HG+PAL treated cells when compared to their expression levels in control treated cells (1.00 ± 0.12 and 1.00 ± 0.15, respectively) (Figure 2.4B and C, respectively). The treatment of HG+PAL showed an augmented effect in terms of enhanced expression of the antioxidant markers, nuclear factor erythroid 2–related factor 2 (*NRF2*) and superoxide dismutase 2 (*SOD2*) (1.48 ± 0.13 and 2.53 ± 0.39), when compared to the cells treated with control media (1.00 ± 0.121 and 1.00 ± 0.107, respectively) (Figure 2.4D and E). Expression levels of various markers included in the current study indicated that stress was induced in the H9c2 cells after HG+PAL exposure.

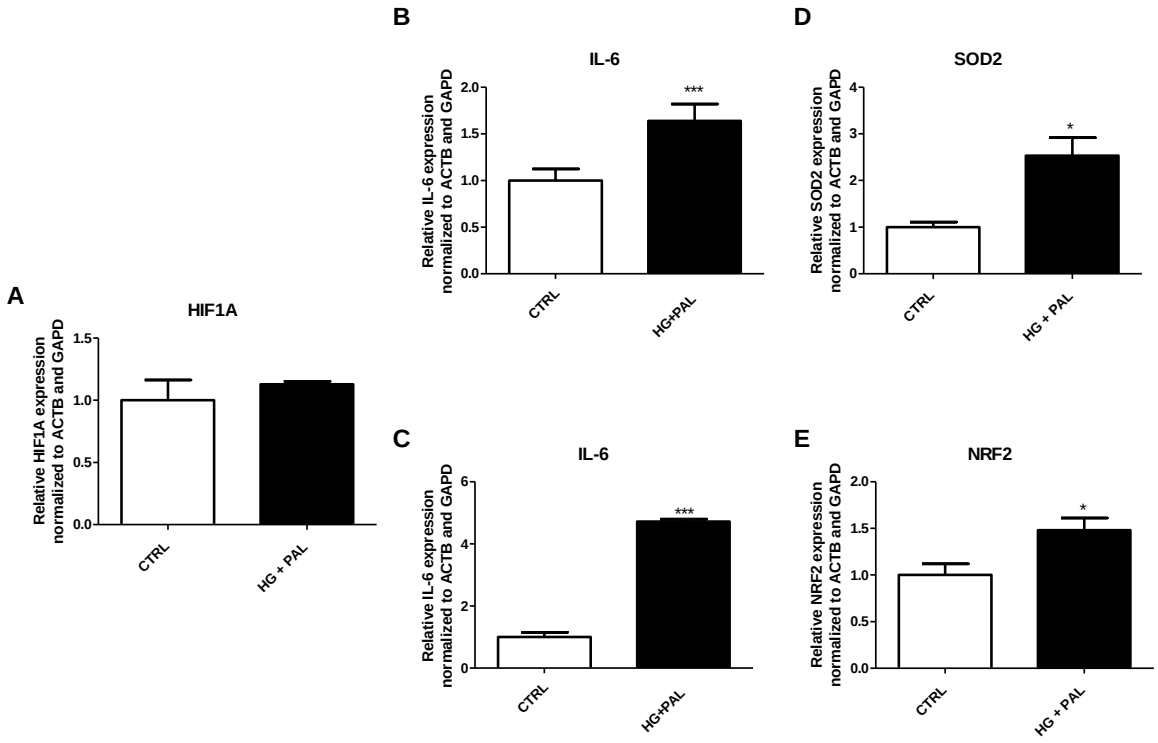

Figure 2.4: Gene expression. RNA expression of oxidative stress marker (A) *HIF1A*, inflammatory markers (B) *IL-6* and (C) *TNF*, and antioxidant markers (D) *NRF2* and (E) *SOD2*. Three independent experiments were conducted with n=3 biological repeats each. A t-test was performed, and statistical significance is depicted as * p≤0.05, ** p≤0.01, and *** p≤0.001.

2.3.4. Determining the effect of AfriplexGRT™ and Aspalathin on mitochondrial bioenergetics

Increased ROS has been directly correlated with altered mitochondrial bioenergetics, and thus these changes were investigated in response to the HG+PAL treatment, using a Seahorse analyzer. Oxidative consumption rate (OCR) and extracellular acidification rate (ECAR) were used to measure oxidative phosphorylation and glycolysis, respectively. An AUC analysis determined that the OCR was slightly increased by the HG+PAL treatment (218.5 ± 27.34) when compared to the control cells (183.1 ± 27.82), and the co-treatment with AfriplexGRT™ (345.2 ± 33.54) and ASP (304.1 ± 27.06) further increased the OCR when compared to the HG+PAL treated cells alone, although this increase was only statistically significant for the cells treated with AfriplexGRT™ (Figure 2.5A). The ECAR was unaffected by the HG+PAL treatment (90.79 ± 15.71) when compared to the control group (88.53 ± 21.15), however, as seen in the OCR, the treatment with AfriplexGRT™ (148.5 ± 16.33) and ASP (137.4 ± 16.69) increased this parameter when compared to the HG+PAL treated cells, however none of these changes were statistically significant (Figure 2.5B).

The measured values of OCR and ECAR were used to calculate further parameters of mitochondrial respiration such as basal respiration (cells demand for energy under basal conditions), proton leakage (indication of mitochondrial damage), maximal respiration (maximum respiration rate achievable by the cells), spare respiratory capacity (the capability of the cell to respond to changes in energy demand, indicating cellular flexibility), ATP production (ATP produced to meet the energy demands of the cell) and coupling efficiency.

Basal respiration was significantly decreased by HG+PAL treatment (7.15 ± 1.14) when compared to the experimental control (13.52 ± 1.66), with both AfriplexGRT™ (13.49 ± 1.10) and ASP (14.20 ± 1.11) again significantly increasing basal respiration when compared to HG+PAL treatment alone, to levels comparable to the experimental control (Figure 2.5C).

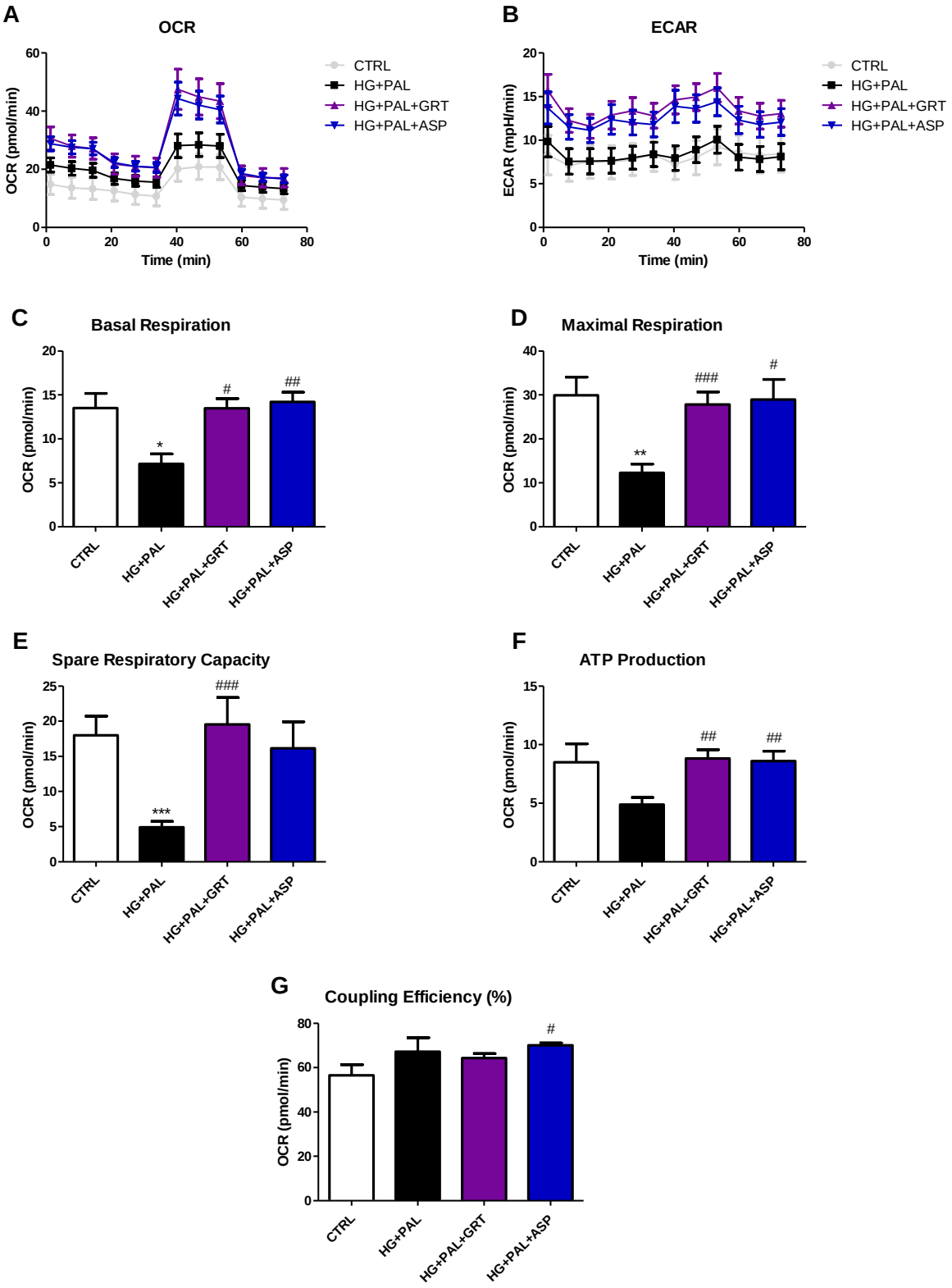

Figure 2.5: Seahorse analysis. Changes in mitochondrial bioenergetics in response to high glucose and palmitate media (HG+PAL) and treatment with AfriplexGRT™ (GRT) or Aspalathin (ASP). Three independent experiments were conducted with n=3 biological repeats each. A one-way ANOVA was performed, and statistical significance is depicted as * p≤0.05, ** p≤0.01 *** p≤0.001 versus the control group and # p≤0.05, ## p≤0.01, ### p≤0.001 versus the HG+PAL group.

Like basal respiration, the cells maximal respiration was significantly decreased by the HG+PAL treatment (12.26 ± 2.02) when compared to the experimental control (29.95 ± 4.12). Further treatment with AfriplexGRT™ (2.85 ± 2.84) and ASP (28.96 ± 4.60) significantly increased the maximum respiration levels induced by the HG+PAL treatment, to levels comparable to the experimental control (Figure 2.5D).

Similarly, spare respiratory capacity was significantly reduced in cells exposed to HG+PAL treatment (4.91 ± 0.56) when compared to the experimental control (18.02 ± 2.71) and both AfriplexGRT™ (19.55 ± 3.84) and ASP (16.15 ± 3.75) treatment reversed the effect of the HG+PAL treatment, although this was only statistically significant for the AfriplexGRT™ treatment (Figure 2.5E).

Although ATP production followed the same trend, the decrease in ATP production by the HG+PAL treatment (109.6 ± 22.52) was not statistically significant when compared to the experimental control (202.9 ± 14.58). Treatment with AfriplexGRT™ (207.8 ± 18.14) and ASP (203.8 ± 18.96), however significantly increased the cells ATP production when compared to the HG+PAL treated cells, to levels comparable to the experimental control (Figure 2.5F).

Although not statistically significant, the HG+PAL treatment (67.16 ± 6.36) marginally increased the coupling efficiency when compared to the experimental control (56.53 ± 4.82), and although AfriplexGRT™ (64.27 ± 2.01) did not induce a change in coupling efficiency, ASP (70.04 ± 1.16) significantly increased coupling efficient when compared to the HG+PAL control (Figure 2.5G).

2.3.5. Determining the effect of AfriplexGRT™ and Aspalathin on mitochondrial membrane potential

Mitochondrial membrane potential is a measure of the cell's mitochondrial energy production, as a representation of cellular activity. JC1 dye was used to determine mitochondrial membrane potential. When there is a high membrane potential, the dye forms J-aggregates within the mitochondria which fluoresce in red. A reduced mitochondrial membrane potential, the JC-1 dye is released from the mitochondria in monomeric form where it exhibits green fluorescence.

These results indicated that the HG+PAL treatment reduced the mitochondrial membrane potential of H9c2 cells (4.22 ± 0.089) when compared to the control cells (6.10 ± 0.26), and the co-treatment with AfriplexGRT™

further significantly decreased membrane potential (2.82 ± 0.20) when compared to the cells exposed to HG+PAL treatment. Treatment with ASP (4.10 ± 0.12) however, had no effect on the mitochondrial potential when compared to the HG+PAL treated group (Figure 2.6).

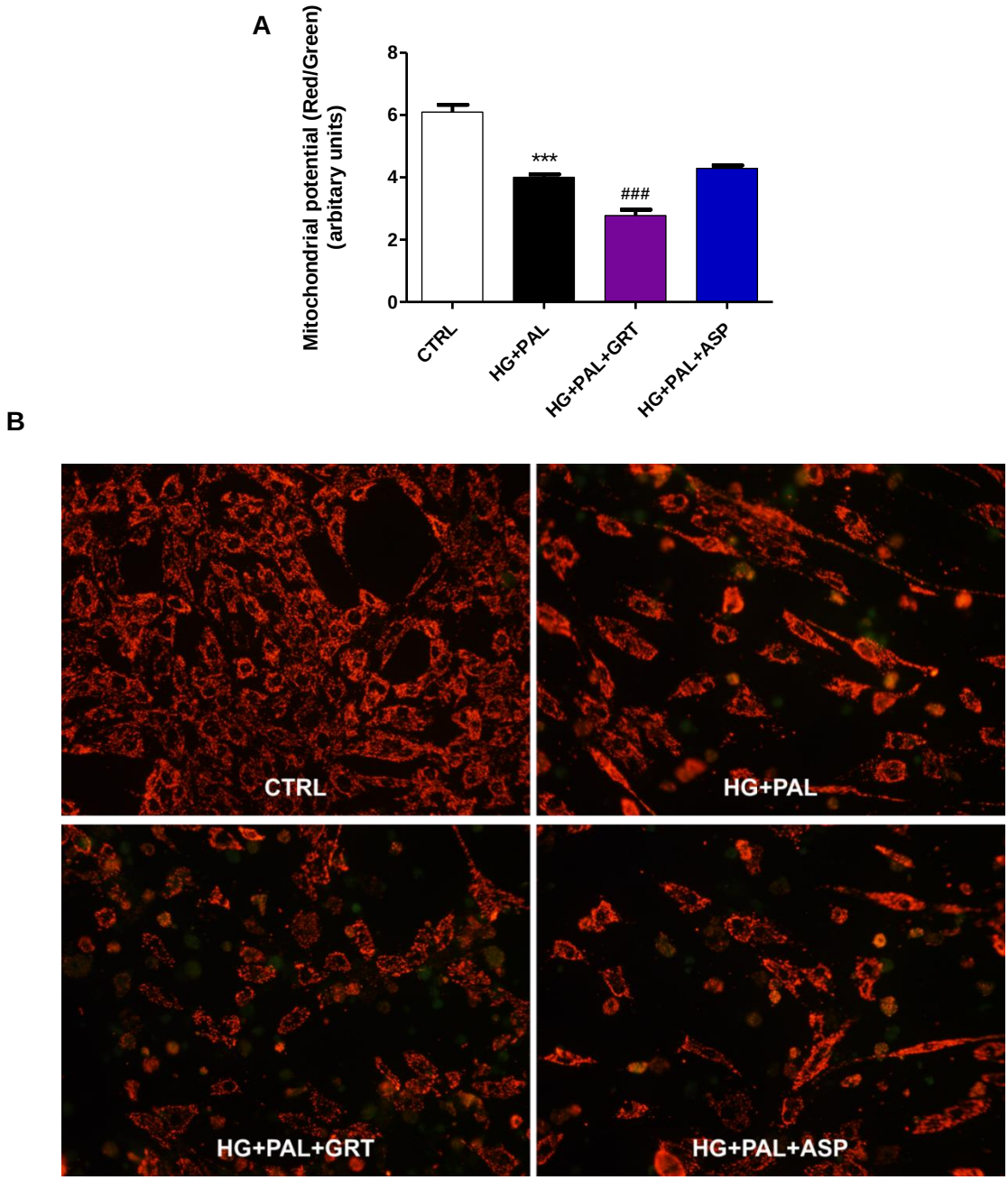

Figure 2.6: JC1 analysis. (A) Graphs and (B) representative fluorescent images showing the effect of AfriplexGRT™ (GRT) or Aspalathin (ASP) on mitochondrial membrane potential using a JC1 stain. Three independent experiments were conducted with n=3 biological repeats each. A one-way ANOVA was performed, and statistical significance is depicted as *** p≤0.001 versus the control group and ### p≤0.001 versus the HG+PAL group.

2.3.6. Determining the effect of AfriplexGRT™ and Aspalathin on apoptosis

Apoptosis was measured as a marker of cellular damage by means of Annexin V and propidium iodide (Pi). The Annexin V can distinguish between live and apoptotic cells, while the Pi can detect necrotic and late apoptotic cells. These results indicate a significant decrease in the proportion of healthy, live cells after HG+PAL treatment (41.66 ± 1.42) when compared to the control cells (81.98 ± 1.14), thus demonstrating a statistically significant increase in early (13.13 ± 0.47) and late (30.68 ± 1.10) apoptotic, as well as necrotic (14.52 ± 1.63) cells in this group (early apoptotic: 7.32 ± 0.74; late apoptotic: 4.89 ± 0.49; necrotic: 5.81 ± 0.089) (Figure 2.7). Neither treatment with AfriplexGRT™ nor ASP could significantly improve the apoptotic state induced by the HG+PAL treatment. Figure 2.8 indicates representative images of the graphs obtained by flow cytometry, indicating the apoptotic status of the cells.

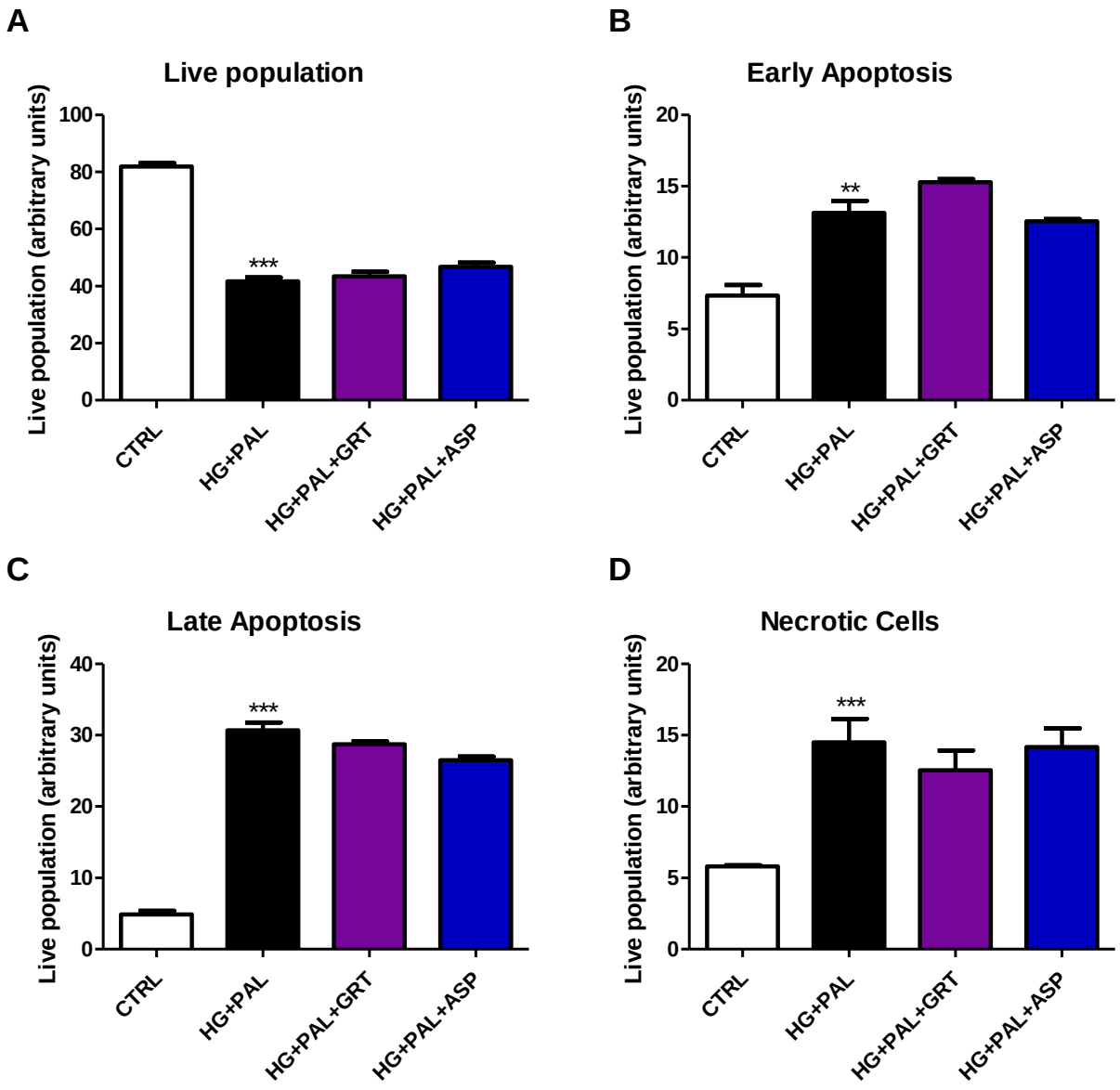

Figure 2.7: Analysis of flow cytometry data. AfriplexGRT™ (GRT) or Aspalathin (ASP) on high glucose and palmitate (HG+PAL)-induced apoptosis. H9c2 cells were exposed to control (CTRL, 5.5 Mm) or high glucose (33 mM) and palmitate (0.3 mM) for 24 hours whereafter, cells were treated with either AfriplexGRT™ or Aspalathin or for 6 hours. Populations of (A) live cells, (B) early apoptotic cells, (C) late apoptotic cells and (D) necrotic cells were analysed and plot. Three independent experiments were conducted with n=3 biological repeats each. A one-way ANOVA was performed, and statistical significance is depicted as ** $p \leq 0.01$ and *** $p \leq 0.001$ versus the control group.

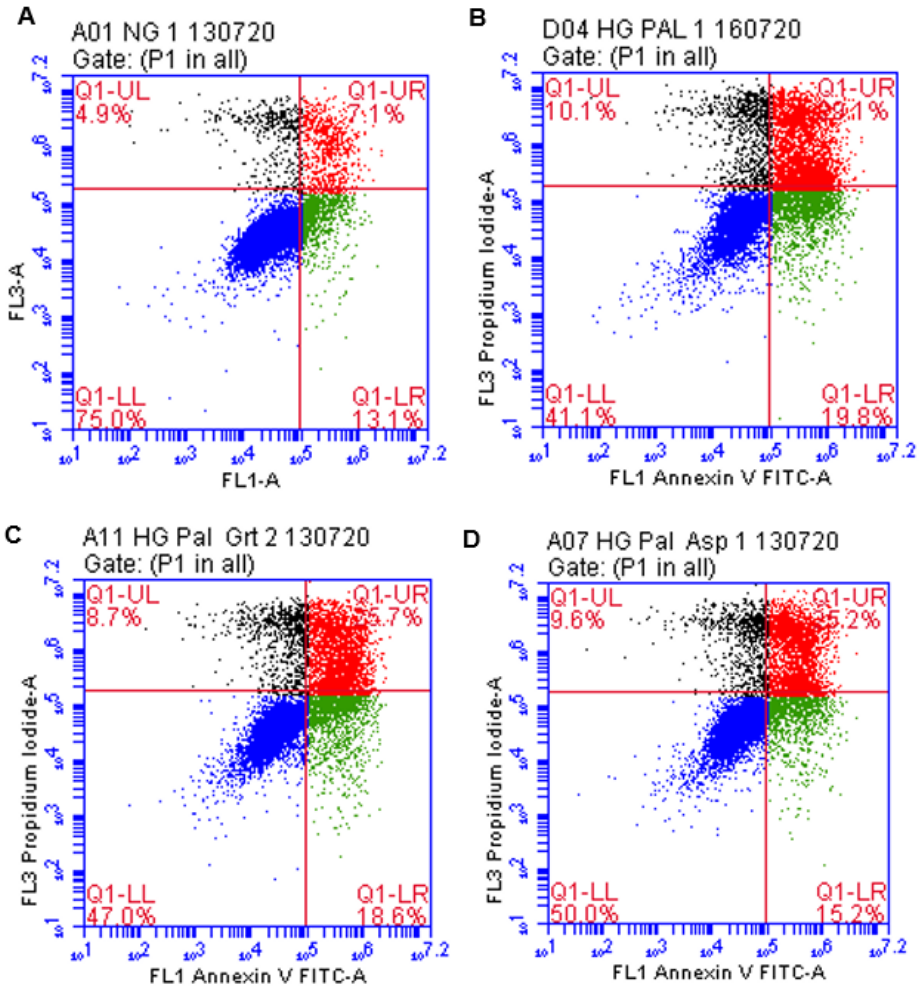

Figure 2.8: Representative images of Annexin and Pi flow cytometry graphs. The effect of AfriplexGRT™ (GRT) or Aspalathin (ASP) on high glucose and palmitate (HG+PAL)-induced apoptosis. (A) control, (B) HG+PAL, (C) HG+PAL+GRT and (D) HG+PAL+ASP treated H9c2 cells were exposed to normal glucose (NG) or high glucose (33 mM) and palmitate (0.3 mM) for 24 hours whereafter, cells were treated with either AfriplexGRT™ or Aspalathin for 6 hours. Three independent experiments were conducted with n=2 biological repeats each.

2.3.6.1. RNA expression

The expression levels for genes involved in the fibrosis signalling pathway that was proposed in chapter 1 were analysed (Figure 1.4). In this pathway, it was proposed that ROS and inflammation lead to the upregulation of inflammatory transcription factor, NFκB which in turn upregulates SMAD2/3 expression and AP1, another master transcription factor in the fibrotic pathway. In turn this activates a signalling cascade resulting in the upregulation of LOXL2, PI3K/AKT/mTOR, and TGFβ signalling. Such activation led to dysregulation in oxygen homeostasis, leading to cardiac dysfunction, or to fibroblast transformation to myofibroblasts. Myofibroblasts express more α-SMA, leading to increased collagen expression and deposition which result in fibrosis. The expression of key genes in this pathway was analysed.

SMAD2 expression was slightly increased in the cells treated with HG+PAL (1.32 ± 0.096) when compared to the control media-treated cells (1.00 ± 0.11) (Figure 2.9A). Treatment with AfriplexGRT™ (1.16 ± 0.13) caused a slight but insignificant decrease, and ASP (1.41 ± 0.30) a slight but insignificant increase in *SMAD2* expression when compared to the cells treated with only HG+PAL (Figure 2.9A). Treatment with 5 µM AZA only slightly increased *SMAD2* expression the groups treated with both control media (1.37 ± 0.048) and HG+PAL (1.67 ± 0.094), when compared to the respective control and HG+PAL controls. A similar trend was observed for the combination treatment with 5 µM AZA and AfriplexGRT™ (2.01 ± 0.42) and ASP (2.32 ± 0.45) which also showed a slight increase in *SMAD2* expression when compared to the HG+PAL group, with the group treated with ASP showing the greatest increase in *SMAD2* expression, although this was not statistically significant. The group treated with HG+PAL plus 20 µM AZA (3.60 ± 1.10), including the groups treated with AfriplexGRT™ (4.15 ± 1.23) and ASP (3.86 ± 0.87) all showed an increase in *SMAD2* expression when compared to the HG+PAL control (Figure 2.9B).

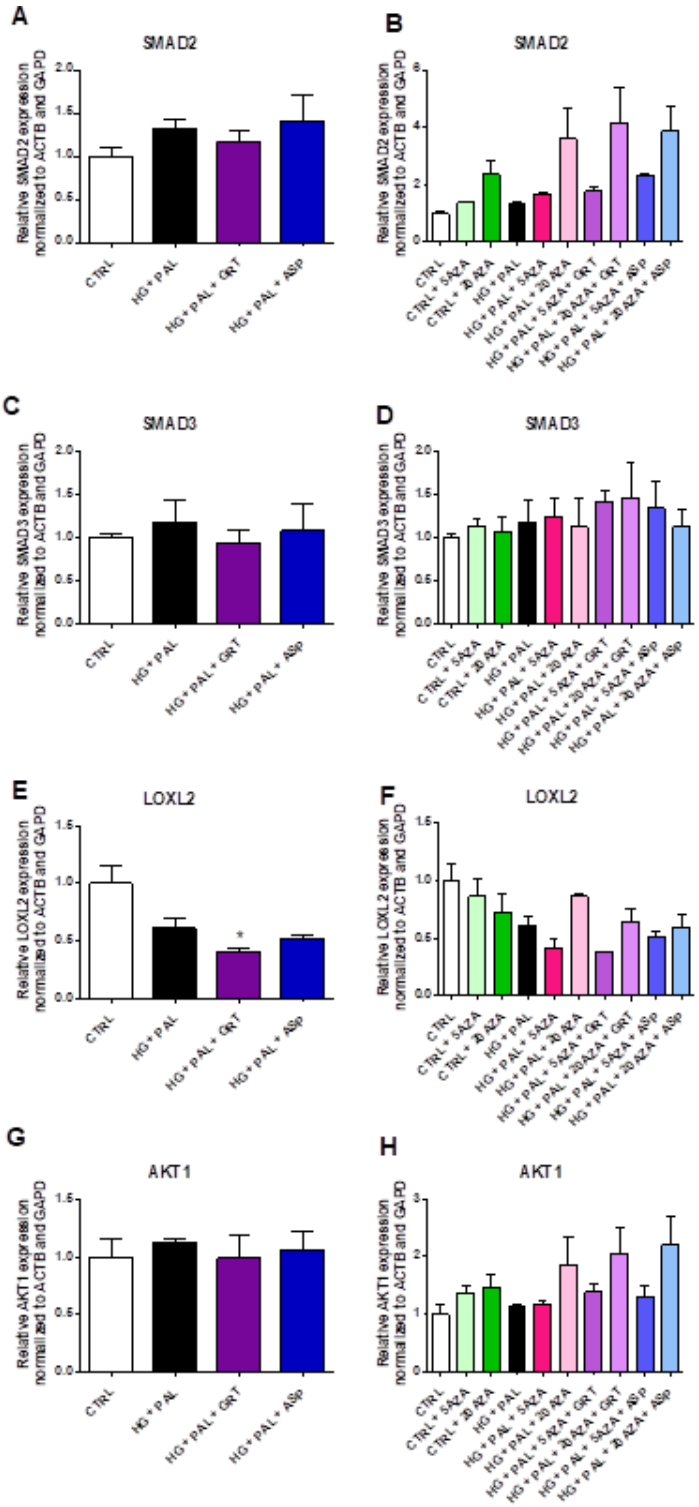

Figure 2.9: Analysis of gene expression of fibrotic markers. Gene expression of (A-B) *SMAD2*, (C-D) *SMAD3,* (E-F) *LOXL2,* and (G-H) *AKT1 after treatment* either control or high glucose media with 0.3 mM palmitate (HG+PAL) for 24 hours, followed by a 6-hour treatment with AfriplexGRT^{TM} (GRT) or Aspalathin (ASP). The HG+PAL cells were also treated with the aforementioned treatment conditions with 5 or 20 µM of AZA. Three independent experiments were conducted with n=3 biological repeats each. A one-way ANOVA was performed, and statistical significance is depicted as * p≤0.05 versus the control group.

SMAD3 showed a similar trend for cells treated with HG+PAL (1.18 ± 0.26) compared to the control media-treated cells (1.00 ± 0.043), as well as for treatment with AfriplexGRT™ (0.93 ± 0.15) and ASP (1.08 ± 0.31) when compared to the HG+PAL only treatment (Figure 2.9C). Treatment with 5 µM and 20 µM AZA resulted in a small and almost equal increase in *SMAD3* expression in the control treated group (1.12 ± 0.079 and 1.07 ± 0.16, respectively) as well as HG+PAL treated group (1.24 ± 0.21 and 1.12 ± 0.33, respectively) when compared to their respective control media and HG+PAL treated control groups, although these increases were not statistically significant. Similarly, the HG+PAL cells treated HG+PAL with 5 µM and 20 µM AZA also increased *SMAD3* expression with AfriplexGRT™ (1.41 ± 0.13 and 1.45 ± 0.41, respectively) and ASP (1.34 ± 0.30 and 1.12 ± 0.20, respectively) treatment when compared to the HG+PAL control, with the biggest increase seen in the *SMAD3* expression level observed in the cells treated with AfriplexGRT™, although none of these increases were statistically significant (Figure 2.9D).

Treatment with HG+PAL caused a decrease in *LOXL2* expression (0.61 ± 0.089) when compared to the control treated cells (1.00 ± 0.15), with a further reduction in expression was observed in the groups treated with AfriplexGRT™ (0.40 ± 0.04) and ASP (0.52 ± 0.035), when compared to the HG+PAL control group (Figure 2.9E). Although these reductions in *LOXL2* expression were not statistically significant, the decreased expression caused by the treatment with AfriplexGRT™ was statistically significant (p=0.0239) when compared to the control media-treated cells. In the control media-treated cells, the addition of 5 µM and 20 µM AZA dose dependently reduced *LOXL2* expression when compared to the control (0.86 ± 0.16 and 0.72 ± 0.17, respectively), however the decreases in expression were not significant for any of the treatments. In the HG+PAL treated groups however, treatment with 5 µM AZA again reduced *LOXL2* expression (0.42 ± 0.068) when compared to the HG+PAL treated cells, and the addition of AfriplexGRT™ (0.38 ± 0.007) and ASP (0.51 ± 0.48) were unable to reverse this, however a slight increase in expression was observed after ASP treatment, but none of these changes were statistically significant. HG+PAL treatment with 20 µM AZA however caused an increase in *LOXL2* expression (0.87 ± 0.018) when compared to the cells without AZA (0.61 ± 0.089, although this was not statistically significant. Further treatment with AfriplexGRT™ and ASP slightly reduced the *LOXL2* expression levels when compared to the HG+PAL with 20 µM AZA to levels

comparable with the HG+PAL only treated cells, however again this was not statistically significant (Figure 2.9F).

AKT1 expression was unaffected by the HG+PAL treatment (1.13 ± 0.024) when compared to the control media-treatment (1.00 ± 0.16), and AfriplexGRT™ (0.99 ± 0.20) and ASP (1.07 ± 0.15) treatment also did not affect the *AKT1* expression levels (Figure 2.9G). When the control media-treated cells were also treated with 5 µM and 20 µM AZA, a slight increase was seen in *AKT1* expression (1.36 ± 0.15 and 1.45 ± 0.24) when compared to cells without AZA. In HG+PAL treated cells however, the addition of 5 µM AZA had no effect on the expression of *AKT1* (1.16 ± 0.055), however the addition of AfriplexGRT™ (1.39 ± 0.13) and ASP (1.31 ± 0.17) slightly increased *AKT1* expression when compared to the HG+PAL and 5 µM AZA treatment, however none of the changes in expression were statistically significant. Addition of 20 µM AZA to the HG+PAL treatment caused an increase in *AKT1* expression (1.87 ± 0.47) when compared to the HG+PAL treatment without AZA, and further treatment with AfriplexGRT™ (2.05 ± 0.46) and ASP (2.20 ± 0.49) were unable to reduce *AKT1* expression again, however these changes in expression were also not statistically significant (Figure 2.9H).

None of the treatment conditions resulted in a statistically significant change in *TGFβ2* expression. The HG+PAL treatment however resulted in a decrease in *TGFβ2* expression (0.77 ± 0.12) when compared to the control cells (1.00 ± 0.19) (Figure 2.10A). The treatment of the HG+PAL-treated cells with AfriplexGRT™ (0.60 ± 0.14) and ASP (0.57 ± 0.14) caused a non-significant decrease in *TGFβ2* expression when compared to cells only treated with HG+PAL (Figure 2.10A). Treatment of cells with 5 µM AZA slightly reduced *TGFβ2* expression in the control (0.82 ± 0.11) and HG+PAL (0.56 ± 0.066) treated cells when compared to their respective controls without AZA treatment, with a further decrease in expression observed with the addition of AfriplexGRT™ (0.46 ± 0.054), but an increase in expression seen with the addition of ASP (0.65 ± 0.15) when compared to cells only treated with HG+PAL with 5 µM AZA. The addition of 20 µM AZA caused a more drastic decrease in *TGFβ2* expression in cells treated with the control media (0.42 ± 0.022) when compared to the control cells, although this was still not statistically significant. In the HG+PAL treated cells however, treatment with 20 µM AZA caused a decrease in *TGFβ2* expression (0.57 ± 0.18) equal to the change caused

by the 5 µM AZA treatment, and the addition of AfriplexGRT™ (0.56 ± 0.14) and ASP (0.55 ± 0.12) was unable to alter the decrease in expression (Figure 2.10B).

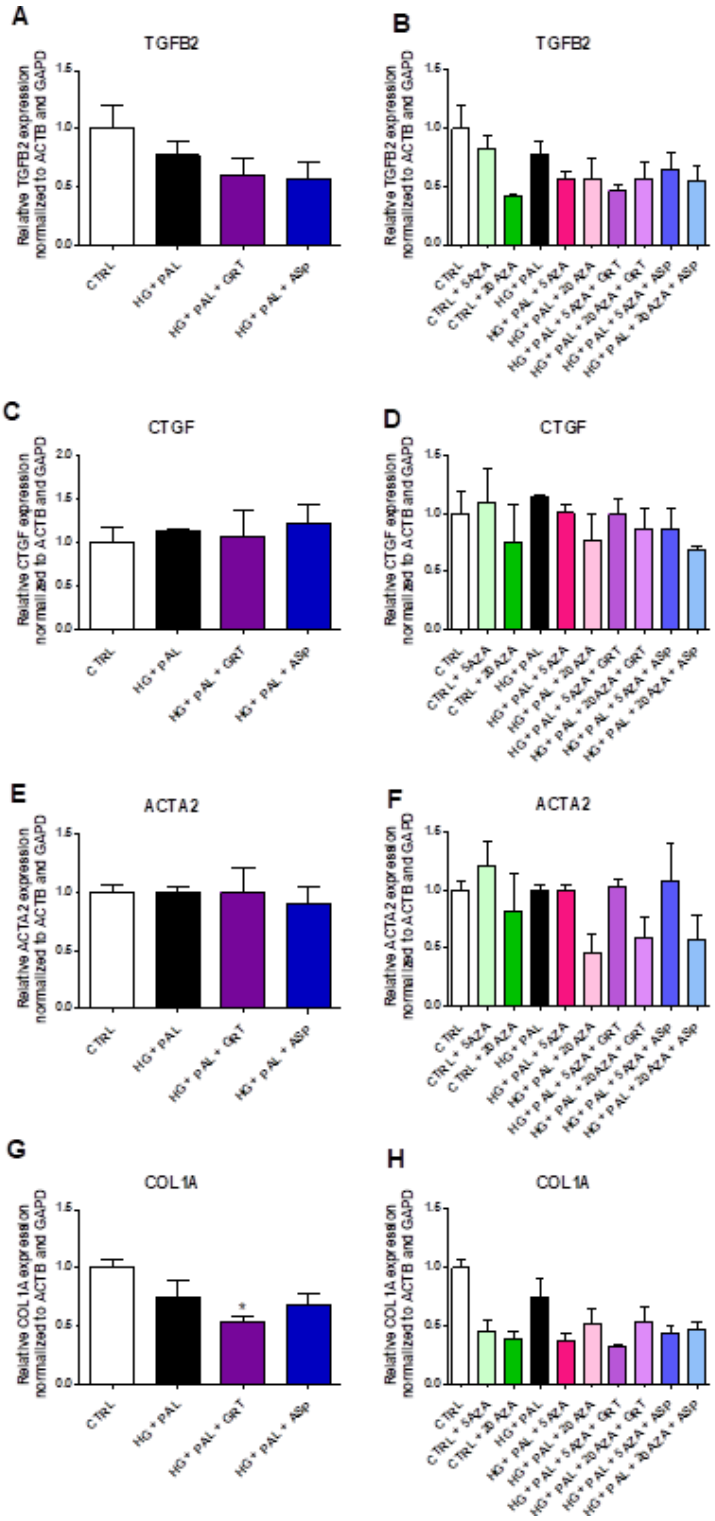

Figure 2.10: Analysis of gene expression of fibrotic markers. Gene expression of (A-B) *TGFβ2*, (C-D) *CTGF,* (E-F) ACTA2*,* and (G-H) *COL1A after treatment* either control or high glucose media with 0.3 mM palmitate (HG+PAL) for 24 hours, followed by a 6-hour treatment with AfriplexGRT™ (GRT) or Aspalathin (ASP). The HG+PAL cells were also treated with the aforementioned treatment conditions with 5 or 20 µM of AZA. Two independent experiments were conducted with n=2 biological repeats each. A one-way ANOVA was performed, and statistical significance is depicted as * p≤0.05 versus the control group.

CTFG expression was marginally increased by the HG+PAL treatment (1.14 ± 0.02) when compared to cells treated with control media (1.00 ± 0.18), although this was not statistically significant, and further treatment with AfriplexGRT™ (1.07 ± 0.29), and ASP (1.23 ± 0.21) did not alter gene expression when compared to the HG+PAL control (Figure 2.10C). Control media-treated cells treated with 5 µM AZA (1.09 ±0.30) did not alter *CTGF* expression when compared to control cells without 5 µM AZA treatment, however a decrease in expression was observed after treatment with 20 µM AZA (0.75 ± 0.32), although this decrease was not statistically significant. The HG+PAL treated cells with 5 µM AZA treatment also marginally decreased *CTGF* expression (1.00 ± 0.073) when compared the HG+PAL control, and treatment with AfriplexGRT™ did not affect *CTGF* expression levels (0.99 ± 0.13), although treatment with ASP (0.87 ± 0.18) slightly decreased expression when compared to the cells treated with HG+PAL and 5 µM AZA. The addition of 20 µM AZA to the HG+PAL treatment however caused a decrease in *CTGF* expression (0.77 ± 0.22) when compared to the HG+PAL control, and treatment with AfriplexGRT™ marginally increased expression (0.87 ± 0.18), however treatment with ASP (0.69 ± 0.026) did not affect *CTGF* when compared to cells treated with HG+PAL and 20 µM AZA alone (Figure 2.10D).

ACTA2 expression was not affected by the HG+PAL treatment (1.00 ± 0.042) when compared to control cells (1.00 ± 0.072), and further treatment with AfriplexGRT™ (0.99 ± 0.22) and ASP (0.91 ± 0.13) also did not result in a change in expression when compared to the HG+PAL-treated cells (Figure 2.10E). Control cells treated with 5 µM AZA caused an increase in *ACTA2* expression (1.20 ± 0.22), when compared to the control cells, where treatment with 20 µM AZA caused a decrease in *ACTA2* expression (0.81 ± 0.34), although these changes were not statistically significant. In the HG+PAL-treated cells, the addition of 5 µM AZA did not change gene expression levels (1.00 ± 0.045) when compared to the HG+PAL control, and while further treatment with AfriplexGRT™ (1.04 ± 0.057) and ASP (1.08 ± 0.31) did not alter gene expression when compared to the HG+PAL. HG+PAL treatment with 20 µM AZA however caused a large but insignificant decrease in *ACTA2* expression (0.46 ± 0.16) when compared to the HG+PAL control, and the addition of AfriplexGRT™ (0.59 ± 0.18) and ASP (0.58 ± 0.20) moderately increased *ACTA2* expression again when compared to the HG+PAL cells treated with 20 µM AZA, however none of these changes were statistically significant (Figure 2.10F).

Lastly, *COL1A1* expression was decreased in cells treated with HG+PAL (0.75 ± 0.15) when compared to the control cells (Figure 2.10G), although this was not statistically significant. Further treatment with AfriplexGRT™ decreased *COL1A1* expression further (0.53 ± 0.47) when compared to the HG+PAL control, although this was only significant when compared to the control media-treated cells. Treatment with ASP (0.68 ± 0.087) however caused no change in *COL1A1* expression when compared to the HG+PAL control (Figure 2.10G). In the control media-treated cells, treatment with 5 (0.45 ± 0.097) and 20 µM (0.39 ± 0.067) AZA reduced *COL1A1* expression when compared to the control cells without AZA treatment, although not significantly. In the cells treated with HG+PAL, the addition of 5 µM AZA reduced gene expression levels of *COL1A1* (0.38 ± 0.059) when compared to the HG+PAL control, and further treatment with AfriplexGRT™ (0.32 ± 0.010) and ASP (0.43 ± 0.058) marginally decreased and increased *COL1A1* expression, respectively, when compared to HG+PAL with 5 µM AZA, however this was not statistically significant. Similarly, the addition of 20 µM AZA reduced *COL1A* expression (0.52 ± 0.13) when compared to the HG+PAL control, however less so than the reduction by the 5 µM AZA. The addition of AfriplexGRT™ to the HG+PAL treatment with 20 µM AZA did not affect *COL1A* expression (0.54 ± 0.12), although the addition of ASP (0.47 ± 0.063) marginally increased expression when compared to the cells treated with HG+PAL with 20 µM AZA, although not significantly (Figure 2.10H).

2.4. Discussion

Cardiac fibrosis is one of the main causes of mortality in cardiovascular disease patients. This fibrotic process is driven by increased ROS and inflammation, often found in cases of obesity and diabetes. The inflammatory response leads to changes in energy metabolism and cell damage. Polyphenols are known to exhibit anti-obesogenic and anti-inflammatory properties which can counteract the effects of ROS and inflammation. Thus, the aim of the current study was to investigate the ameliorative effects of a polyphenol-rich extract AfriplexGRT™, and its bioactive compound, Aspalathin, in mitigating the HG+PAL-induced cardiac damage in an H9c2 cell model.

A dose response experiment (based on concentrations reported in literature) was performed to determine the optimum concentration of PAL to be used in combination with the 33 mM HG media for stress induction. Wei et al. (2013) reported a statistically significant increase in H9c2 cell apoptosis when treating cells with 100 µM and 150 µM PAL after a 12-hour treatment period [17]. They also found a significant reduction in cell viability with the 150 µM PAL treatment after 12 hours. Li et al. (2017), however, treated H9c2 cells with 500 µM PAL for 12 and 24 hours, and found that the 12-hour treatment period was not sufficient to alter glucose consumption when compared to their controls, but that the 24-hour treatment period caused a sufficient insult [18]. In addition, Dludla et al. (2020) reported that palmitate concentrations greater than 250 µM significantly elevated ROS and altered mitochondrial respiration in H9c2 cells, and concentrations of 500 µM or more reduced cell viability because of toxicity [19]. Since these PAL concentrations varied so greatly, the dose response in this study (100-500 µM) was set up to include the PAL concentrations used in literature. After the 24-hour PAL treatment period, the 100, 150, and 200 µM PAL could not induce a sufficient insult to the mitochondrial membrane potential, however the 300 µM reduced the membrane potential by 31%, and the 500 µM PAL concentration further caused a reduction to 8%, when compared to the control group. These findings were similar to those reported by Dludla et al (2020), and thus due to the toxicity of PAL at 500 µM, the 300 µM concentration was used for all further experiments.

Adenosine triphosphate (ATP) is a key energy molecule in cells and is used for various cellular processes. The ATP level decreases under conditions of cellular stress or damage [20], and thus cellular ATP levels were used

to determine the effect of the HG+PAL treatment and AfriplexGRT™ and ASP treatments on the activity of the H9c2 cells. Dludla et al. (2020) made use of an MTT assay to determine metabolic activity of the cells treated with PAL and found that a 200 µM concentration of PAL was sufficient to significantly reduce the metabolic activity when compared to the experimental control [19]. It was thus expected that the HG+PAL treatment would significantly reduce ATP content in this study. Although the reduction in ATP production was not significant when cells were treated with AfriplexGRT™, research by Kroukamp et al (2018) suggested that ingestion of AfriplexGRT™ by rats improved the coupling efficiency and mitochondrial oxygen utilization of primary heart cells of rats on a high fat diet but did not improve the oxidative phosphorylation rate [21]. The data from the current study and literature thus indicate little to no changes to mitochondrial function by AfriplexGRT™. The marginal increase in ATP production by the treatment with ASP was in line with findings reported by Mazibuko-Mbeje et al. (2019) where treatment with ASP significantly improved glucose uptake, MTT activity and ATP production in C3A liver cells that had been treated with 750 µM PAL when compared to PAL treated cells alone [22].

Markers of oxidative stress and inflammation are known to be upregulated as indicators of cellular stress [23]. ROS is upregulated in response to cellular stress such as HG+PAL [24], however, the current study indicated a significant decrease in ROS in response to the HG+PAL treatment when compared to the experimental control. Since this was contrary to what has been reported in literature, gene expression analysis was performed on genes involved in oxidative stress (*HIF1A*), inflammation (*IL-6* and *TNF*) and antioxidation (*NRF2* and *SOD2*). The current study observed that the mRNA expression of *HIF1α* was marginally increased in the current study, however, this upregulation was not statistically significant. A study conducted by Sharma et al. (2020) indicated an increase in *HIF1α* mRNA expression in an obese mouse model when compared to the lean controls [25]. Taken together the increased expression of *HIF1α* confirms the activation of oxidative stress in the H9c2 cell model in response to the HG+PAL treatment.

The expression of both *IL-6* and *TNF* were significantly increased by the HG+PAL treatment when compared to their levels in experimental control cells in the current study, confirming induction of inflammatory pathways by the treatment. This was to be expected since research by Staiger et al. (2004) showed a

significant increase in *IL-6* gene expression in human endothelial cells when exposed to a 500 µM PAL concentration for 20 hours [26]. In addition, Igoillo-Esteve et al. (2010) observed a significant increase in *IL-6* and *TNF* expression in human islet cells cultured with both 6 mM and 28 mM glucose and palmitate when compared to the experimental controls [27].

There is contradictory data in literature about the regulation of antioxidant markers such as NRF2 in response to stress induction such as inflammation. It was reported by da Costa et al. (2019) that NRF2 is activated under conditions whereby ROS levels are higher than the cells' ability to neutralize them [28]. Valenzuela et al. (2017) however, previously reported a decrease in *NRF2* expression in the livers of mice fed a high-fat diet [29]. Additionally, a study by Yu et al. (2020) observed a decrease in SOD activity and *NRF2* in H9c2 cells in response to HG+PAL treatment [30]. Research conducted by Nemecz et al. (2019) revealed a decrease in *SOD2* mRNA expression in response to a 24-hour exposure to 250 µM PAL in β-cells [31]. Most of the literature reported an increase in *NRF2* and decrease in *SOD2* expression when exposed to stress such as that induced by HG+PAL. The *NRF2* expression levels in the current study showed an increase when compared to the experimental control. Although this is contrary to most literature, it could be argued to be an adaptive response by the cells to counteract the increase in ROS caused by the HG+PAL treatment. Alternatively, HG+PAL treatment could have activated the pathways responsible for inflammation and oxidative stress, without the activation of ROS, and since *NRF2* expression is regulated by ROS activation, and that the lack of ROS in the HG+PAL treated cells leads to a decrease in *NRF2* expression, however, additional studies are required to validate these findings. The significant increase in *SOD2* expression in response to HG+PAL treatment in this study, however, corresponds to what is found in literature [32, 33] and is thus expected.

It is known that mitochondrial bioenergetics are affected by a high fat and high glucose conditions, whereby an increase in serum free fatty acids due to a high fat diet can cause a decrease in glucose oxidation and increase in fatty acid metabolism [34, 35]. In addition, Koziel et al. (2012) demonstrated a significant influence of high glucose on mitochondrial bioenergetics parameters of endothelial cells [33]. The study by Koziel et al. reported a decrease in basal respiration, proton leak and maximal respiration after treatment of endothelial cells with high glucose. Similarly, the current study also observed this trend, although the proton leak was

not significantly decreased when compared to the experimental control. These results indicate that HG+PAL conditions reduce the H9c2 cells demand for energy under basal conditions and the maximum respiratory rate achievable by the cells, as well as inducing mitochondrial damage. This results in the mitochondria not being able to sustain the energy demands of the cell and thus cells cannot function efficiently. This is a possible reason for the decrease observed in ATP production. In addition, a study by Alnahdi et al. (2019) observed a decrease in ATP production in HepG2 cells when treated with 300 µM PAL or high glucose, and these effects were more severe when the cells were co-treated with these conditions [32]. The current study also showed the mitochondrial dysfunction mitigation effects of AfriplexGRT™ and ASP by improving basal respiration, maximal respiration, spare respiratory capacity and ATP production of H9c2 cells treated with HG+PAL. Similar results were observed in a C3A cell culture model where cells were treated with 750 µM PAL [22]. Results from this study showed a significant decrease in basal respiration, spare respiratory capacity and ATP production in the cells treated with PAL, however the treatment with 10 µM ASP improved all these parameters to levels comparable with the experimental controls. Taken together, AfriplexGRT™ and ASP play a key role in improving parameters of mitochondrial bioenergetics induced by HG+PAL treatment.

Furthermore, mitochondrial membrane potential was measured to determine the cell's mitochondrial energy production, as a representation of cellular activity. An increase in ROS and change in the cell's energy metabolism can lead to mitochondrial depolarization which is detrimental to the cell. A study by He et al. (2018) found that mitochondrial membrane potential was significantly reduced in neonatal rat cardiomyocytes treated with 300 µM PAL, when compared to the experimental control [36]. The current study is consistent with these findings reporting the reduced mitochondrial potential in HG+PAL treated cells when compared to the control cells. The addition of AfriplexGRT™ caused a further reduction in mitochondrial membrane potential when compared to the HG+PAL control, which corresponds to research conducted by Millar et al. (2020) on C3A cells where treatment of cells with 0.1 mg/mL AfriplexGRT™ caused a reduction in mitochondrial membrane potential [37]. ASP marginally improved mitochondrial membrane potential, which was expected since ASP is the compound within unfermented rooibos that contributes the most antioxidant capacity and is therefore able to reduce ROS caused by the HG+PAL treatment, thereby improving mitochondrial potential [38]. In addition, research by Johnson et al. (2016) showed that ASP could

improve mitochondrial membrane potential in H9c2 cells treated with HG-media [13]. Although the improved mitochondrial bioenergetics after treatment with AfriplexGRT™ seems contradictory to the decrease it caused in MMP, this can be due to proton leakage. It is known that the proton motive force generated for ATP synthesis can also result in protons leaking back into the inner membrane of the mitochondria to stimulate and maintain the activity of the respiratory chain, which can cause a decrease in MMP. In the current study, the decreased MMP was accompanied by an increase in proton leakage after treatment with AfriplexGRT™, however this was not statistically significant (See appendix 3) [39].

Increased ROS and decreased mitochondrial membrane potential can culminate in cellular apoptosis, and thus apoptosis was measured as a marker of cell damage. It was shown by Wei et al. (2013) that apoptosis could be induced in H9c2 cells after treatment with PAL and that the activation of this pathway occurred through ROS and ERK1/2 signalling [17]. This was later confirmed by He et al. (2018) who found that there was a significant increase in apoptosis in neonatal rat cardiomyocytes treated with 30 mM glucose and cells treated with 300 µM PAL when compared to the experimental controls [36]. The data obtained in this study also indicated an increase in apoptosis due to the HG+PAL treatment when compared to the control cells. Treatment with AfriplexGRT™ however did not ameliorate the apoptotic effect induced by the HG+PAL media, which corresponds with research by Millar et al. (2020) who demonstrated that AfriplexGRT™ could not reduce apoptosis in C3A cells treated with 500 µM PAL [37]. In the current study, ASP could not reduce apoptosis in the HG+PAL-treated cells, however, in a study conducted by Johnson et al. (2016), treatment of H9c2 cells with ASP was able to reduce caspase 3/7 activity compared to cells treated with 33 mM glucose, therefore indicating a reduction in apoptosis after ASP treatment [13].

Gene expression analysis was used in the current study to determine the effect of various treatments on a mRNA level. The proposed fibrotic signaling pathway in Figure 2.10, suggested augmented inflammation as a key driver of the fibrotic process. Since the inflammatory markers *IL-6* and *TNF* were upregulated, an upregulation in the role players of the fibrotic pathway was expected. The inflammation would first affect *SMAD2* and *SMAD3* expression. An increase in *SMAD2* and *SMAD3* expression was observed in response to HG+PAL treatment. Although there is limited research reported on SMAD signaling in response to HG+PAL

treatment, Xiao et al. (2021) showed an increase in SMAD2 and TGFβ1 protein expression in kidney fibrosis in a db/db mouse model [40]. In addition, Wu and Gerynck (2009) showed an increased activation of SMAD3 to pSMAD3 induced by a HG treatment in MEF and NRK-52E cells [41]. This could also explain why there is no significant change in *SMAD3* expression in response to the HG+PAL treatment, as the regulation for SMAD3 might not take place on a mRNA level, but rather on the protein level where it is inactivated or activated by phosphorylation. In the current study, *SMAD2* signaling is upregulated in response to the 20 µM AZA treatment, where *SMAD3* expression is unaffected by treatment with AZA, suggesting the *SMAD2* expression might be regulated by DNA methylation, but not *SMAD3* expression, however there is no literature to support this and thus further research is needed to validate these findings.

Since *SMAD2* and *SMAD3* signaling was marginally increased by the HG+PAL treatment, a similar increase was expected in *LOXL2, AKT1* and *TGFβ*2 expression, which should induce upregulation of fibrotic markers *CTGF, ACTA2* (which encodes for α-SMA) and *COL1A*, to cause fibrosis. Instead, the current study observed a moderate decrease in *LOXL2* and *TGFβ2* expression, and a marginal increase in *AKT1* expression in response to HG+PAL treatment. The expression of *CTGF* and *ACTA2* were unaffected by HG+PAL treatment, and *COL1A* was only marginally decreased in the same group, when compared to the experimental controls.

A study by Johnson et al. (2020) observed an increase in *LOXL2* mRNA expression in a db/db mouse model between 11 and 16 weeks when compared to a control db/+ group [42]. Although this is not a diet induced model, the db/db mouse model is one of obesity due to a leptin deficiency, and molecular markers of obesity can drive metabolic disorders. This study also reported no difference in *LOXL2* expression before the animals were 11 weeks old, and thus the lack of LOXL2 upregulation in the current study could be as a result of the treatment being too short, or not severe enough to observe a change in this fibrotic marker after the 24-hour treatment period.

Tam et al. (2015) studied changes in secreted proteins in male C57BL/6 mice fed a 45% fat diet compared to chow control at 5, 10 and 25 weeks. They observed a decrease in *COL1*A expression after 5 and 10 weeks on the high fat diet, however no change in COL1 expression after 25 weeks. Similarly, *CTGF* expression was unaffected by the high fat diet at any of the observed time points, when compared to the controls, however

TGFβ2 expression was marginally decreased after 5 weeks of high fat diet-feeding, and slightly increased compared to the control after 25 weeks on the diet [43]. Similar findings are reported in the current study, and although an increase was expected, particularly in *TGFβ2* expression, the time dependent changes in expression in the study by Tam et al. suggested that perhaps treatment was not carried out for a sufficient period of time to induce a significant increase in these fibrotic markers and that long term treatment may be needed to induce the activation of fibrotic markers.

Although ASP did not significantly alter the expression of these genes of interest, AfriplexGRT™ reduced *LOXL2* and *COL1A* expression significantly when compared to the control group, however the decrease was not significant when compared to cells treated with HG+PAL. Since inflammation drives the fibrotic pathway, and polyphenols such as AfriplexGRT™ are known to have antioxidant properties, it was seen that AfriplexGRT™ reduced ROS as seen in the ROS activity results, which thereby reduces the likelihood of fibroblast to myofibroblast transformation in heart cells and thus reducing collagen deposition and fibrosis in this model. This hypothesis would however need to be further investigated.

Additionally, *LOXL2, TGFβ2, CTGF* and *COL1A* expression was unaffected by AZA treatment, with an increase in AKT1 and ACTA2 expression when treated with 20 µM AZA. Since the majority of these genes are unaffected by AZA treatment, the fibrotic process in this model thus does not seem to be regulated by DNA methylation, but rather through other forms of regulation, such as post-transcriptional regulation. A review by Zhang et al. (2017) suggests that DNA methylation is implicated in cardiac fibrosis, however that only certain environmental stimuli such as hypoxia result in cardiac fibrosis through methylation. This implies that fibrosis could also be activated and driven by different mechanisms independent of DNA methylation [44].

2.5. Conclusion

Taken together, the insult induced in the H9c2 cells by HG+PAL increased inflammation and oxidative stress and reduced mitochondrial membrane potential, increasing apoptosis, however it did not result in a significant change in gene expression related to fibrosis. In addition, treatment with AfriplexGRT™ and Aspalathin did not ameliorate the detrimental effects induced by the HG+PAL treatment. Although changes seen in this study were only marginal, particularly with respect to gene expression levels, literature suggests

longer treatment periods could result in induction of fibrosis, and thus future studies should take into account the length of treatment to induce a fibrotic phenotype. Future research should also focus on the regulation of fibrotic genes by DNA methylation and other epigenetic regulatory factors, because understanding how the fibrotic process is regulated could provide the necessary insight to develop novel treatment plans for fibrotic diseases.

2.6 References

1. World Health Statistics (WHO). New initiative launched to tackle cardiovascular disease, the world's number one killer; *WHO:* Geneva, Switzerland, **2016**.

2. World Health Statistics (WHO). Cardiovascular diseases (CVDs) fact sheet Available online: https://www.who.int/news-room/fact-sheets/detail/cardiovascular-diseases-(cvds) (accessed on Sep 12, 2019).

3. Mittal, M.; Siddiqui, M.R.; Tran, K.; Reddy, S.P.; Malik, A.B. Reactive oxygen species in inflammation and tissue injury. *Antioxidants Redox Signal.* **2014**, *20*, 1126–1167. doi: 10.1089/ars.2012.5149.

4. Travers, J.G.; Kamal, F.A.; Robbins, J.; Yutzey, K.E.; Blaxall, B.C. Cardiac fibrosis: The fibroblast awakens. *Circ. Res.* **2016**, *118*, 1021–1040. doi: 10.1161/CIRCRESAHA.115.306565.

5. Frangogiannis, N.G. The extracellular matrix in ischemic and nonischemic heart failure. *Circ. Res.* **2019**, *125*, 117–146. doi.org/10.1161/CIRCRESAHA.119.311148.

6. Yang, J.; Savvatis, K.; Kang, J.S.; Fan, P.; Zhong, H.; Schwartz, K.; Barry, V.; Mikels-Vigdal, A.; Karpinski, S.; Kornyeyev, D.; et al. Targeting LOXL2 for cardiac interstitial fibrosis and heart failure treatment. *Nat. Commun.* **2016**, *7*, 13710, doi:10.1038/ncomms13710.

7. Baum, J.; Duffy, H.S. Fibroblasts and myofibroblasts: What are we talking about? *J. Cardiovasc. Pharmacol.* **2011**, *57*, 376–379. doi: 10.1097/FJC.0b013e3182116e39.

8. Jang, H.; Serra, C. Nutrition, Epigenetics, and Diseases. *Clin. Nutr. Res.* **2014**, *3*, 1, doi:10.7762/cnr.2014.3.1.1.

9. Zhan, P.; Shen, X.; Qian, Q.; Zhu, J.; Zhang, Y.; Xie, H.-Y.; Xu, C.-H.; Hao, K.; Hu, W.; Xia, N.; et al. Down-regulation of lysyl oxidase-like 2 (LOXL2) is associated with disease progression in lung adenocarcinomas. *Med. Oncol.* **2012**, *29*, 648–655, doi:10.1007/s12032-011-9959-z.

10. Crescenti, A.; Solà, R.; Valls, R.M.; Caimari, A.; del Bas, J.M.; Anguera, A.; Anglés, N.; Arola, L. Cocoa Consumption Alters the Global DNA Methylation of Peripheral Leukocytes in Humans with

Cardiovascular Disease Risk Factors: A Randomized Controlled Trial. *PLoS One* **2013**, *8*, e65744, doi:10.1371/journal.pone.0065744.

11. Link, A.; Balaguer, F.; Goel, A. Cancer chemoprevention by dietary polyphenols: Promising role for epigenetics. *Biochem. Pharmacol.* **2010**, *80*, 1771–1792. doi: 10.1016/j.bcp.2010.06.036.

12. Duthie, S.J. Epigenetic modifications and human pathologies: Cancer and CVD. Proceedings of the Nutrition Society; Proc Nutr Soc, **2011**; Vol. 70, pp. 47–56.

13. Johnson, R.; Dludla, P.; Joubert, E.; February, F.; Mazibuko, S.; Ghoor, S.; Muller, C.; Louw, J. Aspalathin, a dihydrochalcone C-glucoside, protects H9c2 cardiomyocytes against high glucose induced shifts in substrate preference and apoptosis. *Mol. Nutr. Food Res.* **2016**, *60*, 922–934, doi:10.1002/mnfr.201500656.

14. Hu, M.; Ye, P.; Liao, H.; Chen, M.; Yang, F. Metformin Protects H9C2 Cardiomyocytes from High-Glucose and Hypoxia/Reoxygenation Injury via Inhibition of Reactive Oxygen Species Generation and Inflammatory Responses: Role of AMPK and JNK. J. *Diabetes Res.* **2016**, doi:10.1155/2016/2961954.

15. Maeda, M.; Hayashi, T.; Mizuno, N.; Hattori, Y.; Kuzuya, M. Intermittent High Glucose Implements Stress-Induced Senescence in Human Vascular Endothelial Cells: Role of Superoxide Production by NADPH Oxidase. *PLoS One* **2015**, *10*, e0123169, doi:10.1371/journal.pone.0123169.

16. Dludla, P. V.; Muller, C.J.F.; Joubert, E.; Louw, J.; Essop, M.F.; Gabuza, K.B.; Ghoor, S.; Huisamen, B.; Johnson, R. Aspalathin protects the heart against hyperglycemia-induced oxidative damage by up-regulating Nrf2 expression. *Molecules* **2017**, *22*, doi:10.3390/molecules22010129.

17. Wei, C.D.; Li, Y.; Zheng, H.Y.; Tong, Y.Q.; Dai, W. Palmitate induces H9c2 cell apoptosis by increasing reactive oxygen species generation and activation of the ERK1/2 signaling pathway. *Mol. Med. Rep.* **2013**, *7*, 855–861, doi:10.3892/mmr.2013.1276.

18. Li, S.; Li, H.; Yang, D.; Yu, X.; Irwin, D.M.; Niu, G.; Tan, H. Excessive Autophagy Activation and Increased Apoptosis Are Associated with Palmitic Acid-Induced Cardiomyocyte Insulin Resistance. *J. Diabetes Res.* **2017**, *2017*, doi:10.1155/2017/2376893.

19. Dludla, P. V.; Silvestri, S.; Orlando, P.; Mazibuko-Mbeje, S.E.; Johnson, R.; Marcheggiani, F.; Cirilli, I.; Muller, C.J.F.; Louw, J.; Chellan, N.; et al. Palmitate-induced toxicity is associated with impaired mitochondrial respiration and accelerated oxidative stress in cultured cardiomyocytes: The critical role of coenzyme Q9/10. *Toxicol. Vitr.* **2020**, *68*, doi:10.1016/j.tiv.2020.104948.

12. Maehara, Y.; Anai, H.; Tamada, R.; Sugimachi, K. The ATP assay is more sensitive than the succinate dehydrogenase inhibition test for predicting cell viability. *Eur. J. Cancer Clin. Oncol.* **1987**, *23*, 273–276, doi:10.1016/0277-5379(87)90070-8.

21. Kroukamp, M. The effect of chronic ingestion of AfriplexGRT^{TM} on myocardial insulin resistance and mitochondrial function – A preclinical study, Dissertation, Stellenbosch University, **2018**.

22. Mazibuko-Mbeje, S.E.; Dludla, P. V.; Johnson, R.; Joubert, E.; Louw, J.; Ziqubu, K.; Tiano, L.; Silvestri, S.; Orlando, P.; Opoku, A.R.; et al. Aspalathin, a natural product with the potential to reverse hepatic insulin resistance by improving energy metabolism and mitochondrial respiration. *PLoS One* **2019**, *14*, e0216172, doi:10.1371/journal.pone.0216172.

23. Fulda, S.; Gorman, A.M.; Hori, O.; Samali, A. Cellular stress responses: Cell survival and cell death. *Int. J. Cell Biol.* **2010**. doi: 10.1155/2010/245803

24. Ly, L.D.; Xu, S.; Choi, S.-K.; Ha, C.-M.; Thoudam, T.; Cha, S.-K.; Wiederkehr, A.; Wollheim, C.B.; Lee, I.-K.; Park, K.-S. Oxidative stress and calcium dysregulation by palmitate in type 2 diabetes. *Exp. Mol. Med.* **2017**, *49*, e291–e291, doi:10.1038/emm.2016.157.

25. Sharma, M.; Boytard, L.; Hadi, T.; Koelwyn, G.; Simon, R.; Ouimet, M.; Seifert, L.; Spiro, W.; Yan, B.; Hutchison, S.; et al. Enhanced glycolysis and HIF-1α activation in adipose tissue macrophages sustains local and systemic interleukin-1β production in obesity. *Sci. Rep.* **2020**, *10*, 1–12, doi:10.1038/s41598-020-62272-9.

26. Staiger, H.; Staiger, K.; Stefan, N.; Wahl, H.G.; Machicao, F.; Kellerer, M.; Häring, H.U. Palmitate-induced interleukin-6 expression in human coronary artery endothelial cells. *Diabetes* **2004**, *53*, 3209–3216, doi:10.2337/diabetes.53.12.3209.

27. Igoillo-Esteve, M.; Marselli, L.; Cunha, D.A.; Ladrière, L.; Ortis, F.; Grieco, F.A.; Dotta, F.; Weir, G.C.; Marchetti, P.; Eizirik, D.L.; et al. Palmitate induces a pro-inflammatory response in human pancreatic islets that mimics CCL2 expression by beta cells in type 2 diabetes. *Diabetologia* **2010**, *53*, 1395–1405, doi:10.1007/s00125-010-1707-y.

28. Da Costa, R.M.; Rodrigues, D.; Pereira, C.A.; Silva, J.F.; Alves, J. V.; Lobato, N.S.; Tostes, R.C. Nrf2 as a potential mediator of cardiovascular risk in metabolic diseases. *Front. Pharmacol.* **2019**, *10*, 382. doi: 10.3389/fphar.2019.00382

29. Valenzuela, R.; Illesca, P.; Echeverría, F.; Espinosa, A.; Rincón-Cervera, M.Á.; Ortiz, M.; Hernandez-Rodas, M.C.; Valenzuela, A.; Videla, L.A. Molecular adaptations underlying the beneficial effects of hydroxytyrosol in the pathogenic alterations induced by a high-fat diet in mouse liver: PPAR-α and Nrf2 activation, and NF-κB down-regulation. *Food Funct.* **2017**, *8*, 1526–1537, doi:10.1039/c7fo00090a.

30. Yu, H.; Zhen, J.; Yang, Y.; Du, J.; Leng, J.; Tong, Q. Rg1 protects H9c2 cells from high glucose-/palmitate-induced injury via activation of AKT/GSK-3β/Nrf2 pathway. *J. Cell. Mol. Med.* **2020**, *24*, 8194–8205, doi:10.1111/jcmm.15486.

31. Nemecz, M.; Constantin, A.; Dumitrescu, M.; Alexandru, N.; Filippi, A.; Tanko, G.; Georgescu, A. The distinct effects of palmitic and oleic acid on pancreatic beta cell function: The elucidation of associated mechanisms and effector molecules. *Front. Pharmacol.* **2019**, *9*, 1554, doi:10.3389/fphar.2018.01554.

32. Alnahdi, A.; John, A.; Raza, H. Augmentation of glucotoxicity, oxidative stress, apoptosis and mitochondrial dysfunction in hepg2 cells by palmitic acid. *Nutrients* **2019**, *11*, doi:10.3390/nu11091979.

33. Koziel, A.; Woyda-Ploszczyca, A.; Kicinska, A.; Jarmuszkiewicz, W. The influence of high glucose on the aerobic metabolism of endothelial EA.hy926 cells. *Pflugers Arch. Eur. J. Physiol.* **2012**, *464*, 657–669, doi:10.1007/s00424-012-1156-1.

34. Sikder, K.; Shukla, S.K.; Patel, N.; Singh, H.; Rafiq, K. High Fat Diet Upregulates Fatty Acid Oxidation

and Ketogenesis via Intervention of PPAR-γ. *Cell. Physiol. Biochem.* **2018**, *48*, 1317–1331, doi:10.1159/000492091.

35. Nisr, R.B.; Affourtit, C. Palmitate-induced changes in energy demand cause reallocation of ATP supply in rat and human skeletal muscle cells. *Biochim. Biophys. Acta - Bioenerg.* **2016**, *1857*, 1403–1411, doi:10.1016/j.bbabio.2016.04.286.

36. He, Y.; Zhou, L.; Fan, Z.; Liu, S.; Fang, W. Palmitic acid, but not high-glucose, induced myocardial apoptosis is alleviated by N-acetylcysteine due to attenuated mitochondrial-derived ROS accumulation-induced endoplasmic reticulum stress. *Cell Death Dis.* **2018**, *9*, 1–15, doi:10.1038/s41419-018-0593-y.

37. Millar, D.A.; Bowles, S.; Windvogel, S.L.; Louw, J.; Muller, C.J.F. Effect of Rooibos (Aspalathus linearis) extract on atorvastatin-induced toxicity in C3A liver cells. *J. Cell. Physiol.* **2020**, *235*, 9487–9496, doi:10.1002/jcp.29756.

38. Joubert, E.; Winterton, P.; Britz, T.J.; Ferreira, D. Superoxide anion and α, α-diphenyl-β-picrylhydrazyl radical scavenging capacity of rooibos (Aspalathus linearis) aqueous extracts, crude phenolic fractions, tannin and flavonoids. *Food Res. Int.* **2004**, *37*, 133–138, doi:10.1016/j.foodres.2003.09.011.

39. Jastroch, M.; Divakaruni, A.S.; Mookerjee, S.; Treberg, J.R.; Brand, M.D. Mitochondrial proton and electron leaks. *Essays Biochem*. **2010**;47:53-67. doi:10.1042/bse0470053

40. Xiao, Y.; Deng, J.; Li, C.; Gong, X.; Gui, Z.; Huang, J.; Zhang, Y.; Liu, Y.; Ye, X.; Li, X. Epiberberine ameliorated diabetic nephropathy by inactivating the angiotensinogen (Agt) to repress TGFβ/Smad2 pathway. *Phytomedicine* **2021**, *83*, 153488, doi:10.1016/j.phymed.2021.153488.

41. Wu, L.; Derynck, R. Essential Role of TGF-β Signaling in Glucose-Induced Cell Hypertrophy. *Dev. Cell* **2009**, *17*, 35–48, doi:10.1016/j.devcel.2009.05.010.

42. Johnson, R.; Nxele, X.; Cour, M.; Sangweni, N.; Jooste, T.; Hadebe, N.; Samodien, E.; Benjeddou, M.; Mazino, M.; Louw, J.; et al. Identification of potential biomarkers for predicting the early onset of diabetic cardiomyopathy in a mouse model. *Sci. Rep.* **2020**, *10*, 12352, doi:10.1038/s41598-020-

69254-x.

43. Tam, C.S.; Power, J.E.; Markovic, T.P.; Yee, C.; Morsch, M.; McLennan, S. V.; Twigg, S.M. The effects of high-fat feeding on physical function and skeletal muscle extracellular matrix. *Nutr. Diabetes* **2015**, *5*, 187, doi:10.1038/nutd.2015.39.

44. Zhang, X.; Hu, M.; Lyu, X.; Li, C.; Thannickal, V.J.; Sanders, Y.Y. DNA methylation regulated gene expression in organ fibrosis. *Biochim. Biophys. Acta - Mol. Basis Dis.* **2017**, *1863*, 2389–2397. doi: 10.1016/j.bbadis.2017.05.010.

Chapter 3:

AfriplexGRT™ does not display a cardioprotective effect in males compared to female Wistar rats on a high fat-high sugar diet

3.1. Introduction

Cardiovascular disease (CVDs) is a major health burden worldwide, accounting for 31% of all global mortalities [1]. Various lifestyle risk factors such as urbanization, unhealthy diets and sedentary lifestyles, have contributed to this fast-growing CVD epidemic. Additionally, obesity and diabetes are major determinants of cardiovascular-related morbidity and mortality [2]. Unfortunately, current therapies do not provide substantial protection to the myocardium against these metabolic insults, and since CVD consists of many different subtypes, this adds to the complexity of finding a treatment. Furthermore, various scientific evidence serves to support that males have a greater risk of dying as a result of cardiovascular complications compared to their aged-matched premenopausal female counterparts, which is believed to be due to estrogen [3]. However, estrogen is often dysregulated in diabetic females, who have a 5-times increased risk, and thus this protection is lost. Women often go undiagnosed because the development and symptoms of heart disease often present differently compared to their male counterparts [3]. Pre-clinical studies are mostly performed in males, with females majorly underrepresented, and as such a paucity of data exists where the disease pathology is compared in both genders [4–7], with such gender disparity research being necessary especially in the pursuit of precision medicine.

The modern-day individual is faced with an ever-changing environment and high paced lifestyle, resulting in increased stress and a decreased physical demand. The factors of physical, cognitive, emotional and behavioral distress are all warning signs that constitute a preclinical onset of CVD, in which the disease progresses with no phenotypic pathology. This combination of stress, unhealthy eating and decreased physical activity contributes to the development of hyperglycemic induced cardiac fibrosis [8, 9]. Fibrosis is a major contributing factor to CVD related deaths and occurs when there is an overstimulation of the extracellular matrix (ECM) deposition [10]. While the ECM is necessary for cellular structure as well as stabilization after a cardiac event, the continuous deposition causes cardiac stiffness, resulting in reduced contractility, diminished cardiac output, and consequently, heart failure [10].

Lysyl oxidase-like 2 (LOXL2) is the protein responsible for collagen and elastin cross-linking, which is crucial to the structural integrity provided by the ECM. During a normal state, LOXL2 basal level expression is crucial

for cellular maintenance of the myocardium [11]. However, during a disease state, augmented LOXL2 expression is observed. This has been confirmed by Rodriguez et al. (2019) who performed studies in both humans and in animal models and revealed that the abnormal expression/activity of LOXL2 is linked to CVD [12].

Polyphenols have not only been studied as a treatment for fibrosis [13] but also for CVDs [14]. Mounting evidence, including studies from our group, have shown that polyphenols such as AfriplexGRT™, possess strong antioxidant, anti-inflammatory and anti-obesogenic properties and are thus able to protect the myocardium against cardiac dysfunction [15–18]. Furthermore, it has been reported that polyphenols can have gender-specific effects. For example, genistein has divergent effects on the intracellular calcium ion cycles in male guinea pig myocytes compared to their female counterparts, where the cardioprotective effect was found to be greater for females than males [19]. Another example is from the Shanghai Women's Health Study, where soy protein ingestion was positively correlated with reduced CVD incidence in Chinese women, whilst the male counterparts showed an increased CVD risk [20, 21]. Also, it is known that gender may play a role in the bioavailability of polyphenols [7, 22]. For example, Ekstrand et al. (2015) showed that some flavonoids, a subclass of polyphenols, can affect porcine cytochrome P450s in a gender-dependent manner [23]. There is however no previous study that has investigated whether AfriplexGRT™ has gender-specific effects, particularly on LOXL2 expression. As such, this study will investigate whether AfriplexGRT™ can ameliorate the effect of a high fat, high sugar (HFHS) diet on augmented LOXL2 expression, before any onset of disease pathology. Additionally, the study will investigate differential fibrotic gene expression levels in both male and female animals.

3.2. Material and Methods

3.2.1. Reagents and Kits

The RNeasy Fibrous Mini Kit, DNase treatment kit, cDNA synthesis kit, RT^2 First Strand Kit, RT^2 SYBR Green, qPCR Master Mix, Epitect Bisulfite Conversion kit, and all the Pyromark pyrosequencing products were purchased from Qiagen (Valencia, CA, USA). The Qubit assay tubes, and dsDNA Broad Range assay kit were purchased from Thermofisher Scientific (Massachusetts, USA). The RC/DC protein determination kit, BSA

standards, 12% precast gels, gel marker, Laemmli sample buffer, and running buffer were purchased from Bio-Rad (California, USA). The AfriplexGRT™ was obtained from Afriplex (Paarl, South Africa). All other consumables and reagents, unless otherwise specified, were purchased from Sigma-Aldrich Corp. (St. Louis, MO, USA).

3.2.2. Wistar rat model

3.2.2.1. Ethics

Ethical approval was obtained from the Research Ethics Committee on Animal Care at Stellenbosch University (protocol number ACU-2020-14614) and the Ethics Committee for Research Animals at the South African Medical Research Council (ECRA 10/17). All procedures were performed in accordance with the guidelines for ethical conduct in the care and use of animals [24] and the South African National Standard for animal care (SANS 10386:2008) [25].

3.2.2.2. Preparation of AfriplexGRT™ dosage

The dosage was previously determined in a study by our group in a mouse model and Reagen-Shaw conversion method [26] was used to convert the dosage to a relevant dosage in rats. AfriplexGRT™ was prepared daily and administered in the form of jelly cubes. Briefly, 2g AfriplexGRT™ was dissolved in 100 mL boiled water and set in raspberry flavored jelly cubes with the dose per animal (60 mg/kg bodyweight) aliquots made into numbered cubes. The jelly cubes were made one day before to allow the jelly to set. These were individually administered to each animal at the same time every morning for 9 months, ensuring that they ate the full cube, whilst untreated animals received a jelly cube containing no AfriplexGRT™.

3.2.2.3. Study design: Grouping, diet and AfriplexGRT™ treatment of rats

Wistar rats were obtained and housed at the Primate Unit and Delft Animal Centre (PUDAC) of the South African Medical Research Council (SAMRC) in a temperature-controlled environment (23-25°C) with 12 h light/dark cycle and 50±5% relative humidity. Rats received standard laboratory chow, *ad llibitum* and had free access to water. At 5-weeks old, male (n=40) and female (n=40) rats were randomly assigned into one of four groups (n=10 per group) and fed either a: (1) Control diet (standard rat chow diet: containing 16.89% fat), (2) control diet supplemented with AfriplexGRT™ (60mg/kg), (3) high fat. High sugar (HFHS) diet

(containing 40.52% fat) and (4) HFHS diet, supplemented with AfrplexGRT™ (60mg/kg), as depicted in Figure 3.1.

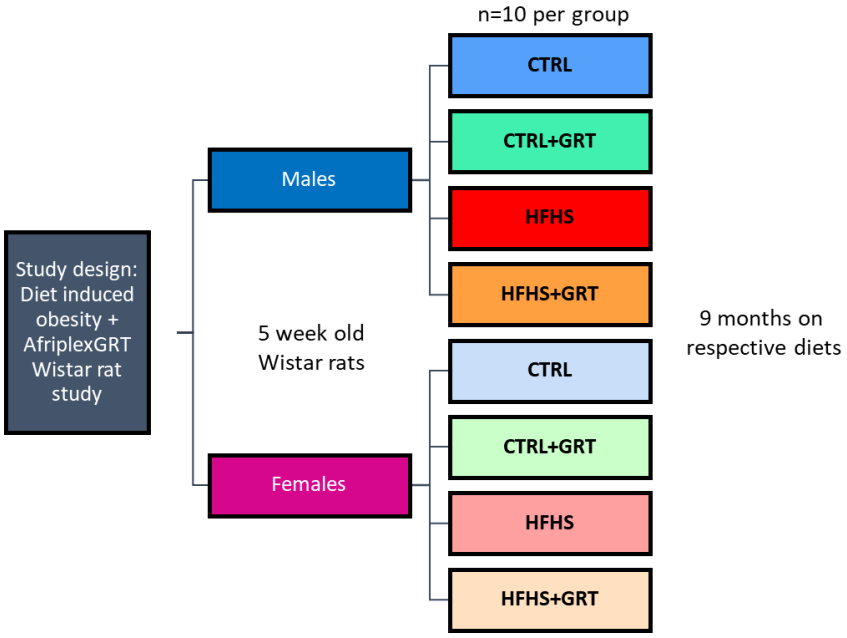

Figure 3.1: Animal study design. Male and female rats (n=40 per group) were each equally split into 4 groups and fed a control diet (CTRL), a control diet supplemented with 60mg/kg AfriplexGRT™ (CTRL+GRT), a high fat, high sugar diet (HFHS) or high fat, high sugar diet, supplemented with 60mg/kg AfrplexGRT™ (HFHS+GRT). Animals were on the respective diets for 9 months.

All rats were individually caged and fed the respective diets for 9 months. The standard rat chow (Rodent breeder laboratory animal diet) was bought from LabChef Research Nutrition™ (Stellenbosch, South Africa, Cat# LAB/RB2005) and the HFHS diet was made in-house at PUDAC (see Supplementary Table A1.1 in Appendix 1 for detailed macronutrient diet composition). Food consumption and water intake were measured twice weekly. Initial bodyweights were recorded at the start of the study and measured weekly thereafter. In addition, oral glucose tolerance tests (OGTTs) were performed every three months and fasting blood glucose was measured by tail-prick monthly. After 9 months on the diet, rats were fasted for 16 hours and anesthetized using isoflurane and sacrificed by exsanguination. The heart weight, fat weight, liver weight, bodyweight and heart/bodyweight ratio were recorded at termination. Heart tissue was collected for RNA, protein and histological analysis, and blood was collected for serum analysis.

3.2.3. Biochemical analysis

3.2.3.1. Bodyweight

The animals were weighed weekly, without prior fasting, using a calibrated gram scale. Values were recorded and an average weight per rat for each group was calculated monthly and plotted. The weight gained throughout the study was calculated as the final bodyweight at termination, minus the bodyweight at the start of feeding when the rats were 5 weeks old.

3.2.3.2. Food and water intake monitoring

Food and water intake were monitored twice weekly and estimated food and water consumption measured as follows: each cage received 150 mL water and a pre-weighed amount of food (pellets for the control diet and patties for the HFHS diet). Estimated food consumption was calculated by subtracting the amount of food remaining after 24 hours from the initial amount. The loss of water in the patties was corrected for by separately weighing a patty before and after feeding and calculating the percentage weight loss to the effect of patties drying out. Estimated water consumption was calculated as water intake per cage by subtracting remaining water after 24 hours from the initial 150 mL. A note was made about water bottles that were empty because of leakage, and their totals removed from the average water consumption calculations.

3.2.3.3. Fasting blood glucose level

After 16 hours of fasting (with only access to tap water, *ad libitium*), blood glucose levels were measured by means of a tail prick. Briefly, the second drop of blood was collected from the tip of the tail and the resulting blood droplet placed onto a OneTouch Select® (LifeScan Inc., California, United States) glucose strip and the glucose concentration determined using the OneTouch Select® glucometer (LifeScan Inc., California, United States).

3.2.3.4. Oral Glucose Tolerance test

Every 3 months an oral glucose tolerance test (OGTT) was performed after 16-hour fasting. Rats were orally gavaged with 4 mL/kg bodyweight dextrose, after which blood glucose concentrations were measured at 15, 30, 60 and 120 minutes by means of a tail prick.

3.2.3.5. Blood collection and tissue harvested

After the 16 hours fast, animals were anaesthetized (0.9 L/min oxygen and 3.5-55 vaporized Isoflurane) and a paddle reflex check done to confirm non-responsiveness. A midline abdominal incision was made, and blood collected from the aorta and transferred to a serum separating tube. Blood aliquots were left at 4°C for 2 hours, whereafter serum was separated by centrifugation at 4 000 rcf for 15 minutes at 4°C. Aliquots were made and stored at -80°C until required. Heart tissue was harvested and stored in either RNA*later* (Life Technology, California, USA) for RNA expression analysis at -20°C or snap-frozen and stored at -80°C until required for DNA and protein expression analysis.

3.2.3.6. HOMA-IR

Fasting blood glucose levels of Wistar rats fasted for 16 hours were measured using a OneTouch Select® glucometer (LifeScan Inc., California, United States). The HOMA-IRs were then calculated by applying the formula [27]: fasting insulin (µU/L) x fasting glucose (nmol/L)/22.5.

3.2.3.7. Lipid Profile and liver enzyme analysis

At termination, 16-hour fasted serum was collected and sent to Pathcare (Cape Town, South Africa) for a lipid profile analysis where the triglyceride, low-density lipoprotein (LDL), high-density lipoprotein (HDL) and total cholesterol levels, as well as liver enzymes aspartate transaminase (AST) and alanine aminotransferase (ALT) levels, were measured.

3.2.3.8. Enzyme-linked immunosorbent assay (ELISA) analysis

3.2.3.8.1. Serum Insulin analysis

Serum insulin levels were determined utilizing a Millipore Sandwich rat/mouse insulin ELISA kit (Merck, Massachusetts, USA) as per the manufacturer's instructions. Briefly, the ELISA uses monoclonal mouse anti-rat insulin antibodies and the binding of biotinylated polyclonal antibodies to the captured insulin and horseradish peroxidase and 3,3',5,5'-tetramethylbenzidine to quantify the insulin. The plate was read at an absorbance of 450 nm and 590 nm using SpectraMax i3 plate reader (Molecular Devices, California, USA).

3.2.3.8.2. Serum LOXL2 analysis

Serum LOXL2 levels were determined using a rat lysyl oxidase-like protein 2 (LOXL2) sandwich ELISA kit (MyBioSource, California, United States, cat#: MBS2705848) as per manufacturer's instructions. Briefly, the ELISA makes use of a LOXL2 specific antibody and biotin-conjugated antibodies to the captured LOXL2 and Avidin-conjugated horseradish peroxidase and TMB substrate to quantify the LOXL2. The plate was read at an absorbance of 450 nm using SpectraMax i3 plate reader (Molecular Devices, California, USA).

3.2.3.9. Histology and microscopy analysis

Heart tissue was fixed in 10% formalin and embedded in paraffin immediately upon collection according to a previously described protocol [28]. Sections of 5µm were cut from the paraffin-embedded blocks, fixed onto glass slides and stained with either hematoxylin and eosin stain (Merck-Millipore, Billerica, USA), trichrome (staining collagen) (Abcam, Cambridge, United Kingdom, cat# ab150686) or probed with anti-LOXL2 antibody (Biocom Africa, Johannesburg, South Africa, cat# AB96233), as per manufacturer's instructions. For histological analysis, 5 random areas of each of the 10 sections per group were digitized using an Olympus BX50 light microscope (20x and 40x magnification) and NIS-Elements BR 3.0 computerized image analysis software (Nikon, Tokyo, Japan).

3.2.3.9.1. Haemotoxylin & Eosin staining

Hematoxylin and Eosin stain (H&E) (Merck-Millipore, Billerica, USA) was performed by standard laboratory procedures. Briefly, tissue was stained with haematoxylin for 12 minutes and washed in distilled water. Slides were then placed under running tap-water for 10 minutes to allow the blue colour to develop. The tissue was then counterstained in 1% aqueous eosin stain for 2 minutes and washed with distilled water. The slides were dehydrated with alcohol, cleared with xylene and dried after which a coverslip was mounted with DPX. For histological analysis, 5 random areas of each of the 10 sections per group were digitized using an Olympus BX50 light microscope (20x and 40x magnification) and NIS-Elements BR 3.0 computerized image analysis software (Nikon, Tokyo, Japan). These slides were then sent to Idexx Laboratories (Johannesburg, South Africa) for analysis.

3.2.3.9.2. Trichrome staining

Trichrome staining is performed by standard laboratory procedures. Briefly, slides were placed in preheated Bouin's fluid and rinsed with water. Slides were stained with Weigert's iron haematoxylin stain followed by Biebrich scarlet/acid fuchsin solution. The stain was then differentiated in phosphomolybic/phosphotungstic acid solution followed by aniline blue solution (Sigma-Aldrich, Missouri, USA). Slides were cleared with xylene, then dried, whereafter a cover slip was mounted with DPX. For histological analysis, 5 random areas of each of the 10 sections per group were digitized using an Olympus BX50 light microscope (20x and 40x magnification) and NIS-Elements BR 3.0 computerized image analysis software (Nikon, Tokyo, Japan). These slides were then sent to Idexx Laboratories (Johannesburg, South Africa) for analysis.

3.2.3.9.3. Immunohistochemistry – LOXL2

Heart tissue slides was immunohistochemically labelled with anti-LOXL2 using standard laboratory procedures. Briefly, after the dewaxing process, the tissue was blocked for endogenous peroxidases in 3% hydrogen peroxide and rinsed. Slides were then treated in a 0.01 M citrate buffer (pH 6.0) in a Pascal pressure chamber (125°C for 30 seconds, then 90°C for 10 seconds) and allowed to cool for 20 minutes and rinsed with water. Slides were washed with Tris-buffered saline (TBS) (pH 7.2) then placed in a moisture chamber and normal goat serum (1:20) applied. After removal of the goat serum, slides were incubated overnight at 4°C in anti-LOXL2 primary antibody (1:50). Slides were then washed with TBS (pH 7.2), after which the secondary anti-rabbit IgG (1:200) was applied for 30 minutes at room temperature followed by the incubation with Vectastain for 60 minutes at room temperature. After washing with TBS, liquid DAB+ substrate solution added for 5 minutes followed by a haemotoxylin counterstain. The slides were rinsed in tap water for the blue colour to develop and then dried and a cover slip was mounted with DPX. For histological analysis, 5 random areas of each of the 10 sections per group were digitized using an Olympus BX50 light microscope (20x and 40x magnification) and NIS-Elements BR 3.0 computerized image analysis software (Nikon, Tokyo, Japan).

3.2.4. Gene and Protein expression analysis

Pyrosequencing analysis was done to assess changes in DNA methylation patterns as a result of altered diet, whilst quantitative real-time polymerase reaction (qRT-PCR) analysis was used to assess mRNA expression levels in the heart. Protein was extracted to assess whether changes in mRNA expression were translated to protein expression levels in the rat hearts.

3.2.4.1. Investigating methylation signatures

3.2.4.1.1. Pyrosequencing primer design

The LOXL2 DNA sequence was obtained from Ensembl and the relevant highly methylated region or region of interest was identified from literature [29, 30]. For *LOXL2*, pyrosequencing primers were designed using the Pyromark Assay Design 2.0 software. Primer sequences used are listed in Table 3.1.

Table 3.1: A list of the methylation sequencing primers used for pyrosequencing.

Primers designed using Pyromark Assay Design 2.0 software		
Gene	**Forward Primer**	**Reverse Primer**
LOXL2	AGAGTTTAAATATATAGGTGGAAGATA	ACTATCCAATACTTATCACAAATCTACT*

3.2.4.1.2. DNA extraction

Approximately 20-25mg frozen heart tissue was weighed into a clean 2 mL Eppendorf tube containing a steel bead followed by the addition of 1 mL lysis buffer (400 mM NaCl, 10 mM Tric-Cl, pH 8.0) and 10 µL Proteinase K. The tissue was homogenized using a Qiagen 85210 tissue lyser (Hilden, Germany) five times at 25 Hz followed by incubation overnight at 56°C. After incubation, 333 µL 5/6 M NaCl was added and mixed vigorously after which the cell debris was pelleted by centrifugation at maximum speed for 10 minutes. The aqueous phase was transferred to a clean tube followed by the addition of 500 µL cold isopropanol and incubation for 30 minutes at -80°C. The DNA was then pelleted by centrifugation at maximum speed for 10 minutes, followed by washing of the pellet with 500 µL ethanol four times to remove any salt in the pellet. The pellet was then air-dried and resuspended in 100 µL Ambion nuclease-free water (Thermo Fisher Scientific, Massachusetts, USA). The product was stored at -20°C until use.

3.2.4.1.3. DNA concentration determination

DNA concentration was determined using a Qubit dsDNA Broad Range assay kit (Thermo Fisher Scientific, Massachusetts, USA) as per the manufacturer's instructions. Briefly, reagents were allowed to reach room temperature, after which Qubit reagent was made up by combining Qubit dsDNA BR Reagent with the Qubit dsDNA BR Buffer in a 1:200 ratio. Next, 10 µL of each of the two standards and 2 µL of each sample were placed in separate 0.5 mL tubes and Qubit reagent added to a final volume of 200 µL. After incubation for 2 minutes at room temperature, the concentrations were determined using a Qubit fluorometer (Thermo Fisher Scientific, Massachusetts, USA).

3.2.4.1.4. Bisulfite conversion and clean-up

Using an Epitect Fast DNA Bisulfite Conversion Kit (Qiagen, Hilden, Germany), 500 ng of the extracted DNA was bisulfite converted following the manufacturer's instructions. The conversion was done in an Applied Biosystems™ Veriti™ 96-Well Thermal Cycler (Thermo Fisher Scientific, Massachusetts, USA, cat# 4375786) using the following conditions: denaturation at 95°C for 5 minutes, incubation at 60°C for 20 minutes, denaturation at 95°C for 5 minutes and incubation at 60°C for 20 minutes followed by an infinite hold at 20°C. This was followed by a clean-up step, where the bisulfite converted product was transferred to a 1.5 mL Eppendorf tube and buffer BL added, followed by the addition of 250 µL of absolute ethanol and mixing with a vortex. This mixture was then transferred to a MiniElute DNA spin column and centrifuged at maximum speed (15000 rpm) for one minute, and the flow-through discarded. The column was then washed with buffer BW and again the flow-through was discarded. Thereafter Buffer BD was added to the column and incubated for 15 minutes at room temperature before centrifugation at maximum speed for one minute, and the flow-through discarded. Following a further 2 washes with buffer BW, absolute ethanol was added to each column and centrifuged twice for 1 minute at maximum speed, and incubation for 5 minutes at 60°C to ensure that there is no liquid left in the column. The columns were then placed into a new 1.5 mL collection tubes and the DNA eluted in 15 µL buffer EB, and the product stored at -20°C until use.

3.2.4.1.5. PCR

The bisulfite converted DNA was amplified using a Pyromark PCR kit (Qiagen, Hilden, Germany) as per the manufacturer's instructions. Briefly, the PCR reaction consisted of 33 ng bisulfite converted DNA, and final concentrations of 1x PCR master mix, 1x coral load, 2.5 mM $MgCl_2$, and 0.2µM of each primer in a final volume of 25 µL. Thermocycling conditions were as follows: PCR activation hold at 95°C for 5 minutes, followed by 94°C for 30 seconds, 56°C for 30 seconds, and 72°C for 30 seconds for 45 cycles, followed by a final extension at 72°C for 10 minutes. This PCR product was run on a 1% agarose gel containing 10 µL GelStar gel stain, for 1 hour at 100 volts and visualized using a Chemidoc MP imaging system (Bio-Rad, California, USA) to check for contamination of the PCR product.

3.2.4.1.6. Pyrosequencing

Pyrosequencing was performed on the PCR product using a Pyromark Q96 ID platform (Qiagen, Hilden, Germany), as per the manufacturer's instructions. Briefly, a master mix was made up containing 1.5 µL Streptavidin beads, 40 µL binding buffer and 28.5 µL nuclease-free water per sample, after which 70 µL of this master mix was combined with 10 µL PCR product in a 96-well PCR plate. These were then mixed on an orbital shaker at 1400 rpm for 10 minutes. A second mix was made up containing a final concentration of 0.4 µM sequencing primer in annealing buffer, and 40 µL of this mix was aliquoted into each corresponding well in a Pyromark Q96 plate low.

After flushing of the Pyromark Q96 ID platform probe, the probe was placed in the PCR plate and the beads collected after which it was washed with 70% ethanol, denaturation buffer and wash buffer, respectively. The probe was then placed above the plate low, the vacuum turned off and the beads were shaken out into the plate low. The plate low was then incubated at 80°C for 2 minutes and allowed to cool to room temperature.

Reconstituted enzyme and substrate mixes, as well as the required volumes of NTPs, were added to a cartridge, which was placed in the Pyromark Q96 instrument. The plate low was added to the instruments plate chamber and the run initiated according to pre-set-up files and respective NTP dispensation orders of the specific primers. The results were then analyzed using the PyroMark Q96 SW software.

3.2.4.2. mRNA expression analysis

3.2.4.2.1. RNA extraction

Total RNA was extracted from tissue stored in Invitrogen Ambion RNA later solution (Life Technologies, California, USA, cat# AM7021), using a Qiagen RNeasy Fibrous Mini Kit (The Scientific Group, South Africa, cat# QIA/74704) as per manufacturer's instructions. Briefly, 25 mg of heart tissue was homogenized in a mixture of buffer RLT and proteinase K, using a Qiagen 85210 tissue lyser (Hilden, Germany) followed by incubation at 55°C for 10 minutes. The mixture was then centrifuged at 10 000 rcf for the cell debris to pellet, and the supernatant transferred to a new tube where 0.5 volumes of absolute ethanol were added, and the contents of the tube transferred to a RNeasy Mini column and spun down at 8 000 rcf for 15 seconds. Following, buffers RW1 and RPE were added to the column, which was then subjected to centrifugation at 8000 rcf for 15 seconds, and the flow-through was discarded each time. The RNA was eluted from the column by the addition of 30 µL RNase-free water, followed by centrifugation at 8 000 rcf for 1 minute.

3.2.4.2.2. RNA quantification

The mRNA concentrations were then measured using a NanoDrop One system (Thermo Fisher Scientific, Massachusetts, USA), using RNase-free water as a blank and taking readings of 1 µL of each sample in duplicate. The average of each reading was used as the final concentration, and the 260/280 and 260/230 ratios were used as an indicator of RNA integrity and purity.

3.2.4.2.3. DNase treatment

DNase treatment was performed on 20 µg of RNA using an Invitrogen Ambion DNase kit (Thermo Fisher Scientific, Massachusetts, USA) as per the manufacturer's instructions. Briefly, 20 ng total RNA was incubated with 5 µL DNase buffer and 1 µL DNase made up to a final volume of 49 µL with nuclease-free water. The sample was incubated for 30 minutes at 37°C, followed by the addition of another 1 µL DNase and incubation for a further 30 minutes. Thereafter, 10 µL DNAse inactivation reagent was added and incubated for 5 minutes at room temperature, after which the tubes were centrifuged at 10 000 rcf for 1.5 minutes and the RNA transferred to a clean tube while avoiding the precipitated inactivation reagent.

3.2.4.2.4. cDNA synthesis

Total RNA was reverse transcribed to complementary DNA (cDNA) using a High-Capacity cDNA Reverse transcription kit (Thermo Fisher Scientific, Massachusetts, USA) as per the manufacturer's instructions. Briefly, an RT positive and RT negative mixture was made for each sample containing a final concentration of 1µg RNA, 2x RT buffer, 2x dNTP mix, 2x random primers, 20 U RNase inhibitor (Thermo Fisher Scientific, Massachusetts, USA), 1 µL reverse transcriptase and nuclease-free water to a total reaction volume of 20 µL, where the RT negative reactions did not contain the reverse transcriptase. The PCR reaction was run in an Applied Biosystems™ Veriti™ 96-Well Thermal Cycler (Thermo Fisher Scientific, Massachusetts, USA) at 25°C for 10 minutes, 37°C for 120 minutes, 85°C for 5 seconds ending with an infinite hold at 4°C.

3.2.4.2.5. Assessment of genomic DNA contamination

In order to assess whether the synthesized cDNA contains and genomic DNA, 1 µL of the RT-positive and RT-negative reactions was added to a PCR plate and 24 µL of a master mix containing 1x SYBR Green PCR mix, 400 nM each, β-actin forward and reverse primers and RNase-free water. The PCR was run on the Quantstudio 7 Flex Real-Time PCR system (Thermo Fisher Scientific, Massachusetts, USA). Thermocycling conditions were as follows: PCR activation at 95°C for 15 minutes, followed by denaturation at 94°C for 15 seconds, annealing at 60°C for 20 seconds and extension at 95°C for 35 seconds for 40 cycles, followed by an infinite hold at 4°C.

Upon completion of the run, the generated Ct values obtained for the RT-positive reactions were subtracted from the Ct values obtained from the RT-negative reactions, and a difference of 10 cycles or more was considered to have insignificant genomic DNA contamination. Only the RT-positive reactions were used for further analysis.

3.2.4.2.6. Quantitative Real-Time PCR (qRT-PCR)

cDNA was used for expression analysis by means of qRT-PCR. Briefly, Taqman® Gene Expression assays were purchased from Thermofisher Scientific (Massachusetts, USA). The genes analyzed are found in Table 3.2.

Table 3.2: Taqman® Gene Expression assay list.

Gene Name	Description	Taqman® Assay ID
LOXL2	Lysyl oxidase-like 2	Rn01466080_m1
COL1A1	Collagen, type I, alpha 1	Rn01463848_m1
α-SMA (ACTA2)	Actin alpha 2 (alpha-smooth muscle actin)	Rn01759928_g1
SMAD2	Mothers against decapentaplegic homolog 2	Rn00569900_m1
SMAD3	Mothers against decapentaplegic homolog 3	Rn00565331_m1
CTGF	Connective tissue growth factor	Rn01537279_g1
TGFβ2	Transforming growth factor beta-2	Rn00676060_m1
HIF1A	Hypoxia-inducible factor 1-alpha	Rn01472831_m1
AKT1	Protein kinase B	Rn00583646_m1
SOD2	Superoxide dismutase 2	Rn00690588_g1
NRF2 (NFE2L2)	Nuclear factor erythroid 2-related factor 2	Rn00582415_m1
ACTβ	Beta-actin	Rn00667869_m1
HPRT	Hypoxanthine-guanine phosphoribosyltransferase 1	Rn01527840_m1

A standard curve set up to determine the relative expression of each gene; for the standard curve, equal volumes of each of the samples to be run were combined in one tube and a 10-fold dilution series made of this mixture. For qRT-PCR, 10 µL reactions were prepared, containing 1 µL DNA, 5 µL Applied Biosystems™ TaqMan™ Fast Advanced Master Mix (Thermo Fisher Scientific, Massachusetts, USA), 0.5 µL probe and 3.5 µL nuclease-free water for a total reaction volume of 10 µL per well.

These samples were run on a Quantstudio 7 Flex Real-Time PCR system (Thermo Fisher Scientific, Massachusetts, USA). Thermocycling conditions were as follows: hold at 95°C for 20 seconds, followed by 95°C for 1 second, 60°C for 20 seconds for 40 cycles.

3.2.4.2.7. RT^2 PCR Rat Fibrosis Profiler Array

A profiler PCR array specifically aimed at analyzing the expression of fibrotic genes was performed to identify quantify other genes that could be affecting fibrosis in the heart tissue, not initially studied in the qRT-PCR analysis. These profiler arrays were performed as per the manufacturer's instructions. Briefly, the DNase treated RNA was converted to cDNA using a RT^2 First Strand kit (Qiagen, Hilden, Germany) as per the

manufacturer's instructions. The Fibrosis profiler array (QIA/330231_PARN-120ZA-2) was set up with 2 control samples and 2 HFHS diet-fed rat samples per array plate. The array was run on a Quantstudio 7 Flex Real-Time PCR system (Thermo Fisher Scientific, Massachusetts, USA). Thermocycling conditions were as follows: hold at 95°C for 10 minutes, followed by 95°C for 15 seconds, 55°C for 40 seconds and 72°C for 30 seconds, for 45 cycles.

The array data was analyzed by using a Microsoft Excel Macro provided by Qiagen GeneGlobe (https://dataanalysis2.qiagen.com/static/templates/RT2_Profiler_Custom_PCR_Array_Template.xlsx) and uploading it to the GeneGlobe analysis website. Data was normalized to housekeeping genes beta-actin (*ACTβ*), beta-2-(β2)-microglobulin (*β2M*), hypoxanthine phosphoribosyltransferase 1 (*HPRT1*), lactate dehydrogenase A (*LDHA*), and large ribosomal subunit protein P1 (*RPLP1*). The ΔΔCt method was used to analyse the quantification of each gene, and candidates with Ct values > 35 were excluded from the analysis.

3.2.4.3. Protein expression analysis

3.2.4.3.1. Protein extraction

Rat heart tissue was cut, and 20-25 mg of tissue was added to tissue lysis buffer containing protease inhibitor and phosphor inhibitor tablets and 1mM PMSF. The tissue was then homogenized using a steel bead, on a Qiagen 85210 tissue lyser (Hilden, Germany) 4 times at 25Hz for 1 minute, followed by centrifugation at 10 000 rcf for 5 minutes, and the supernatant transferred to a clean tube.

3.2.4.3.2. Quantification of proteins

Protein concentration was determined by means of a reducing agent compatible and detergent compatible (RC/DC) Protein Assay (Bio-Rad, California, USA) according to the manufacturer's instructions. Briefly, 20 µL DC reagent S was aged to every 1 mL of DC reagent A to make reagent A'. 5 µL BSA protein concentration standards (0, 0.125, 0.25, 0.5, 0.75, 1, 1.5 and 2.0 mg/mL) and 20x dilution of each unknown sample were pipetted into a 96-well clear plate in duplicate and 25 µL reagent A' added to each well. 200 µL of DC reagent B was then added to each well and after mixing on a plate shaker for 10 seconds, the absorbance measured 695nm using a SpectraMax i3 plate reader (Molecular Devices, California, USA) and protein concentrations extrapolated from the BSA standard curve generated.

3.2.4.3.3. Western Blot analysis

For western blot analysis, 30 µg of the extracted proteins were run on a 12% precast gel (BioRad Laboratories, California, USA) and transferred to a nitrocellulose membrane. The membrane was stained for total protein with Ponceau stain for 5 minutes on an orbital shaker and imaged, after which the stain was reversed by washing in 1x Tris Buffered Saline with Tween 20 (TBST). The membrane was then blocked with 5% (w/v) skim milk (Sigma) in TBST for minimum of 2 hours on a shaker, after which it was incubated overnight with the primary antibody in 1x TBST. The antibodies and their dilutions used are listed below.

Table 3.3: List of primary antibodies and their dilutions used for Western Blot analysis.

Antibody	Company	Cat#	Dilution
CTGF	Santa Cruz	Sc-365970	1:500
p-SMAD2	Abcam	Ab53100	1:250
LOXL2	Abcam	Ab96233	1:500
β-actin	Santa Cruz	Sc-47778	1:2000

The membrane was washed for 3x 10 minutes with TBST, after which it was incubated with secondary antibody in 2.5% skim milk in 1xTBST at room temperature for 1-1.5 hours and again washed for 3x 10 minutes with TBST. The detection was done using a Clarity Western ECL substrate chemiluminescent detection kit (Bio-Rad, California, USA) and visualized using a Chemidoc MP imaging system (Bio-Rad, California, USA). If stripped, the blot was washed with 1 x TBST for 2 minutes and incubated in Restore Plus Western blot stripping buffer (Thermo Fisher Scientific, Massachusetts, USA,) for 7-8 minutes, followed by another wash step as before.

3.2.5. Statistical Analysis

All data were analyzed using GraphPad Prism 5.04 (GraphPad Software, California, USA) and expressed as mean ± the standard error of the mean (SEM). Data was tested for normal distribution using a Shapiro-Wilks

test, followed by a one-way ANOVA with a Tukey's multiple comparison post hoc or a two-way ANOVA with a Bonferroni post hoc, where applicable. A p-value of < 0.05 was considered to be statistically significant.

3.3. Results

Male and female animals were each split into one of four groups and fed either a: (1) Control diet (standard rat chow diet), (2) control diet supplemented with AfriplexGRT™ (60mg/kg), (3) HFHS diet, or (4) HFHS diet, supplemented with AfriplexGRT™ (60 mg/kg) (Figure 3.1). After 9 months on their respective diets, the tissue was collected for subsequent molecular experiments to assess the effect of both gender and the diets on fibrosis of the heart.

3.3.1. Biochemical Analysis

3.3.1.1. Nutritional composition of diets

Samples of the control (CTRL) diet pellets and HFHS patties were sent to Microchem Lab Services (Pty) Ltd for chemical composition analysis to ascertain the amount of fat, protein, carbohydrates and fiber contained within each individual diet.

Table 3.4: Diet composition of the standard rodent diet compared to the high fat patty.

Component	CTRL diet	HFHS diet
Fat (g/100g)	5.89	10.61
Protein (g/100g)	26.8	9.1
Dietary Fiber (g/100g)	17.2	5.3
Carbohydrates (g/100g)	43.8	22.3
Total calories (kcal/g)	**3.01**	**2.10**

3.3.1.2. Caloric intake

The energy intake was estimated and expressed as caloric intake per gram of food (kcal/g). The caloric intake for all diet groups is given in Figure 3.2. As per the diet composition analysis, animals fed a standard rodent chow and a high fat diet received 3.01 kcal/g and 2.1 kcal/g, respectively, with the latter containing more moisture (Table 3.4). The control diet-fed animals received tap water, therefore no extra calories were added,

whereas the HFHS fed animals received water *ad libitum* containing sucrose and fructose, thus adding a further 0.569 kcal/mL of water consumed (Table 3.4 and Figure 3.2).

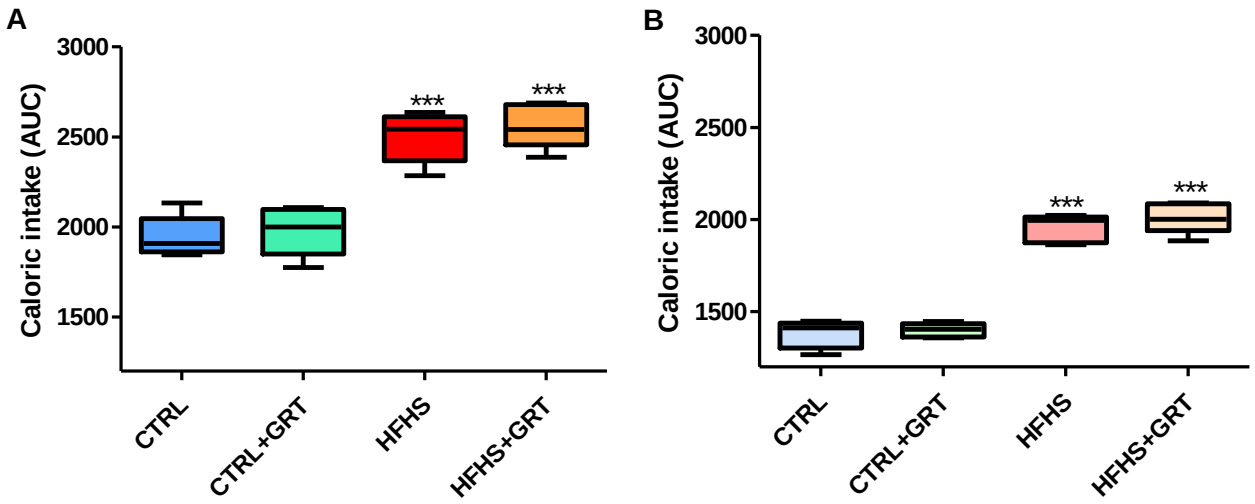

Figure 3.2: Area under the curve (AUC) analysis of the caloric intake. Box and whisker plots display AUC of the caloric intake of A) male and B) female Wistar rats over the 9-month period on their respective diets. The AUC was calculated over the full 9-month period. Data are presented as the mean ± SEM of n=10 animals per group. A one-way ANOVA was performed, and statistical significance is depicted as *** p≤0.001 versus control group.

The area under the curve (AUC) analysis was performed for the evaluation of caloric intake. The AUC over the 9-month feeding period showed that the caloric intake was 1945 ± 50.6 kcal and 1979 ± 60.5 kcal for the male CTRL and CTRL+AfriplexGRT™ groups, respectively, and 2500 ± 62.0 kcal and 2563 ± 54.8 kcal for the male HFHS and HFHS+AfriplexGRT™ fed groups respectively (Figure 3.2). This reveals that male animals fed the HFHS diet consumed significantly higher calories when compared to those fed the CTRL diet. An increase of almost 25% in calories consumed was observed for the males over the study period, however AfriplexGRT™ did not have any effect on the consumption in either group.

AUC analysis performed for the females showed an area of 1379 ± 33.6 kcal and 1400 ± 16.5 kcal for the CTRL and CTRL+AfriplexGRT™ groups, respectively, and 1954 ± 33.15 kcal and 2010 ± 37.1 kcal for the HFHS and HFHS+AfriplexGRT™ fed groups respectively. Female animals fed the HFHS diet also demonstrated a higher

energy intake when compared to the female control group. A 43% increase in calories consumed by the females was observed over the study period, however AfriplexGRT™ did not have any effect on the consumption in either group.

Although the trend of caloric consumption was the same between the male and female animals, the overall caloric intake of the males (Control: 1945 ± 50.60; HFHS: 2500 ± 62.01) was more than the females (Control: 1379 ± 33.63; HFHS: 1954 ±33.15) for all the groups, with males consuming roughly 550 calories more than female animals ($p<0.001$) (Figure 3.2).

3.3.2. Morphometric analysis

3.3.2.1. The effect of HFHS diet on the body weight of Wistar rats

At the start of the study, the mean bodyweight of male and female rats was 207.8 ± 3.31 g and 149.8 ± 1.94 g, respectively. The weight gain per month for all the diet groups is depicted in Figure 3.3. Over the 9-month feeding period, a consistent increase in bodyweight was observed for all animal groups. A significant rise (11%) in the bodyweight was observed in the male animals fed a HFHS diet (447.7 ± 11.06 g) after a feeding period of 5 months, when compared to the animals fed the control diet (402.8 ± 9.33 g). This trend continued until the end of the study and resulted in a final weight of 529.6 ± 17.0 g for the HFHS diet-fed rats, with a 16.8% increase in comparison to their control diet counterparts (453.3 ± 9.50 g). A similar trend was observed in the male group fed the HFHS diet supplemented with AfriplexGRT™ (530.5 ± 17.0 g), however this increase was not significant when compared to the HFHS group, even though the HFHS+AfriplexGRT™ group had a 17.0% increase in body weight when compared to the control group. The AfriplexGRT™ supplementation of the control diet (442.7 ± 11.34 g) showed no significant change in bodyweight with a 2.3% decrease when compared to the control group (Figure 3.3A).

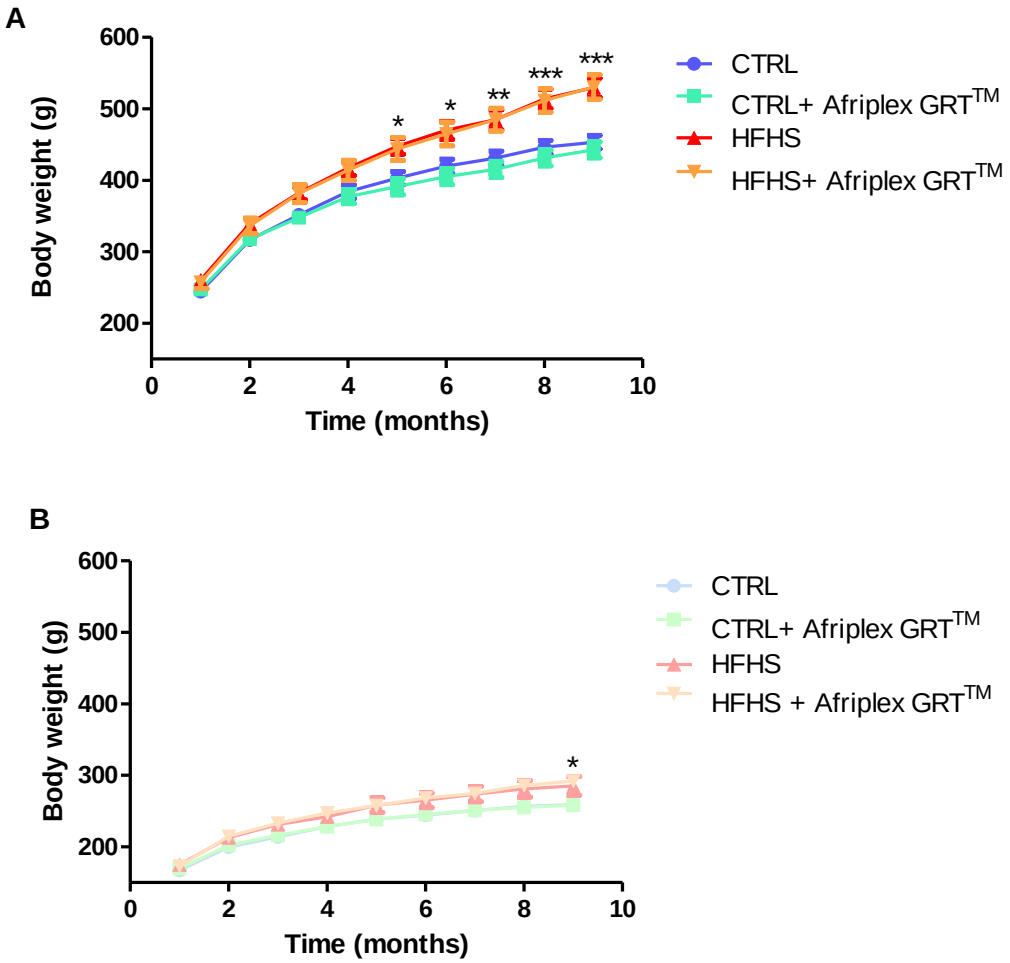

Figure 3.3: Body weights of Wistar rats after 9 months of treatment. Bodyweight graphs for A) male and B) female Wistar rats over 9 months on their respective diets. Data presented as the mean ± SEM of n=10 animals per group. A one-way ANOVA was performed, and statistical significance is depicted as * p≤0.05, **p≤0.01, *** p≤0.001 control versus vs HFHS diet groups.

In the female groups, the mean bodyweight for the HFHS diet-fed group and animals fed a control diet was 174.8 ± 6.19g and 166.9 ±3.90 g, respectively, after one month on their respective diets. The body weight of all female animal groups increased gradually throughout the study period however, difference in bodyweight over monthly intervals was not statistically significant. A significant gain (10.2% increase) in body weight was only reflected at the 9th month of feeding in the HFHS diet-fed group (285.3 ± 13.15 g) when compared to their control counterparts (258.9 ± 6.28 g). There was no significant difference in the bodyweights of HFHS diet-fed animals supplemented AfriplexGRT^{TM} (291.8 ± 6.26 g) when compared to the HFHS diet-fed group.

Supplementation of the control diet with AfriplexGRT™ (258.1 ± 6.18 g) did not cause any significant change on the bodyweight when compared to the control group.

Taken together, although both genders had a significantly increased caloric intake in the HFHS-diet fed rats compared the controls, only the male animals significantly differed in weight before the last month of the study. The HFHS males increased in bodyweight from 260.3 ± 5.23g in month 1 to 529.6 ±13.32 g in month 9 in comparison to the female animals which increased from 174.8 ± 6.19g to 285.3 ± 13.15g over the study period. Male rats thus gained weight at a faster rate than their female counterparts, in addition being significantly larger and heavier than the females ($p<0.001$), even from the beginning of the study (Figure 3.3).

3.3.2.2. The effect of HFHS diet on heart weight, abdominal fat weights and liver weights in male and female rats

The organ weights recorded no significant change in heart weights between the male control (2.16 ± 0.09 g) and HFHS (2.25 ± 0.072 g) diet-fed groups. The CTRL+AfriplexGRT™ (2.19 ± 0.063 g) and HFHS+AfriplexGRT™ (2.45 ± 0.079 g) groups also show no difference in heart weights compared to their non-AfriplexGRT™ treated counterparts. Similar findings were observed in all female diet groups, with no significant gain in heart weight between the HFHS diet-fed animals (1.72 ± 0.049 g) and animals fed the control diet (1.63 ± 0.038 g) (Figure 3.4B). The mean heart weight of animals fed HFHS+AfriplexGRT™ was 1.76 ± 0.092 g and this was not significantly different from the animals fed only HFHS diet. The trend remained the same for both the control group animals (with and without AfriplexGRT™ supplementation). The male hearts were however significantly heavier (2.26 ± 0.256 g) than the female rats (1.68 ± 0.19 g) of the same age ($p<0.01$) (Figure 3.4A).

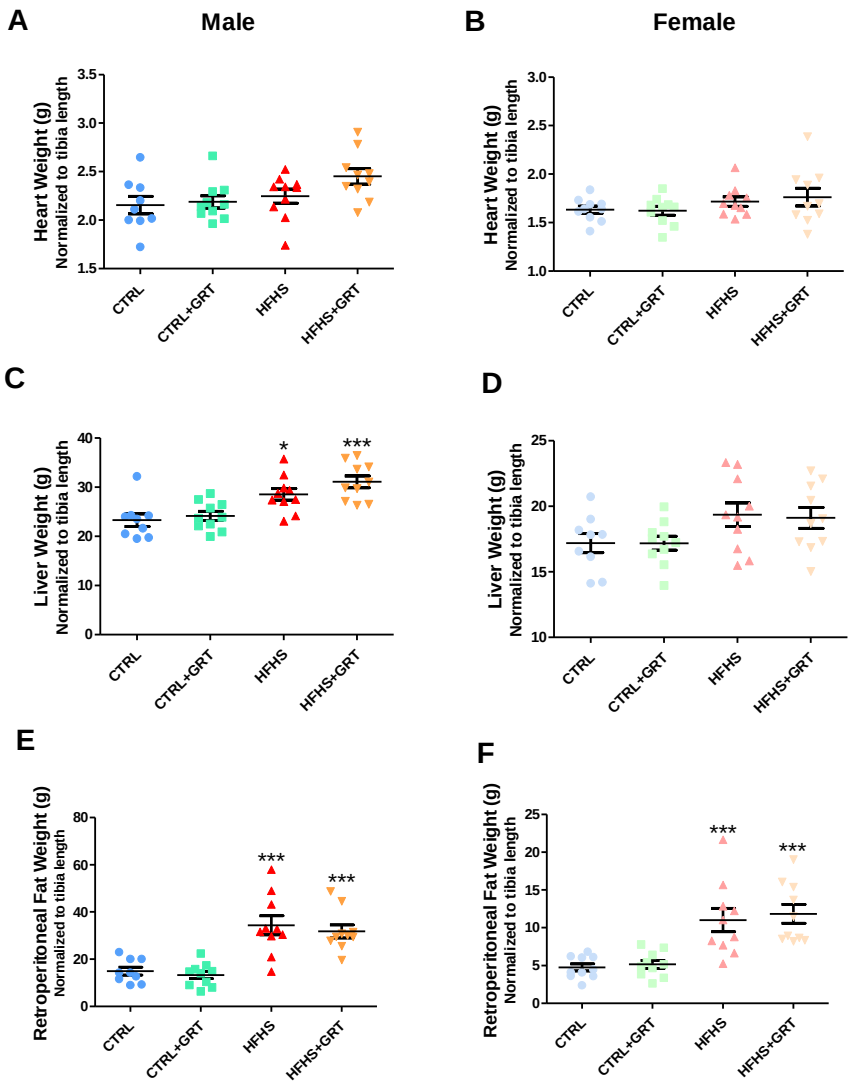

Figure 3.4: Organ weights of Wistar rats after 9 months of treatment. Organ weights for male A) heart, C) liver and E) retroperitoneal fat, and female B) heart, D) liver and F) retroperitoneal fat after 9 months on their respective diets. Data presented as the mean ± SEM of n=10 animals per group. A one-way ANOVA was performed, and statistical significance is depicted as * p≤0.05, *** p≤0.001 versus control.

Liver weights were significantly higher in male rats fed the HFHS diet (28.6 ± 1.17 g) when compared to their control counterparts (23.3 ± 1.28 g, $p < 0.05$). The liver weights of animals fed HFHS diet supplemented with AfriplexGRT™ (31.1 ± 1.21 g) was not statistically different when compared to males fed only the HFHS diet. AfriplexGRT™ did not have an impact on the liver weights of the control group (24.2 ± 0.91 g) (Figure 3.4C). The mean liver weight for the female animals fed the HFHS diet (19.36 ± 0.91 g) was increased when

compared to animals fed the control diet (17.19 ± 0.72 g), however, there was no statistically significant difference in the liver weights of these two groups. Similar results were seen in the animals fed the control diet (17.19 ± 0.53 g) and HFHS diet (19.12 ± 0.80 g) supplemented with AfriplexGRT™ did not have an effect on the respective non-supplemented control groups. Figure 3.4C and D showed that the diet influenced liver weight in male rats but not in females, however male livers were significantly heavier than female livers ($p<0.001$).

The retroperitoneal fat (RF) pad weight was significantly increased in the HFHS-fed groups in both the males (34.36 ± 4.03 g, $p < 0.001$) and females (11.0 ± 1.55 g, $p < 0.001$) when compared to their control counterparts (14.93 ± 1.67 g and 4.75 ± 0.46 g respectively) (Figure 3.4 E and F). Supplementation with AfriplexGRT™ did not influence RF pad weight in male (13.30 ± 1.54 g) and female (5.15 ± 0.53 g) groups fed the control diet. Similarly, the AfriplexGRT™ supplementation did not decrease the RF weight gain in the male (31.79 ± 2.72 g) or female (11.84 ± 1.25 g) groups fed the HFHS diet. Thus, diet but not gender played a role in the RF fat mass, and supplementation with AfriplexGRT™ left liver weights unaffected in either gender. Liver weights were however significantly heavier in the male rats when compared to the females ($p<0.001$).

3.3.2.3. The effect of HFHS diet on fasting blood glucose levels in both male and female rats

Fasting blood glucose (FBG) levels were measured monthly. They remained stable over the 9-month feeding period in all female diet groups, with a slight fluctuation observed at month 6 in the male HFHS diet-fed group. FBG levels of male animals fed HFHS diet were significantly higher at the 6th month (5.31 ± 0.30 mmol/L) when compared to the control group (4.33 ± 0.097 mmol/L) ($p<0.0065$), however, this was in the normal range. FBG levels dropped again to 4.98 ± 0.15 mmol/L for the HFHS diet-fed group in month 7 compared to 4.57 ± 0.14 mmol/L for the control group and remained unchanged till the end of the feeding period. Supplementation with AfriplexGRT™ did not significantly change the FBG levels for the control or HFHS diet-fed groups and did not significantly reduce the higher serum glucose levels at month 6 when compared to the HFHS diet-fed group (Figure 3.5A).

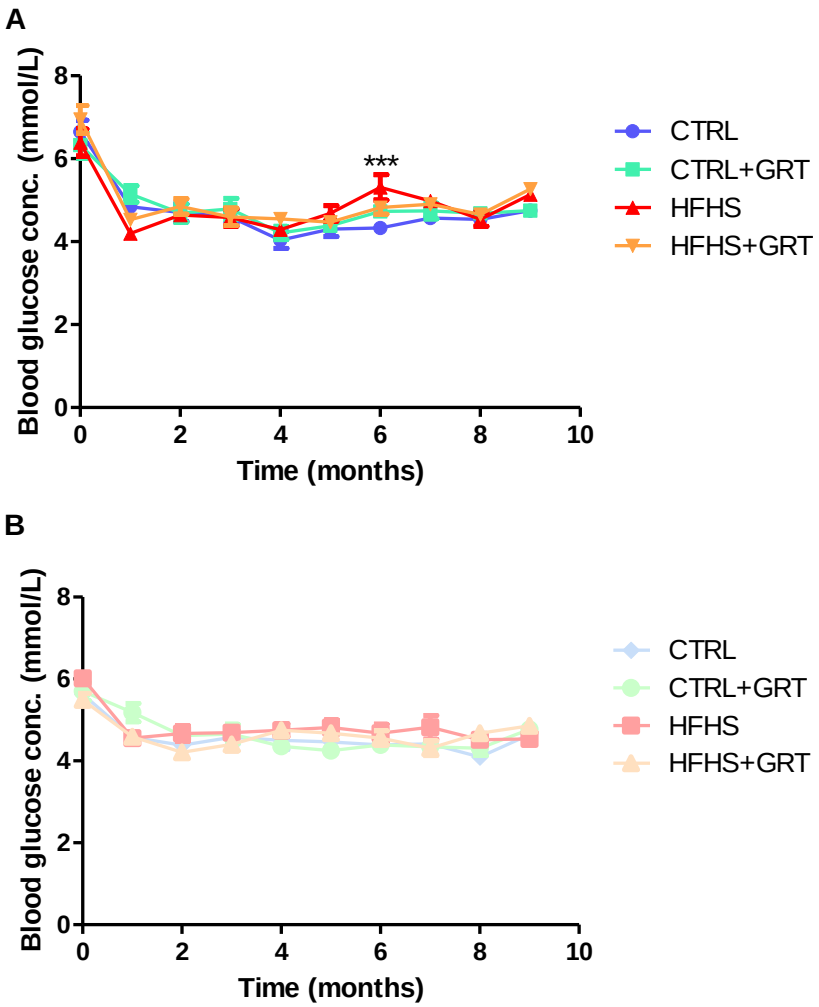

Figure 3.5: Fasting blood glucose of (A) male and (B) female Wistar rats. Circulating glucose concentration measured after 16 hours of fasting. Data are represented as the mean ± SEM of n=10 animals per group. A one-way ANOVA was performed, and statistical significance is depicted as *** p≤0.001 male control versus HFHS.

FBG levels remained unchanged in the female cohort when comparing HFHS diet-fed animals (4.81 ± 0.14 mmol/L) to their control counterparts (4.57 ± 0.13 mmol/L) as well as after supplementation with AfriplexGRT™ across different diet groups (4.65 ± 0.11 mmol/L and 4.66 ± 0.15 mmol/L, respectively) (Figure 3.5B). In addition, the global FBG mean levels fell within a normal range of 4-5.5 mmol/L, suggesting that the rats were not insulin resistant.

3.3.2.4. The effect of HFHS diet on Oral glucose tolerance test (OGTT) in male and female Wistar rats

OGTTs were performed over 120 minutes after the rats were orally gavaged with dextrose after 16 hours of fasting. This was performed to investigate whether the HFHS diet causes β-cell dysfunction in the Wistar rat model. Results obtained showed that male rats fed the HFHS diet had significantly higher AUC when compared to the control group, at month 3 (942.8 ± 16.80 compared to 815.1 ± 16.41, p-value 0.0004), 6 (910.8 ± 18.58 compared to 778.1 ± 26.13, p-value 0.001) and 9 (926.5 ± 33.3 compared to 768.9 ± 18.24, p-value 0.0005), respectively. As seen in Figure 3.6, the blood glucose levels for all male groups at all 3 timepoints peaked at 15 minutes after which it gradually decreased towards a normal level, however after the 2-hour monitoring period, the blood glucose levels had not fully recovered to basal levels. Similarly, supplementation with AfriplexGRT™ followed a similar trend where AUC showed a significant increase at month 3 (944.3 ± 34.97 vs 815.1 ± 16.41, p-value 0.0058), 6 (891.2 ± 43.8 compared to 778.1 ± 26.13, p-value 0.0172) and 9 (934.4 ± 24.3 compared to 768.9 ± 18.24, p-value 0.0001) (Table 3.5 and Figure 3.6).

Table 3.5: Oral glucose tolerance test, area under the curve (AUC).

Gender	Group	Month 3	Month 6	Month 9
Male	CTRL	815.1 ± 16.41	778.1 ± 26.13	768.9 ± 18.24
	CTRL+GRT	796.8 ± 15.09	855.6 ± 22.85	809.0 ± 22.97
	HFHS	**942.8 ± 16.80****	**910.8 ± 18.58***	**926.5 ± 33.33*****
	HFHS+GRT	**944.3 ± 34.97****	891.2 ± 43.82	**934.4 ± 24.34*****
Female	CTRL	857.4 ± 30.85	774.3 ± 19.26	751.9 ± 21.80
	CTRL+GRT	888.1 ± 52.24	762.6 ± 12.39	727.9 ± 14.56
	HFHS	905.3 ± 17.79	824.8 ± 43.20	796.1 ± 20.46
	HFHS+GRT	879.9 ± 21.99	877.9 ± 20.99	780.3 ± 25.37

AUC calculations for oral glucose tolerance tests performed at 3, 6, and 9 months. Data represent mean ±SEM of n=10 animals per group. Statistical significance is depicted as * p≤0.05, ** p≤0.01, *** p≤0.001 versus the control group.

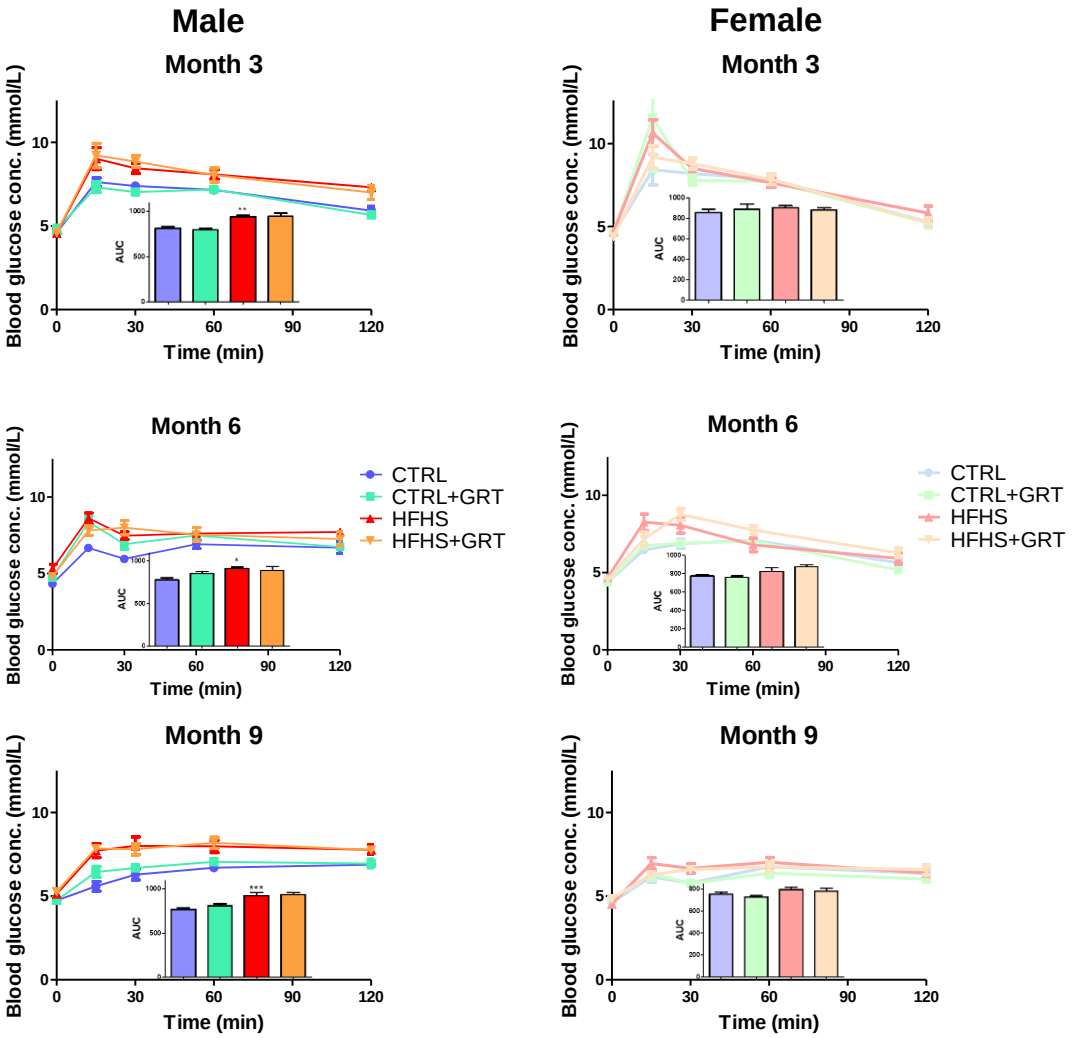

Figure 3.6: Glucose response observed during oral glucose tolerance test (OGTT) and examined as the area under the curve (AUC) plots. Blood glucose measured over 120 minutes after dextrose administration at months 3, 6 and 9. Data represent the mean ± SEM of n=10 animals per group. AUC calculated from these plots. Data are represented as the mean ± SEM of n=10 animals per group. A one-way ANOVA was performed, and statistical significance is depicted as * p≤0.05, ** p≤0.01, ***p≤0.001 versus the control group.

The female rats however, showed no significant difference in the OGTT AUC between the control and HFHS diet-fed groups at months 3 (857.4 ± 30.85 vs 905.3 ± 17.79), 6 (774.3 ± 19.26 vs 824.8 ± 43.20) or 9 (751.9 ± 21.8 vs 796.1 ± 20.46) (Figure 3.6 and Table 3.5). Additionally, supplementation with AfriplexGRT^{TM} also had no effect on AUC for the control or HFHS diet-fed females at month 3 (888.1 ± 52.24 and 879.9 ± 21.99

respectively), 6 (762.6 ± 12.39 and 877.9 ± 20.99 respectively) or 9 (727.9 ± 14.56 and 780.3 ± 25.37 respectively). Similar to their male counterparts, the female blood glucose levels for at all 3 timepoints peaked at 15 minutes (except for the HFHS group supplemented with AfriplexGRT™ at month 6, peaking at 30 minutes), after which it gradually decreased towards a normal level. While the males and females had a similar initial response to the dextrose, the females cleared the glucose effectively in all groups, whereas the male's ability for glucose clearance was slightly hindered.

3.3.2.5. The effect of HFHS diet on serum liver enzymes of male and female Wistar rats

Serum AST and ALT levels were measured as indicators of liver damage after HFHS feeding. As shown in Figure 3.7, ALT (> 48 U/L) but not AST (> 55 U/L) liver enzymes were in the normal range. Unexpectedly, serum AST levels were slightly decreased in the male HFHS diet-fed group (46.40 ± 3.65 IU/L) when compared to their control counterparts (58.56 ± 2.98 IU/L), although the difference was not statistically significant. Supplementation with AfriplexGRT™ (59.33 ± 3.06 IU/L), however, significantly increased ($p<0.05$) AST levels above the normal range when compared to the HFHS diet-fed group, augmenting the effect of the diet. A slight but insignificant decrease was seen in the serum ALT levels after the control group was exposed to AfriplexGRT™ (53.10 ± 3.05 IU/L) when compared to the control diet-fed group (58.56 ± 2.98 IU/L) without AfriplexGRT™ supplementation.

The mean AST levels were reduced in the female HFHS diet-fed group (56.30 ± 3.24 IU/L) when compared to rats fed the control diet (72.67 ± 6.05 IU/L), although this decrease was not statistically significant. Diet supplementation with AfriplexGRT™ did not have any influence on the AST levels of both the HFHS diet-fed group (49.67 ± 3.11 IU/L) when compared to the HFHS diet group or the control diet-fed animals (73.80 ± 4.74 IU/L) when compared to the control diet group. When comparing the male and female groups, the females (control: 72.67 ± 6.05; HFHS: 56.30 ±3.24) had elevated AST levels when compared to the males (control: 58.56 ± 2.98; HFHS: 46.40 ± 3.65) although this was not statistically significant, however, AfriplexGRT™ supplementation increased the AST levels in the males, but not the females (Figure 3.7A and C).

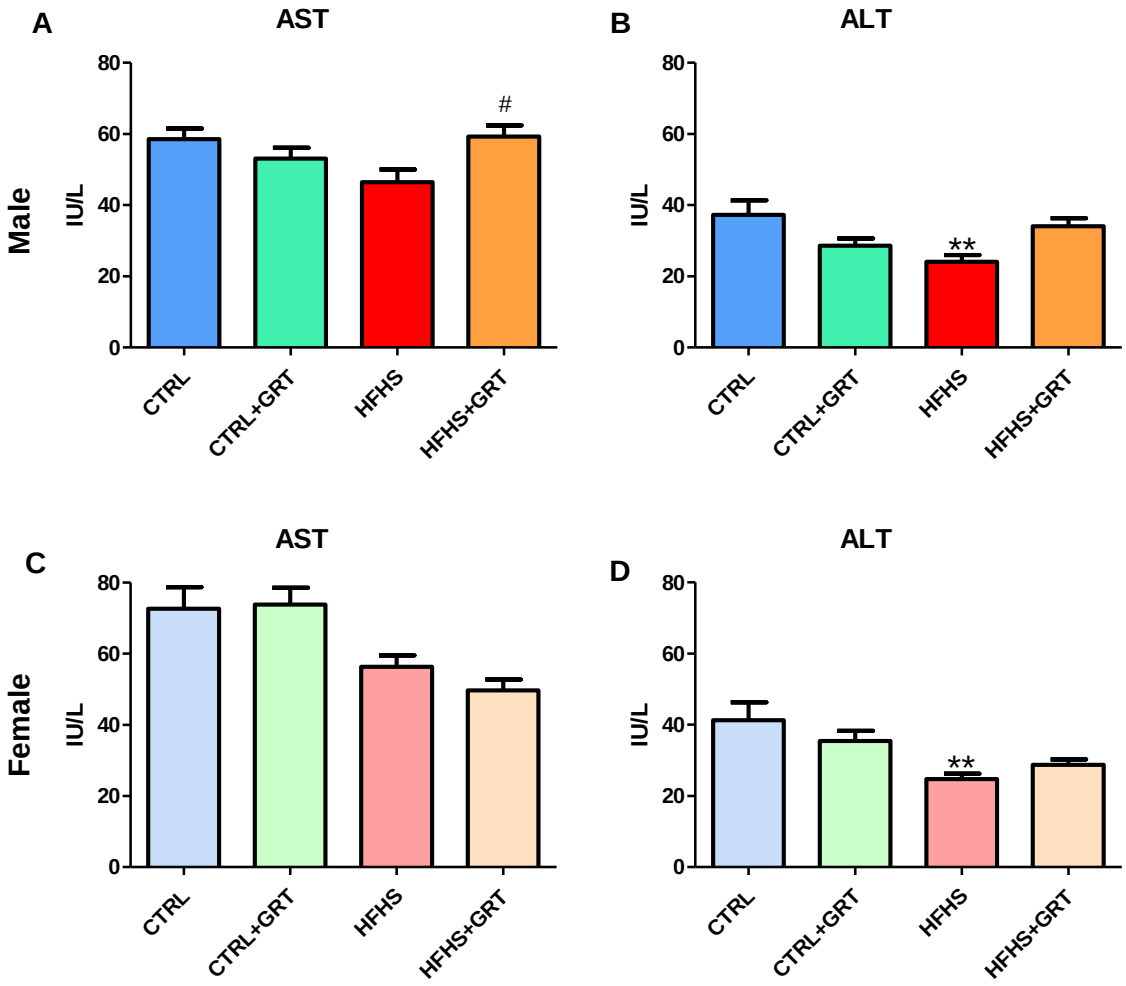

Figure 3.7: Serum AST and ALT levels as an indicator of liver damage. AST (A and C) and ALT (B and D) levels of the Wistar rats after 9 months on their respective diets. Data represent the mean ± SEM of n=10 animals per group. A one-way ANOVA was performed, and statistical significance is depicted as * p≤0.05, ** p≤0.01 versus the control group; # p≤0.05 versus HFHS.

The ALT levels were reduced in the male HFHS diet-fed group (24.10 ± 1.88 IU/L) when compared to their control counterparts (37.30 ± 4.08 IU/L), however, supplementation with AfriplexGRT™ reduced the ALT levels in the control diet-fed animals (28.60 ± 2.03 IU/L) but increased it in the HFHS diet-fed group (34.00 ± 2.31 IU/L), though the differences were not statistically significant. Similarly, the females demonstrated a decrease in the ALT levels in the HFHS diet-fed group (24.80 ± 1.51 IU/L) when compared to their control counterparts (41.30 ± 5.02 IU/L) and supplementation with AfriplexGRT™ had the same effect as seen in the male groups (Figure 3.7C and D).

While ALT levels show the same trend in both male and female groups, the AST levels in response to diet are similar between the genders, however, AfriplexGRT™ supplementation had a different effect in the male and female cohorts. It is however important to note that normal reference ranges for AST and ALT are between 50-150 IU/L and 10-40 IU/L, respectively [31]. As such, data presented showed that both AST and ALT levels for both males and females were within the normal range, except for the AST levels in both genders being slightly lower in response to the HFHS diet on its own.

3.3.2.6. The effect of HFHS diet on serum lipid profiles of male and female Wistar rats

Serum lipid profiles are known measurements to predict cardiovascular risk. The serum triglyceride levels were significantly elevated in male (3.10 ± 0.34) and female (1.82 ± 0.29) Wistar rats on the HFHS diet when compared to their respective control groups (1.23 ± 0.11 and 0.76 ± 0.11 respectively). Diet supplementation with AfriplexGRT™ was however unable to decrease serum triglycerides levels for either the male control (1.13 ± 0.14) or HFHS (3.55 ± 0.38) group. A similar trend was observed for the triglyceride levels in female rats supplemented with AfriplexGRT™ for both the control diet-fed group (2.05 ± 0.22) and HFHS diet-fed group (0.77 ± 0.088) (Figure 3.8A and B). The trends of the effect of diet and consumption of AfriplexGRT™ however were the same when comparing the male and female groups, however, the overall triglyceride levels were slightly elevated in the male rats when compared to the females, particularly in the groups fed the HFHS diet.

There was however no significant change in total cholesterol in the male (1.63 ± 0.098) and female (1.90 ± 0.12) groups on the HFHS diet when compared to their control counterparts (1.54 ± 0.096 and 1.57 ± 0.084, respectively). Supplementation with AfriplexGRT™ was unable to change total-cholesterol levels in both the male control (1.43 ± 0.087) and HFHS groups (1.96 ± 0.090) and well as the female control (1.49 ± 0.086) and HFHS (1.98 ± 0.10) groups (Figure 3.8C and D).

Similar results were observed for HDL-cholesterol in either the male (0.80 ± 0.033) and female (1.19 ± 0.063) groups on the HFHS diet when compared to their control counterparts (0.97 ± 0.05 and 1.12 ± 0.057, respectively). Supplementation with AfriplexGRT™ was unable to change HDL-cholesterol levels in both the

male control (1.00 ± 0.056) and HFHS groups (0.85 ± 0.040) and well as the female control (1.07 ± 0.072) and HFHS (1.24 ± 0.058) groups (Figure 3.8E and F).

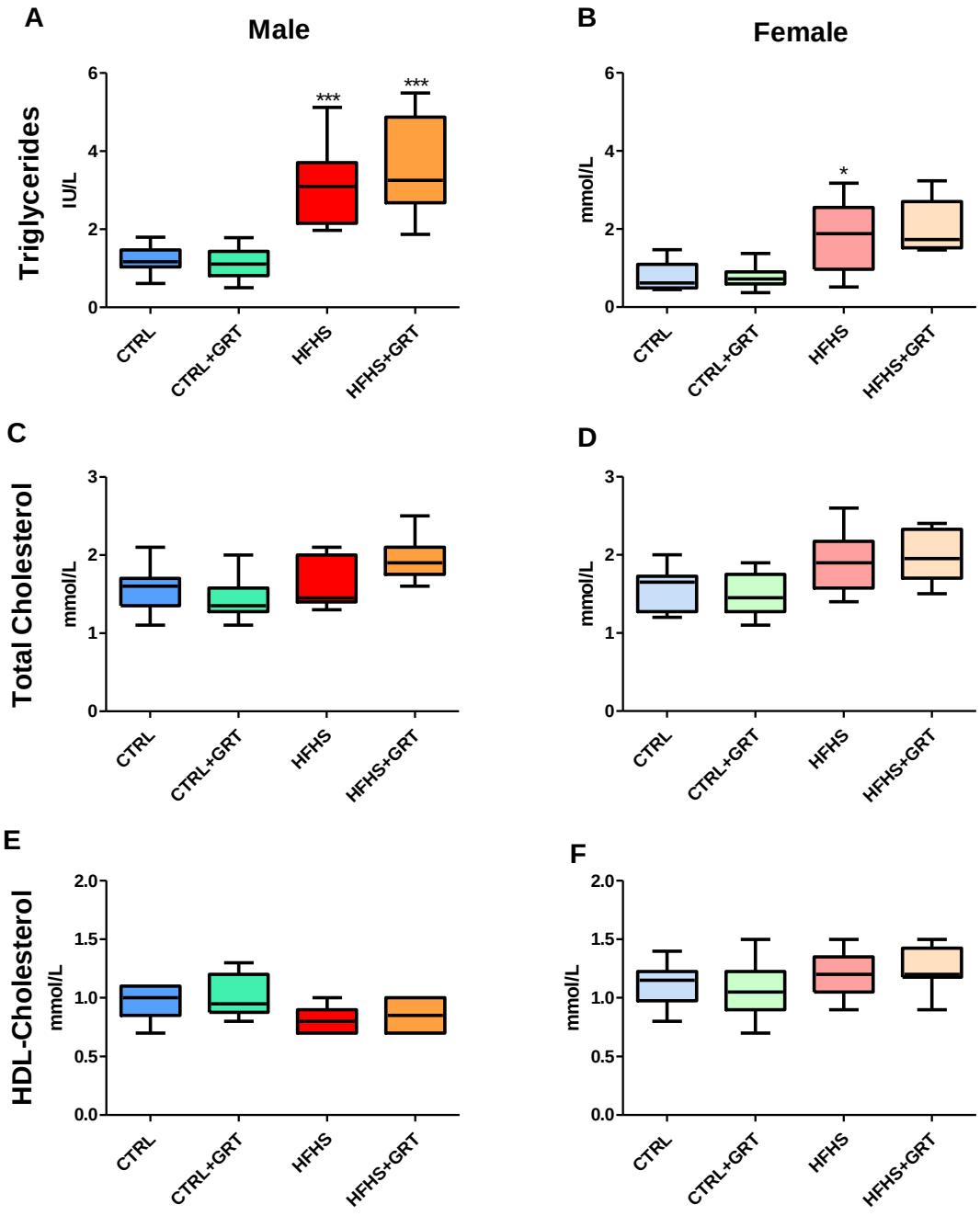

Figure 3.8: Serum triglycerides, total cholesterol, and HDL-cholesterol. Box and whisker plots of the serum triglycerides and cholesterols of male and female Wistar rats after 9 months on their respective diets. Data represent the mean ± SEM of n=10 animals per group. A one-way ANOVA was performed, and statistical significance is depicted as * p≤0.05, ** p≤0.01, *** p≤0.001 versus the control group.

3.3.3. Molecular analysis to study the effects of HFHS diet feeding

3.3.3.1. The effect of HFHS diet on serum insulin levels

Insulin resistance is a known indicator of metabolic syndrome and thus insulin levels were determined using a serum ELISA kit. Males that consumed the HFHS diet showed increased serum insulin levels when compared to the normal control group (6.57 ± 1.36 compared to 3.06 ± 0.66), although not significant. Treatment with the AfriplexGRT^{TM} did not decrease serum insulin levels in the control (2.92 ± 0.60) or HFHS diet-fed (7.01 ± 1.92) groups (Figure 3.9A). Upon analysis of serum insulin levels of female Wistar rats, no significant changes could be observed on rats fed the HFHS diets (0.80 ± 0.22) when compared to the controls (0.67 ± 0.12), and AfriplexGRT^{TM} supplementation also did not affect the insulin level in either the control (0.80 ± 0.22) or HFHS diet-fed groups (0.73 ± 0.16) (Figure 3.9B). Then comparing the serum insulin levels between the male and female groups, there was a non-significant increase in insulin levels between male (3.06 ± 0.66) and female (0.67 ± 0.12) control groups, however in the HFHS diet-fed animals, the male rats (6.57 ± 1.36) has significantly higher insulin levels when compared to the females (0.80 ± 0.10) on the same diet ($p<0.001$).

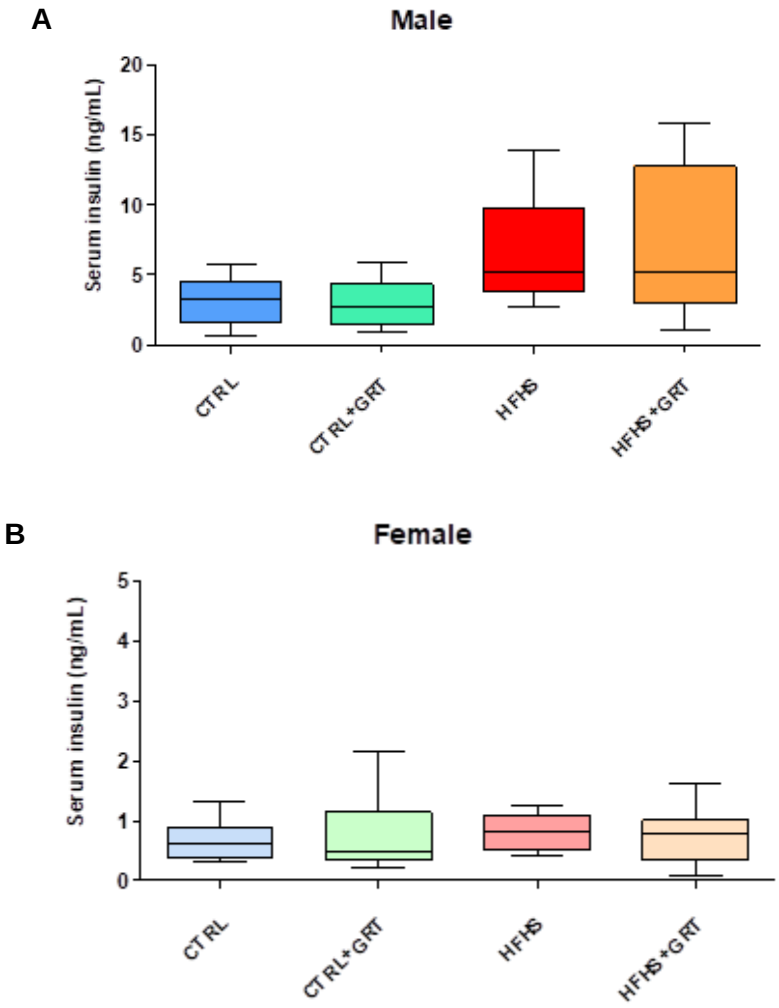

Figure 3.9: Serum insulin levels. Effect of diet on serum insulin levels of A) male and B) female Wistar rats fed a control diet (CTRL), control diet supplemented with 60 mg/kg AfriplexGRT™ (CTRL+GRT), high fat, high sugar diet (HFHS), or high fat, high sugar diet supplemented with AfriplexGRT™ (HFHS+GRT). A one-way ANOVA was performed. Data represent the mean ± SEM of n=9 animals per group.

3.3.3.2. HOMA-IR calculation as a measurement of insulin resistance

The HOMA-IR index relates to the level of insulin resistance and can be interpreted as the higher the HOMA-IR value, the greater the degree of insulin resistance. HOMA-IR below 1 is indicative of insulin sensitivity whereas, increased levels above 1 are an indication of insulin resistance. HOMA-IR calculations were done according to the formula [32]:

$$\text{HOMA-IR} = \text{Fasting insulin } (\mu\text{U/L}) \text{ x fasting glucose } (\text{nmol/L})/22.5$$

Results obtained showed that HFHS-diet feeding resulted in an increased HOMA-IR index for both males (1.57 ± 0.30) and females (1.56 ± 0.016), when compared to their control groups (0.60 ± 0.12 and 0.14 ± 0.024), although differences were not statistically significant. However, treatment with the AfriplexGRT™ extract did not significantly reduce the HOMA-IR insulin levels in both male (1.42 ± 0.38) and female (0.16 ± 0.036) Wistar rats fed the HFHS diet (Figure 3.10). Although the HOMA-IR trend was similar for the male and female animals, female HOMA-IR after HFHS-diet feeding remained below 1 for all groups, whereas males had levels higher than 1.

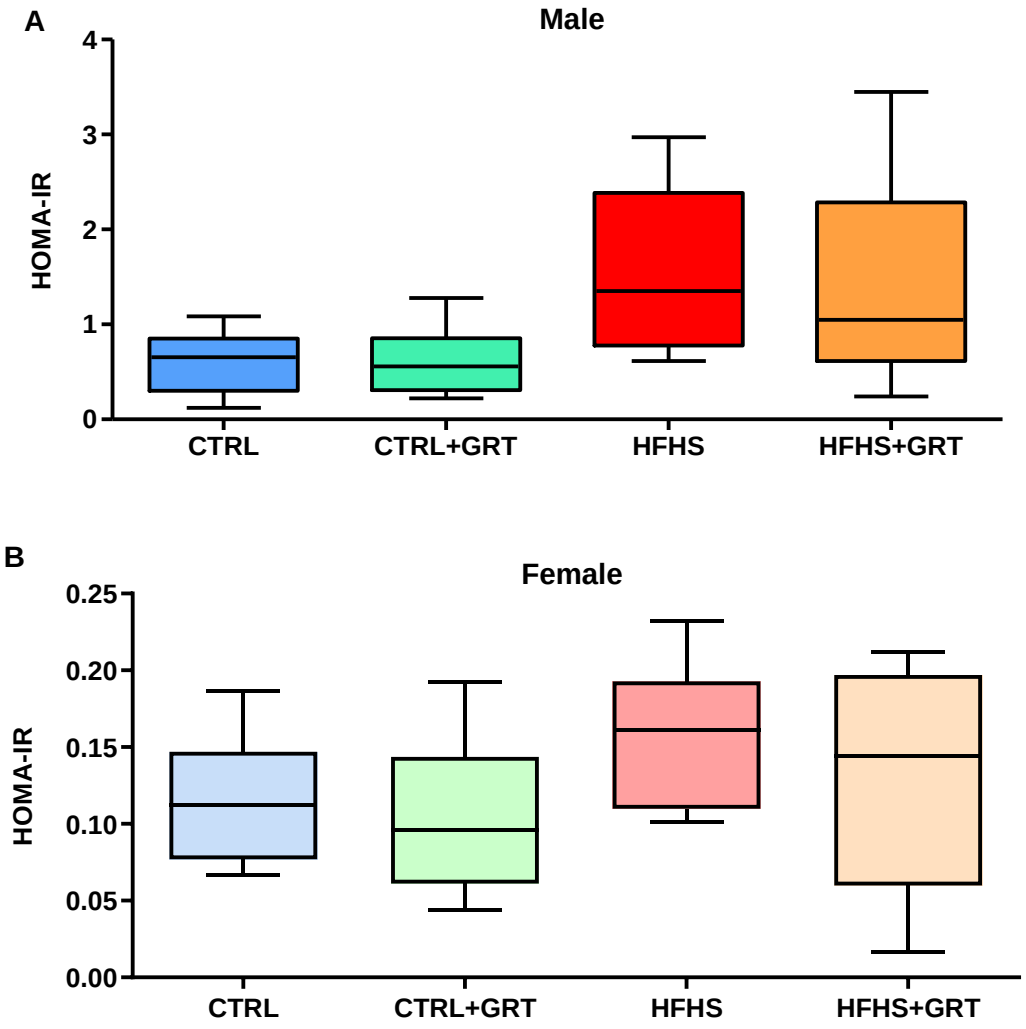

Figure 3.10: HOMA-IR. Graph of calculated HOMA-IR values from Insulin ELISA of A) male and B) female Wistar rats fed a control diet (CTRL), control diet supplemented with 60mg/kg AfriplexGRT™ (CTRL+GRT), high fat, high sugar diet (HFHS), or high fat, high sugar diet supplemented with AfriplexGRT™ (HFHS+GRT). A one-way ANOVA was performed, and data represent the mean ± SEM of n=9 animals per group.

3.3.3.3. Serum LOXL2 levels as an early indicator of fibrosis before clinical diagnosis

Serum LOXL2 levels were only performed on male Wistar rats due to the greater dietary effects being observed in these animals. Increased serum LOXL2 is a marker of the preclinical onset of fibrosis [33]. Expression of serum LOXL2 is elevated in heart failure patients, correlating with left ventricular dysfunction, with reported use as an asymptomatic cardiac biomarker [33, 34]. Yang et al. (2016), reported that LOXL2 higher than 0.1 ng/mL correlated with the amount of crosslinked collagen that was associated with the development of interstitial fibrosis, ventricular stiffness and diastolic dysfunction in pathological, stressed hearts in human subjects. The serum ELISA showed there was an increase in the serum LOXL2 concentration in Wistar rats on HFHS diet when compared to the control diet-fed group (0.76 ± 0.113 compared 0.54 ± 0.089), while the AfriplexGRT™ slightly reduced the LOXL2 concentration in both the control (0.30 ± 0.072) and HFHS (0.59 ± 0.084) diet groups when compared to their control counterparts (Figure 3.11). However, the observed effect was not significant.

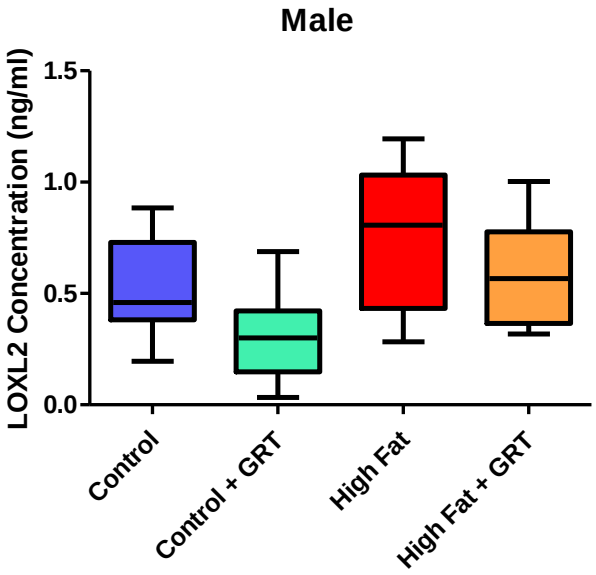

Figure 3.11: Serum ELISA-based LOXL2 expression. LOXL2 serum concentrations determined by an ELISA in male Wistar rats fed a control diet (CTRL), control diet supplemented with 60mg/kg AfriplexGRT™ (CTRL+GRT), high fat, high sugar diet (HFHS), or high fat, high sugar diet supplemented with AfriplexGRT™ (HFHS+GRT). A one-way ANOVA was performed, and data represent the mean ± SEM of n=10 animals per group.

Table 3.6: Summary of metabolic parameters that differ in males versus females control and high fat diets. Data represent the mean ± SEM of n=10 animals per group. Statistical significance is depicted as * p≤0.05, ** p≤0.01, *** p≤0.001 versus the respective control group.

	Males		**Females**		**Male vs female**
Metabolic characteristics	**CTRL**	**HFHS**	**CTRL**	**HFHS**	**HFHS**
Bodyweight (g) month 9	453.3 ± 9.50	**529.6 ± 13.32*****	258.9 ± 6.28	**285.3 ± 13.15***	**P<0.001*****
Calories intake (AUC)	1945 ± 50.60	**2500 ± 62.01*****	1379 ± 33.63	**1954 ± 33.15*****	**P<0.001*****
Blood glucose (mmol/L)	4.73 ± 0.23	4.88 ± 0.20	4.57 ± 0.13	4.81 ± 0.14	**P=0.0165***
OGTT 3 months AUC (mm^2)	815.1 ± 16.41	**942.8 ± 16.80****	857.4 ± 30.85	905.3 ± 17.79	ns
OGTT 6 months AUC (mm^2)	778.1 ± 26.13	**910.8 ± 18.58***	774.3 ± 19.26	751.9 ± 21.80	ns
OGTT 9 months AUC (mm^2)	768.9 ± 18.24	**926.5 ± 33.33*****	824.8 ± 43.20	796.1 ± 20.46	ns
Insulin (ng/mL)	3.06 ± 0.66	6.57 ± 1.36	0.67 ± 0.12	0.80 ± 0.16	**P<0.001*****
HOMA-IR	0.60 ± 0.12	1.57 ± 0.30	0.14 ± 0.02	0.16 ± 0.04	**P<0.001*****
Triglycerides (mmol/L)	1.23 ± 0.11	**3.10 ± 0.34*****	0.76 ± 0.11	**1.82 ± 0.29***	**ns**
HDL (mmol/L)	0.97 ± 0.05	0.80 ± 0.03	1.12 ± 0.06	1.24 ± 0.06	**P<0.001*****

3.3.4. The effect of a HFHS diet on histology for both male and female rats

Stained tissue sections from the control and HFHS groups were evaluated by an independent company (Idexx Laboratories, Kyalami, South Africa) for complete objectivity, and the results reported as per their findings.

3.3.4.1. The effect of HFHS diet on Hematoxylin and Eosin-stained (H&E) heart sections of both male and female Wistar rats

In the control tissue sections, multifocal variation was seen in the eosinophilia of the myocardial fibre cytoplasm, and the fibres often had a granular cytoplasmic appearance. The control groups displayed striated muscle fibres with a branched cellular network. Intercalating disks were visible with normal cardiomyocytes nuclei being observed. No degenerative changes could be observed under H&E stain.

Tissue sections of Wistar rats fed a HFHS diet, displayed scattered small groups of fibres, and sometimes individual scattered cells, that showed mild swelling of myocardial fibres with increased eosinophilia of the cytoplasm with a hyalinised (degenerate) smudged appearance. Mild swelling of the fibres with a slightly granular cytoplasm appearance could be observed. Fibres were slightly separated. Single blood vessel walls revealed a slightly smudged appearance of the tunica media while some scattered small blood vessels had slightly hyalinised tunica media. Few fibres also contained vacuoles in the cytoplasm and individualisation of fibres or mild increase in the interstitial space between fibres due to possible interstitial oedema or increased cell poor stroma. In single areas, mildly increased numbers of fibroblasts are present interstitially between these fibres (Figure 3.12). AfriplexGRT^{TM} was unable to reverse any mild interstitial oedema observed in animals on the HFHS diet.

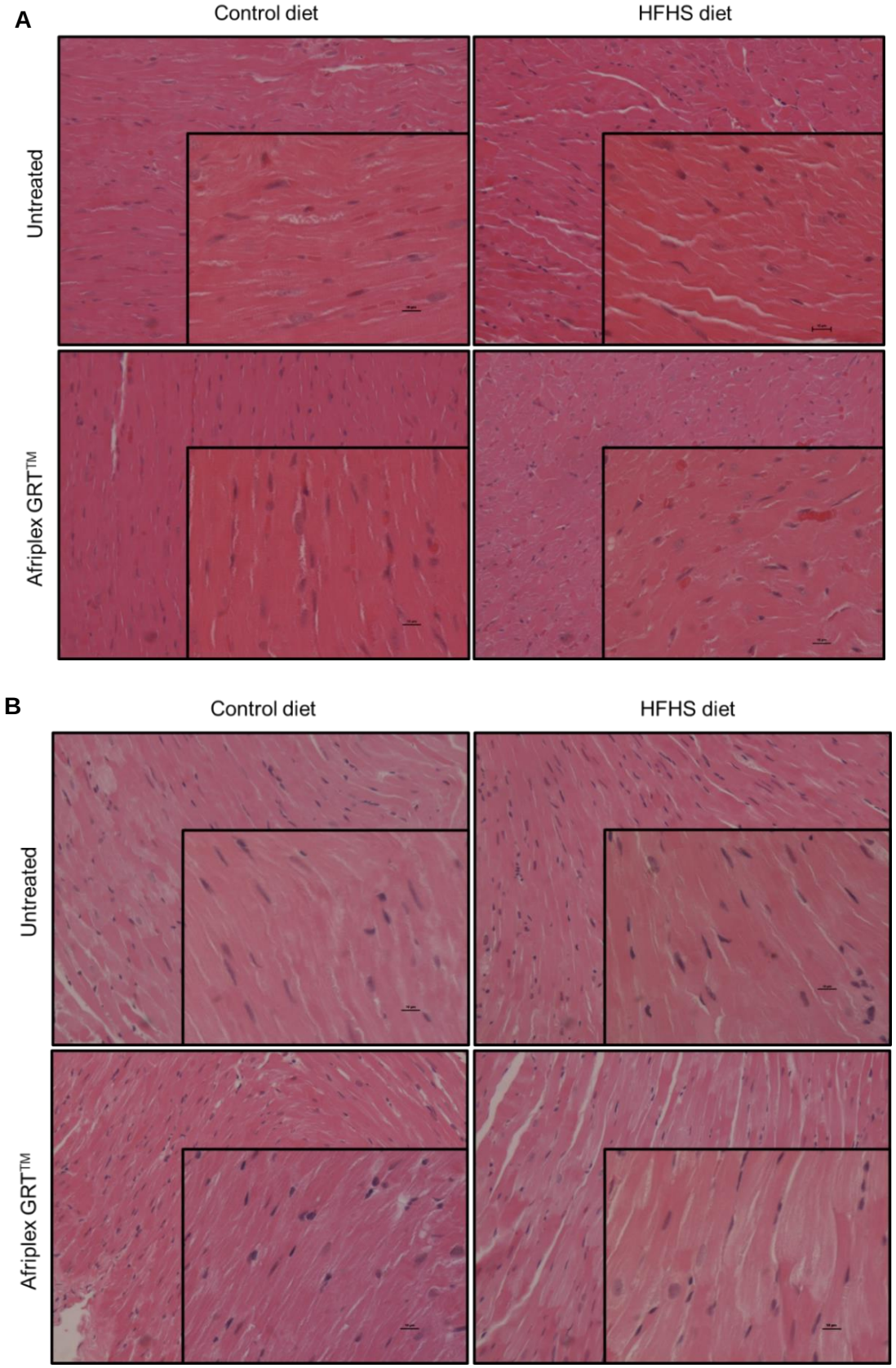

Figure 3.12: Photomicrograph showing hematoxylin and eosin-stained heart sections. Representative images of H&E-stained sections from A) male Wistar rats and, B) female Wistar rats, where AfriplexGRT™ supplementation was at 60 mg/kg.

3.3.4.2. The effect of HFHS diet on trichrome stained heart sections of both male and female Wistar rats

In the control tissue sections, collagen was present around blood vessels, especially larger vascular structures as would be normally expected in association with the vasculature. Collagen appeared more prominent around medium-sized blood vessels. Multifocal few areas also yield mild increase in interstitial collagen between fibres; however, mild collagen presence is associated with the epicardium and endocardium. Minimal amounts of collagen were present in the interstitial spaces between small groups of fibres and did not appear increased in few areas with the degenerate appearance of fibres.

In the HFHS tissue sections, collagen appeared prominent around larger blood vessels, with small amounts also visible between groups of fibres and minimally associated with the epicardium and endocardium. Single areas showed minimally increased collagen interstitially between individual fibres, however epicardial and endocardial structures reveal poor collagen staining.

As a whole, the collagen appeared quite scant in most regions and only increased around blood vessels as would be normally expected or in areas possibly minimally increased above normal, however, this change was considered insignificant (Figure 3.13).

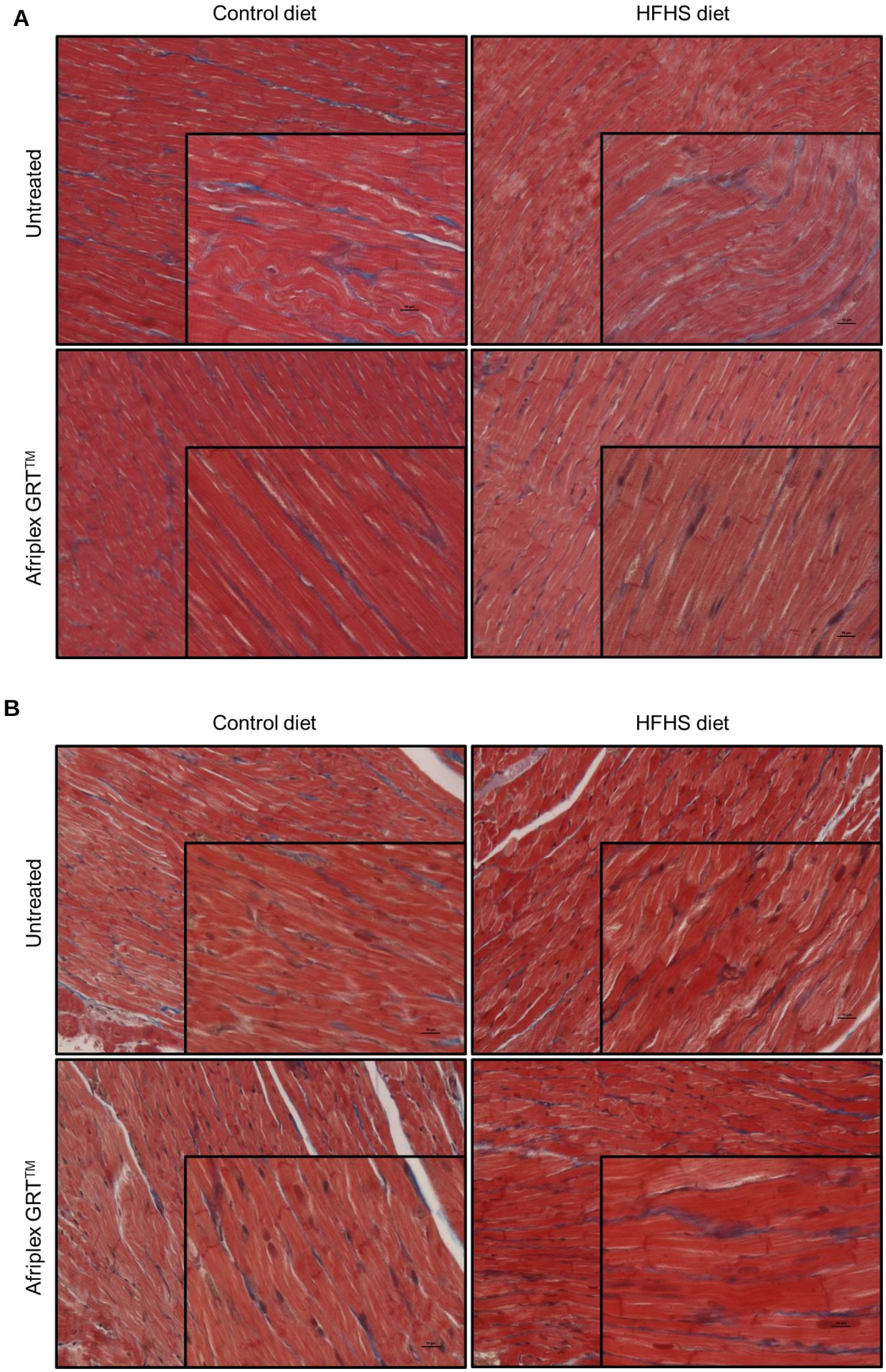

Figure 3.13: Trichrome stained heart sections. Representative images of trichrome stained sections from A) male Wistar rats and, B) female Wistar rats, where AfriplexGRT™ supplementation was at 60 mg/kg.

3.3.4.3. The effect of HFHS diet on LOXL2 immunohistochemical heart sections of both male and female Wistar rats

In both control and HFHS groups in both the male and female tissue sections, there was a high degree of variability in the LOXL2 staining (Figure 3.14). All groups and genders showed clear striations of the myocardial cells and an increased LOXL2 protein expression around blood vessels. As a whole there is no significant difference in LOXL2 protein expression in the myocardial tissue.

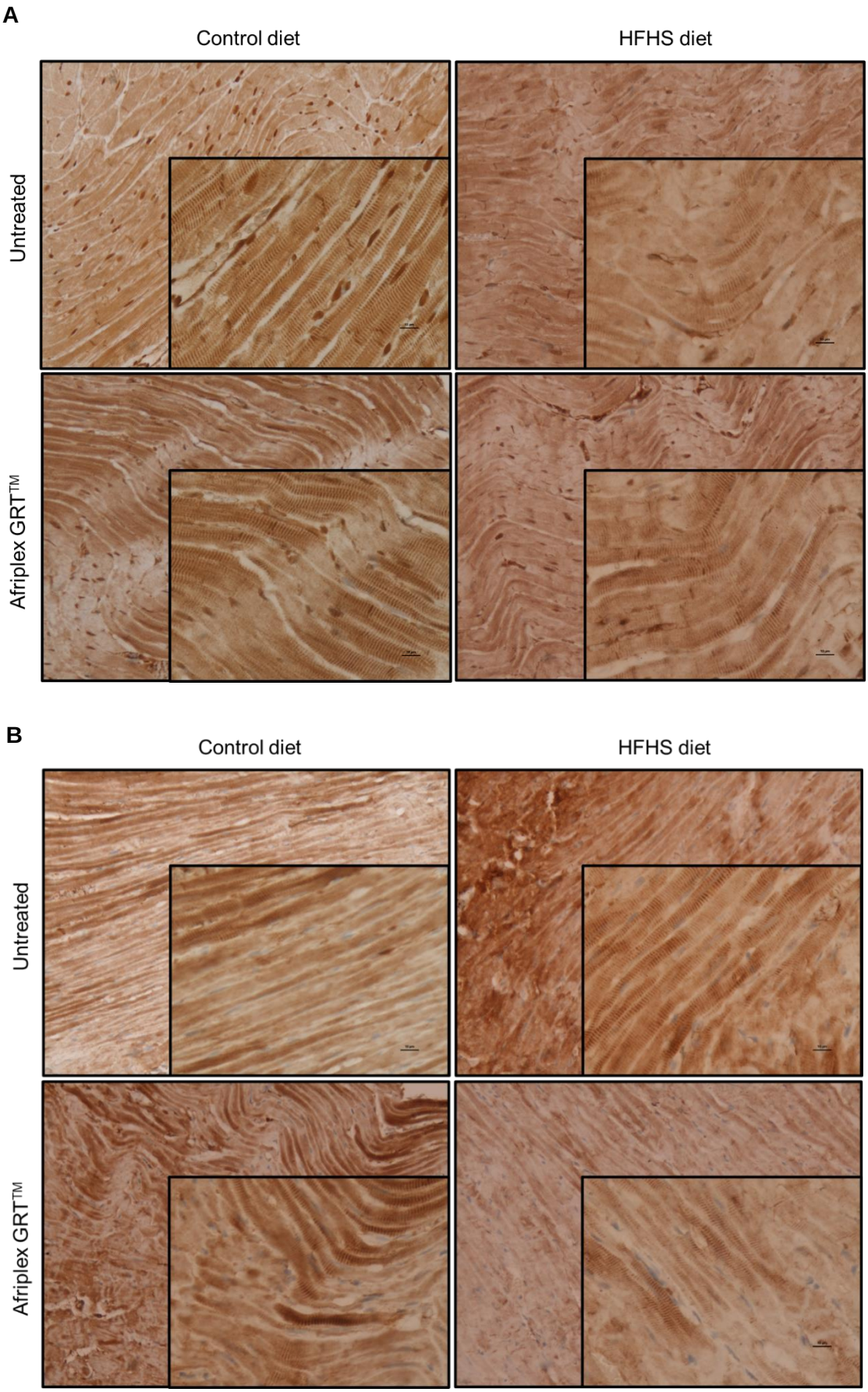

Figure 3.14: LOXL2 immunohistochemical probing. Representative images of LOXL2 immunostained heart sections from A) male and, B) female Wistar rats, where AfriplexGRT™ supplementation was at 60 mg/kg.

3.3.5. Gene Expression analysis

3.3.5.1. DNA methylation analysis

DNA methylation is an epigenetic mechanism used by cells to regulate gene expression. It is known that LOXL2 expression is affected by DNA methylation where demethylation increases LOXL2 expression. This increase of LOXL2 expression is associated with increased fibrosis, and Johnson et al. (2020) showed an increase in LOXL2 expression in the serum and hearts of db/db mice confirming LOXL2 upregulation in a diabetic state [34]. Five LOXL2 CpG sites within *LOXL2* promoter region have been identified (Figure 3.15) which are all conserved between humans, rats and mice.

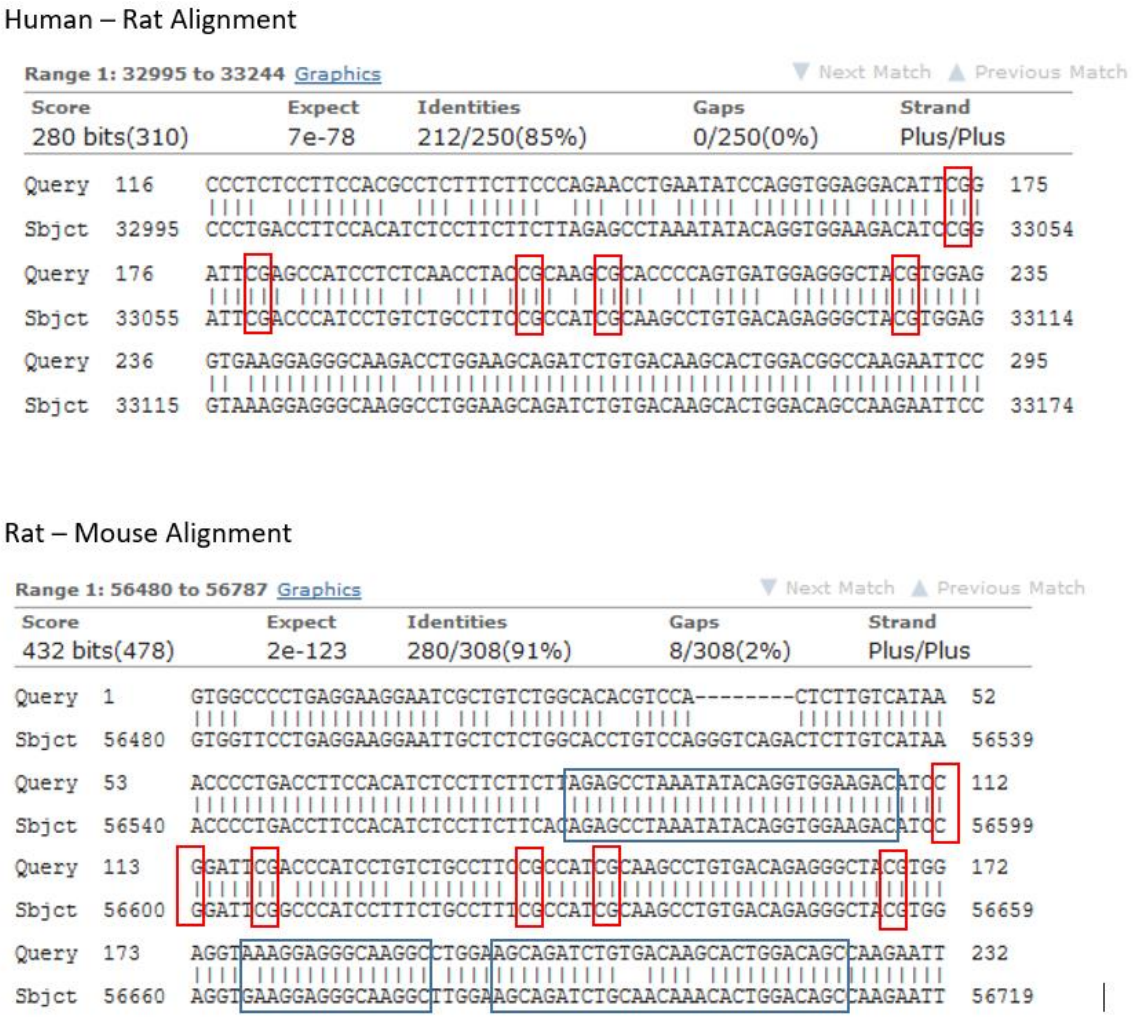

Figure 3.15: LOXL2 promotor alignment and CpG identification. NCBI human to rat alignment (A) and rat to mouse alignment (B) of the *LOXL2* promotor sequence, with the conserved CpG sites indicated by the red blocks and the forward, reverse and sequencing primer positions indicated by the blue blocks.

Results obtained revealed no significant change in methylation status at any of the 5 identified CpG sites for any of the groups. There was however a general trend whereby the methylation was slightly increased in the HFHS diet-fed male (53.9 ± 4.65 compared to 47.5 ± 4.42) and female (52.92 ± 5.65 compared to 51.1 ± 4.84) rats when compared to their respective control groups. There was a slight reduction in the methylation levels for the male HFHS diet group receiving AfriplexGRT™ (49.9 ± 4.20 and 50.0 ± 4.87) when compared to their HFHS diet counterparts, but a slight increase in the methylation levels for the male control group receiving AfriplexGRT™ (48.44 ± 4.27) when compared to its unsupplemented control group. However, supplementation with AfriplexGRT™ did not have any influence on the methylation levels of (48.60 ± 4.78) female rats receiving the HFHS diet (HFHS diet+AfriplexGRT) when compared to their HFHS diet-fed control counterparts. These changes were however very small and are thus inconclusive. Interestingly though, the methylation site with the highest level of methylation was CpG site 3 which had approximately 15-30% higher methylation than the other sites, irrespective of diet or gender (Figure 3.16).

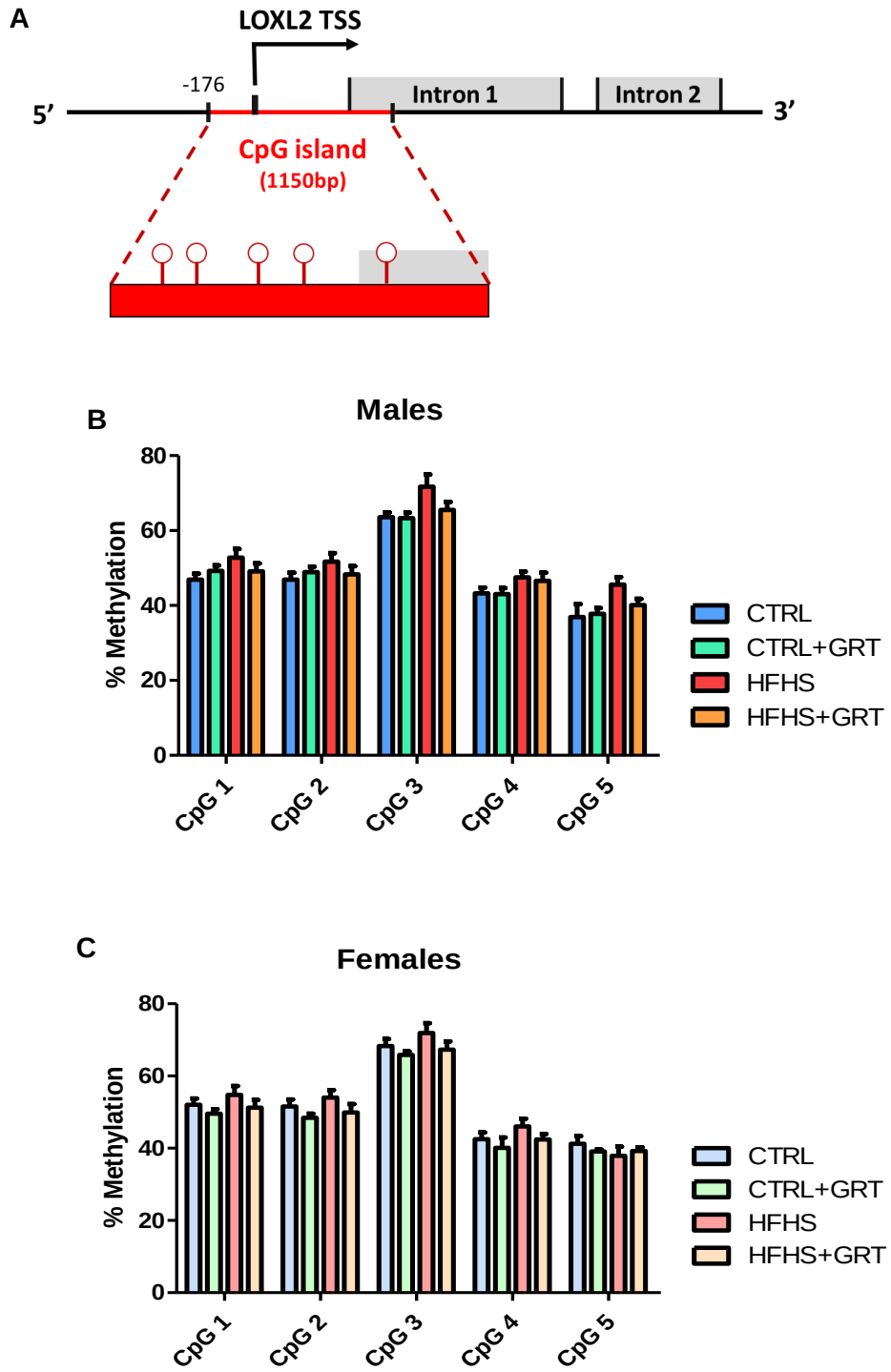

Figure 3.16: LOXL2 pyrosequencing analysis. (A) Graphical representation of the location of the 5 CpG sites investigated. Bar graph showing the percentage methylation of 5 identified methylation sites within the promoter and first exon of *LOXL2*, in both B) male and C) female Wister rats after 9 months on their respective diets. A one-way ANOVA was performed, and data represent the mean ± SEM of n=10 animals per group.

3.3.5.2. RNA expression

Differential gene expression was performed on genes involved in the fibrotic pathway that were located up and downstream of LOXL2. These genes included *COL1A1, SMAD2, SMAD3, TGFβ2, ACTA2, PIK3cg, AKT1, HIF1A1*, and *CTGF*. When comparing the control and HFHS groups, no significant differences were observed in the expression levels of any of the aforementioned genes analyzed.

LOXL2 expression was unchanged in the male (1.00 ± 0.070) group fed the control diet when compared to animals exposed to the HFHS diet (1.00 ± 0.072). A similar trend was observed in the female group fed the HFHS diet (0.97 ± 0.073) when compared to their control diet counterparts (1.00 ± 0.074). Its expression was however slightly increased in both the control male (1.09 ± 0.050) and female (1.12 ± 0.083) groups and the HFHS male (1.19 ± 0.033) and female (1.06 ± 0.093) groups when their diets were supplemented with AfriplexGRT™ when compared to their relative controls (Figure 3.17 and 3.18A).

The HFHS diet in did not influence the expression levels of *COLA1* (0.917 ± 0.137) in the female cohort compared to the control group (1.00 ± 0.090). However, *COL1A1* expression levels were increased slightly in the HFHS diet group (1.18 ± 0.17) and control group (1.31 ± 0.21) supplemented with AfriplexGRT™ when compared to their unsupplemented counterparts. This trend was however not followed in the male cohort where consumption of the HFHS diet resulted in a decrease in *COL1A1* expression in the HFHS group when compared to the control group (0.80 ± 0.069 compared to 1.00 ± 0.11). Supplementation with AfriplexGRT™ had no effect on *COL1A1* expression in the control (0.929 ± 0.070) or HFHS diet-fed (0.879 ± 0.059) male rats (Figure 3.17 and 3.18B).

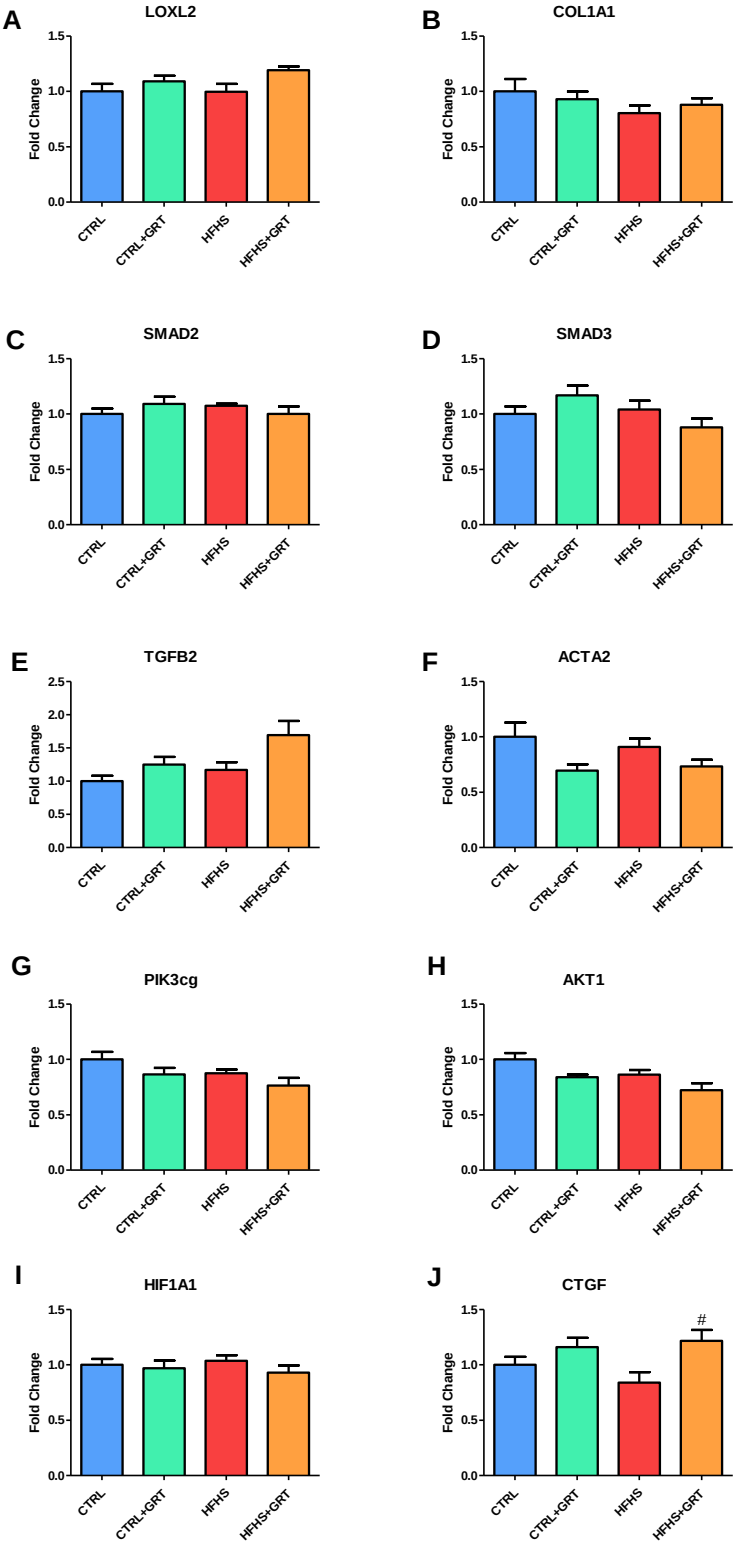

Figure 3.17: RNA expression in male rats. RNA expression of A) *LOXL2*, B) *COL1A1*, C) *SMAD2*, D) *SMAD3*, E) *TGFβ*, F) *α-SMA (ACTA2)*, G) *PI3K (PIK3cg)*, H) *AKT1*, I) *HIF1A*, J) CTGF in the hearts of male Wistar rats after 9 months on their respective diets. Data represents the mean ± SEM of n=10 animals per group. A one-way ANOVA was performed, and statistical significance is depicted as # p≤0.05 versus the control group.

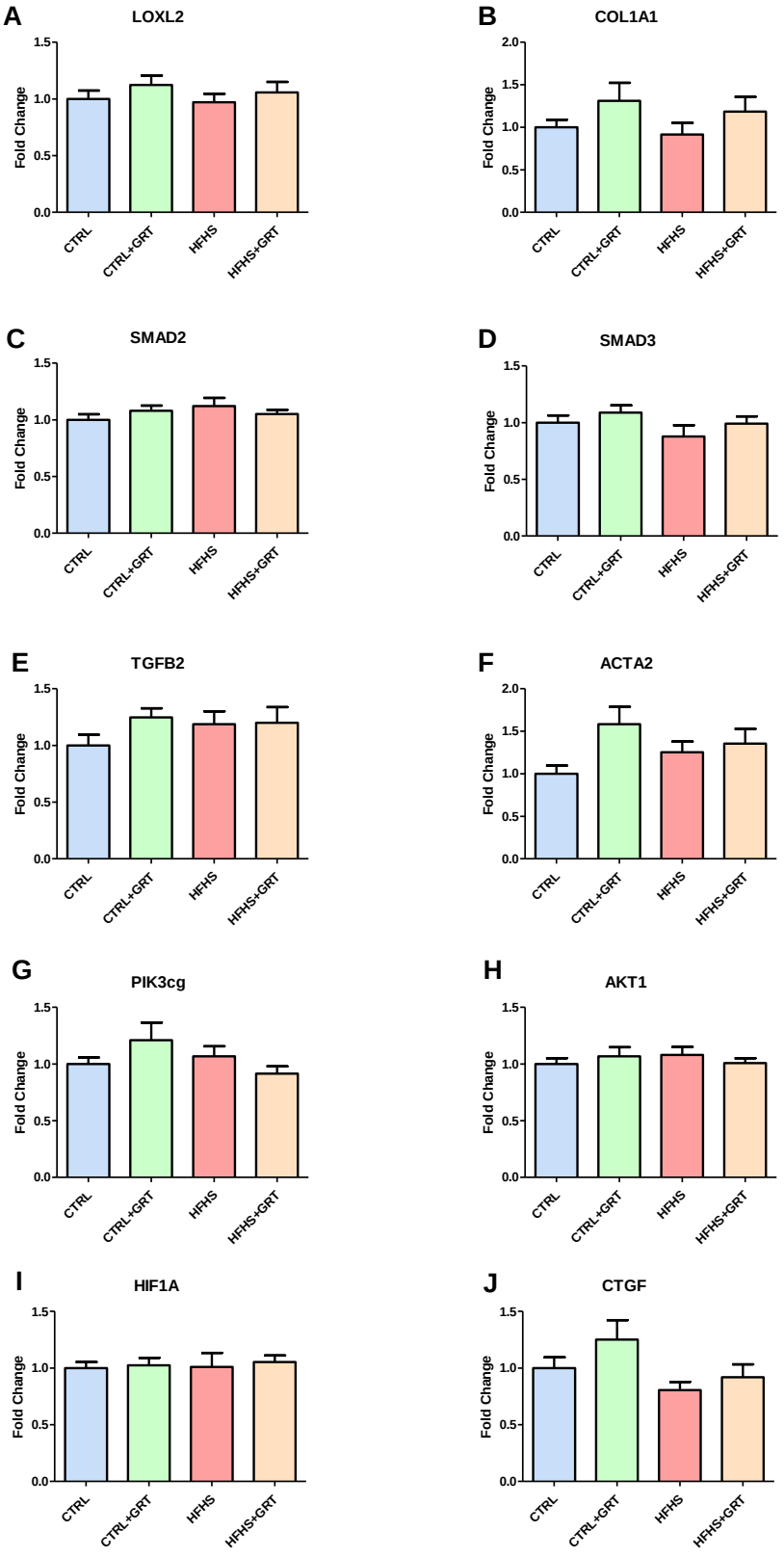

Figure 3.18: RNA expression of female rats. RNA expression of A) *LOXL2*, B) *COL1A1*, C) *SMAD2*, D) *SMAD3*, E) *TGFβ*, F) *α-SMA (ACTA2)*, G) *PI3K (PIK3cg)*, H) *AKT1*, I) *HIF1A*, J) *CTGF* in the hearts of female Wistar rats after 9 months on their respective diets. A one-way ANOVA was performed, and data represents the mean ± SEM of n=10 animals per group.

SMAD2, PIK3cg, AKT1 and *HIF1A* seemed largely unaffected by diet (Figure 3.16 and 3.17C, G-I). There was no change in the expression levels of *SMAD3* in the male animal group fed the HFHS diet when compared to their control counterparts (1.04 ± 0.080 compared to 1.00 ± 0.070), however, expression levels of *SMAD3* reflected a slight decrease in the female HFHS diet-fed group when compared to the control diet-fed animals (0.88 ± 0.099 compared to 1.00 ± 0.063). Supplementation with AfriplexGRT™ seemed to slightly increase *SMAD3* expression in the control diet-fed animals in both the male (1.17 ± 0.089) and female (1.089 ± 0.063) groups. In the HFHS diet-fed animals however, *SMAD3* expression slightly increased in the female animal group receiving AfriplexGRT™ supplementation (0.99 ± 0.064), whereas a decrease in expression level was observed among male animal group (0.88 ± 0.078), when compared to their untreated dietary controls (Figure 3.17 and 3.18D).

HFHS diet-feeding did not induce a significant change in the expression levels of *TGF-β2* in either the males and the females, however, *TGF-β2* was slightly upregulated in both male (1.17 ± 0.12 compared to 1.00 ± 0.079) and female (1.19 ± 0.12 compared to 1.00 ± 0.094) groups fed HFHS diet. AfriplexGRT™ supplementation in male HFHS diet group (1.69 ± 0.21), and control diet fed group (1.25 ± 0.12), increased *TGF-β2* expression compared to the untreated HFHS diet group and control diet fed group, respectively, although this difference was also insignificant (Figure 3.17 and 3.18E). *TGF-β2* expression was unchanged by AfriplexGRT™ supplementation in female animal group fed the HFHS diet (1.20 ± 0.14), however, it was increased in the female animal group fed control diet (1.25 ± 0.082) after having been exposed to AfriplexGRT™.

HFHS diet feeding decreased *ACTA2* expression (0.91 ± 0.076) in males when compared to their control diet-fed counterparts (1.00 ± 0.129). In contrast, *ACTA2* expression levels were slightly elevated in the females HFHS diet group (1.26 ± 0.13 vs 1.00 ± 0.95) when compared to the control group. AfriplexGRT™ supplementation of male and female HFHS diet group resulted in decreased and increased *ACTA2* expression levels respectively, in males (0.70 ± 0.056) and in females (1.36 ± 0.17), however, differences were not statistically significant. Interestingly, *ACTA2* expression was different between the male and female cohorts, with the males experiencing a decrease in the groups treated with AfriplexGRT™ when compared to their

control counterparts. Conversely, in the female cohort, AfriplexGRT™ supplementation increased the expression of *ACTA2* in both the control (1.85 ± 0.20) and HFHS diet-fed groups (Figure 3.17 and 3.18F).

Analysis of *CTGF* expression showed a slight decrease in the groups fed the HFHS diet in both the male (0.84 ± 0.093 vs 1.00 ± 0.074) and female (0.81 ± 0.070 vs 1.00 ± 0.094) groups, when compared to the animals on the control diets. An increased gene expression was observed after AfriplexGRT™ supplementation in all groups however this increase was statistically significant in the male cohort fed a HFHS diet (1.22 ± 0.10 vs 0.84 ± 0.09) (Figure 3.17 and 3.18J).

3.3.5.3. RT^2 PCR Rat Fibrosis Profiler Array

A RT^2 PCR profiler array was conducted to confirm the qRT-PCR gene expression analysis results of the genes from the proposed LOXL2 fibrosis signaling pathway, and to identify additional genes involved in fibrosis. The fibrosis profiler array did not investigate *LOXL2* or *COL1A1* expression, but instead *LOX* and *COL1A2* expression which is not directly comparable but an indication of expression of the genes of interest. Male animals saw a more than 2-fold decrease in *AKT1, LOX* and *SMAD3*, while females saw a similar decrease in *ACTA2, AKT1, COL1A2, CTGF* and *TGFβ2* in the HFHS diet-fed animals when compared to their control counterparts (Table 3.7).

Additional markers of fibrosis were selected for genes that were up- or down-regulated more than 10-fold. No genes were differentially regulated more than 4-fold in male rats fed the HFHS diet when compared to their control counterparts. Female animals on the HFHS diet, however, observed 17 genes with more than 10-fold downregulation (Table 3.7). The majority of the genes identified were inflammatory cytokines and chemokines (*CCL12, CCR2, CXCR4, IL10* and *ILK*). For the full list of genes on the array and the observed fold changes in male and female animals, see Supplementary Table A2.1 in Appendix 2.

Table 3.7: PCR Profiler Array results for genes of interest from the proposed fibrotic signaling pathway and possible additional markers for diet-induced fibrosis with greater than 10-fold regulation.

Gene	Description	Male Fold regulation	Female Fold regulation
Genes involved in Proposed Fibrosis Pathway			
Acta2	Smooth muscle alpha-actin	-1.60	**-5.85**
Akt1	V-akt murine thymoma viral oncogene homolog 1	**-2.21**	**-3.33**
Col1a2	Collagen, type I, alpha 2	-1.36	**-10.81**
Ctgf	Connective tissue growth factor	-1.63	**-7.04**
Lox	Lysyl oxidase	**-2.57**	1.35
Smad2	SMAD family member 2	-1.84	-1.48
Smad3	SMAD family member 3	**-2.69**	1.62
Tgfb2	Transforming growth factor, beta 2	-1.07	**-6.48**
Additional Markers for diet-induced Fibrosis			
Cav1	Caveolin 1, caveolae protein	-	**-16,43**
Ccl12	Chemokine (C-C motif) ligand 12	-	**-24,62**
Ccr2	Chemokine (C-C motif) receptor 2	-	**-22,27**
Col1a2	Collagen, type I, alpha 2	-	**-10,81**
Cxcr4	Chemokine (C-X-C motif) receptor 4	-	**-10,76**
Dcn	Decorin	-	**-10,81**
Il10	Interleukin 10	-	**-19,92**
IlK	Integrin-linked kinase	-	**-87,87**
Itgb3	Integrin, beta 3	-	**-23,82**
Itgb5	Integrin, beta 5	-	**-10,80**
Jun	Jun oncogene	-	**-101,83**
Serpinh1	Serine (or cysteine) peptidase inhibitor, clade H, member 1	-	**-39,47**
Smad7	SMAD family member 7	-	**-11,50**
Tgfb3	Transforming growth factor, beta 3	-	**-19,96**
Timp1	TIMP metallopeptidase inhibitor 1	-	**-64,48**
Timp3	TIMP metallopeptidase inhibitor 3	-	**-10,25**
Timp4	Tissue inhibitor of metalloproteinase 4	-	**-40,20**

3.3.5.4. Protein expression

To determine protein expression of some of the key proteins in the fibrotic pathway within the heart, western blot analysis was performed. In the male rats, the HFHS diet caused a decrease in pSMAD2 (46061 ± 20034), CTGF (45508 ± 15954), and LOXL2 (265339 ± 52701) expression, when compared to their levels in control diet-fed animals (26729 ± 8232; 97534 ± 24681; and 217763 ± 82538, respectively), however, this was not statistically significant. AfriplexGRT™ however had no effect on CTGF (9.82 ± 2.62 compared to 6.66 ± 2.34) expression in the HFHS diet-fed group compared to their HFHS controls. It however caused a non-significant increase in the pSMAD2 (16.25 ± 9.71 compared to 4.05 ± 1.53) and LOXL2 (48.96 ± 21.45 compared to 11.52 ± 2.61) expression (Figure 3.19A). The females however did not follow this pattern of expression where they saw a slight increase in pSMAD2 (0.011 ± 0.0034 compared to 0.0079 ± 0.0023) and LOXL2 (0.074 ± 0.029 compared to 0.052 ± 0.019) expression in the groups fed a HFHS diet when compared to their control counterparts. AfriplexGRT™ did not attenuate this in pSMAD2 (0.011 ± 0.0017) or LOXL2 (0.091 ± 0.034). There was also no change in the CTGF expression in the HFHS diet-fed animals compared to their control counterparts (0.043 ± 0.011 compared to 0.053 ± 0.016), and AfriplexGRT™ had no effect (0.045 ± 0.013) (Figure 3.19B).

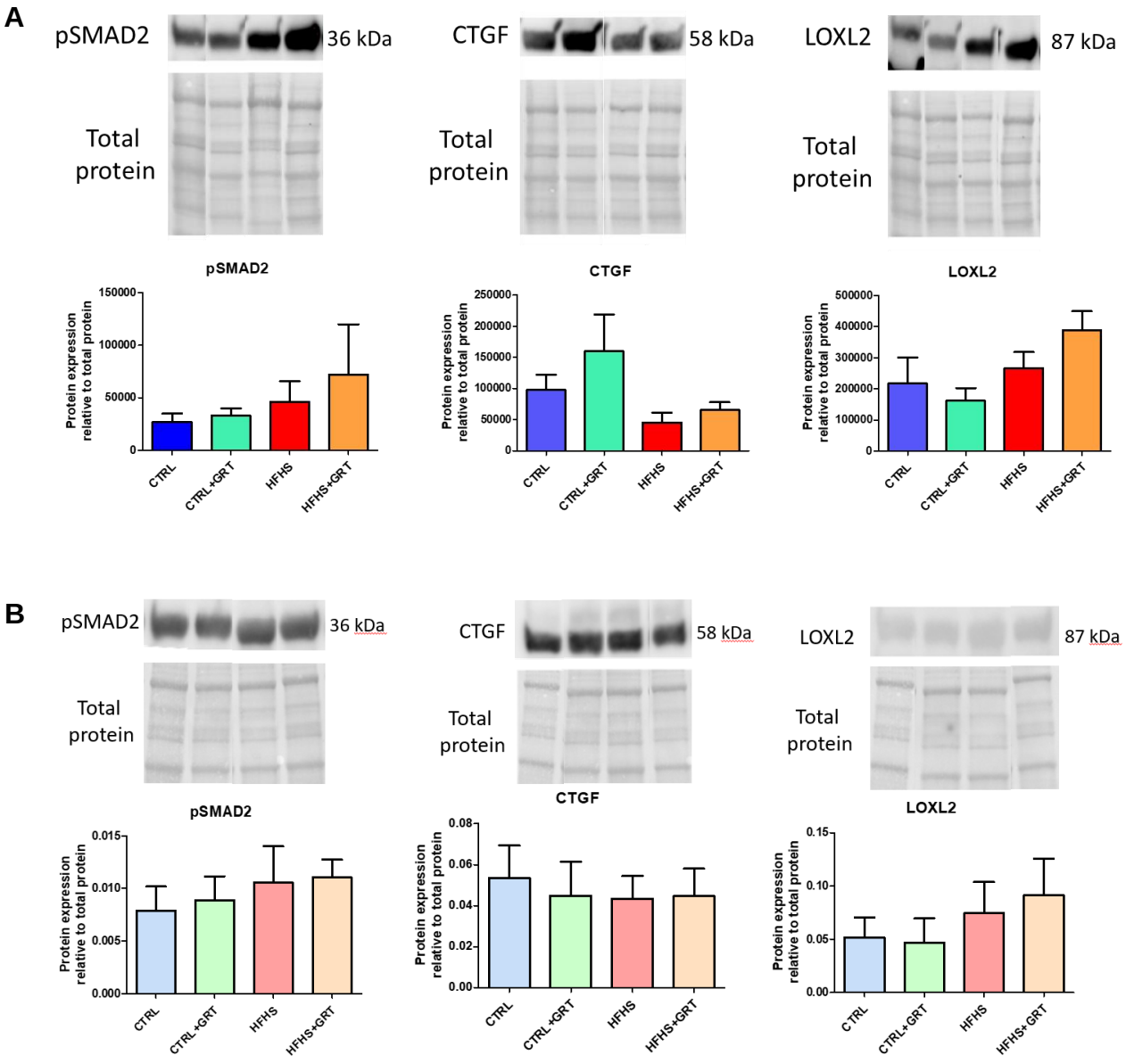

Figure 3.19: Western blot analysis of proteins extracted from heart tissue. pSMAD2, CTGF and LOXL2 protein expression from heart tissue from A) male and B) female Wistar rats. A one-way ANOVA was performed, and data represents the mean ± SEM of n=9 animals per group.

3.4. Discussion

There is accumulating evidence that augmented expression of LOXL2 in both humans and in animal models is linked to CVDs [12]. Yang et al. (2016) as well as Johnson et al. (2020) have more specifically shown that it is linked to cardiac fibrosis [33, 34]. This fibrosis in the heart can be caused by bad lifestyle choices such as unhealthy diet, lack of exercise, and smoking, leading to the increase of CVD risk factors [2]. It has also been observed that premenopausal women are protected against CVD development due to their hormones [3]. The current study thus aimed to investigate changes in markers of fibrosis and cardiac dysfunction in a diet-induced obesity Wistar rat model, by examining myocardial collagen deposition, and whether gender influences disease onset. The second aim was to investigate the prophylactic effect of AfriplexGRT^{TM}, for the maintenance of good metabolic health, against HFHS-diet-induced cardiac modulation in a Wistar rat.

3.4.1. The effect of caloric intake

To induce an experimental model of cardiac risk, Wistar rats were fed either a control diet (carbohydrates accounting for 54% of the total calories, with 22% calories from fat) or a HFHS diet (38% calories from carbohydrates) for 9 months. Since the HFHS diet-fed animals received extra calories from added sucrose and fructose in the water, both groups received high-calorie contents from their diet and thus the severity of the impact of our HFHS diet could be reduced when compared to the control groups since the diets were so similar. In addition, the control diet consisted of 22% calories from fat, while the HFHS diet consisted of 41% calories from fat. Since 22% fat in a diet is a considerably high amount, this could cause increased weight-gain similar to that caused by consuming our HFHS diet, since both diets were high in fat. In a study by Akiyama et al. (1996) where the caloric intake of rats was doubled compared to a control group, it was demonstrated that the higher caloric intake resulted in a significantly increased bodyweight, elevated serum cholesterol and triglyceride as well as free fatty acid levels, and the rats on the higher calorie intake group had worse glucose clearance than their control counterparts, after only 28 days [35]. Additionally, research conducted by Moreno-Fernández et al. (2018) showed that Wistar rats that were fed a diet composing of 22.5% fat and water supplemented with 25% dextrose was sufficient to induce a significant weight gain and could induce metabolic syndrome when compared to their control diet-fed counterparts over 20 weeks [36].

It was thus expected that the rats on the HFHS diet would have shown more significant signs of metabolic syndrome development after 9 months on the diet. Fat is known to positively affect the palatability of food [37] and could contribute to food intake differences. This could also contribute to a lower food intake in our HFHS group, leading to a less pronounced effect caused by this diet. The amount of protein was the same in both diets at ~15%, since lower protein could cause changes in insulin signaling [38].

3.4.2. The effect of HFHS diet on bodyweight, FBG, and HOMA-IR

The results from the animal study showed a steady increase in body weight for all the groups across the 9-month feeding period, however, the increase is more prominent for animals on the HFHS-diet. The significant increase in body weight due to the different diets occurred much earlier in male rats than their female counterparts, which is in part to be expected as male animals tend to eat much more than their female counterparts [39] and thus the effect of the diet might be seen earlier. The overall calories consumed were thus expectedly higher in male groups than the females. In our study, a significant weight gain was only seen after 9 months for the female rats fed the HFHS diet when compared to their control group. Similar findings were observed in a study done by Taraschenko et al. (2011) on Sprague-Dawley rats, where animals were fed either a high-fat (45% calories from fat) or a low-fat (10% calories from fat) diet for 30 or 34 days. It was found that male rats consuming a high-fat diet quickly exhibited an increased fat deposition and body weight when compared to their control counterparts, however, females on the same high-fat diet did not become obese [40]. In the current study, although both males and females were exposed to the same composition of HFHS diet, the males gained significantly higher weight than their age matched female counterparts. These gender-specific changes in body weight have been previously reported in Wistar rats even when using different diets such as a high-fructose diet in a study by Pektaş et al. [41]. In the study by Pektaş et al. (2015) rats were fed a standard rat chow diet with either tap water, or tap water containing 10% fructose for 24 weeks, after which male rats saw a statistically significant increase in bodyweight on the diet with fructose when compared to their control counterparts, however the weight gain in the female rats was minimal. In the current study, no significant change in bodyweight was observed in the male or female cohorts when the diets were supplemented with AfriplexGRT^{TM}, although caloric intake was significantly higher in HFHS diet-

fed groups for both genders. This indicates that AfriplexGRT™ is likely not involved in reducing weight gain in obesity and could indicate an increased hyperphagic response, which remains to be investigated.

The next aim of this study was to investigate the effect of the HFHS diet and AfriplexGRT™ on heart weight, retroperitoneal fat weight and liver weight in male and female rats. The HFHS diet caused a slight increase in the heart weight when compared to hearts of the control diet-fed animals, and even more so when supplemented with AfriplexGRT™, in both the male and female group, although this increase was not statistically significant. This could be indicative of a slight change in heart morphology due to the diet. An enlarged heart or liver could indicate hypertrophy or hyperplasia which are an increase in tissue size due to an increase in cell size or cell number, respectively, both of which could cause instability or dysfunction within the tissue. These results have previously been demonstrated by Zeng et al. (2015) in a mouse model, where mice fed a high-fat diet had a significant increase in heart weight when compared to their control diet-fed counterparts which was an indication of left ventricular hypertrophy [42].

The liver reflected an increase in weight in all rats fed the HFHS diet, however, this increase in weight was only significant in the male rats. This increase in liver weight was expected due to the liver being one of the first organs affected by metabolic changes, and it is particularly sensitive to the high amounts of fats ingested and results in non-alcoholic fatty liver disease in more severe cases [43]. In a study by Milagro et al. (2006), male Wistar rats were fed either a control standard chow diet or a high-fat diet for 56 days, after which they reported a statistically significant increase in the rats' bodyweights, fat content and liver weights [44]. Furthermore, features of metabolic syndrome, such as non-alcoholic fatty liver disease and increased retroperitoneal fat, have frequently been associated with an increased risk of cardiovascular disease [45, 46].

Retroperitoneal fat is a type of adipose tissue that accumulates between the organs; an increase in this fat depot is associated with lower metabolic health due to the movement of fat and pro-inflammatory cytokines into the liver (portal theory), thus leading to hepatic IR and steatosis [47]. In addition, the increase in circulating fat in the body leads to hepatic lipid accumulation, and this is often the driver of downstream metabolic dysfunctions [48]. In the current study, the retroperitoneal fat pad was significantly increased in all the groups fed the HFHS diet, with AfriplexGRT™ supplementation not affecting fat accumulation.

Stemmer et al. (2012) conducted a study whereby male Wistar rats were fed a high-fat diet (40% calories from fat) for 11 months and found that the animals with the higher caloric intake developed significantly larger fat depots when compared to the rats with lower daily calorie intake. More specifically their epididymal, retroperitoneal and subcutaneous fat pads were significantly larger than the corresponding depots of the lower calorie intake rats [49].

Impaired glucose tolerance is one of the markers of metabolic syndrome and as such, FBG levels were measured and OGTTs conducted. The effect of impaired fasting glucose occurs when the liver becomes intolerant to insulin, resulting in a reduction in glucose production suppression by insulin and also increases liver triglycerides [50–52]. There was however no significant change in FBG levels for males or females across the 9-month feeding period for all groups, except for the male HFHS diet-fed group at month 6 where they showed a brief increase in FBG levels. AUC results for the OGTTs indicated an impaired glucose-lowering capability within the male rats fed the HFHS diet when compared to their control counterparts, indicating a decrease in insulin sensitivity, which is often an indication of diabetes development, which is a known risk factor for cardiovascular disease. However, this impaired glucose clearance was not seen in the female cohort where the glucose was sufficiently cleared within 120-minutes.

Though this was not investigated in this study, it was interesting to note that females seem to have protection most likely conferred by their sex hormones, more specifically estrogen [53]. Furthermore, the same trend has been seen in pre-menopausal women were found to be protected against cardiovascular disease when compared to age-matched men, implicating that sex-hormones in the protective effect [54]. In addition, it has been suggested that 17β-estradiol, an oestrogen hormone, offers protection against the development of diabetes through increased β-cell survival [54]. While the rats FBG levels were expected to be elevated in the animals fed the HFHS diet, the impaired glucose clearance indicated by the OGTT results for the males was expected, however the females' lack of glucose intolerance was not in line with what is found in the literature. Atamni et al. (2016) conducted a study whereby 683 mice were fed either a control or high-fat diet for 16 weeks and the response in male and female groups compared [55]. They observed an increase in the FBG levels for both the male and female animals, although this increase was consistently higher in the male cohort

and an increase in the AUC for the OGTTs for both the male and female animals. A study in the same year by Lamont et al. (2016) fed NZO mice a standard chow control diet or a low carbohydrate, high-fat diet for 9 weeks and found an increase in FBG as well as a decrease in glucose tolerance indicated by the OGTT results for the animals on the low carbohydrate, high-fat diet when compared to their control counterparts [56]. In the current study, supplementation with AfriplexGRT™ did not improve glucose tolerance, even in the male cohort with impaired glucose clearance. These findings however do not correspond directly with literature where consumption of polyphenols exhibit improved glucose tolerance. For example, a study by Bozzetto et al. (2015) obese patients were placed on a control diet or a diet high in polyphenols for 8 weeks, whereafter an OGTT indicated that patients on the high polyphenolic diet had improved glucose clearance when compared to patients on the control diet [57].

The liver is often the first organ to be affected by metabolic dysfunction. Thus, to investigate whether changes occurred in the liver, AST and ALT levels were measured as markers of liver injury. These markers were found to be lower in the HFHS diet-fed rats for both genders when compared to the control group, indicating no liver damaged. Since the liver is one of the first organs to be affected during IR, these results indicate that metabolic syndrome is unlikely to have developed. This is however unusual since the rats were on the diet for 9 months, and other studies have shown metabolic derangement after a shorter time on a high-fat diet. Roux et al. (2011) showed changes in a Wistar rat model after 3 months on a 40% fat diet [58], while Pheiffer et al. showed a significant change in metabolic parameters in male Wistar rats after 7 months on the same HFHS diet [59]. These studies indicate that there must be additional factors, besides gender and diet composition that play a part in disease initiation and development.

3.4.3. Diets and lipids

It is known that obesity is often accompanied by metabolic derangement which presents as an increase in triglycerides and LDL cholesterol, impaired glucose tolerance, insulin resistance (often presenting with higher systemic insulin [60]), as well as an increase in pro-inflammatory cytokines [61] and adipose fibrosis [62]. Furthermore, diets high in fats usually cause an increase in serum triglyceride and cholesterol levels. There was however no change in the cholesterols, however, the triglycerides were significantly increased in all HFHS

diet-fed rats, regardless of gender. Since excess sugar and calories are converted to triglycerides [63], it is expected that triglyceride levels will be increased in the HFHS diet-fed rats. This increased in triglycerides corresponded to the reduced glucose clearance in males. A study by Moreno-Fernández et al. (2018) fed Wistar rats a control diet, a high-fat diet, a high-fat diet supplemented with fructose or a high-fat diet supplemented with glucose for 20 weeks and found that serum triglycerides were increased for all three groups on the high-fat diet when compared to their control counterparts, however, the total cholesterol and HDL-cholesterol levels were unaffected by the diet [36]. These data confirm the trend seen in the current study.

Hyperinsulinemia is often a symptom of metabolic syndrome, thus fasting serum insulin levels were measured. Although not significant, there was an increase in serum insulin levels in the HFHS groups, particularly in males. This is however expected because the HFHS-diet has a higher sugar content, and thus more insulin would be produced to control the blood glucose levels. A study by Moreno-Fernández et al. (2018) also observed significantly increased insulin levels in Wistar rats fed a high-fat diet, as well as a high-fat diet supplemented with either glucose or fructose, when compared to their control counterparts [36]. In addition, Lamont et al. (2016) also observed an increase in plasma insulin levels in mice fed a low carbohydrate, high-fat diet when compared to their control diet-fed counterparts, although this increase was not significant in the fasted animals [56]. As metabolic syndrome or IR starts to develop, the fasting insulin levels would also start to increase as more insulin is required to have the same glucose uptake effect. There was however no significant change in FBG levels or HOMA-IR, which is a ratio of insulin and FBG, either.

3.4.4. The effect of diet on markers of fibrosis

According to Yang et al. (2016), cardiac fibrosis is a major predictor of cardiovascular dysfunction and subsequent heart failure severity. More specifically, in recent years, LOXL2 has been identified as a possible predictor of cardiac fibrosis, however, as yet, LOXL2 has not been used as a therapeutic target of diet-induced obesity and cardiac dysfunction due to the paucity of data that exist [64]. Nonetheless, apart from the Yang et al. (2016) study, this was confirmed by Cavalera (2014) and later Zhao et al. (2017), who reported a positive correlation between serum LOXL2 levels, obesity and cardiac fibrosis [65, 66]. Yang et al. (2016) confirmed

this and reported that LOXL2 levels were elevated in the serum of end-stage heart failure patients as well as in mechanically stressed mice hearts [33], suggesting a pathological role of LOXL2 in cardiac fibrosis. Therefore, the current study measured serum LOXL2 levels as a marker of asymptomatic onset of diet-induced cardiac fibrosis. The most predominant effects were seen in the male rats, therefore the serum LOXL2 levels were only measured in the male groups. Although not significant, there was an increase in serum LOXL2 levels in the HFHS group when compared to the controls, and interestingly, the supplementation with AfriplexGRT™ reduced the LOXL2 levels. Since fibrosis, particularly involving the ECM, is known to be upregulated in states of obesity and IR, and with LOXL2 being a fibrotic marker, the increased level is expected. The effect of the AfriplexGRT™ could also be expected since polyphenols have been previously shown to decrease cytokines that drive the fibrotic process [67, 68].

To confirm the morphometric and molecular analysis, histological changes were also analyzed. The H&E-stained sections showed changes of multifocal hyalinisation (degradation) of fibres with increased interstitial oedema and minimum collagen fibres in cardiac interstitials space, known to cause contractile abnormalities. These minute histology changes were aligned with increased serum LOXL2 levels as well as decreased glucose clearance, which might be indicative of the pre-clinical onset of a cardiovascular insult.

3.4.5. LOXL2 mRNA expression and its downstream regulators as early marker of diet-induced fibrosis

Next, the fibrotic gene regulatory network was studied, to see whether the HFHS diet or AfriplexGRT™ supplementation caused changes on a molecular level. This study showed that mRNA expression analysis of *TGFβ2* was marginally upregulated by the HFHS-diet, and more so in the diets supplemented with AfriplexGRT™. A study by Sousa-Pinto et al. (2016) saw minimal changes to the *TGFβ2* expression in the adipose tissue of rats fed a high-fat diet when compared to rats fed a control diet [69]. Jiang et al. (2020) however found that consumption of a high-fat diet increased *TGFβ* expression in the hearts of C57BL/6J mice, when compared to their control group [70]. Taken together, these studies indicate that changes in *TGFβ2* expression are dependent on the model used. The minimal change in *TGFβ2* expression is however expected to result in equally insignificant changes in the expression of its downstream targets such as *LOXL2* and *COL1A1*.

There was no significant change in *LOXL2* expression due to differences in diet, treatment or gender. This was confirmed in by evaluating several downstream targets of *TGFβ2*. *LOXL2* showed a similar pattern of expression in the male and female cohorts with a non-significant, but slightly higher expression in the groups supplemented with AfriplexGRT™. There was however no effect on *LOXL2* expression caused by the different diets. In a study by Lytle et al. (2016), in a model of non-alcoholic steatohepatitis (NASH), mice fed a HFHS diet for 24 weeks showed increased *LOX* expression in the liver when compared to their controls, resulting in liver fibrosis [71]. This indicates the ability of a HFHS diet to induce the upregulation of fibrotic genes within a diet-induced disease state. Because, in the current study, there was no metabolic disease state, the minimal changes to *LOXL2* expression were expected.

Since *LOXL2* expression was not significantly altered by diet, no change was expected in collagen (*COL1A1*) or α-SMA (*ACTA2*) expression. Both *COL1A1* and *ACTA2* had an increase in expression in both the control and HFHS diet-fed groups supplemented with AfriplexGRT™ in the female cohort, however, this was not significant, and was also not observed in the male cohort. Because this was different in the male and female cohorts it could indicate a gender-specific effect for AfriplexGRT™, however, this cannot be confirmed since none of these changes were significant. *SMAD2/3*, *PI3K, AKT* and *HIF1A* are all involved in the fibrotic pathway, however, there was also no significant change in the expression of these genes. These all confirm that metabolic syndrome could not be induced in the Wistar rats included in the current study.

Furthermore*, CTGF* was investigated as a marker of cardiac damage to confirm what was seen in the histological analysis. A study by Jeckel et al. (2014) showed no significant changes in *CTGF* expression in the left ventricular tissue of male Wistar rats after 12 weeks of high-fat diet consumption when compared to their control diet counterparts [72]. As in the study by Jeckel at al., the results from the current study showed no significant change in the expression of *CTGF* in any of the other groups when compared to the control counterparts, however, there is a slight increase in expression in groups treated with AfriplexGRT™ when compared to the respective diet controls. This difference was indeed significant in the male group between the HFHS diet-fed group and its AfriplexGRT™ treated counterparts. These results confirm the scant changes observed in the histology, however, does seem to suggest that supplementation with AfriplexGRT™ could

result in a worse effect after long term use instead of being protective as hypothesised. This effect would however need to be further investigated, particularly in a model where metabolic syndrome was induced.

3.4.6. LOXL2 and DNA methylation

Gene expression is regulated by DNA methylation [73], which is an epigenetic modification. DNA methylation is the addition of a methyl group to a cytosine residue within the DNA, which can result in the repression of expression by inhibiting the binding of transcription factors to the DNA, thereby blocking transcription from taking place. The *LOXL2* gene has been previously identified to have CpG sites within its promoter region and its expression was suggested to be regulated by DNA methylation [29, 33]. Primers were designed to span the region identified in the literature to contain the CpG sites within the promotor of the *LOXL2* gene and pyrosequencing methylation analysis was performed on this region. These results indicated that there was no difference at any of the 5 identified methylation sites for male or female rats due to the diet, and supplementation with AfriplexGRT^{TM} also had no significant effect on the DNA methylation profile. The gene expression results for *LOXL2* thus correlated with the *LOXL2* DNA methylation results.

3.4.7. LOXL2 and pSMAD2 activation correspond to increased serum levels

Yang et al. (2016) reported that LOXL2 is transcriptionally activated in the stress heart and together with TGFβ2, pSMAD and COL1A it provides the primary signal that triggers the deposition of collagen in the stress heart. This study showed that a HFHS diet indeed increase pSMAD2 and pLOXL2 protein and not mRNA expression, which was particularly evident in the male rats. This infers that LOXL2 expression might not be regulated DNA methylation but rather by some post-translation modification which requires further investigation [74]. There are however many factors that influence the rates of transcription and translation [75], such as regulatory sequences, mRNA stability, gene silencing and promotor selection, all of which cause transcription and translation to proceed at different rates. It is thus possible that the rate of translation could be faster than the rate of transcription for pSMAD2 and LOXL2, and thus more of the RNA has been translated to proteins, resulting in an insignificant increase in the RNA expression, but a greater expression difference on the protein expression level. CTGF however seems to be slightly decreased in the HFHS diet-fed rats on both the RNA and protein level. Since CTGF is an indication of cardiac damage, these data suggest that even

though there is very little to no damage to the heart, the markers of fibrosis and its signalling pathway are upregulated due to the diet. From the proposed mechanism (Chapter 1), the question still remains whether LOXL2 and SMAD2 are upstream or downstream of CTGF and TGFβ signalling, however the data suggests that they might be upstream since the CTGF signalling was unaltered.

In addition to the factors studied, the age of the rats needs to be taken into account. Globally, more women are obese than men [76], however these statistics are reversed when it comes to CVD development [77] with a high prevalence of CVD among men. When taking age into account, however, there is a low incidence of CVDs in pre-menopausal women, where it is suspected that their hormones play a role in protecting their hearts from developing CVDs [78]. A sharp rise in CVD incidences is however seen in menopausal women or women over the age of 45 years [78]. When relating the rats' age in the current study to human ages, the rats were 5 weeks at the beginning of the study and 41 weeks at the end of the study. This correlates to a human age of 2.5 years old at the beginning of the study and around 25 years old by the end of the study [79, 80]. The female rats fall into the pre-menopausal category, and thus the gender differences seen in this study could be as a result of the protective effects of the female hormones. Future studies might consider a longer feeding period to compare the effects of the respective diets on pre- and post-menopausal animals and their CVD development.

Taken together, gender-specific differences in bodyweights, liver weights, OGTTs and the gene expression levels (*COL1A1, SMAD3, ACTA2* and *PIK3cg*) indicate that sex hormones could play a role in the development of metabolic diseases, or at the very least, in the rats' sensitivity and physiological responses to the development of diet-induced obesity. A serious limitation of this study however is that the animals did not develop metabolic syndrome, irrespective of gender. Since the current study focused on the heart, which is one of the last organs to see changes in metabolic diseases, the results do not conclusively show the effect of the diet or AfriplexGRT™ on developing cardiac injury or fibrosis. In order to study this effect, further research thus needs to be conducted whereby a different diet is used to induce metabolic disease or the study needs to be conducted for a minimum of 12 months. In addition, the levels of the rats' sex hormones

should be measured in order to determine whether the observed effects are indeed due to hormonal influences.

3.4.8. Additional markers for diet-induced fibrosis

The rat fibrosis profiler array was used to identify genes that could possibly be used as early detection markers for cardiac fibrosis. Genes with 10-fold regulation or higher were selected as additional markers of interest, which resulted in 17 down-regulated, however these were only changed in the female rats. The results indicated that of the 17 genes: four were ECM remodelling enzymes (*SERPINH1, TIMP1, TIMP3* and *TIMP4*), two were cell adhesion molecules (*ITGB3* and *ITGB5*), four were involved in signal transduction (*CAV1, DCN, SMAD7* and *TGFB3*) one was a transcription factor (*JUN*), one was a collagen gene (*COL1A2*) and five were inflammatory cytokines and chemokines (*CCL12, CCR2, CXCR4, IL10* and *ILK*) were also down regulated. These cellular processes should be further studied in terms of their mechanisms within diet-induced cardiac fibrosis and could serve as potential markers of cardiac risk.

Interestingly, these genes identified were only downregulated 10-fold or more in female rats, indicating that the fibrotic pathway was not activated within the females. This corresponds with the metabolic and molecular parameters assessed which indicated that the males were at higher risk of CVD development than their female counterparts. This matches with literature, where men are at higher risk of developing CVD than women [77].

3.5. Conclusion

In conclusion, results from this study showed that the HFHS-diet did not induce the desired metabolic derangement, as demonstrated by the normal FBG levels, HOMA-IR, liver enzymes, serum cholesterol and absence of cardiac pathology. Because of this, the effect of AfriplexGRT™ could not be effectively studied. However, gender-specific differences were evident in terms of increased body weight, fat accumulation, handling OGTT, triglycerides levels, OGTT, serum insulin, serum LOXL2 and increased LOXL2 and pSMAD2 protein expression associated with early onset of cardiac fibrosis. Interestingly, the female rats seem to be less prone to metabolic perturbations caused by a HFHS diet which could explain the lack of weight gain or changes in glucose tolerance when compared to their male counterparts. Since research is predominantly focused on male subjects [77], these results warrant further investigation into female animal models and humans to elucidate gender-specific variations in disease development and treatment with a specific focus on the role LOXL2 plays. Finally, the inability of AfriplexGRT™ to reverse HFHS-induced weight gain and metabolic dysfunction in our study may suggest that it may be ineffective as a preventative anti-obesity nutraceutical. Nonetheless, the current findings contributed toward knowledge production on diet-induced sex-differences and elaborated on the role serum and LOXL2 might play as an early marker and contributor to cardiac fibrosis. Future studies should consider the addition of alternative fibrotic markers to predict cardiac risk.

3.6. References

1. World Health Statistics (WHO). Monitoring health for the SDGs; *WHO:* Geneva, Switzerland, **2019**.

2. World Health Statistics (WHO). Cardiovascular diseases (CVDs) fact sheet Available online: https://www.who.int/news-room/fact-sheets/detail/cardiovascular-diseases-(cvds) (accessed on Sep 12, 2019).

3. Maas, A.H.E.M.; Appelman, Y.E.A. Gender differences in coronary heart disease. *Netherlands Hear. J.* **2010**, *18*, 598–603. doi: 10.1007/s12471-010-0841-y

4. Clayton, J.A. Studying both sexes: A guiding principle for biomedicine. *FASEB J.* **2016**, *30*, 519–524, doi:10.1096/fj.15-279554.

5. Yoon, D.Y.; Mansukhani, N.A.; Stubbs, V.C.; Helenowski, I.B.; Woodruff, T.K.; Kibbe, M.R. Sex bias exists in basic science and translational surgical research. *Surg. (United States)* **2014**, *156*, 508–516, doi:10.1016/j.surg.2014.07.001.

6. Beery, A.K.; Zucker, I. Sex bias in neuroscience and biomedical research. *Neurosci. Biobehav. Rev.* **2011**, *35*, 565–572. doi: 10.1016/j.neubiorev.2010.07.002

7. Campesi, I.; Marino, M.; Cipolletti, M.; Romani, A.; Franconi, F. Put “gender glasses” on the effects of phenolic compounds on cardiovascular function and diseases. *Eur. J. Nutr.* **2018**, *57*, 2677–2691. doi: 10.1007/s00394-018-1695-0.

8. Zheng, J.; Cheng, J.; Zheng, S.; Zhang, L.; Guo, X.; Zhang, J.; Xiao, X. Physical Exercise and Its Protective Effects on Diabetic Cardiomyopathy: What Is the Evidence? *Front. Endocrinol. (Lausanne).* **2018**, *9*, doi:10.3389/fendo.2018.00729.

9. Booth, F.W.; Roberts, C.K.; Laye, M.J. Lack of exercise is a major cause of chronic diseases. *Compr. Physiol.* **2012**, *2*, 1143–1211, doi:10.1002/cphy.c110025.

10. Travers, J.G.; Kamal, F.A.; Robbins, J.; Yutzey, K.E.; Blaxall, B.C. Cardiac fibrosis: The fibroblast awakens. *Circ. Res.* **2016**, *118*, 1021–1040. doi: 10.1161/CIRCRESAHA.115.306565.

11. González, A.; López, B.; Ravassa, S.; San José, G.; Díez, J. The complex dynamics of myocardial interstitial fibrosis in heart failure. Focus on collagen cross-linking. *Biochim. Biophys. Acta - Mol. Cell Res.* **2019**, *1866*, 1421–1432, doi:10.1016/J.BBAMCR.2019.06.001.

12. Rodríguez, C.; Martínez-González, J. The Role of Lysyl Oxidase Enzymes in Cardiac Function and Remodeling. *Cells* **2019**, *8*, 1483, doi:10.3390/cells8121483.

13. Janel, N.; Noll, C. Protection and Reversal of Hepatic Fibrosis by Polyphenols. In *Polyphenols in Human Health and Disease*; Elsevier Inc., **2013**; Vol. 1, pp. 665–679 ISBN 9780123984562.

14. Michalska, M.; Bluba, A.; Mikhailidis, D.P.; Nowak, P.; Bielecka-Dabrowa, A.; Rysz, J.; Banach, M. The role of polyphenols in cardiovascular disease. *Med. Sci. Monit.* **2010**, *16*, 110–9.

15. Lamuela-Raventos, R.M.; Quifer-Rada, P. Effect of dietary polyphenols on cardiovascular risk. *Heart* **2016**, *102*, 1340–1341. doi: 10.1136/heartjnl-2016-309647.

16. Khurana, S.; Venkataraman, K.; Hollingsworth, A.; Piche, M.; Tai, T.C. Polyphenols: Benefits to the cardiovascular system in health and in aging. *Nutrients* **2013**, *5*, 3779–3827. doi: 10.3390/nu5103779

17. Tressera-Rimbau, A.; Arranz, S.; Eder, M.; Vallverdú-Queralt, A. Dietary Polyphenols in the Prevention of Stroke. **2017**, 7467962. doi.org/10.1155/2017/7467962

18. Pantsi, W.G.; Marnewick, J.L.; Esterhuyse, A.J.; Rautenbach, F.; Van Rooyen, J. Rooibos (Aspalathus linearis) offers cardiac protection against ischaemia/reperfusion in the isolated perfused rat heart. *Phytomedicine* **2011**, *18*, 1220–1228, doi:10.1016/j.phymed.2011.09.069.

19. Liew, R.; Stagg, M.A.; Chan, J.; Collins, P.; MacLeod, K.T. Gender determines the acute actions of genistein on intracellular calcium regulation in the guinea-pig heart. *Cardiovasc. Res.* **2004**, *61*, 66–76, doi:10.1016/j.cardiores.2003.10.006.

20. Yu, D.; Zhang, X.; Xiang, Y.B.; Yang, G.; Li, H.; Fazio, S.; Linton, M.; Cai, Q.; Zheng, W.; Gao, Y.T.; et al. Association of soy food intake with risk and biomarkers of coronary heart disease in Chinese men. *Int. J. Cardiol.* **2014**, *172*, e285, doi:10.1016/j.ijcard.2013.12.200.

21. Zhang, X.; Ou Shu, X.; Gao, Y.-T.; Yang, G.; Li, Q.; Li, H.; Jin, F.; Zheng, W. Soy Food Consumption Is Associated with Lower Risk of Coronary Heart Disease in Chinese Women | The Journal of Nutrition | Oxford Academic. **2003**, 2874–2878.

22. D'Archivio, M.; Filesi, C.; Varì, R.; Scazzocchio, B.; Masella, R. Bioavailability of the polyphenols: Status and controversies. *Int. J. Mol. Sci.* **2010**, *11*, 1321–1342. doi: 10.3390/ijms11041321

23. Ekstrand, B.; Rasmussen, M.K.; Woll, F.; Zlabek, V.; Zamaratskaia, G. In Vitro Gender-Dependent Inhibition of Porcine Cytochrome P450 Activity by Selected Flavonoids and Phenolic Acids. *Biomed Res. Int.* **2015**, *2015*, doi:10.1155/2015/387918.

24. Guidelines for Ethical Conduct in the Care and Use of Animals Available online: https://www.apa.org/science/leadership/care/guidelines (accessed on Aug 30, 2020).

25. South African Bureau of Standards *South African National Standard: The care and use of animals for scientific purposes (SANS 10386:2008)*; Groenkloof, Pretoria: SABS Standards Division., 2008;

26. Reagan-Shaw, S.; Nihal, M.; Ahmad, N. Dose translation from animal to human studies revisited. *FASEB J.* **2008**, *22*, 659–661, doi:10.1096/fj.07-9574lsf.

27. Salgado, A.L.F.D.A.; De Carvalho, L.; Oliveira, A.C.; Dos Santos, V.N.; Vieira, J.G.; Parise, E.R. Insulin resistance index (HOMA-IR) in the differentiation of patients with non-alcoholic fatty liver disease and healthy individuals. *Arq. Gastroenterol.* **2010**, *47*, 165–169, doi:10.1590/S0004-28032010000200009.

28. Fischer, A.H.; Jacobson, K.A.; Rose, J.; Zeller, R. Paraffin embedding tissue samples for sectioning. *Cold Spring Harb. Protoc.* **2008**, *3*, pdb.prot4989, doi:10.1101/pdb.prot4989.

29. Fong, S.F.T.; Dietzsch, E.; Fong, K.S.K.; Hollosi, P.; Asuncion, L.; He, Q.; Parker, M.I.; Csiszar, K. Lysyl oxidase-like 2 expression is increased in colon and esophageal tumors and associated with less differentiated colon tumors. *Genes, Chromosom. Cancer* **2007**, *46*, 644–655, doi:10.1002/gcc.20444.

30. Zhan, P.; Shen, X.; Qian, Q.; Zhu, J.; Zhang, Y.; Xie, H.-Y.; Xu, C.-H.; Hao, K.; Hu, W.; Xia, N.; et al. Down-regulation of lysyl oxidase-like 2 (LOXL2) is associated with disease progression in lung

adenocarcinomas. *Med. Oncol.* **2012**, *29*, 648–655, doi:10.1007/s12032-011-9959-z.

31. Hasan, K.M.M.; Tamanna, N.; Haque, M.A. Biochemical and histopathological profiling of Wistar rat treated with Brassica napus as a supplementary feed. *Food Sci. Hum. Wellness* **2018**, *7*, 77–82, doi:10.1016/j.fshw.2017.12.002.

32. Matthews, D.R.; Hosker, J.P.; Rudenski, A.S.; Naylor, B.A.; Treacher, D.F.; Turner, R.C. Homeostasis model assessment: insulin resistance and β-cell function from fasting plasma glucose and insulin concentrations in man. *Diabetologia* **1985**, *28*, 412–419, doi:10.1007/BF00280883.

33. Yang, J.; Savvatis, K.; Kang, J.S.; Fan, P.; Zhong, H.; Schwartz, K.; Barry, V.; Mikels-Vigdal, A.; Karpinski, S.; Kornyeyev, D.; et al. Targeting LOXL2 for cardiac interstitial fibrosis and heart failure treatment. *Nat. Commun.* **2016**, *7*, 13710, doi:10.1038/ncomms13710.

34. Johnson, R.; Nxele, X.; Cour, M.; Sangweni, N.; Jooste, T.; Hadebe, N.; Samodien, E.; Benjeddou, M.; Mazino, M.; Louw, J.; et al. Identification of potential biomarkers for predicting the early onset of diabetic cardiomyopathy in a mouse model. *Sci. Rep.* **2020**, *10*, 12352, doi:10.1038/s41598-020-69254-x.

35. Akiyama, T.; Tachibana, I.; Shirohara, H.; Watanabe, N.; Otsuki, M. High-fat hypercaloric diet induces obesity, glucose intolerance and hyperlipidemia in normal adult male Wistar rat. *Diabetes Res. Clin. Pract.* **1996**, *31*, 27–35, doi:10.1016/0168-8227(96)01205-3.

36. Moreno-Fernández, S.; Garcés-Rimón, M.; Vera, G.; Astier, J.; Landrier, J.F.; Miguel, M. High fat/high glucose diet induces metabolic syndrome in an experimental rat model. *Nutrients* **2018**, *10*, doi:10.3390/nu10101502.

37. Manabe, Y.; Matsumura, S.; Fushiki, T. Preference for High-Fat Food in Animals. In; CRC Press/Taylor & Francis, **2009**; pp. 243–264 ISBN 9781420067750.

38. Araujo, E.P.; Amaral, M.E.C.; Filiputti, E.; de Souza, C.T.; Laurito, T.L.; Augusto, V.D.; Saad, M.J.A.; Boschero, A.C.; Velloso, L.A.; Carneiro, E.M. Restoration of insulin secretion in pancreatic islets of protein-deficient rats by reduced expression of insulin receptor substrate (IRS)-1 and IRS-2. *J.*

Endocrinol. **2004**, *181*, 25–38, doi:10.1677/joe.0.1810025.

39. van Hest, A.; van Haaren, F.; van de Poll, N.E. The behavior of male and female Wistar rats pressing a lever for food is not affected by sex differences in food motivation. *Behav. Brain Res.* **1988**, *27*, 215–221, doi:10.1016/0166-4328(88)90118-0.

40. Taraschenko, O.D.; Maisonneuve, I.M.; Glick, S.D. Sex differences in high fat-induced obesity in rats: Effects of 18-methoxycoronaridine. *Physiol. Behav.* **2011**, *103*, 308–314, doi:10.1016/j.physbeh.2011.02.011.

41. Pektaş, M.B.; Sadi, G.; Akar, F. Long-Term Dietary Fructose Causes Gender-Different Metabolic and Vascular Dysfunction in Rats: Modulatory Effects of Resveratrol. *Cell. Physiol. Biochem.* **2015**, *37*, 1407–1420, doi:10.1159/000430405.

42. Zeng, H.; Vaka, V.R.; He, X.; Booz, G.W.; Chen, J.X. High-fat diet induces cardiac remodelling and dysfunction: Assessment of the role played by SIRT3 loss. *J. Cell. Mol. Med.* **2015**, *19*, 1847–1856, doi:10.1111/jcmm.12556.

43. Marina, A.; Delfino Von Frankenberg, A.; Suvag, S.; Holly, S.; Kratz, M.; Richards, T.L.; Utzschneider, K.M.; Kratz, M. Effects of dietary fat and saturated fat content on liver fat and markers of oxidative stress in overweight/obese men and women under weight-stable conditions. *Nutrients* **2014**, *6*, 4678–4690, doi:10.3390/nu6114678.

44. Milagro, F.I.; Campión, J.; Martíez, J.A. Weight gain induced by high-fat feeding involves increased liver oxidative stress. *Obesity* **2006**, *14*, 1118–1123, doi:10.1038/oby.2006.128.

45. Ismaiel, A.; Dumitraşcu, D.L. Cardiovascular Risk in Fatty Liver Disease: The Liver-Heart Axis—Literature Review. *Front. Med.* 2019, *6*.

46. Adams, L.A.; Anstee, Q.M.; Tilg, H.; Targher, G. Non-Alcoholic fatty liver disease and its relationship with cardiovascular disease and other extrahepatic diseases. *Gut* **2017**, *66*, 1138–1153, doi:10.1136/gutjnl-2017-313884.

47. Item, F.; Konrad, D. Visceral fat and metabolic inflammation: The portal theory revisited. *Obes. Rev.* **2012**, *13*, 30–39, doi:10.1111/j.1467-789X.2012.01035.x.

48. Geisler, C.E.; Renquist, B.J. Hepatic lipid accumulation: Cause and consequence of dysregulated glucoregulatory hormones. *J. Endocrinol.* **2017**, *234*, R1–R21. doi: 10.1530/JOE-16-0513.

49. Stemmer, K.; Perez-Tilve, D.; Ananthakrishnan, G.; Bort, A.; Seeley, R.J.; Tschöp, M.H.; Dietrich, D.R.; Pfluger, P.T. High-fat-diet-induced obesity causes an inflammatory and tumor-promoting microenvironment in the rat kidney. *DMM Dis. Model. Mech.* **2012**, *5*, 627–635, doi:10.1242/dmm.009407.

50. Kim, S.P.; Ellmerer, M.; Van Citters, G.W.; Bergman, R.N. Primacy of hepatic insulin resistance in the development of the metabolic syndrome induced by an isocaloric moderate-fat diet in the dog. *Diabetes* **2003**, *52*, 2453–2460, doi:10.2337/diabetes.52.10.2453.

51. Arita, Y.; Kihara, S.; Ouchi, N.; Takahashi, M.; Maeda, K.; Miyagawa, J.I.; Hotta, K.; Shimomura, I.; Nakamura, T.; Miyaoka, K.; et al. Paradoxical decrease of an adipose-specific protein, adiponectin, in obesity. *Biochem. Biophys. Res. Commun.* **1999**, *257*, 79–83, doi:10.1006/bbrc.1999.0255.

52. Berg, A.H.; Combs, T.P.; Du, X.; Brownlee, M.; Scherer, P.E. The adipocyte-secreted protein Acrp30 enhances hepatic insulin action. *Nat. Med.* **2001**, *7*, 947–953, doi:10.1038/90992.

53. Bakir, S.; Mori, T.; Durand, J.; Chen, Y.-F.; Thompson, J.A.; Oparil, S. Estrogen-Induced Vasoprotection Is Estrogen Receptor Dependent. *Circulation* **2000**, *101*, 2342–2344, doi:10.1161/01.CIR.101.20.2342.

54. Cignarella, A.; Bolego, C.; Cignarella, A. Mechanisms of estrogen protection in diabetes and metabolic disease. *Horm. Mol. Biol. Clin. Investig.* **2010**, *4*, 575–580, doi:10.1515/HMBCI.2010.084.

55. Atamni, H.J.A.T.; Mott, R.; Soller, M.; Iraqi, F.A. High-fat-diet induced development of increased fasting glucose levels and impaired response to intraperitoneal glucose challenge in the collaborative cross mouse genetic reference population. *BMC Genet.* **2016**, *17*, doi:10.1186/s12863-015-0321-x.

56. Lamont, B.J.; Waters, M.F.; Andrikopoulos, S. A low-carbohydrate high-fat diet increases weight gain

and does not improve glucose tolerance, insulin secretion or β-cell mass in NZO mice. *Nutr. Diabetes* **2016**, *6*, e194, doi:10.1038/nutd.2016.2.

57. Bozzetto, L.; Annuzzi, G.; Pacini, G.; Costabile, G.; Vetrani, C.; Vitale, M.; Griffo, E.; Giacco, A.; De Natale, C.; Cocozza, S.; et al. Polyphenol-rich diets improve glucose metabolism in people at high cardiometabolic risk: a controlled randomised intervention trial. *Diabetologia* **2015**, *58*, 1551–1560, doi:10.1007/s00125-015-3592-x.

58. Roux, C.R. β-cell response to high fat diet induced metabolic demands in the obese Wistar rat, 2011.

59. Pheiffer, C.; Jacobs, C.; Patel, O.; Ghoor, S.; Muller, C.; Louw, J. Expression of UCP2 in Wistar rats varies according to age and the severity of obesity. *J. Physiol. Biochem.* **2016**, *72*, 25–32, doi:10.1007/s13105-015-0454-4.

60. Klop, B.; Elte, J.W.F.; Cabezas, M.C. Dyslipidemia in Obesity: Mechanisms and Potential Targets. *Nutrients* 2013, *5*, 1218–1240. doi: 10.3390/nu5041218

61. Wang, T.; He, C. Pro-inflammatory cytokines: The link between obesity and osteoarthritis. *Cytokine Growth Factor Rev.* 2018, *44*, 38–50. doi: 10.1016/j.cytogfr.2018.10.002.

62. Buechler, C.; Krautbauer, S.; Eisinger, K. Adipose tissue fibrosis. *World J. Diabetes* **2015**, *6*, 548, doi:10.4239/wjd.v6.i4.548.

63. Haberland, M.; Carrer, M.; Mokalled, M.H.; Montgomery, R.L.; Olson, E.N. Redundant control of adipogenesis by histone deacetylases 1 and 2. *J. Biol. Chem.* **2010**, *285*, 14663–14670, doi:10.1074/jbc.M109.081679.

64. Miana, M.; Galán, M.; Martínez-Martínez, E.; Varona, S.; Jurado-López, R.; Bausa-Miranda, B.; Antequera, A.; Luaces, M.; Martínez-González, J.; Rodríguez, C.; et al. The lysyl oxidase inhibitor β-aminopropionitrile reduces body weight gain and improves the metabolic profile in diet-induced obesity in rats. *DMM Dis. Model. Mech.* **2015**, *8*, 543–551, doi:10.1242/dmm.020107.

65. Cavalera, M.; Wang, J.; Frangogiannis, N.G. Obesity, metabolic dysfunction, and cardiac fibrosis:

Pathophysiological pathways, molecular mechanisms, and therapeutic opportunities. *Transl. Res.* **2014**, *164*, 323–335. doi: 10.1016/j.trsl.2014.05.001.

66. Zhao, Y.; Tang, K.; Tianbao, X.; Wang, J.; Yang, J.; Li, D. Increased serum lysyl oxidase-like 2 levels correlate with the degree of left atrial fibrosis in patients with atrial fibrillation. *Biosci. Rep.* **2017**, *37*, doi:10.1042/BSR20171332.

67. Yahfoufi, N.; Alsadi, N.; Jambi, M.; Matar, C. The immunomodulatory and anti-inflammatory role of polyphenols. *Nutrients* **2018**, *10*. The immunomodulatory and anti-inflammatory role of polyphenols.

68. Borthwick, L.A.; Wynn, T.A.; Fisher, A.J. Cytokine mediated tissue fibrosis. *Biochim. Biophys. Acta - Mol. Basis Dis.* **2013**, *1832*, 1049–1060. doi: 10.1016/j.bbadis.2012.09.014.

69. Sousa-Pinto, B.; Gonçalves, L.; Rodrigues, A.R.; Tomada, I.; Almeida, H.; Neves, D.; Gouveia, A.M. Characterization of TGF-β expression and signaling profile in the adipose tissue of rats fed with high-fat and energy-restricted diets. *J. Nutr. Biochem.* **2016**, *38*, 107–115, doi:10.1016/j.jnutbio.2016.07.017.

70. Jiang, J.; Li, Y.; Liang, S.; Sun, B.; Shi, Y.; Xu, Q.; Zhang, J.; Shen, H.; Duan, J.; Sun, Z. Combined exposure of fine particulate matter and high-fat diet aggravate the cardiac fibrosis in C57BL/6J mice. *J. Hazard. Mater.* **2020**, *391*, 122203, doi:10.1016/j.jhazmat.2020.122203.

71. Lytle, K.A.; Jump, D.B. Is Western Diet-Induced Nonalcoholic Steatohepatitis in Ldlr-/- Mice Reversible? *PLoS One* **2016**, *11*, e0146942, doi:10.1371/journal.pone.0146942.

72. Jeckel, K.M.; Bouma, G.J.; Hess, A.M.; Petrilli, E.B.; Frye, M.A. Dietary fatty acids alter left ventricular myocardial gene expression in Wistar rats. *Nutr. Res.* **2014**, *34*, 694–706, doi:10.1016/j.nutres.2014.07.011.

73. Moore, L.D.; Le, T.; Fan, G. DNA methylation and its basic function. *Neuropsychopharmacology* **2013**, *38*, 23–38. doi.org/10.1038/npp.2012.112

74. Ralston, A. Simultaneous Gene Transcription and Translation in Bacteria. *Nat. Educ.* **2008**, *1*, 4.

75. Hausser, J.; Mayo, A.; Keren, L.; Alon, U. Central dogma rates and the trade-off between precision and economy in gene expression. *Nat. Commun.* **2019**, *10*, 1–15, doi:10.1038/s41467-018-07391-8.

76. Garawi, F.; Devries, K.; Thorogood, N.; Uauy, R. Global differences between women and men in the prevalence of obesity: Is there an association with gender inequality? *Eur. J. Clin. Nutr.* **2014**, *68*, 1101–1106, doi:10.1038/ejcn.2014.86.

77. Mosca, L.; Barrett-Connor, E.; Kass Wenger, N. Sex/gender differences in cardiovascular disease prevention: What a difference a decade makes. *Circulation* **2011**, *124*, 2145–2154, doi:10.1161/CIRCULATIONAHA.110.968792.

78. Crosignani, P.G.; Farley, T.; Fauser, B.; Glasier, A.; Greer, I.; Hanson, M.A.; La Vecchia, C.; Mishell, D.; Rosano, G.; Simon, T.; et al. Hormones and cardiovascular health in women. *Hum. Reprod. Update* **2006**, *12*, 483–497, doi:10.1093/humupd/dml028.

79. Sengupta, P. The laboratory rat: Relating its age with human's. *Int. J. Prev. Med.* **2013**, *4*, 624–630.

80. Andreollo, N.A.; Santos, E.F. dos; Araújo, M.R.; Lopes, L.R. Rat's age versus human's age: what is the relationship? *Arq. Bras. Cir. Dig.* **2012**, *25*, 49–51. doi: 10.1590/s0102-67202012000100011.

Chapter 4:

Impact of an obesogenic diet and AfriplexGRT™ administration on fibrosis in hearts of male Wistar rats

4.1. Introduction

Cardiovascular disease (CVD) remains the leading cause of mortality worldwide [1] with a higher prevalence of well-known independent risk factors such as obesity and insulin resistance and type 2 diabetes mellitus (T2DM). This high CVD-associated mortality indicates inadequate available treatment options and highlights an urgent need for an innovative mechanistic paradigm for the treatment of cardiovascular disease.

Obesity is a major risk factor for CVD development, and various endocrine, autocrine, and paracrine properties of adipose tissue have highlighted its profound role in the coordination of metabolic disturbances and cardiovascular insults [2, 3]. Various obesity-associated risk factors can culminate in the development of cardiac fibrosis and myocardial dysfunction [4]. Cardiac fibrosis is a significant global health problem and is linked to various forms of heart disease [5, 6] characterized by excessive deposition of extracellular matrix (ECM) proteins, adverse tissue compliance, and ventricular dysfunction [7]. Excessive collagen type 1 deposition leads to cardiac dysfunction. Therefore, any molecule or pathway involved in ECM homeostasis and remodeling may provide novel potential targets for the treatment of cardiac fibrosis.

Lysyl oxidase (LOX) proteins are a family of five copper-dependent enzymes which play a key role in ECM homeostasis and remodelling. Their primary role is to oxidize lysine and hydroxylysine residues of collagen and elastin chains into aldehydes, which can subsequently form covalent cross-linkages after reacting with amino groups and other aldehydes [8, 9].

There is increasing evidence to support that abnormal activity of LOX proteins is linked with cardiovascular diseases [8, 10]. Excessive myocardial collagen deposition and crosslinking, a process governed by LOX enzymes, make a substantial contribution to cardiac fibrosis and can cause myocardial stiffness and cardiac dysfunction [11, 12]. Among five LOX enzymes, lysyl oxidase-like 2 (LOXL2) is a key player in cardiac fibrosis [13]. Yang et al. (2016) reported that LOXL2 expression levels were upregulated in the diseased hearts of humans and mice [13]. Elevated LOXL2 expression leads to enhanced TGFβ2 production, activating fibroblast transformation to myofibroblasts with augmented collagen deposition and crosslinking in abnormally thickened regions of stressed hearts. These effects result in interstitial fibrosis and cardiac dysfunction. Furthermore, various studies have also reported that dietary composition may also play a critical role in

cardiac dysfunction, and with a deeper understanding of the relationship between dietary composition and CVD risk profile, novel approaches can be identified for the treatment of CVD [4, 14, 15].

Although some conventional drugs have been shown to alleviate cardiac fibrosis in clinical trials, there is a paucity of efficacious therapies that can and inhibit or reverse cardiac fibrosis and prevent its progression in heart patients [16]. Various plant-derived polyphenols have been proposed as attenuators of cardiac fibrosis in several cardiovascular disease models [17]. Additionally, some dietary polyphenols have not only shown promise in protecting the heart but also reduce cardiac fibrosis development by decreasing oxidative stress as well as serum markers of fibrosis [17]. Of interest to this study is an *Aspalathus linearis* (commonly known as rooibos) derived polyphenol known as Aspalathin. A*. linearis* is a fynbos plant that is endemic to South Africa and occurs in two forms, i.e. unfermented (green) or fermented (red). Importantly, Aspalathin is the major bioactive compound present in unfermented green rooibos extract (AfriplexGRT^{TM}). Various health-related benefits of rooibos such as antidiabetic [18], anti-hypertensive [19], cholesterol lowering [20], anti-inflammatory [21, 22], and anti-obesity [23] effects have been attributed to its flavonoid content. Therefore, in the current study, we investigated the prophylactic effect of an Aspalathin-rich green rooibos extract (AfriplexGRT^{TM}) against cardiac fibrosis, specifically focusing on the modulation of LOXL2 and its downstream target genes in the hearts of obesogenic male Wistar rats. In brief, this study first evaluated the basic metabolic parameters and changes to morphological parameters, serum and genetic expressions of LOXL2 and its downstream target genes that are associated with an obesogenic diet (34% and 66% calories from fat), and then the therapeutic effects of AfriplexGRT^{TM} on modulating the abnormal levels on various parameters.

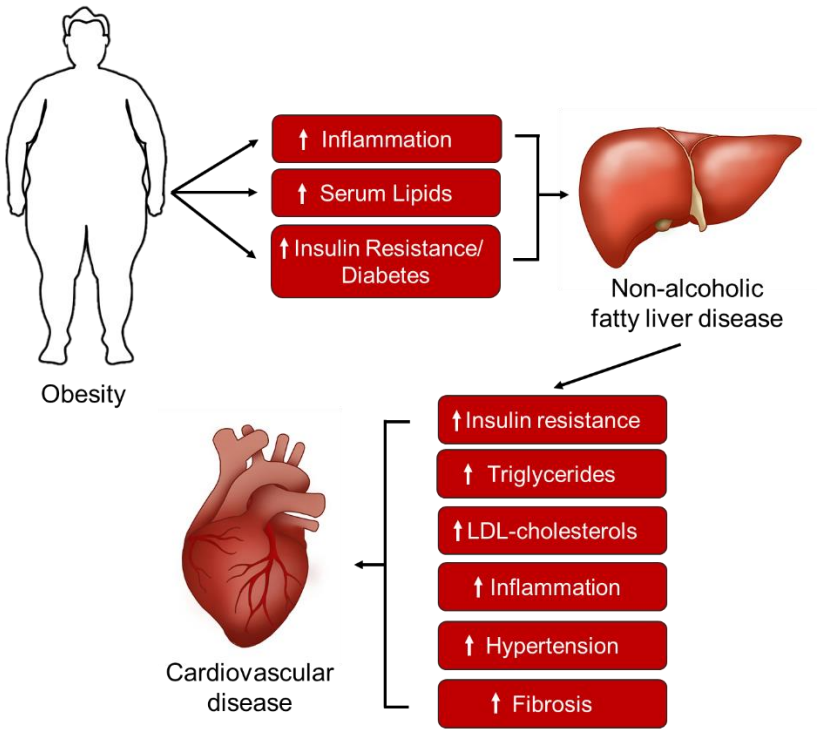

Figure 4.1: Obesity can lead to increased risk of cardiovascular disease (CVD) development. Obesity causes an increase in CVD risk factors such as an increase in serum triglycerides and inflammation, which can lead to non-alcoholic fatty liver disease and cardiovascular disease.

4.2. Material and Methods

4.2.1. Reagents and Kits

The RNeasy Fibrous Mini Kit, DNase treatment kit, cDNA synthesis kit, RT^2 First Strand Kit, RT^2 SYBR Green, and qPCR Master Mix were purchased from Qiagen (Valencia, CA, USA). The RC/DC protein determination kit, BSA standards, 12% precast gels, gel marker, Laemmli sample buffer, and running buffer were purchased from Bio-Rad (California, USA). All other consumables and reagents, unless otherwise specified, were purchased from Sigma-Aldrich Corp. (St. Louis, MO, USA).

4.2.2. Wistar rat model

4.2.2.1. Ethics

Ethical approval was obtained from the Research Ethics Committee on Animal Care at Stellenbosch University (protocol number ACU-2018-6786). All procedures were performed following the guidelines for ethical

conduct in the care and use of animals [24] and the South African National Standard for animal care (SANS 10386:2008) [25].

4.2.2.2. Study design: Grouping, diet and AfriplexGRT™ treatment of rats

Male Wistar rats were obtained and housed at the Animal Research Facility of the Faculty of Medicine and Health Sciences on Tygerberg campus, Stellenbosch University, in a temperature-controlled environment (23-25°C) with 12 h light/dark cycle and 50 ± 5% relative humidity. All rats received standard laboratory chow, *ad libitum,* and had free access to water. At 4-weeks post-weaning, at an age of 6 weeks, rats (n=72) were randomly allocated into three groups (n=24 per group) and fed either a (1) control diet (standard rat chow diet), (2) obesogenic 1 (OB1) diet (containing cooking fat, sucrose and condensed milk), or (3) obesogenic 2 (OB2) diet (containing cooking fat, condensed milk, fructose, cholesterol and casein) for 10 weeks (Figure 4.2) (see Supplementary Table A1.2 in Appendix 1 for detailed macronutrient diet composition). Thereafter, each group was further subdivided (n=12 per group) and their diets supplemented with or without AfriplexGRT™ (60 mg/kg) for a further 7 weeks. The Aspalathin-rich green rooibos extract (Afriplex GRT™) was obtained from Afriplex Pharmaceuticals PTY (LTD) (Paarl, South Africa). The treatment dosage was previously determined in a study by our group in a mouse model and the Reagen-Shaw conversion method [28] was used to convert the dosage to a relevant dosage in rats. AfriplexGRT™ was prepared daily and administered in the form of jelly cubes (60 mg/kg body weight). Briefly, jelly was prepared by mixing 1g gelatin powder per 1.92g raspberry flavored jelly powder in 12 mL of cold water. This mixture was stirred and heated in a microwave for 10 seconds at a time until the powders were dissolved, and the mixture left to cool. AfriplexGRT™ was dissolved in the cooled mixture (60°C) and set in jelly trays with the dose per animal (60 mg/kg bodyweight) aliquoted into numbered cubes at 4°C. These cubes were individually administered to each animal daily for the treatment period, ensuring that they ate the full cube, whilst untreated animals received a jelly cube containing no AfriplexGRT™.

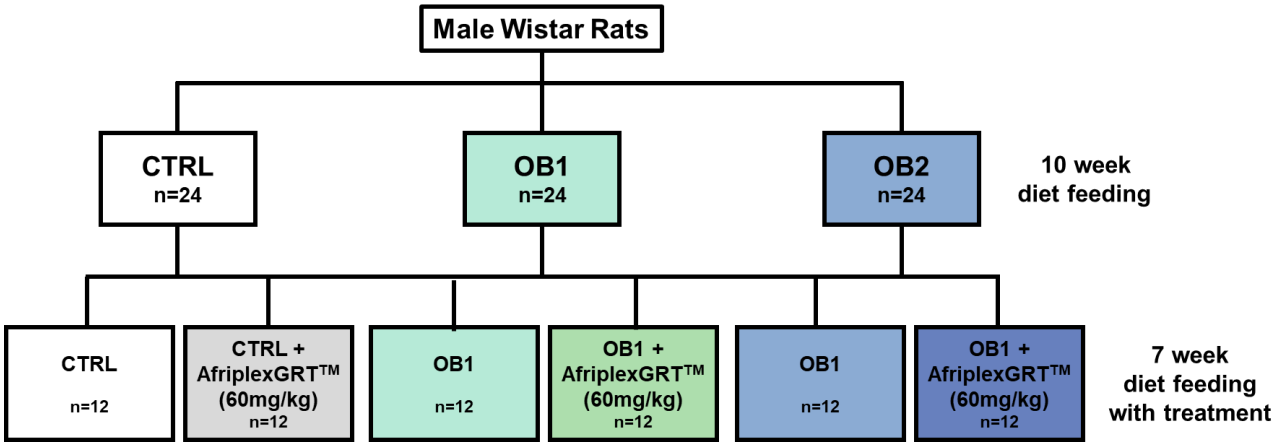

Figure 4.2: Animal study design. Male Wistar rats (n=72) were equally split into 3 groups (n=24 each) and fed a control diet (CTRL), an obesogenic 1 diet (OB1) or an obesogenic 2 diet (OB2) for 10 weeks. Each group was then split into two (n=12 animals/group) with their respective diets supplemented with or without 60 mg/kg AfriplexGRT™ for a further 7 weeks.

Animals were housed 4 animals per cage for the 16-week study period. The standard rat chow (Rodent breeder customized laboratory animal diet) was bought from LabChef Research Nutrition™ (Stellenbosch, South Africa). Food and water intake were monitored daily, and animal body weight was measured weekly, however, fasting blood glucose and oral glucose tolerance tests (OGTT) were only measured once, a week before terminations.

4.2.2.3. Sample collection

A week before concluding the study, animals were fasted for 16 hours and sedated with 10 mg of sodium pentobarbitone and anaesthetized with a 2% isoflurane. Fasting blood glucose levels were measured, and 1 mL blood was collected from the carotid artery into serum-separating tubes for serum analysis. Serum was used for the analysis of lipid profiles, liver enzymes, as well as insulin. At the termination of the study, animals were euthanized overdose with 160 mg/kg sodium pentobarbitone, followed by exsanguination. This blood collected from the vena cava was also collected in serum-separating tubes and the serum used for serum LOXL2 analysis. Heart tissue was also collected and snap-frozen for storage at -80°C till further analysis.

4.2.3. Biochemical analysis

4.2.3.1. Fasting Blood glucose

The animals blood glucose was measured by tail prick where a needle was used to prick the end of the tail and the resulting blood droplet used to measure the glucose concentration using a Glucoplus™ glucometer (Glucoplus, Montreal, Canada).

4.2.3.2. Plasma insulin

At termination, without fasting the rats, blood was collected into serum separator tubes, put on ice for 2 hours before centrifugation at maximum speed for 10 minutes. Serum aliquots were made and stored at -80°C until further use. The serum was used to perform an insulin ELISA analysis according to the manufacturer's protocol to determine the rat plasma insulin levels.

4.2.3.3. HOMA-IR

Wistar rats were fasted for 16 hours before their fasting glucose levels were measured. The HOMA-IRs were then calculated by fasting insulin (µU/L) x fasting glucose (nmol/L)/22.5.

4.2.3.4. Oral Glucose Tolerance test (OGTT)

After 15 weeks of the study, an oral glucose tolerance test (OGTT) was performed. The animals were fasted for 16 hours and their basal blood glucose concentrations measured. Thereafter they were administered 1 g/kg bodyweight 50% sucrose using oral gavage. Blood glucose concentrations were then measured at 3, 5, 10, 20, 30, 45, 60, 90 and 120 minutes after sucrose administration by means of a tail prick.

4.2.3.5. Lipid Profile analysis

After the 17-week study period, the serum collected after 16 hours of fasting was sent to Pathcare Medical Diagnostic Laboratories, South Africa for lipid profile analysis, where triglyceride, low-density lipoprotein (LDL), high-density lipoprotein (HDL) and total cholesterol levels were measured. In addition, liver enzymes aspartate aminotransferase (AST) and alanine aminotransferase (ALT) were also quantified.

4.2.3.6. Enzyme-linked immunosorbent assay (ELISA) analysis

4.2.3.6.1. Serum Insulin analysis

Serum insulin levels were determined by means of a Millipore Sandwich rat/mouse insulin ELISA kit (Merck, Massachusetts, USA) as described in chapter 3, section 3.2.3.8.1. The homeostatic model assessment for insulin resistance (HOMA2-IR) was calculated as a measurement of insulin resistance within the animal model and was calculated as fasting insulin (µU/L) x fasting glucose (nmol/L)/22.5 [26].

4.2.3.6.2. Serum LOXL2 analysis

Serum LOXL2 levels were determined using a rat lysyl oxidase-like protein 2 (LOXL2) sandwich ELISA kit (MyBiosource, California, United States, cat#: MBS2705848) as per manufacturer's instructions, as described in chapter 3, section 3.2.3.8.2.

4.2.3.7. Histology and microscopy analysis of heart tissue sections

The tissue was flash-frozen using liquid nitrogen upon collection. Using a Leica CM1860 cryostat (Leica, Wetzlar, Germany) 5µm sections were cut from the frozen tissue. These were then fixed onto glass slides and stained with hematoxylin and eosin stain (Merck-Millipore, Billerica, USA), as per the manufacturer's instructions. For histological analysis, 5 random areas of each of the sections were digitized using an Olympus BX50 light microscope (20x and 40x magnification) and NIS-Elements BR 3.0 computerized image analysis software (Nikon, Tokyo, Japan).

4.2.3.7.1. Hematoxylin & Eosin staining

Hematoxylin and Eosin stain (H&E) (Merck-Millipore, Billerica, USA) was performed by standard laboratory procedures described in chapter 3, section 3.2.3.9.1. These slides were then sent to Idexx Laboratories (Johannesburg, South Africa) for analysis.

4.2.4. Gene and Protein expression analysis

Expression analysis was carried out in the hearts of the control, OB1, OB1+AfriplexGRT^{TM}, OB2 and OB2+AfriplexGRT^{TM} rat groups. Quantitative real-time polymerase reaction (qRT-PCR) analysis was used to assess mRNA expression levels in the heart, while protein was extracted to assess whether changes in mRNA expression were translated to protein expression levels in the rat hearts.

4.2.4.1. RNA extraction

Total RNA was extracted from frozen heart tissue, using a Qiagen RNeasy Fibrous Mini Kit (The Scientific Group, South Africa, cat# QIA/74704) as described in chapter 3, section 3.2.4.2.1.

4.2.4.1.1. RNA quantification

The mRNA concentrations were then measured as described in chapter 3, section 3.2.4.2.2.

4.2.4.1.2. DNase treatment

DNase treatment was performed on 5 µg of RNA using an Invitrogen Ambion DNase kit (Thermo Fisher Scientific, Massachusetts, USA) as described in chapter 3, section 3.2.4.2.3.

4.2.4.1.3. cDNA conversion and assessment of genomic DNA contamination

Total RNA was reverse transcribed to complementary DNA (cDNA) using a High-Capacity cDNA Reverse transcription kit (Thermo Fisher Scientific, Massachusetts, USA) as described in chapter 3, section 3.2.4.2.4.

To assess whether the synthesized cDNA contained any genomic DNA, a PCR was run on the Quantstudio 7 Flex Real-Time PCR system (Thermo Fisher Scientific, Massachusetts, USA) as described in chapter 3, section 3.2.4.2.5.

4.2.4.1.4. Quantitative Real-Time PCR (qRT-PCR)

cDNA was used for expression analysis by means of qRT-PCR. Briefly, Taqman® Gene Expression assays were purchased from Thermofisher Scientific (Massachusetts, USA). The genes analyzed are found in Table 4.1.

Table 4.1: Taqman® Gene Expression assay list.

Gene Name	Description	Taqman® Assay ID
LOXL2	Lysyl oxidase-like 2	Rn01466080_m1
COL1A1	Collagen, type I, alpha 1	Rn01463848_m1
α-SMA (ACTA2)	Actin alpha 2 (alpha-smooth muscle actin)	Rn01759928_g1
SMAD2	Mothers against decapentaplegic homolog 2	Rn00569900_m1
SMAD3	Mothers against decapentaplegic homolog 3	Rn00565331_m1
CTGF	Connective tissue growth factor	Rn01537279_g1
TGFβ2	Transforming growth factor beta-2	Rn00676060_m1
HIF1A	Hypoxia-inducible factor 1-alpha	Rn01472831_m1
AKT1	Protein kinase B	Rn00583646_m1
PI3K (PIK3cg)	Phosphatidylinositol-4,5-Bisphosphate 3-Kinase Catalytic Subunit Gamma	Rn01769524_m1
SOD2	Superoxide dismutase 2	Rn00690588_g1
NRF2 (NFE2L2)	Nuclear factor erythroid 2-related factor 2	Rn00582415_m1
ACTβ	Beta-actin	Rn00667869_m1
HPRT	Hypoxanthine-guanine phosphoribosyltransferase 1	Rn01527840_m1

A standard curve set up to determine the relative expression of each gene as described in chapter 3, section 3.2.4.2.6. Expression results were normalized to the expression of housekeeping genes ACTβ and HPRT.

4.2.4.2. Protein expression analysis

4.2.4.2.1. Protein extraction

Protein was extracted from rat heart tissue as described in chapter 3, section 3.2.4.3.1.

4.2.4.2.2. Quantification of proteins

Protein concentration was determined by means of a reducing agent compatible and detergent compatible (RC/DC) Protein Assay (Bio-Rad, California, USA), as described in chapter 3, section 3.2.4.3.2.

4.2.4.2.3. Western Blot analysis

Western blot analysis was performed as described in chapter 3, section 3.2.4.3.3. The antibodies and their dilutions used are listed below (Table 4.2).

Table 4.2: List of primary antibodies and their dilutions used for Western Blot analysis.

Antibody	Company	Cat#	Dilution
CTGF	Santa Cruz	Sc-365970	1:500
p-SMAD2	Abcam	Ab53100	1:250
LOXL2	Abcam	Ab96233	1:500

4.2.5. Statistical Analysis

All data were analyzed using GraphPad Prism 5.04 (GraphPad Software, California, USA) and expressed as mean ± the standard error of the mean (SEM). Data was tested for normal distribution using a Shapiro-Wilks test, followed by a one-way ANOVA with a Tukey's multiple comparison post hoc or a two-way ANOVA with a Bonferroni post hoc, where applicable. A p-value of < 0.05 was considered statistically significant.

4.3. Results

4.3.1. Biochemical analysis

4.3.1.1. Nutritional composition of diets

Samples of the respective diets were sent to Microchem Lab Services (Pty) Ltd for chemical composition analysis to ascertain the amount of fat, protein, carbohydrates, and fiber contained within each diet.

Table 4.3: Diet composition. Composition analysis of the control, obesogenic 1 (OB1) and obesogenic 2 (OB2) diets as per the Microchem analysis.

Component	Control diet	OB1 diet	OB2 diet
Fat (g/100g)	5.04	8.80	24.09
Protein (g/100g)	25.8	9.0	12.9
Dietary Fiber (g/100g)	16.8	4.0	5.5
Carbohydrates (g/100g)	44.2	31.0	17.0
Fructose (g/100g)	0.3	0.1	4.4
Sucrose (g/100g)	4.6	17.5	1.5

4.3.1.2. Food and caloric intake

The food intake was measured over the 10-week initial feeding period, and this showed a significant increase in the amount of food consumed by rats on the OB1 diet when compared to the control diet (219.0 ± 2.39 compared to 170.4 ± 5.69). The rats on the OB2 diet had the same food intake per week as the control diet-fed animals (163.8 ± 2.34) over the 10 weeks. When comparing the food intake for the OB1 and OB2 groups, the OB1 diet-fed rats consumed significantly more food than their OB2 diet-fed counterparts (Figure 4.3A).

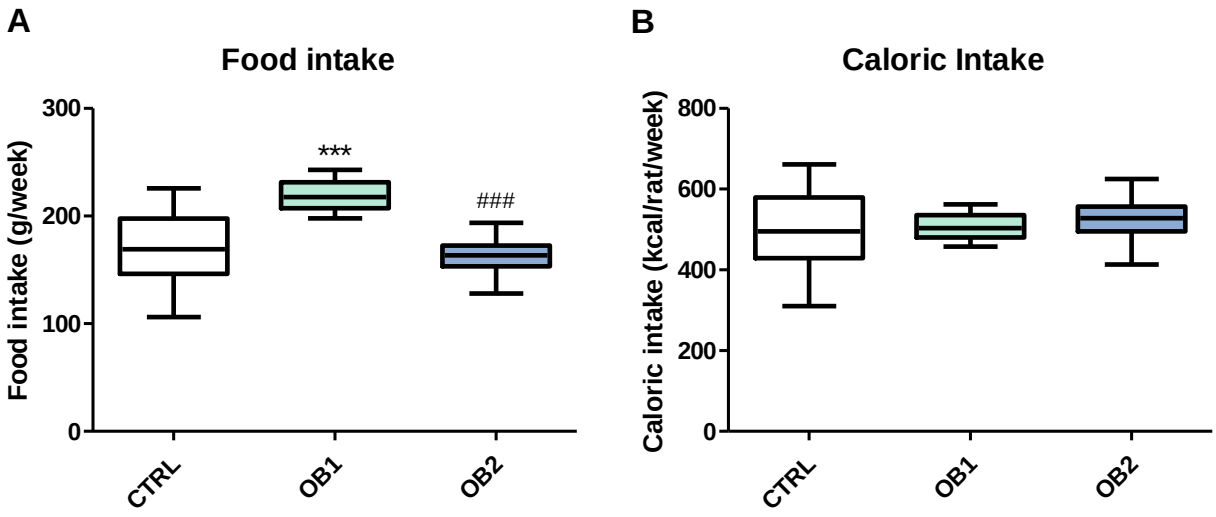

Figure 4.3: Food and caloric intake of animals on the obesogenic diets. Box and whisker plot of (A) the amount of food consumed and (B) the caloric intake per week of rats on their respective diets during the initial 10-week feeding period. Data are presented as the mean ± SEM of n=6 animals per group. Data represents the mean ± SEM of n=12 animals per group. A one-way ANOVA was performed, and statistical significance is depicted as *** $p \leq 0.001$ versus the control group and ### $p \leq 0.001$ versus the OB1 group.

From the diet composition analysis, the number of calories for each diet was calculated and was 2.93 kcal/g for the control diet, 2.32 kcal/g for the OB1 diet and 3.23 kcal/g for the OB2 diet. When evaluating the caloric intake, there was no significant difference in the calories consumed by the OB1 diet-fed (507.1 ± 5.53) and OB2 diet-fed (529.1 ± 7.74) animals when compared to the control rats (499.2 ± 16.67), or when compared to each other (Figure 4.3B). This indicates that although the OB1 group consumed more food, the caloric intake for the different groups remained unchanged. Upon administration with AfriplexGRT^{TM}, the animals were cohabitated, and thus the effect of AfriplexGRT^{TM} on food intake could not be determined.

4.3.2. Morphometric analysis

4.3.2.1. The effect of diet composition on the bodyweights of male Wistar rats

Wister rat groups fed on OB1 or OB2 diets for 10 weeks showed a gradual increase in bodyweight over the study period, however, significant differences were only observed in the OB1 group at 16 and 17 weeks (407.1 ± 33.55 and 416.5 ± 35.53 respectively), when compared to the control rats (364.3 ± 31.51 and 378.9 ± 33.58 respectively). The extract was administered in the form of jelly cubes from week 11 onwards and animals in the control groups received jelly without AfriplexGRT™. No significant difference in body weight was observed in rats fed an OB1 diet supplemented with or without AfriplexGRT™. In contrast, the bodyweight of the OB2 group supplemented with AfriplexGRT™ was briefly increased significantly at week 13 (416.5 ± 39.46) when compared to the OB2 diet-fed group (380.1 ± 24.01), but this significant increase in bodyweight was not maintained during the rest of the study period.

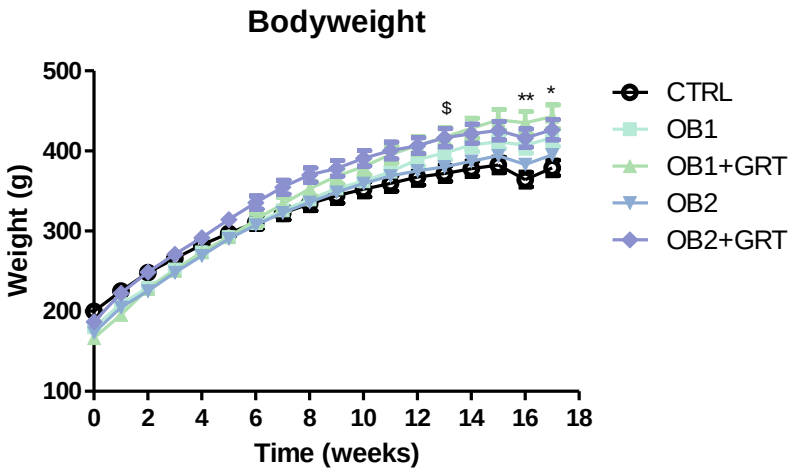

Figure 4.4: Body weights of Wistar rats after the 17-week treatment period. A bodyweight graph for male Wistar rats over the 17 weeks on their respective diets. Data presented as the mean ± SEM of n=12 animals per group. A one-way ANOVA was performed, and statistical significance is depicted as * p≤0.05, ** p≤0.01 control versus the OB1 group; and $ p≤0.05 OB2 versus the OB2+GRT group.

4.3.2.2. The effect of diet composition on fasting blood glucose

The normal range for fasting blood glucose (FBG) levels in normal Wistar rats is between 3.95-5.65 mmol/L [27]. In the current study, 16-hour FBG levels were measured by tail prick before termination and were slightly elevated in all groups when compared to normal values, however, no significant differences could be seen in fasting blood glucose levels for animals fed on different obesogenic diets and diets supplemented with or without AfriplexGRT™ (Figure 4.5).

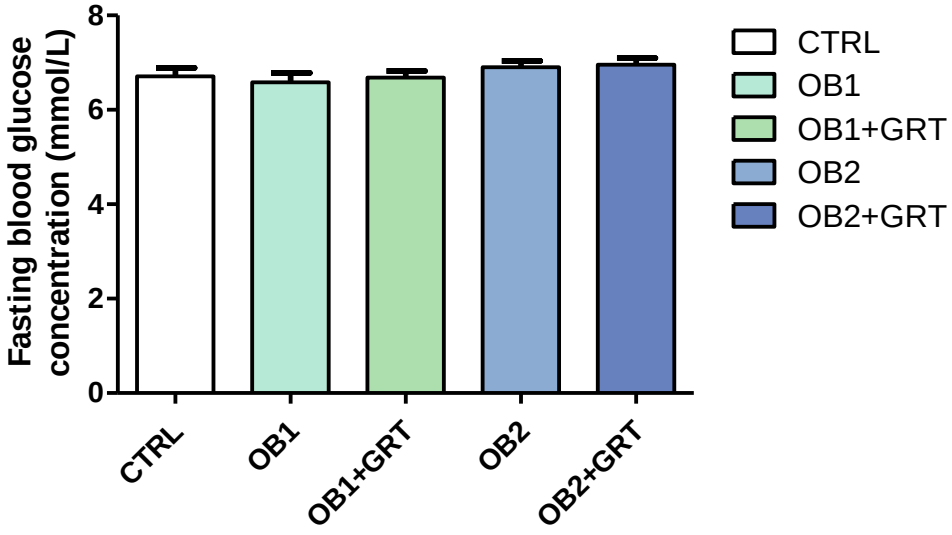

Figure 4.5: Fasting blood glucose of Wistar rats after 16 weeks. Circulating glucose concentration measured after 16 hours of fasting. A one-way ANOVA was performed, and data represent the mean ± SEM of n=12 animals per group.

4.3.2.3. The effect of diet composition on glucose clearance

OGTTs were utilized for the determination of fasting whole-body glucose homeostasis to determine the rat's ability to clear glucose after following the oral ingestion of sucrose. OGTTs were performed over 120 minutes after the rats were orally gavaged with 50% sucrose after 16 hours of fasting. This was performed to investigate whether diet composition differences cause changes in β-cell dysfunction in the Wistar rat model. Results obtained showed that there was a significantly higher area under the curve (AUC) in the OB2 diet-fed group supplemented with AfriplexGRT™ (798.1 ± 137.5) when compared to the OB2 group (670.6 ± 84.72) (Table 4). It is however interesting to note that, although non-significant, the OB1 diet-fed group with

AfriplexGRT™ also exhibited increased AUC (746.8 ± 56.58) than their diet control counterparts (725.8 ± 75.17), indicating impaired glucose clearance (Figure 4.6).

Table 4.4: Oral glucose tolerance test. Area under the curve (AUC) calculations for oral glucose tolerance tests performed.

Group	OGTT AUC
CTRL	661.5 ± 51.89
OB1	725.8 ± 75.17
OB1+GRT	**746.8 ± 56.58***
OB2	670.6 ± 84.72
OB2+GRT	**798.1 ± 137.5** #**

Data represent the mean ±SEM of n=12 animals per group. A one-way ANOVA was performed, and statistical significance is depicted as * p≤0.05, ** p≤0.01 versus the control group; # p≤0.05 versus the OB2 group.

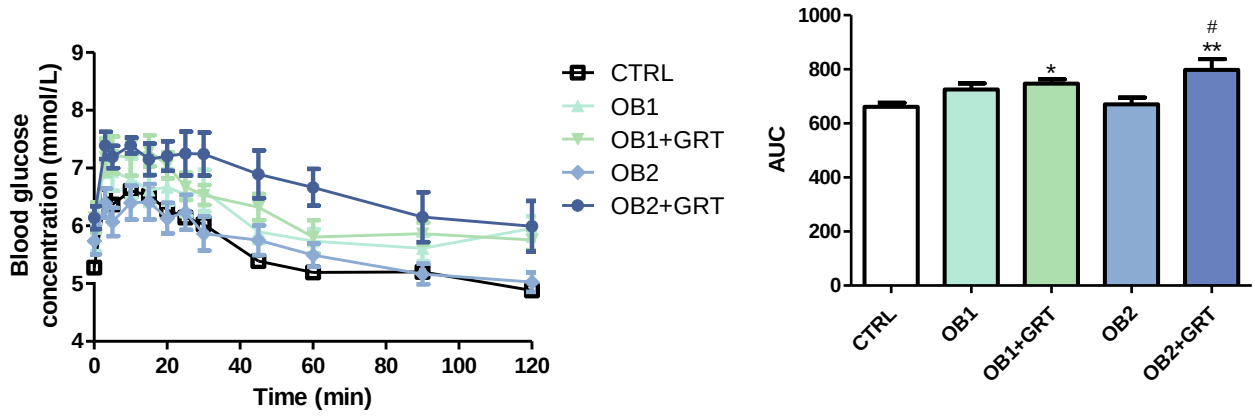

Figure 4.6: Oral glucose tolerance test AUC plots: The effect of AfriplexGRT™ on glucose metabolism. Glucose tolerance assessed after 16-hour fasting over 120 minutes after 50% sucrose administration. A one-way ANOVA was performed, and data represent the mean ± SEM of n=12 animals per group. AUC calculated from these plots.

4.3.2.4. The effect of diet composition on serum liver enzymes and serum lipid profiles of male Wistar rats

Serum lipid profiles are known measurements for the prediction of cardiovascular risk [28]. The serum triglyceride levels were significantly elevated in both the OB1 diet-fed group (1.357 ± 0.272, $p<0.001$) as well as the OB2 diet-fed group (1.324 ± 0.382, $p<0.001$) when compared to the normal control group animals (0.600 ± 0.114) (Figure 4.7A). Supplementation with AfriplexGRT™ did not affect serum triglycerides levels in both the OB1-fed (1.114 ± 0.301) or OB2-fed (1.212 ± 0.466) groups when compared to their control counterparts. (1.357 ± 0.272 and 1.324 ± 0.382, respectively). The OB2 diet (3.083 ± 0.674 and 1.282 ± 0.475 respectively) significantly increased total cholesterol levels ($p<0.05$) and LDL-cholesterol ($p<0.001$) when compared to the control diet (1.918 ± 0.289 and 0.300 ± 0.00), however, HDL-cholesterol levels remained unchanged in all the groups. The OB1 diet-fed group had no change in either total- (1.673 ± 3.133) or LDL-cholesterol (0.333 ± 0.116), and supplementation with AfriplexGRT™ also had no effect on total or LDL-cholesterol for any of the diets (Figure 4.7B and C).

The serum AST and ALT levels were measured as indicators of liver damage. The serum AST and ALT levels were again significantly increased ($p<0.05$ and $p<0.001$, respectively) in the OB2 diet-fed group (171.1 ± 70.71 and 179.5 ± 117.8) when compared to the normal controls (103.2 ± 17.97 and 36.09 ± 4.42), where the OB1 diet had no effect on these levels (95.09 ± 11.05 and 40.64 ± 12.30). Supplementation with AfriplexGRT™ also did not affect AST and ALT levels. Normal reference ranges for AST and ALT are between 50-150 IU/L and 10-40 IU/L, respectively [29]. As such, the data presented showed that both AST and ALT levels were within the normal range for the control and OB1 diet groups, but higher than the normal range for the OB2 group for both AST and ALT levels (Figure 4.7E and F).

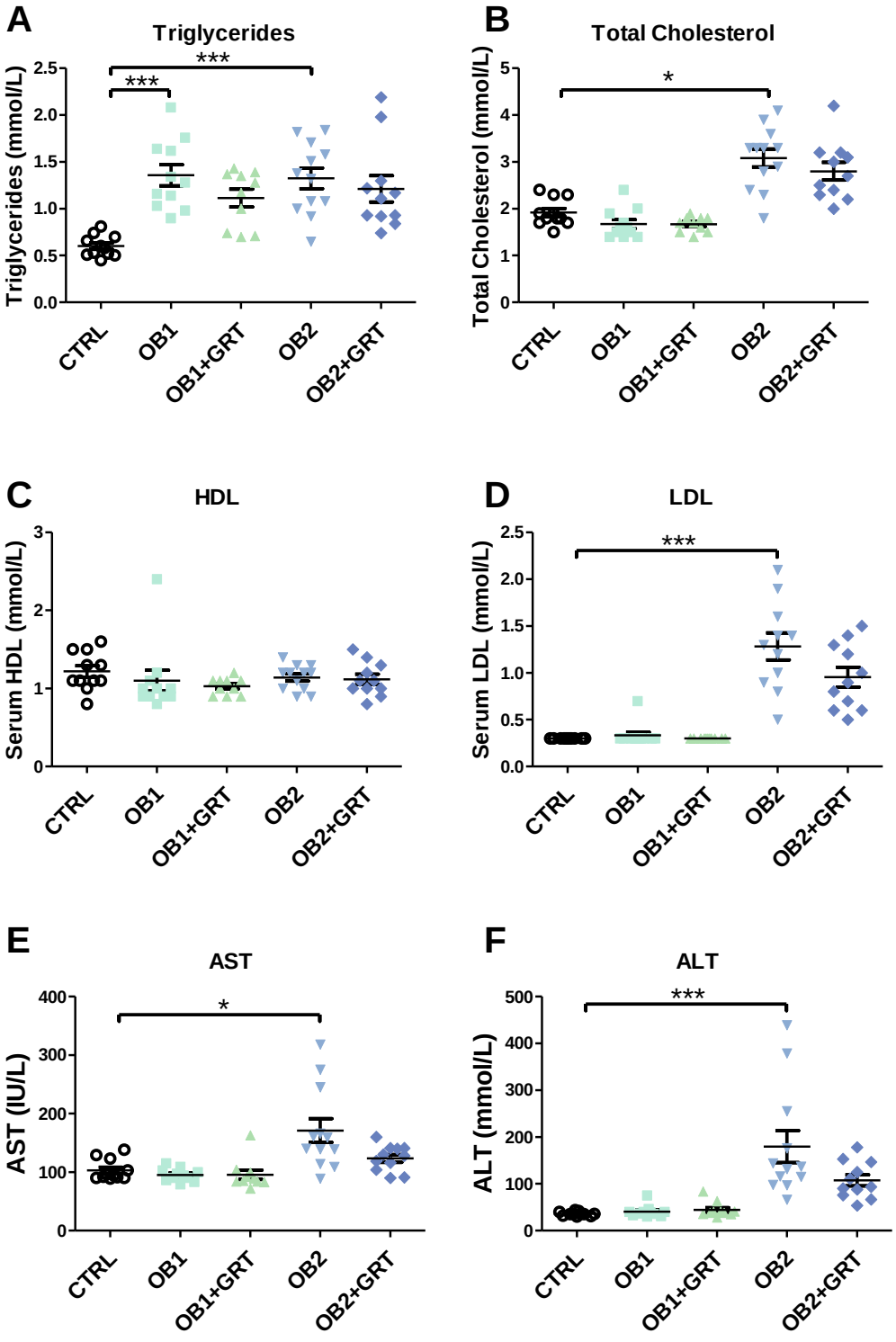

Figure 4.7: Serum triglycerides, total cholesterol, and HDL-cholesterol and serum AST and ALT levels as an indicator of liver damage. Scatter plots of the serum triglycerides, cholesterols, and AST and ALT levels of the male Wistar rats after 17 weeks on their respective diets. Data represent the mean ± SEM of n=12 animals per group. A one-way ANOVA was performed, and statistical significance is depicted as * p≤0.05, *** p≤0.001 versus the control group.

4.3.3. Molecular analysis

4.3.3.1. The effect of diet composition on serum insulin levels

Serum insulin levels were determined using a serum ELISA kit to assess possible insulin resistance. The OB1 diet-fed animals had significantly increased serum insulin levels (3.987 ± 2.1, p<0005) when compared to the normal controls (1.584 ± 0.819), and supplementation with AfriplexGRT™ (3.424 ± 1.326) was unable to alter this increase. The OB2 diet caused a slight increase in serum insulin levels (2.324 ± 1.087) although not significant, and AfriplexGRT™ supplementation further increased this (3.183 ± 1.692), although still not significant (Figure 4.8).

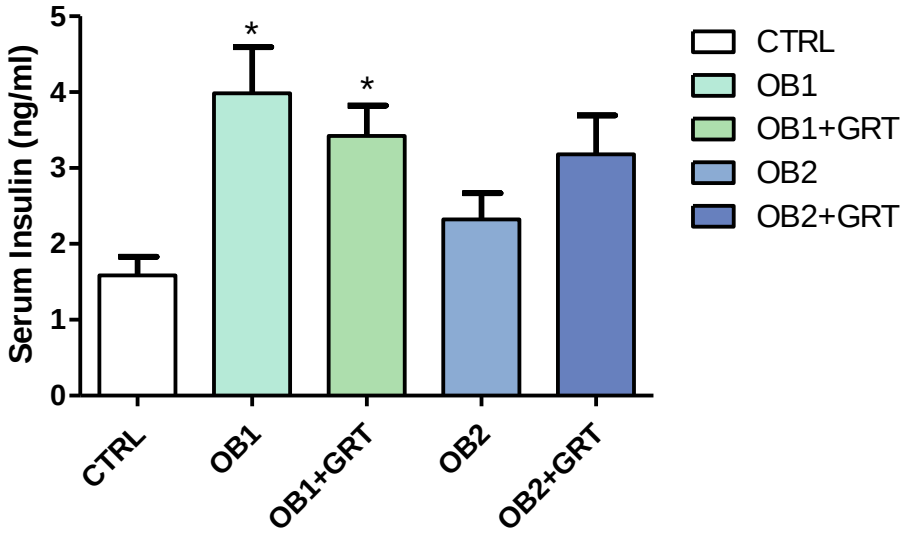

Figure 4.8: Fasting serum insulin levels at 17 weeks of diet feeding. Insulin ELISA of male Wistar rats fed a control diet (CTRL), obesogenic 1 (OB1) diet, OB1 diet supplemented with 60 mg/kg GRT (OB1+GRT), obesogenic 2 (OB2) diet, or OB2 diet supplemented with GRT (OB2+GRT). Data represents the mean ± SEM of n=10-12 animals per group. A one-way ANOVA was performed, and statistical significance is depicted as * p≤0.05 versus the control group.

4.3.3.2. HOMA-IR calculation as a measurement of insulin resistance

The HOMA-IR index relates to the level of insulin resistance with a low HOMA-IR being indicative of insulin sensitivity, and HOMA-IR >1 is an indication of insulin resistance. HOMA-IR calculations were done according to the formula [26]:

$$\text{HOMA-IR} = \text{Fasting insulin } (\mu U/L) \text{ x fasting glucose } (\text{nmol}/L)/22.5$$

Results obtained in the current study showed both the OB1 and OB2 diets increased the HOMA-IR levels (0.265 ± 0.111 and 0.194 ± 0.106 respectively) in both OB1 fed and OB2 fed animals when compared to the control (0.123 ± 0.067), however, the differences were not statistically significant. The supplementation with AfriplexGRT™ did not lower this but rather marginally increased HOMA-IR levels in both the OB1 and OB2 diet-fed groups (0.301 ±0.134 and 0.292 ± 0.174), respectively (Figure 4.9). The increased HOMA-IR levels were still within a normal physiological range.

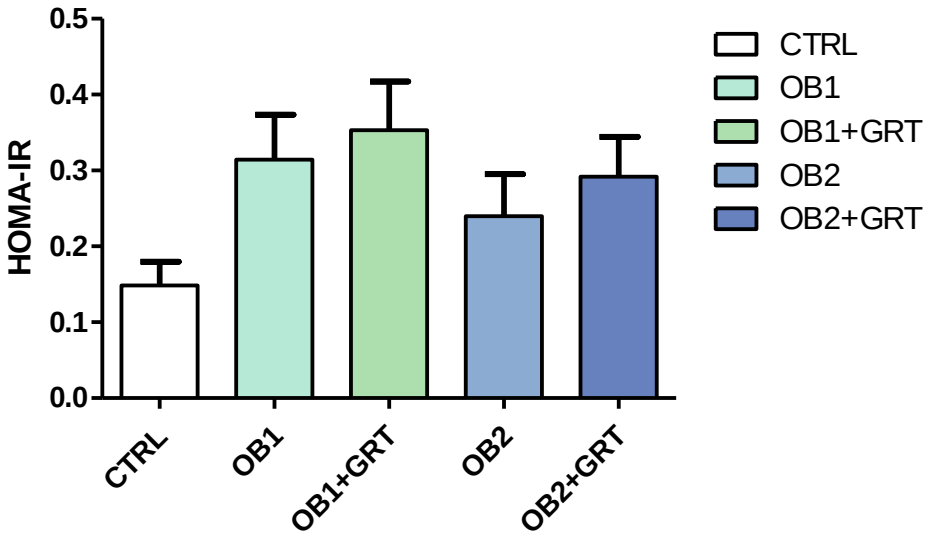

Figure 4.9: HOMA-IR calculation analysis. Graph of calculated HOMA-IR values from Insulin ELISA of male Wistar rats fed a control diet (CTRL), obesogenic 1 (OB1) diet, OB1 diet supplemented with 60 mg/kg GRT (OB1+GRT), obesogenic 2 (OB2) diet, or OB2 diet supplemented with GRT (OB2+GRT). A one-way ANOVA was performed, and data represents the mean ± SEM of n=10-12 animals per group.

4.3.3.3. Serum LOXL2 levels as an indicator of fibrosis

Serum LOXL2 levels were only performed on the animals fed the OB2 diet since most of the serum triglycerides and other CVD risk predictors were seen to be more severe in these groups. Increased serum LOXL2 is a marker of the preclinical onset of fibrosis [13]. The serum ELISA showed an increase in the serum LOXL2 concentration of Wistar rats fed the OB2 diet (0.544 ± 0.347) when compared to the rats fed the control diet (0.191 ± 0.104), while supplementation with AfriplexGRT™ (0.582 ± 0.257) did not affect reducing the LOXL2 concentration when compared to its dietary control (Figure 4.10).

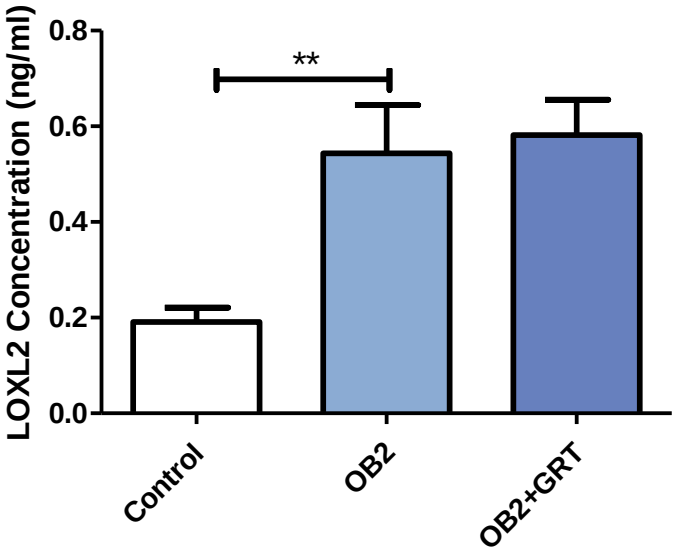

Figure 4.10: Serum LOXL2 concentrations after 17 weeks of feeding. LOXL2 serum concentrations were determined by an ELISA of male Wistar rats fed a control diet (CTRL), obesogenic 1 (OB1) diet, OB1 diet supplemented with 60 mg/kg GRT (OB1+GRT), obesogenic 2 (OB2) diet, or OB2 diet supplemented with GRT (OB2+GRT). Data represents the mean ± SEM of n=10-12 animals per group. A one-way ANOVA was performed, and statistical significance is depicted as ** p≤0.01 versus the control group.

Table 4.5: Summary of metabolic parameters that differ between the control, OB1 and OB2 diets. A one-way ANOVA was performed, and statistical significance is depicted as * p≤0.05, and *** p≤0.001 versus the control group and ### p≤0.001 versus the OB1 group.

Metabolic characteristics	CTRL	OB1	OB2
Bodyweight (g) week 17	378.9 ± 9.70	416.5 ± 10.71	395.1 ± 7.49
Food intake (g/week)	170.4 ± 5.69	**219.0 ± 2.39*****	**163.8 ± 2.40**$^{###}$
Calories intake (AUC)	499.2 ± 16.67	507.1 ± 5.53	529.1 ± 7.74
Blood glucose (mmol/L)	6.71 ± 0.18	6.58 ± 0.20	6.90 ± 0.14
OGTT AUC (mm^2)	661.5 ± 14.98	725.8 ± 22.06	670.6 ± 24.46
Insulin (ng/mL)	1.58 ± 0.25	**3.99 ± 0.61***	2.32 ± 0.34
HOMA-IR	0.12 ± 0.02	0.27 ± 0.04	0.19 ± 0.003
Triglycerides (mmol/L)	0.60 ± 0.03	**1.36 ± 0.11*****	**1.32 ± 0.11*****
Total Cholesterol (mmol/L)	1.92 ± 0.09	1.67 ± 0.09	**3.08 ± 0.19*****
LDL (mmol/L)	0.30 ± 0.00	0.33 ± 0.03	**1.28 ± 0.14*****
AST (IU/L)	103.2 ± 5.42	95.1 ± 3.33	**171.2 ± 20.41***
ALT (IU/L)	36.09 ± 1.33	40.64 ± 3.71	**179.5 ± 34.01*****

4.3.4. The effect of effect of diet composition on histology

Stained tissue sections from each group were evaluated by an independent company (Idexx Laboratories, Kyalami, South Africa) for complete objectivity, and the results reported as per their findings.

4.3.4.1. The effect of diet composition on Hematoxylin and Eosin-stained heart sections

All stained sections showed marked freeze artefacts that severely hampered the examination, and thus one sample from each group was evaluated as a representation. In the control section, myocardial fibres

appeared normal although striations were poorly visible and stromal support cells are minimally visible, and only in few areas, where the OB1-diet section shows very prominent striations, but still very few stromal support cells were present (Figure 4.11). Supplementation with AfriplexGRT™ however made the cardiac fibres to appear slightly thin with smudged cytoplasm, with interstitial support cells present but minimal in number. The OB2 diet seemed to cause a mild variation in fibre diameter but many appear slightly thin and with slightly smudged cytoplasm and still few stromal support cells which appear more prominent diffusely in the interstitium and slightly more noticeable were associated with blood vessels. Supplementation with AfriplexGRT™ however caused the same mild variation in fibre diameter with the cytoplasm appearing eosinophilic and slightly smudged. Interstitial stromal support cells were still visible between fibres and although they are not numerous, they were more prominent throughout this sample.

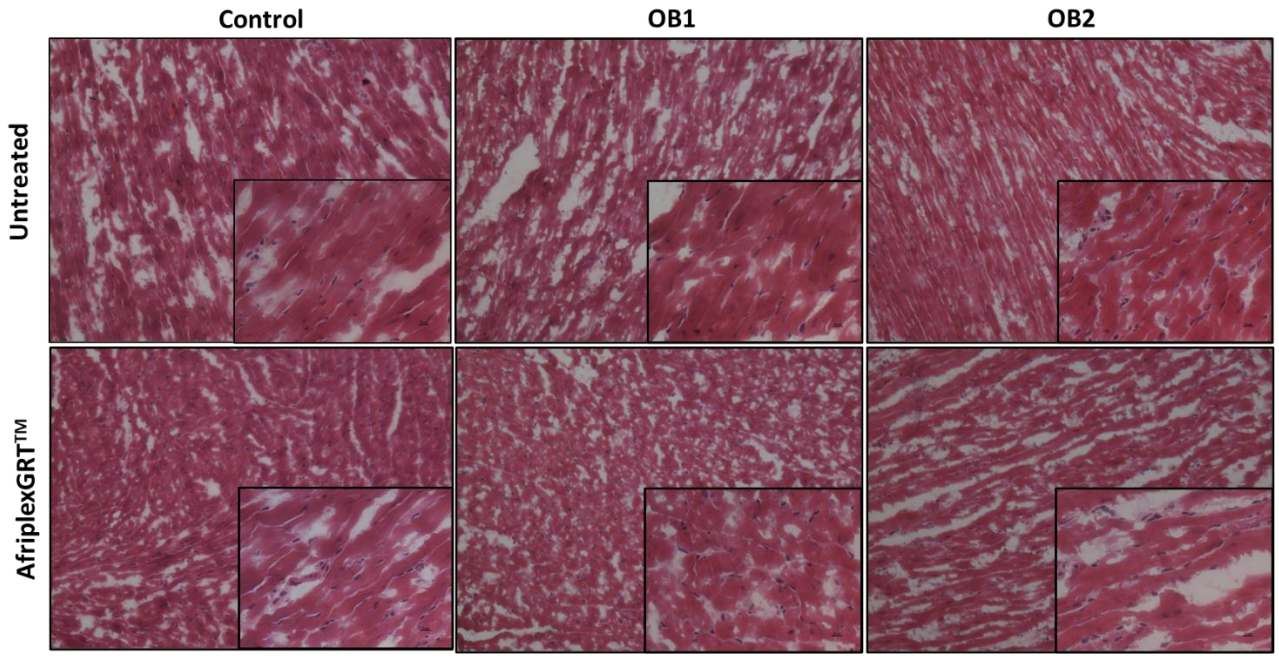

Figure 4.11: Hematoxylin and eosin-stained heart sections. Representative 10x and 40x magnification images of H&E-stained sections from male Wistar rats fed control, OB1 or OB2 diets, where GRT supplementation was at 60 mg/kg.

The histological appearance of the myocardial fibres varies minimally between the groups, and the variation appeared to be due to artefacts. There was very mild variation in the number of interstitial support cells between myocardial fibres between the different groups, although they remain few. These cells were focally more prominent around blood vessels in some groups, particularly those fed the OB2 diet. The control group showed minimal visibility of interstitial support cells between the myocardial fibres, while in the OB2 and OB2+AfriplexGRT™ groups these cells are diffusely more prominent, but still only visible in small numbers. The interstitial spaces were thus not expanded, nor with notable stromal infiltrates, and the interstitial support cells do not clearly represent fibrosis.

4.3.4.2. RNA expression

Differential gene expression was performed on genes involved in the fibrotic pathway that were located up and downstream of LOXL2. These genes included *COL1A1, SMAD2, SMAD3, TGFβ2, ACTA2, PIK3cg, AKT1, HIF1A1*, and *CTGF*. No significant differences were observed in the expression levels of any of the aforementioned genes for rats fed the OB1 or OB2 diets when compared to the control diet-fed animals, and diet supplementation with AfriplexGRT™ did not affect gene expression. Analysis of *LOXL2* expression showed an increased gene expression with animals on the OB2 diet (1.243 ± 0.289) when compared to the OB1 diet (1.067 ± 0.123) and the normal control diet (1.023 ± 0.250). AfriplexGRT™ treatment had little if any effect on the expression levels of *LOXL2* in OB1 (0.954 ± 0.245) and OB2 (1.232 ± 0.166) diet-fed animals (Figure 4.12A). *COL1A1* expression was slightly increased in the OB1diet-fed animals (0.258 ± 0.163) but decreased in the OB2 diet-fed animals (3.760 ± 0.312). However, an enhanced expression of *COL1A1* was observed in animals fed the OB1 (3.823 ± 0.365) and OB2 (5.098 ± 6.792) supplemented with AfriplexGRT™ when compared to the control group (1.679 ± 2.110), (Figure 4.12B). *SMAD2, CTGF* and *HIF1A* expression seemed largely unaffected by diets (Figure 4.12C, I and J), except for an increase in *HIF1A* due to the OB2 diet (2.251 ± 1.563) when compared to the controls (1.032 ± 0.274) (Figure 4.12I). *TGF-β2* expression, however, was increased in the OB1 (1.274 ± 0.545) and OB2 (1.356 ± 0.383) diet-fed animals when compared to their control counterparts (1.025 ± 0.237), and treatment with AfriplexGRT™ reduced these levels again (0.790 ± 0.305 and 0.807 ± 0.255) when compared to the control group (Figure 4.12E). Interestingly, *PIK3cg* expression was unaffected by the OB1 diet (1.274 ± 0.376), however it was marginally increased by the OB2 diet (1.731

± 0.512) when compared to the controls (1.181 ± 0.634), and its expression was further increased by treatment with AfriplexGRT™ in both the OB1 (1.563 ± 0.385) and OB2 (1.792 ± 1.034) diet groups (Figure 4.11G). In contrast, *AKT1* expression was slightly decreased by both the OB1 (0.781 ± 0.121) and OB2 (0.840 ± 0.108) diets when compared to their control counterparts (1.023 ± 0.223), and AfriplexGRT™ supplementation slightly increased the expression again (0.986 ± 0.257 and 0.913 ± 0.014 respectively), although these changes were not significant (Figure 4.12H).

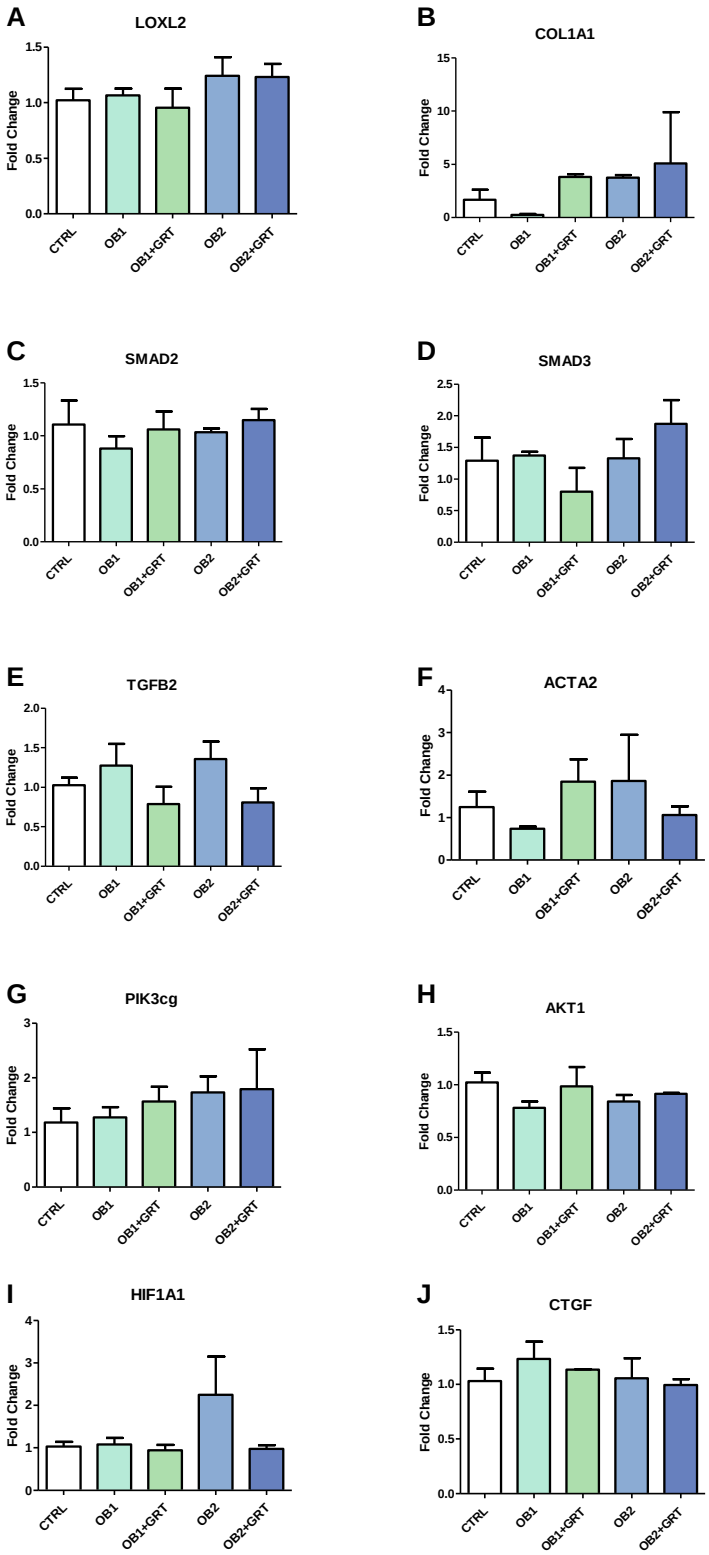

Figure 4.12: RNA expression in male rats. RNA expression of A) *LOXL2*, B) *COL1A1*, C) *SMAD2*, D) *SMAD3*, E) **TGFβ2**, F) *α-SMA (ACTA2)*, G) *PI3K (PIK3cg)*, H) *AKT1*, I) *HIF1A*, and J) *CTGF* in the hearts of male Wistar rats after 17 weeks on their respective diets. A one-way ANOVA was performed, and data represents the mean ± SEM of a varying number of animals per group.

4.3.4.3. Protein expression

To determine the protein expression of some of the key proteins in the fibrotic pathway within the heart, western blot analysis was performed. OB1 (0.0211 ± 0.007) and OB2 diet (0.0215 ± 0.015) feeding did not significantly change the LOXL2 expression in the heart, however, animals fed OB1 and OB2 diets supplemented with AfriplexGRT™ had decreased LOXL2 expression (OB1: 0.015 ± 0.009; OB2: 0.0197 ± 0.001) when compared to the control animals (0.030 ± 0.0324) (Figure 4.13A). The OB1 diet caused a decrease of both pSMAD2 (0.0042 ± 0.004 compared to 0.0163 ± 0.0196) and CTGF expression (0.0562 ± 0.0161 compared to 0.1852 ± 0.0931) expression compared to the controls, although the results were only statistically significant for CTGF expression and treatment with AfriplexGRT™ was unable to attenuate this effect (Figure 4.12B and C). The pSMAD2 (0.0111 ± 0.0164) and CTGF (0.1705 ± 0.1105) expression remain unchanged by consumption of the OB2 diet when compared to their control counterparts, and supplementation with AfriplexGRT™ only reduced CTGF expression (0.07678 ± 0.0128), although this change was not significant (Figure 4.13B and C).

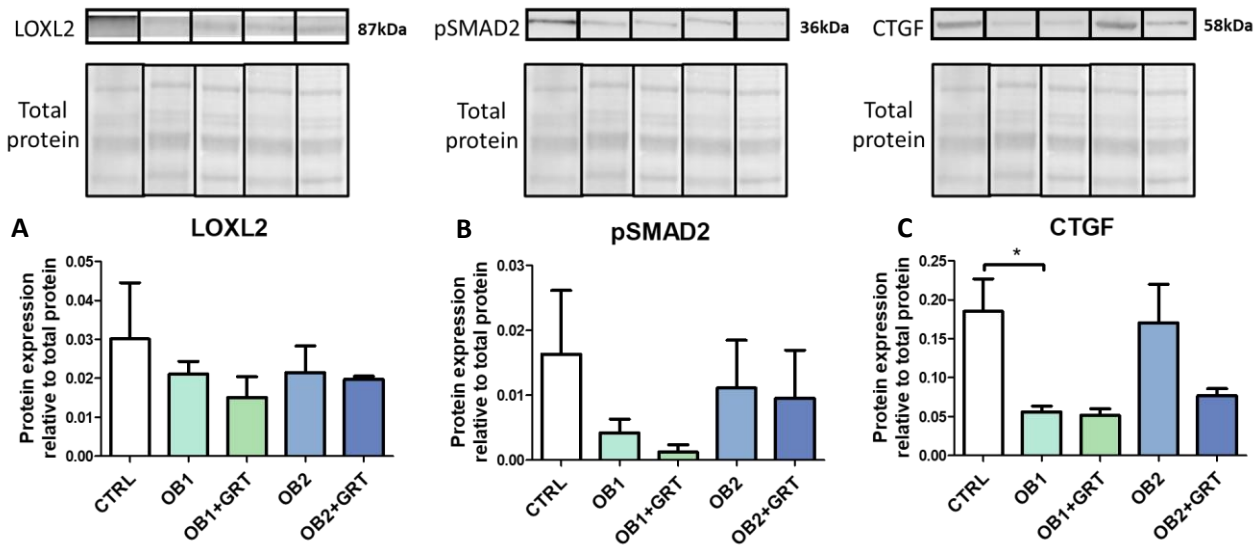

Figure 4.13: Western blot analysis of proteins extracted from heart tissue. (A) LOXL2, (B) pSMAD2 and (C) CTGF protein expression from heart tissue from male Wistar rats. A one-way ANOVA was performed, and data represents the mean ± SEM of a varying number of animals per group.

4.4. Discussion

The World Health Organization has proposed to focus on various dietary interventions that may prevent and reduce various CVD risk factors such as obesity, hypertension and diabetes [30]. Vast amounts of research exist that focuses on the effect of diet on disease development, specifically linking diet and lifestyle to obesity [31–33], hypertension [34–37], dyslipidemia [33, 38], diabetes [39, 40] and other cardiovascular disease risk factors. Additionally, a previous study from our group (Johnson et al., 2020) highlighted the role of LOXL2 in cardiac dysfunction, however, there is a paucity of research on the role of LOXL2 in cardiac fibrosis, a hallmark of cardiac dysfunction [41]. Therefore, understanding the regulatory mechanisms of LOXL2 and the role of dietary composition in modulating expression levels of LOXL2 may provide new avenues for controlling its abnormal expressions, and discovery of novel treatment for fibrosis induced CVDs. Interestingly, polyphenols have also been known to have the potential to ameliorate various metabolic complications, however, the effect of AfriplexGRT™ in diet-induced metabolic and morphological parameters, and in regulating the expression levels of LOXL2, remains to be elucidated. Therefore, this study primarily aimed to assess the effect of the OB1 and OB2 diets on the cardiovascular profile of the diet-induced obesogenic Wistar rat model. The second aim was to evaluate the cardioprotective potential of AfriplexGRT™ in attenuating the augmented levels of LOXL2 and its downstream effectors. To our knowledge, this was the first study investigating the role of an obesogenic diet on LOXL2 expression and to determine if AfriplexGRT™ can counteract the deleterious effect.

4.4.1 Diet composition risk on cardiac metabolic injury

Diet composition plays a significant role in the development of obesity, which is a major risk factor for CVD. This was elaborated on in a study performed by Bray et al. (2010) where concerns were raised on the detrimental metabolic risk of consuming high energy-dense food and sugar-sweetened beverages. In the current study, the impact of two obesogenic diets on metabolic health were investigated, and the results obtained showed a diverse metabolic profile between rats who consumed the OB1 (medium-fat/34% calories from fat) versus the OB2 diet (high-fat/66% calories from fat). Animals on the OB1 diet presented with hyperinsulinemia compared to animals on the OB2 diet who become hypercholesterolemic, while both diets

induced hyperlipidemia when compared to the control diet. It can be speculated that the diverse metabolic response can be ascribed to diet composition, whereas both the OB1 and OB2 diet contained added sugars with the OB1 diet containing a higher amount of sucrose (where sucrose composition is 1:1; sucrose: fructose, thus the specific diet contains the free fructose plus 50% of the sucrose as fructose, meaning that OB1 diet would contribute more fructose than the OB 2 diet. While both sucrose and fructose are unhealthy, increased fructose consumption has been linked to the development of obesity, hypertension, diabetes and cardiovascular disease [39, 42]. In addition, the OB2 diet contains cholesterol, making it higher in fat content than the control or OB1 diets. Suggesting that the high-fat content in the OB2 diet could trigger inflammation and it is known that prolonged high fat consumption has been shown to increase serum triglycerides, increasing the risk of atherosclerosis and heart failure [43, 44].

4.4.2 Diet-induced obesity as a risk for CVD

All animals including the control group had slightly elevated blood glucose, near the pre-diabetic range (5.6 - 6.5mmol/L), but, with no indication of severe metabolic insult concerning blood glucose and HDL. It was noteworthy that the respective diets had similar caloric values (isocaloric diet), despite OB1 diet-fed animals showing a significant increase in body weight compared to the control diet-fed animals in the last 2 weeks. These dietary-associated differences were expected due to the significantly increased food consumption of the OB1 group when compared to both the control and OB2 diet counterparts. In addition, it is known that diets high in sugars, particularly fructose, upregulate the expression of ghrelin, which stimulates appetite [45]. Taking into consideration that the OB1 diet contained higher amounts of sucrose and that sucrose composition is 50% sucrose and 50% free fructose, it would explain this study's findings that the OB1 diet resulted in pronounced weight gain and subsequent hyperinsulinemia. Conversely, increased consumption of foods high in fat and fructose has been shown to induce obesity [46], and it was thus expected for the OB2 diet-fed animals to also have an increased weight. However, the study has utilized a diet-induced model over a very short 16-week period, and it was thus suspected that the time the animals were exposed to their respective diets might not have been long enough to see a significant increase in weight gain. In addition, it is also known that diets containing more fat and protein better stimulate satiety, with the protein content

having a greater effect than that of the fat content [47]. Since the OB2 diet contained almost triple the amount of fat and 30% more protein than the OB1 diet, the reduced food intake by the OB2 diet-fed animals compared to the OB1 diet-fed group is to be expected and this could be a key factor in the lack of significant weight gain by the OB2 groups in this study.

4.4.3 Insulin resistance as a risk of CVD

Insulin resistance is often an indicator of metabolic derangement due to diet, which results in increased circulating levels of both insulin and glucose, as well as increased liver triglycerides [48–50]. There was however no significant change in fasting blood glucose for any of the different diet groups, however, interestingly, when looking at the rats' ability to clear glucose, none of the diets were able to significantly alter glucose clearance, except for the groups treated with AfriplexGRT™. This indicates that although the diet composition did not affect insulin sensitivity, AfriplexGRT™ may negatively affect this parameter. This directly contradicts findings from Muller et al. (2012) that showed AfriplexGRT™ to have glucose-lowering effects by increasing glucose uptake in both a muscle C2C12 cell culture model, as well as an STZ-induced diabetic rat model [51]. Serum insulin levels of the rats were measured, where only the OB1 diet-fed groups significantly increased circulating insulin levels. AfriplexGRT™ administration decreased serum insulin levels in the OB1 but not OB2 diet. Since the OB1 diet contained the highest concentration of sugar and fructose, this result is expected, as increased consumption of fructose and sucrose impair insulin-mediated glucose control. To confirm this, the HOMA-IR calculation was used as an indication of insulin sensitivity, and although a more prominent increase was observed in the OB1 diet-fed group, the HOMA-IR levels were still within the normal range, indicating that there was likely no significant metabolic derangement, however, the increase may indicate that metabolic changes were beginning to incur but that the duration of the study was not long enough to show a significant metabolic alteration.

4.4.4 Hyperlipidemia and CVD

Symptoms of metabolic derangement include increased triglycerides, LDL cholesterol, pro-inflammatory cytokines [52] and adipose fibrosis [53]. Both diets caused an increase in triglyceride levels, although significantly elevated levels of LDL-cholesterol were only seen with the OB2 diet-fed group. The observed

triglyceride levels can be a result of excessive consumption of both fat and sugar [54], which can occur in the presence or absence of high LDL [55], which could explain what was observed in the OB1 diet-fed group since excess sugar and calories are converted to triglycerides [56]. Noteworthy, diets high in fat have been shown to increase triglycerides and LDL-cholesterols as seen in the OB2 diet-fed group. This was confirmed in research conducted by Retterstol et al. (2018) where individuals were fed a diet low in carbohydrates but high in fat after which they observed an increase in LDL-cholesterol, total-cholesterol and free fatty acid levels [57]. Furthermore, dyslipidemia is characteristic of NAFLD [58] and plays a profound role in the development of CVD [59]. In the current study, the AST and ALT levels were measured as markers of liver injury. This study showed that hepatic AST and ALT enzymes levels were elevated in the OB2 diet-fed animals, suggesting that the OB2 and not OB1 diet-induced liver damage increasing CVD risk with concomitant insulin and glucose dysregulation. Furthermore, data presented showed that AfriplexGRT^{TM} was unable to protect the myocardium against various diet-induced cardiometabolic risk parameters that were observed in GRT groups, compared to their corresponding non-GRT diet groups.

4.4.5 Diet effect on cardiac pathology and serum LOXL2

To determine whether the metabolic risk parameters induced cardiac pathology, histological analysis by H&E staining were performed and showed minimal fibrosis, however, the analysis was challenging due to artefacts induced by sample preservation. This was thus followed up by measuring serum LOXL2 levels as an indicator of fibrosis. LOXL2 is the protein responsible for collagen and elastin cross-linking [60], as well as for ECM deposition, and thus an increase in this protein is linked to augmented fibrosis. In humans, an increase in serum LOXL2 levels was observed in end-stage heart failure patients [13]. Since the risk predictors and liver damage were more severely altered in the OB2 diet-fed group, LOXL2 levels were only measured in these groups compared to the controls. The LOXL2 levels were significantly increased in the OB2 group, which suggest possible early onset of mechanical dysfunction of the pathological diet-induced stressed heart. However, these findings would require confirmation using echocardiograph analysis, which was not performed in the current study. However, in a study done by Johnson et al. (2020), it was confirmed that increased serum LOXL2 levels are indicative of cardiac fibrosis in the absence of cardiac pathology. This was

further confirmed in studies done by Yang et al. (2016), Rodriguez et al. (2019), and Zhao et al. (2017) where serum LOXL2 was targeted as fundamental diagnostic markers of cardiac interstitial fibrosis and subsequent cardiac dysfunction. Due to the severity of the OB2 diet treatment with AfriplexGRT™ was unable to attenuate LOXL2 levels in the OB2 diet-fed groups. While the evidence of overt pathology was not seen in the histology, several metabolic derangements were induced through the respective diets. This warranted evaluation of gene and protein expression levels of various downstream targets of LOXL2 to ascertain the effect of diet composition and treatment with AfriplexGRT™ on a molecular level.

4.4.6 LOXL2 and its downstream effectors

In a study by Yang et al. (2016), they observed that LOXL2 expression was upregulated by mechanical stress in the heart which upregulated collagen development with the activation of the PI3k/AKT/mTOR pathway and TGF-β signalling, as well as collagen crosslinking through LOXL2 [13]. In the current study, *TGFβ2*, a master regulator involved in the regulation of LOXL2 and collagen expression, was upregulated by both the OB1 and OB2 diets and reduced by supplementation with AfriplexGRT™. Since *LOXL2* expression was not significantly altered by diet, no change was expected in collagen or α-SMA expression. There was however a slight increase in *LOXL2, COL1A1* and *ACTA2* in the groups fed the OB2 diet when compared to the levels in the control group. The results were not consistent in the OB1 and AfriplexGRT™ supplemented groups concerning the expression of *COL1A1*, *ACTA2*, *SMAD2* and *AKT1* are also involved in the fibrotic pathway, however, the expression of these genes seems to be minimally decreased due to both diets, however, supplementation with AfriplexGRT™ increased these levels again similar to the level of the control group. *PIK3cg* expression was increased by the OB2 diet but further increased by supplementation with AfriplexGRT™. *HIF1A*, a marker of oxidative stress, was only increased in the OB2 group, although this was not statistically significant. *CTGF* was investigated as a marker of cardiac damage, however, there was no significant change in its expression, although there was a slight increase in the OB1 group, and the treatment with AfriplexGRT™ seemed to slightly decrease its expression when compared to the respective diet controls. Although none of these changes observed was significant, they indicate slight changes in the fibrotic markers due to the different diets and require further investigation. This corresponded to the cardiac pathology

showing the absence of severe fibrosis after 16-weeks of OB2 diet feeding and should echocardiography have been performed, early onset of left ventricular dysfunction might have been detected.

Lastly, the protein expression analysis showed no significant change in the LOXL2 expression, confirming the gene expression results, although there was high variation in the control group. The expression of pSMAD2 and CTGF were decreased in the OB1 diet, with a less pronounced decrease seen in the OB2 group. There was however again high variation in the control group as well as the OB2 diet groups. Since CTGF is an indication of cardiac damage and no significant increase was seen in its expression, these data suggest that there was no damage in the heart and could explain why the markers of fibrosis and its signalling pathway cascade were only minimally dysregulated. A limitation of this study is the small sample size for the gene and protein expression, thus lacking statistical power.

Taken together, only minimal diet-induced changes were seen in bodyweights, OGTTs, histology and gene expression, however, more prominent changes were seen in the insulin, triglyceride, LDL-cholesterol and serum LOXL2 levels. These data could indicate that molecular changes can occur before metamorphic changes, and that diet composition plays a major role in the development of the metabolic syndrome. The limitations of this study are the sample number for gene and protein analysis and the absence of echocardiography. Since there is still a debate about whether it is sugar or fat that causes hypothalamic inflammation [61, 62] as well as what is the primary cause of metabolic disease, it could have been useful to observe the effects of sugar and high fat individually. Further research therefore should be conducted on separate diet constituents as well as in combination to discern their contribution to altering the fibrotic pathway and CVD risk. In addition, AfriplexGRT^{TM} only significantly improved glucose tolerance in the rats on the OB2 diet when compared to the untreated OB2 diet-fed group, it also seemed to marginally reduce the serum cholesterol and triglyceride levels, as well as the markers of liver damage. There is however no current research on the effect of AfriplexGRT^{TM} on the fibrotic pathway, although Aspalathin (the main active ingredient in AfriplexGRT^{TM}) has been shown to reduce oxidative stress [63] and apoptosis [64] within the heart. Further research should thus also be conducted on the effect of both Aspalathin and AfriplexGRT^{TM} on the fibrotic pathway within the myocardium.

4.5. Conclusion

These data indicate that molecular changes can occur before metamorphic changes, and that diet composition plays a major role in the development of metabolic syndrome, which is a known risk factor for CVD. Hyperinsulinemia, hyperglycemia, hypertriglyceridemia and hyperlipidemia are known risk predictors of CVDs [65–67]. Diet composition plays a profound role in the development of cardiac dysfunction. In this study we investigated 2 obesogenic diets, OB1 and OB2. The OB1 diet was able to induce hyperinsulinemia and hypertriglyceridemia and caused weight gain, increased insulin and HOMA-IR, with no effect on liver enzymes. Conversely, the OB2 diet, which was a high fat, high fructose diet, caused a more prominent increase in triglycerides and LDL-cholesterol, as well as indicators of liver toxicity. The OB2 diet showed increased levels of serum LOXL2 expression, however no significant differences could be observed on both the RNA and protein levels, which require further investigation.

Taken together, a diet high in fat and sugar could cause an activation of the LOXL2 fibrotic pathway to some extent, and thus a larger sample size may have given more clarity to the effect of diet composition on modulating the expression levels of various fibrotic markers. In addition, AfriplexGRT™ was unable to attenuate the changes induced by the OB1 and OB2 diets, and conflicting gene expression results with the AfriplexGRT™ co-treatment in improving cardiac fibrosis needs to be further investigated.

4.6. References

1. World Health Statistics (WHO). Cardiovascular diseases (CVDs) fact sheet Available online: https://www.who.int/news-room/fact-sheets/detail/cardiovascular-diseases-(cvds) (accessed on Sep 12, 2019).

2. Govindarajan, G.; Alpert, M.A.; Tejwani, L. Endocrine and Metabolic Effects of Fat: Cardiovascular Implications. *Am. J. Med.* **2008**, *121*, 366–370. doi: 10.1016/j.amjmed.2008.01.032.

3. Bertaso, A.G.; Bertol, D.; Duncan, B.B.; Foppa, M. Epicardial fat: Definition, measurements and systematic review of main outcomes. *Arq. Bras. Cardiol.* **2013**, *101*, doi:10.5935/abc.20130138.

4. Cavalera, M.; Wang, J.; Frangogiannis, N.G. Obesity, metabolic dysfunction, and cardiac fibrosis: Pathophysiological pathways, molecular mechanisms, and therapeutic opportunities. *Transl. Res.* **2014**, *164*, 323–335. doi: 10.1016/j.trsl.2014.05.001.

5. Steenman, M.; Lande, G. Cardiac aging and heart disease in humans. *Biophys. Rev.* **2017**, *9*, 131–137. doi: 10.1007/s12551-017-0255-9

6. Biernacka, A.; Frangogiannis, N.G. Aging and cardiac fibrosis. *Aging Dis.* **2011**, *2*, 158–173.

7. Mohammed, S.F.; Hussain, S.; Mirzoyev, S.A.; Edwards, W.D.; Maleszewski, J.J.; Redfield, M.M. Coronary microvascular rarefaction and myocardial fibrosis in heart failure with preserved ejection fraction. *Circulation* **2015**, *131*, 550–559, doi:10.1161/CIRCULATIONAHA.114.009625.

8. Rodriguez, C.; Martinez-Gonzalez, J.; Raposo, B.; Alcudia, J.F.; Guadall, A.; Badimon, L. Regulation of lysyl oxidase in vascular cells: lysyl oxidase as a new player in cardiovascular diseases. *Cardiovasc. Res.* **2008**, *79*, 7–13, doi:10.1093/cvr/cvn102.

9. Kagan, H.M.; Li, W. Lysyl oxidase: Properties, specificity, and biological roles inside and outside of the cell. *J. Cell. Biochem.* **2003**, *88*, 660–672, doi:10.1002/jcb.10413.

10. López, B.; González, A.; Hermida, N.; Valencia, F.; De Teresa, E.; Díez, J. Role of lysyl oxidase in myocardial fibrosis: From basic science to clinical aspects. *Am. J. Physiol. - Hear. Circ. Physiol.* **2010**,

299. doi: 10.1152/ajpheart.00335.2010

11. Badenhorst, D.; Maseko, M.; Tsotetsi, O.J.; Naidoo, A.; Brooksbank, R.; Norton, G.R.; Woodiwiss, A.J. Cross-linking influences the impact of quantitative changes in myocardial collagen on cardiac stiffness and remodelling in hypertension in rats. *Cardiovasc. Res.* **2003**, *57*, 632–641, doi:10.1016/S0008-6363(02)00733-2.

12. López, B.; Querejeta, R.; González, A.; Beaumont, J.; Larman, M.; Díez, J. Impact of treatment on myocardial lysyl oxidase expression and collagen cross-linking in patients with heart failure. *Hypertens. (Dallas, Tex. 1979)* **2009**, *53*, 236–42, doi:10.1161/HYPERTENSIONAHA.108.125278.

13. Yang, J.; Savvatis, K.; Kang, J.S.; Fan, P.; Zhong, H.; Schwartz, K.; Barry, V.; Mikels-Vigdal, A.; Karpinski, S.; Kornyeyev, D.; et al. Targeting LOXL2 for cardiac interstitial fibrosis and heart failure treatment. *Nat. Commun.* **2016**, *7*, 13710, doi:10.1038/ncomms13710.

14. Fontana, L. Modulating human aging and age-associated diseases. *Biochim. Biophys. Acta - Gen. Subj.* **2009**, *1790*, 1133–1138. doi: 10.1016/j.bbagen.2009.02.002.

15. Aguila, M.B.; Alberto Mandarim-de-Lacerda, C. Blood pressure, ventricular volume and number of cardiomyocyte nuclei in rats fed for 12 months on diets differing in fat composition. *Mech. Ageing Dev.* **2001**, *122*, 77–88, doi:10.1016/S0047-6374(00)00215-3.

16. Heymans, S.; González, A.; Pizard, A.; Papageorgiou, A.P.; Lõpez-Andrés, N.; Jaisser, F.; Thum, T.; Zannad, F.; Díez, J. Searching for new mechanisms of myocardial fibrosis with diagnostic and/or therapeutic potential. *Eur. J. Heart Fail.* **2015**, *17*, 764–771. doi: 10.1002/ejhf.312.

17. Zhang, N.; Wei, W.Y.; Li, L.L.; Hu, C.; Tang, Q.Z. Therapeutic potential of polyphenols in cardiac fibrosis. *Front. Pharmacol.* **2018**, *9*, 122. doi: 10.3389/fphar.2018.00122

18. Joubert, E.; Louw, J.; Fey, S.J.; Larsen, P.M. An anti-diabetic extract of rooibos, **2008**.

19. Persson, I.A.L.; Persson, K.; Hägg, S.; Andersson, R.G.G. Effects of green tea, black tea and Rooibos tea on angiotensin-converting enzyme and nitric oxide in healthy volunteers. *Public Health Nutr.* **2010**, *13*,

730–737, doi:10.1017/S1368980010000170.

20. Marnewick, J.L.; Rautenbach, F.; Venter, I.; Neethling, H.; Blackhurst, D.M.; Wolmarans, P.; MacHaria, M. Effects of rooibos (Aspalathus linearis) on oxidative stress and biochemical parameters in adults at risk for cardiovascular disease. *J. Ethnopharmacol.* **2011**, *133*, 46–52, doi:10.1016/j.jep.2010.08.061.

21. Smith, C.; Swart, A.C. Rooibos (Aspalathus linearis) facilitates an anti-inflammatory state, modulating IL-6 and IL-10 while not inhibiting the acute glucocorticoid response to a mild novel stressor in vivo. *J. Funct. Foods* **2016**, *27*, 42–54, doi:10.1016/j.jff.2016.08.055.

22. Baba, H.; Ohtsuka, Y.; Haruna, H.; Lee, T.; Nagata, S.; Maeda, M.; Yamashiro, Y.; Shimizu, T. Studies of anti-inflammatory effects of Rooibos tea in rats. *Pediatr. Int.* **2009**, *51*, 700–704, doi:10.1111/j.1442-200X.2009.02835.x.

23. Najafian, M.; Najafian, B.; Najafian, Z. The Effect of Aspalathin on Levels of Sugar and Lipids in Streptozotocin-Induced Diabetic and Normal Rats. *Zahedan J. Res. Med. Sci.* **2016**, *In Press*, doi:10.17795/zjrms-4963.

24. Guidelines for Ethical Conduct in the Care and Use of Animals Available online: https://www.apa.org/science/leadership/care/guidelines (accessed on Aug 30, 2020).

25. South African Bureau of Standards *South African National Standard: The care and use of animals for scientific purposes (SANS 10386:2008)*; Groenkloof, Pretoria: SABS Standards Division., 2008;

26. Matthews, D.R.; Hosker, J.P.; Rudenski, A.S.; Naylor, B.A.; Treacher, D.F.; Turner, R.C. Homeostasis model assessment: insulin resistance and β-cell function from fasting plasma glucose and insulin concentrations in man. *Diabetologia* **1985**, *28*, 412–419, doi:10.1007/BF00280883.

27. Wang, Z.; Yang, Y.; Xiang, X.; Men, Y.; He, M. Estimation of the normal range of blood glucose in rats. *J. Hyg. Res.* **2010**, *39*, 133–137.

28. Dayimu, A.; Wang, C.; Li, J.; Fan, B.; Ji, X.; Zhang, T.; Xue, F. Trajectories of Lipids Profile and Incident Cardiovascular Disease Risk: A Longitudinal Cohort Study. *J. Am. Heart Assoc.* **2019**, *8*,

doi:10.1161/JAHA.119.013479.

29. Hasan, K.M.M.; Tamanna, N.; Haque, M.A. Biochemical and histopathological profiling of Wistar rat treated with Brassica napus as a supplementary feed. *Food Sci. Hum. Wellness* **2018**, *7*, 77–82, doi:10.1016/j.fshw.2017.12.002.

30. WHO | World Health Statistics 2019: Monitoring health for the SDGs. *WHO* **2019**.

31. Wadden, T.A.; Webb, V.L.; Moran, C.H.; Bailer, B.A. Lifestyle modification for obesity: New developments in diet, physical activity, and behavior therapy. *Circulation* **2012**, *125*, 1157–1170. doi: 10.1161/CIRCULATIONAHA.111.039453

32. Drewnowski, A. The Real Contribution of Added Sugars and Fats to Obesity. *Epidemiol. Rev.* **2007**, *29*, 160–171, doi:10.1093/epirev/mxm011.

33. Kang, Y.J.; Wang, H.W.; Cheon, S.Y.; Lee, H.J.; Hwang, K.M.; Yoon, H.S. Associations of Obesity and Dyslipidemia with Intake of Sodium, Fat, and Sugar among Koreans: a Qualitative Systematic Review. *Clin. Nutr. Res.* **2016**, *5*, 290, doi:10.7762/cnr.2016.5.4.290.

34. Myrie, S.B.; McKnight, L.L.; King, J.C.; McGuire, J.J.; Van Vliet, B.N.; Bertolo, R.F. Effects of a diet high in salt, fat, and sugar on telemetric blood pressure measurements in conscious, unrestrained adult yucatan miniature swine (Sus scrofa). *Comp. Med.* **2012**, *62*, 282–290.

35. Farquhar, W.B.; Edwards, D.G.; Jurkovitz, C.T.; Weintraub, W.S. Dietary sodium and health: More than just blood pressure. *J. Am. Coll. Cardiol.* **2015**, *65*, 1042–1050. doi: 10.1016/j.jacc.2014.12.039

36. Sakurai, M.; Stamler, J.; Miura, K.; Brown, I.J.; Nakagawa, H.; Elliott, P.; Ueshima, H.; Chan, Q.; Tzoulaki, I.; Dyer, A.R.; et al. Relationship of dietary cholesterol to blood pressure: The INTERMAP study. *J. Hypertens.* **2011**, *29*, 222–228, doi:10.1097/HJH.0b013e32834069a5.

37. Mansoori, S.; Kushner, N.; Suminski, R.R.; Farquhar, W.B.; Chai, S.C. Added Sugar Intake is Associated with Blood Pressure in Older Females. *Nutrients* **2019**, *11*, 2060, doi:10.3390/nu11092060.

38. DiNicolantonio, J.J.; Lucan, S.C.; O'Keefe, J.H. The Evidence for Saturated Fat and for Sugar Related to

Coronary Heart Disease. *Prog. Cardiovasc. Dis.* **2016**, *58*, 464–472. doi: 10.1016/j.pcad.2015.11.006

39. Johnson, R.J.; Sánchez-Lozada, L.G.; Andrews, P.; Lanaspa, M.A. Perspective: A historical and scientific perspective of sugar and its relation with obesity and diabetes. *Adv. Nutr.* **2017**, *8*, 412–422, doi:10.3945/an.116.014654.

40. Hemmingsen, B.; Gimenez-Perez, G.; Mauricio, D.; Roqué i Figuls, M.; Metzendorf, M.I.; Richter, B. Diet, physical activity or both for prevention or delay of type 2 diabetes mellitus and its associated complications in people at increased risk of developing type 2 diabetes mellitus. *Cochrane Database Syst. Rev.* 2017. doi: 10.1002/14651858.CD003054.pub4.

41. Johnson, R.; Nxele, X.; Cour, M.; Sangweni, N.; Jooste, T.; Hadebe, N.; Samodien, E.; Benjeddou, M.; Mazino, M.; Louw, J.; et al. Identification of potential biomarkers for predicting the early onset of diabetic cardiomyopathy in a mouse model. *Sci. Rep.* **2020**, *10*, 12352, doi:10.1038/s41598-020-69254-x.

42. Malik, V.S.; Hu, F.B. Fructose and Cardiometabolic Health What the Evidence from Sugar-Sweetened Beverages Tells Us. *J. Am. Coll. Cardiol.* **2015**, *66*, 1615–1624. doi: 10.1016/j.jacc.2015.08.025

43. Talayero, B.G.; Sacks, F.M. The role of triglycerides in atherosclerosis. *Curr. Cardiol. Rep.* **2011**, *13*, 544–552, doi:10.1007/s11886-011-0220-3.

44. Nordestgaard, B.G. Triglyceride-Rich Lipoproteins and Atherosclerotic Cardiovascular Disease: New Insights from Epidemiology, Genetics, and Biology. *Circ. Res.* **2016**, *118*, 547–563, doi:10.1161/CIRCRESAHA.115.306249.

45. Lowette, K.; Roosen, L.; Tack, J.; Vanden Berghe, P. Effects of High-Fructose Diets on Central Appetite Signaling and Cognitive Function. *Front. Nutr.* **2015**, *2*. doi: 10.3389/fnut.2015.00005

46. Kopp, W. How western diet and lifestyle drive the pandemic of obesity and civilization diseases. *Diabetes, Metab. Syndr. Obes. Targets Ther.* **2019**, *12*, 2221–2236, doi:10.2147/DMSO.S216791.

47. Paddon-Jones, D.; Westman, E.; Mattes, R.D.; Wolfe, R.R.; Astrup, A.; Westerterp-Plantenga, M.

Protein, weight management, and satiety. In Proceedings of the American Journal of Clinical Nutrition; American Society for Nutrition, **2008**; 87, pp. 1558S-1561S.

48. Kim, S.P.; Ellmerer, M.; Van Citters, G.W.; Bergman, R.N. Primacy of hepatic insulin resistance in the development of the metabolic syndrome induced by an isocaloric moderate-fat diet in the dog. *Diabetes* **2003**, *52*, 2453–2460, doi:10.2337/diabetes.52.10.2453.

49. Arita, Y.; Kihara, S.; Ouchi, N.; Takahashi, M.; Maeda, K.; Miyagawa, J.I.; Hotta, K.; Shimomura, I.; Nakamura, T.; Miyaoka, K.; et al. Paradoxical decrease of an adipose-specific protein, adiponectin, in obesity. *Biochem. Biophys. Res. Commun.* **1999**, *257*, 79–83, doi:10.1006/bbrc.1999.0255.

50. Berg, A.H.; Combs, T.P.; Du, X.; Brownlee, M.; Scherer, P.E. The adipocyte-secreted protein Acrp30 enhances hepatic insulin action. *Nat. Med.* **2001**, *7*, 947–953, doi:10.1038/90992.

51. Muller, C.J.F.; Joubert, E.; De Beer, D.; Sanderson, M.; Malherbe, C.J.; Fey, S.J.; Louw, J. Acute assessment of an aspalathin-enriched green rooibos (Aspalathus linearis) extract with hypoglycemic potential. *Phytomedicine* **2012**, *20*, 32–39, doi:10.1016/j.phymed.2012.09.010.

52. Wang, T.; He, C. Pro-inflammatory cytokines: The link between obesity and osteoarthritis. *Cytokine Growth Factor Rev.* 2018, *44*, 38–50. doi: 10.1016/j.cytogfr.2018.10.002.

53. Buechler, C.; Krautbauer, S.; Eisinger, K. Adipose tissue fibrosis. *World J. Diabetes* **2015**, *6*, 548, doi:10.4239/wjd.v6.i4.548.

54. Schwingshackl, L.; Hoffmann, G. Comparison of Effects of Long-Term Low-Fat vs High-Fat Diets on Blood Lipid Levels in Overweight orObese Patients: A Systematic Review and Meta-Analysis. *J. Acad. Nutr. Diet.* **2013**, *113*, 1640–1661, doi:10.1016/j.jand.2013.07.010.

55. Bitzur, R.; Cohen, H.; Kamari, Y.; Shaish, A.; Harats, D. Triglycerides and HDL cholesterol: stars or second leads in diabetes? *Diabetes Care* **2009**, *32 Suppl 2*, S373. doi: 10.2337/dc09-S343.

56. Haberland, M.; Carrer, M.; Mokalled, M.H.; Montgomery, R.L.; Olson, E.N. Redundant control of adipogenesis by histone deacetylases 1 and 2. *J. Biol. Chem.* **2010**, *285*, 14663–14670,

doi:10.1074/jbc.M109.081679.

57. Retterstol, K.; Svendsen, M.; Narverud, I.; Holven, K.B. Effect of low carbohydrate high fat diet on LDL cholesterol and gene expression in normal-weight, young adults: A randomized controlled study. *Atherosclerosis* **2018**, *279*, 52–61, doi:10.1016/j.atherosclerosis.2018.10.013.

58. Katsiki, N.; Mikhailidis, D.P.; Mantzoros, C.S. Non-alcoholic fatty liver disease and dyslipidemia: An update. *Metabolism.* **2016**, *65*, 1109–1123. doi: 10.1016/j.metabol.2016.05.003.

59. Pol, T.; Held, C.; Westerbergh, J.; Lindbäck, J.; Alexander, J.H.; Alings, M.; Erol, C.; Goto, S.; Halvorsen, S.; Huber, K.; et al. Dyslipidemia and risk of cardiovascular events in patients with atrial fibrillation treated with oral anticoagulation therapy: Insights from the ARISTOTLE (Apixaban for Reduction in Stroke and Other Thromboembolic Events in Atrial Fibrillation) trial. *J. Am. Heart Assoc.* **2018**, *7*, doi:10.1161/JAHA.117.007444.

60. Lucero, H.A.; Kagan, H.M. Lysyl oxidase: An oxidative enzyme and effector of cell function. *Cell. Mol. Life Sci.* **2006**, *63*, 2304–2316. doi: 10.1007/s00018-006-6149-9.

61. Gao, Y.; Bielohuby, M.; Fleming, T.; Grabner, G.F.; Foppen, E.; Bernhard, W.; Guzmán-Ruiz, M.; Layritz, C.; Legutko, B.; Zinser, E.; et al. Dietary sugars, not lipids, drive hypothalamic inflammation. *Mol. Metab.* **2017**, *6*, 897–908, doi:10.1016/j.molmet.2017.06.008.

62. Wang, X.; Ge, A.; Cheng, M.; Guo, F.; Zhao, M.; Zhou, X.; Liu, L.; Yang, N. Increased hypothalamic inflammation associated with the susceptibility to obesity in rats exposed to high-fat diet. *Exp. Diabetes Res.* **2012**, *2012*, doi:10.1155/2012/847246.

63. Dludla, P. V.; Muller, C.J.F.; Joubert, E.; Louw, J.; Essop, M.F.; Gabuza, K.B.; Ghoor, S.; Huisamen, B.; Johnson, R. Aspalathin protects the heart against hyperglycemia-induced oxidative damage by up-regulating Nrf2 expression. *Molecules* **2017**, *22*, doi:10.3390/molecules22010129.

64. Johnson, R.; Dludla, P.; Joubert, E.; February, F.; Mazibuko, S.; Ghoor, S.; Muller, C.; Louw, J. Aspalathin, a dihydrochalcone C-glucoside, protects H9c2 cardiomyocytes against high glucose induced shifts in substrate preference and apoptosis. *Mol. Nutr. Food Res.* **2016**, *60*, 922–934,

doi:10.1002/mnfr.201500656.

65. Basa, A.L.; Garber, A.J. Cardiovascular disease and diabetes: modifying risk factors other than glucose control. *Ochsner J.* **2001**, *3*, 132–7.

66. Ormazabal, V.; Nair, S.; Elfeky, O.; Aguayo, C.; Salomon, C.; Zuñiga, F.A. Association between insulin resistance and the development of cardiovascular disease. *Cardiovasc. Diabetol.* **2018**, *17*, 122. doi.org/10.1186/s12933-018-0762-4.

67. Ye, X.; Kong, W.; Zafar, M.I.; Chen, L.-L. Serum triglycerides as a risk factor for cardiovascular diseases in type 2 diabetes mellitus: a systematic review and meta-analysis of prospective studies. *Cardiovasc. Diabetol.* **2019**, *18*, 48, doi:10.1186/s12933-019-0851-z.

Chapter 5:

Discussion, Conclusion and Future Studies

5.1 Discussion

Results from the current study demonstrated that a cardiac insult was induced in the H9c2 cells after exposure to HG+PAL as confirmed by reduced ATP production, increased apoptosis and mitochondrial dysfunction. This confirmed previous finding from our research group that either high glucose, or PAL are able to induce cardiac insult in a H9c2 cell culture model [1]. AfriplexGRT™ and ASP have proven to have the ability to improve mitochondrial function [2–4] as confirmed by enhanced basal and maximal respiration, ATP production and spare respiratory capacity of the H9c2 cells after the co-treatment with AfriplexGRT™ or ASP.

It is well accepted that cardiac interstitial fibrosis is linked to augmented LOXL2 expression [5]. However, in the current study, the expression levels of *LOXL2* and its downstream effectors involved in the fibrotic pathway, were not significantly altered. This contradicts previous finding from our group where LOXL2 expression was enhanced after the cells were treated with PAL (unpublished data). The lack of altered LOXL2 expression indicated that either there was no change in the methylation status of LOXL2, or that DNA methylation was not responsible for the regulation of LOXL2 gene expression. A methylation inhibitor, AZA, was thus used in the H9c2 cell culture model to demonstrate the known ameliorative effect of polyphenols on the AZA-induced hypomethylation [6, 7]. Findings showed the co-treatment of AZA (20 µM) with HG+PAL reduced the expression levels of key fibrotic markers (Figure 2.12). As such, this was validated in a diet-induced animal model.

Diet composition plays a significant role in the development of obesity [8, 9], which is a major risk factor for CVD [10]. This was elaborated on in a study performed by Bray et al. (2010) where concerns were raised on the detrimental metabolic risk of consuming high energy-dense food and sugar-sweetened beverages [11], especially in females, since females have a higher incidence of obesity [12]. Additionally, gender differences have also been reported in pathophysiological manifestations of obesity and CVDs [13]. Therefore, the current study aimed to investigate changes in markers of fibrosis and cardiac dysfunction in an obesogenic, diet-induced Wistar rat model in both males and females. The study also examined myocardial collagen deposition and investigated the role of gender in the disease pathophysiology. The prophylactic effect of

AfriplexGRT^{TM}, for the maintenance of good metabolic health, against HFHS-diet-induced cardiac modulation in a Wistar rat was also investigated.

The findings from this objective demonstrated that even though the diets consumed amongst males and females were the same, the calorie intake was higher in males compared to females. This resulted in males having increased body weight when compared to females. This increase contributed to males having significantly heavier RF pads when compared to females. The increase in RF weight was concomitant with the enhanced serum triglyceride levels in males compared to females, which could be associated with the observed inability of males to clear glucose back to basal levels. However, rats on the respective diets did not develop insulin resistance, nor was AfriplexGRT^{TM} able to improve any of the metabolic parameters (Table 5.1). Mechanistically, serum LOXL2 levels, a marker of early cardiovascular disfunction, were significantly increased in male Wistar rats consuming the HFHS diet. However, no significant differences could be observed on an mRNA expression level and DNA methylation profile. As such, protein LOXL2 expression levels were increased, matching heightened LOXL2 serum levels. These results may imply that an early event of cardiac fibrosis may have been activated and thus require further validation. This would suggest that LOXL2-induced fibrosis could have been driven by a different mechanism, independent of DNA methylation. DNA methylation signatures change in response to environmental changes, such as diet. The HFHS diet, however, was unable to induce any significant metabolic insult and thus did not alter DNA methylation patterns to cause changes in gene expression and thus, unfortunately the current study could not focus solely on aberrant DNA methylation signatures in response to diet.

Table 5.1: Summary of metabolic and molecular parameters that differ between the diet groups when compared to their control counterparts. Statistical significance is depicted as * p≤0.05, ** p≤0.01, *** p≤0.001 versus the respective control group.

Metabolic characteristics	**HFHS (male)**	**OB1**	**OB2**
Final bodyweight (g)	↑***	↑	↑
Food intake (g/week)	N/A	↑***	↑
Caloric intake (AUC)	↑***	-	-
OGTT AUC (mm^2)	↑***	↑	↑
Insulin (ng/mL)	↑	↑*	↑
HOMA-IR	↑	↑	↑
Triglycerides (mmol/L)	↑***	↑***	↑***
Total Cholesterol (mmol/L)	-	-	↑***
LDL (mmol/L)	N/A	-	↑***
AST (IU/L)	↓	-	↑*
ALT (IU/L)	↓**	-	↑***
Serum LOXL2 (ng/ml)	↑	N/A	↑**
Gene Expression	**HFHS (male)**	**OB1**	**OB2**
LOXL2	-	-	↑
COL1A	↓	↓	↑
SMAD2	↑	↓	-
SMAD3	-	-	-
TGFβ2	↑	↑	↑
ACTA2	↓	↓	↑
PIK3cg	↓	-	↑
AKT1	↓	↓	↓
HIF1A	↑	-	↑
CTGF	↓	↑	-

Since the HFHS did not induce the desired metabolic derangement, it was concluded that diet composition may have played a role. As reported by various studies [14–18], the diet composition plays a profound role in the development of cardiac dysfunction. As such, the next objective investigated the role played by different obesogenic diets on the CVD risk profile. This study also investigated the cardioprotective potential of AfriplexGRT™ on the modulation of LOXL2 and its downstream targets.

Indeed, a diet high in fat and fructose caused not only an increase in triglycerides, but also LDL-cholesterol, and indicators of liver toxicity. As expected, serum LOXL2 levels were increased in the OB2 diet, however no significant increase in the gene and protein expression levels of key fibrotic markers was observed, thus DNA methylation was not explored in this study, and thus required further investigation. Additionally, AfriplexGRT™ was unable to attenuate the changes induced by the OB1 and OB2 diets.

There were however limitations to this study. The major limitations include:

- Although there were perturbations in metabolic parameters, the diet could not induce a metabolic insult that is linked to cardiac dysfunction.
- No functional parameters were measured in the form of echocardiography.
- There were varied levels of fat and sugar in the different obesogenic diets, resulting in the inability to have an effective comparative analysis.
- A larger sample size was required to confirm the serum LOXL2 activity assay on a gene and protein expression level.

5.2 Conclusion

In conclusion, contradictory to previous findings, this study showed that HG+PAL was unable to induce increased *LOXL2* expression. However, various *in vitro* obesogenic Wistar rat models showed higher levels of LOXL2 activity in serum, which has previously been linked to the early onset of cardiac fibrosis [19, 20]. This study found that increased LOXL2 activity is not regulated by DNA methylation, or that methylation profiles could not be appropriately studied as a result of insufficient onset of metabolic syndrome. In addition, it was concluded that AfriplexGRT™ was unable to mitigate diet-induced cardiac insults or LOXL2-induced fibrosis.

5.3 Future Studies

Future studies should include:

- To induce a more severe, diet-induced *in vivo* model of cardiac pathology, using both male and female animals, with echocardiography to verify decreased cardiac function. To use this model to confirm the role of LOXL2 in myocardial pathology, and to investigate the effect of AfriplexGRT^{TM} in end-stage cardiac dysfunction. Additionally, to elaborate on gender differences in the highly regulated markers identified in the Fibrosis Profiler Array.
- Investigate the regulatory processes governing LOXL2 expression, and the role epigenetics plays in the modulation of its downstream targets.
- *In vitro* functional analysis of LOXL2 and its effect on its downstream genes in order to decipher the pathophysiology of cardiac fibrosis.

5.4 References

1. Johnson, R.; Dludla, P.; Joubert, E.; February, F.; Mazibuko, S.; Ghoor, S.; Muller, C.; Louw, J. Aspalathin, a dihydrochalcone C-glucoside, protects H9c2 cardiomyocytes against high glucose induced shifts in substrate preference and apoptosis. *Mol. Nutr. Food Res.* **2016**, *60*, 922–934, doi:10.1002/mnfr.201500656.

2. Dludla, P. V.; Johnson, R.; Mazibuko-Mbeje, S.E.; Muller, C.J.F.; Louw, J.; Joubert, E.; Orlando, P.; Silvestri, S.; Chellan, N.; Nkambule, B.B.; et al. Fermented rooibos extract attenuates hyperglycemia-induced myocardial oxidative damage by improving mitochondrial energetics and intracellular antioxidant capacity. *South African J. Bot.* **2020**, *131*, 143–150, doi:10.1016/j.sajb.2020.02.003.

3. Mazibuko-Mbeje, S.E.; Dludla, P. V.; Johnson, R.; Joubert, E.; Louw, J.; Ziqubu, K.; Tiano, L.; Silvestri, S.; Orlando, P.; Opoku, A.R.; et al. Aspalathin, a natural product with the potential to reverse hepatic insulin resistance by improving energy metabolism and mitochondrial respiration. *PLoS One* **2019**, *14*, e0216172, doi:10.1371/journal.pone.0216172.

4. Uličná, O.; Vančová, O.; Kucharská, J.; Janega, P.; Waczulíková, I. Rooibos tea (Aspalathus linearis) ameliorates the CCl 4 -induced injury to mitochondrial respiratory function and energy production in rat liver. *Gen. Physiol. Biophys.* **2019**, *38*, 15–25, doi:10.4149/gpb_2018037.

5. Johnson, R.; Nxele, X.; Cour, M.; Sangweni, N.; Jooste, T.; Hadebe, N.; Samodien, E.; Benjeddou, M.; Mazino, M.; Louw, J.; et al. Identification of potential biomarkers for predicting the early onset of diabetic cardiomyopathy in a mouse model. *Sci. Rep.* **2020**, *10*, 12352, doi:10.1038/s41598-020-69254-x.

6. Fang, M.; Chen, D.; Yang, C.S. Dietary Polyphenols May Affect DNA Methylation. *J. Nutr.* **2007**, *137*, 223S-228S, doi:10.1093/jn/137.1.223S.

7. Crescenti, A.; Solà, R.; Valls, R.M.; Caimari, A.; del Bas, J.M.; Anguera, A.; Anglés, N.; Arola, L. Cocoa Consumption Alters the Global DNA Methylation of Peripheral Leukocytes in Humans with Cardiovascular Disease Risk Factors: A Randomized Controlled Trial. *PLoS One* **2013**, *8*, e65744,

doi:10.1371/journal.pone.0065744.

8. Qi, L. Personalized nutrition and obesity. *Ann. Med.* **2014**, *46*, 247–252, doi:10.3109/07853890.2014.891802.

9. Hensrud, D.D. Diet and obesity. *Curr. Opin. Gastroenterol.* **2004**, *20*, 119–124. doi: 10.1097/00001574-200403000-00012.

10. Akil, L.; Anwar Ahmad, H. Relationships between obesity and cardiovascular diseases in four southern states and Colorado. *J. Health Care Poor Underserved* **2011**, *22*, 61–72, doi:10.1353/hpu.2011.0166.

11. Bray, M.S.; Tsai, J.Y.; Villegas-Montoya, C.; Boland, B.B.; Blasier, Z.; Egbejimi, O.; Kueht, M.; Young, M.E. Time-of-day-dependent dietary fat consumption influences multiple cardiometabolic syndrome parameters in mice. *Int. J. Obes.* **2010**, *34*, 1589–1598, doi:10.1038/ijo.2010.63.

12. Mosca, L.; Barrett-Connor, E.; Kass Wenger, N. Sex/gender differences in cardiovascular disease prevention: What a difference a decade makes. *Circulation* **2011**, *124*, 2145–2154, doi:10.1161/CIRCULATIONAHA.110.968792.

13. Gao, Z.; Chen, Z.; Sun, A.; Deng, X. Gender differences in cardiovascular disease. *Med. Nov. Technol. Devices* **2019**, *4*, 100025, doi:10.1016/j.medntd.2019.100025.

14. Martins Matias, A.; Murucci Coelho, P.; Bermond Marques, V.; dos Santos, L.; Monteiro de Assis, A.L.E.; Valentim Nogueira, B.; Lima-Leopoldo, A.P.; Soares Leopoldo, A. Hypercaloric diet models do not develop heart failure, but the excess sucrose promotes contractility dysfunction. *PLoS One* **2020**, *15*, e0228860, doi:10.1371/journal.pone.0228860.

15. Casas, R.; Castro-Barquero, S.; Estruch, R.; Sacanella, E. Nutrition and cardiovascular health. *Int. J. Mol. Sci.* **2018**, *19*. doi: 10.3390/ijms19123988.

16. Stanley, W.C.; Dabkowski, E.R.; Ribeiro, R.F.; O'Connell, K.A. Dietary fat and heart failure: Moving from lipotoxicity to lipoprotection. *Circ. Res.* **2012**, *110*, 764–776. doi: 10.1161/CIRCRESAHA.111.253104.

17. Brandhorst, S.; Longo, V.D. Dietary Restrictions and Nutrition in the Prevention and Treatment of

Cardiovascular Disease. *Circ. Res.* **2019**, *124*, 952–965. doi.org/10.1161/CIRCRESAHA.118.313352

18. Korakas, E.; Dimitriadis, G.; Raptis, A.; Lambadiari, V. Dietary composition and cardiovascular risk: A mediator or a Bystander? *Nutrients* **2018**, *10*. doi: 10.3390/nu10121912.

19. Yang, J.; Savvatis, K.; Kang, J.S.; Fan, P.; Zhong, H.; Schwartz, K.; Barry, V.; Mikels-Vigdal, A.; Karpinski, S.; Kornyeyev, D.; et al. Targeting LOXL2 for cardiac interstitial fibrosis and heart failure treatment. *Nat. Commun.* **2016**, *7*, 13710, doi:10.1038/ncomms13710.

20. Zhao, Y.; Tang, K.; Tianbao, X.; Wang, J.; Yang, J.; Li, D. Increased serum lysyl oxidase-like 2 levels correlate with the degree of left atrial fibrosis in patients with atrial fibrillation. *Biosci. Rep.* **2017**, *37*, doi:10.1042/BSR20171332.

Appendix 1:

Detailed Diet Composition

Supplementary Table A3.1 The macronutrient composition of the control and HSHF diets utilized in the first obesogenic diet induced obesity study.

	Control	HFHS
Energy (kJ/100g)	878	650
Glycaemic carbohydrate (g/100g)	16.9	18.3
Starch (g/100g)	8.0	13.2
Total sugar (g/100g)	5.1	8.9
Glucose (g/100g)	0.3	0.5
Sucrose (g/100g)	2.3	6.5
Fructose (g/100g)	0.4	0.5
Other sugars (maltose, lactose, galactose, trehalose) (g/100g)	2.1	1.3
Total fat (g/100g)	4.37	10.61
% kJ from fat	24	45
Saturated fat (g/100g)	1.58	5.73
Mono-unsaturated fat (g/100g)	2.11	3.63
Poly-unsaturated fat (g/100g)	0.69	1.25
Cholesterol (mg/100g)	35	88
Protein (g/100g)	7.7	9.1
Fibre (g/100g)	5.9	5.3

Supplementary Table A4.2 The macronutrient composition of the control, OB1 and OB2 diets utilized in the second obesogenic diet study.

	Control	OB1	OB2
Energy (kJ/100g)	1225	968	1350
Glycaemic carbohydrate (g/100g)	27.4	27	11.5
Starch (g/100g)	22.1	6.9	4.7
Total sugar (g/100g)	5.2	20.1	6.7
Glucose (g/100g)	0.1	0	0.2
Sucrose (g/100g)	4.6	17.5	1.5
Fructose (g/100g)	0.3	0.1	4.4
Other sugars (maltose, lactose, galactose, trehalose) (g/100g)	0.2	2.5 (consisting solely of lactose)	0.7
Total fat (g/100g)	5.04	8.80	24.09
% kJ from fat	15.4	33.6	66.0
Saturated fat (g/100g)	1.28	5.26	14.3
Mono-unsaturated fat (g/100g)	1.28	2.61	7.42
Poly-unsaturated fat (g/100g)	2.48	0.94	2.38
Cholesterol (mg/100g)	44	11	440
Protein (g/100g)	25.8	9	12.9
Fibre (g/100g)	16.8	4.0	5.5

Appendix 2:

RT^2 PCR Profiler Array Results

Supplementary Table A2: PCR Fibrosis profiler array results. Fold regulation of genes up- or down-regulated by the HFHS diet in male and femal wistar rats.

Gene	Description	Fold Regulation	
		Males	Females
Acta2	Smooth muscle alpha-actin	-1.60	**-5.85**
Agt	Angiotensinogen (serpin peptidase inhibitor, clade A, member 8)	**-2.63**	**-2.34**
Akt1	V-akt murine thymoma viral oncogene homolog 1	**-2.21**	**-3.33**
Bcl2	B-cell CLL/lymphoma 2	-1.77	**-9.80**
Bmp7	Bone morphogenetic protein 7	1.67	1.62
Cav1	Caveolin 1, caveolae protein	-1.28	**-16.83**
Ccl11	Chemokine (C-C motif) ligand 11	-1.54	-1.36
Ccl12	Chemokine (C-C motif) ligand 12	1.03	**-24.62**
Ccl3	Chemokine (C-C motif) ligand 3	-1.15	**-7.76**
Ccr2	Chemokine (C-C motif) receptor 2	-1.27	**-22.27**
Cebpb	CCAAT/enhancer binding protein (C/EBP), beta	-1.96	-1.52
Col1a2	Collagen, type I, alpha 2	-1.36	**-10.81**
Col3a1	Collagen, type III, alpha 1	-1.37	**5.77**
Ctgf	Connective tissue growth factor	-1.63	**-7.04**
Cxcr4	Chemokine (C-X-C motif) receptor 4	-1.54	**-10.76**
Dcn	Decorin	-1.10	**-10.81**
Edn1	Endothelin 1	-1.47	**5.01**
Egf	Epidermal growth factor	1.03	**-8.38**
Eng	Endoglin	-1.32	**-3.06**
Faslg	Fas ligand (TNF superfamily, member 6)	**-2.26**	1.62
Grem1	Gremlin 1, cysteine knot superfamily, homolog (Xenopus laevis)	-1.40	1.62
Hgf	Hepatocyte growth factor	-1.50	**5.18**
Ifng	Interferon gamma	**-2.60**	1.62

Il10	Interleukin 10	-1.40	**-19.92**
Il13	Interleukin 13	-1.00	**-7.54**
Il13ra2	Interleukin 13 receptor, alpha 2	1.16	1.62
Il1a	Interleukin 1 alpha	-1.32	1.26
Il1b	Interleukin 1 beta	-1.61	1.62
Il4	Interleukin 4	1.01	**-6.56**
Il5	Interleukin 5	1.48	**-6.95**
Ilk	Integrin-linked kinase	-1.13	**-87.87**
Inhbe	Inhibin beta E	-1.72	-1.17
Itga1	Integrin, alpha 1	-1.46	**-6.17**
Itga2	Integrin, alpha 2	-1.52	1.62
Itga3	Integrin, alpha 3	-1.46	**-6.97**
Itgav	Integrin, alpha V	-1.93	**-2.83**
Itgb1	Integrin, beta 1	-1.41	**-2.33**
Itgb3	Integrin, beta 3	-1.28	**-23.82**
Itgb5	Integrin, beta 5	-1.60	**-10.80**
Itgb6	Integrin, beta 6	-1.24	**-3.55**
Itgb8	Integrin, beta 8	-1.32	**-2.79**
Jun	Jun oncogene	**-2.01**	**-101.83**
Lox	Lysyl oxidase	**-2.57**	1.35
Ltbp1	Latent transforming growth factor beta binding protein 1	-1.79	**-4.92**
Mmp13	Matrix metallopeptidase 13	-1.12	1.62
Mmp14	Matrix metallopeptidase 14 (membrane-inserted)	-1.99	**-3.00**
Mmp1	Matrix metallopeptidase 1a (interstitial collagenase)	-1.70	**-8.71**
Mmp2	Matrix metallopeptidase 2	-1.56	**-6.07**
Mmp3	Matrix metallopeptidase 3	-1.47	1.36
Mmp8	Matrix metallopeptidase 8	-1.36	-1.18
Mmp9	Matrix metallopeptidase 9	**-2.46**	**-6.94**

Myc	Myelocytomatosis oncogene	-1.66	1.62
Nfkb1	Nuclear factor of kappa light polypeptide gene enhancer in B-cells 1	**-2.02**	1.91
Pdgfa	Platelet-derived growth factor alpha polypeptide	-1.72	**-3.97**
Pdgfb	Platelet-derived growth factor beta polypeptide (simian sarcoma viral (v-sis) oncogene homolog)	-1.61	**-2.10**
Plat	Plasminogen activator, tissue	-1.31	**-2.38**
Plau	Plasminogen activator, urokinase	**-2.28**	1.62
Plg	Plasminogen	-1.46	**-2.47**
Serpina1	Serpin peptidase inhibitor, clade A (alpha-1 antiproteinase, antitrypsin), member 1	1.12	-1.08
Serpine1	Serpin peptidase inhibitor, clade E (nexin, plasminogen activator inhibitor type 1), member 1	**-3.04**	**-3.92**
Serpinh1	Serine (or cysteine) peptidase inhibitor, clade H, member 1	-1.90	**-39.47**
Smad2	SMAD family member 2	-1.84	-1.48
Smad3	SMAD family member 3	**-2.69**	1.62
Smad4	SMAD family member 4	-1.62	**-8.22**
Smad6	SMAD family member 6	-1.59	**-3.98**
Smad7	SMAD family member 7	-1.74	**-11.50**
Snai1	Snail homolog 1 (Drosophila)	-1.05	**-6.28**
Sp1	Sp1 transcription factor	-1.92	**-2.18**
Stat1	Signal transducer and activator of transcription 1	-1.79	**-3.72**
Stat6	Signal transducer and activator of transcription 6	-1.40	**-2.93**
Tgfb1	Transforming growth factor, beta 1	-1.54	-1.01
Tgfb2	Transforming growth factor, beta 2	-1.07	**-6.48**
Tgfb3	Transforming growth factor, beta 3	-1.34	**-19.96**
Tgfbr1	Transforming growth factor, beta receptor 1	-1.72	**-9.46**
Tgfbr2	Transforming growth factor, beta receptor II	-1.93	**-7.22**
Tgif1	TGFB-induced factor homeobox 1	-1.21	**-8.49**
Thbs1	Thrombospondin 1	**-2.45**	-1.71
Thbs2	Thrombospondin 2	-1.39	**-7.06**
Timp1	TIMP metallopeptidase inhibitor 1	1.06	**-64.48**

Timp2	TIMP metallopeptidase inhibitor 2	-1.10	**-9.31**
Timp3	TIMP metallopeptidase inhibitor 3	-1.59	**-10.25**
Timp4	Tissue inhibitor of metalloproteinase 4	-1.26	**-40.20**
Tnf	Tumor necrosis factor (TNF superfamily, member 2)	**-2.12**	**-4.88**
Vegfa	Vascular endothelial growth factor A	-1.91	**-3.50**

Appendix 3:

Proton Leak Results

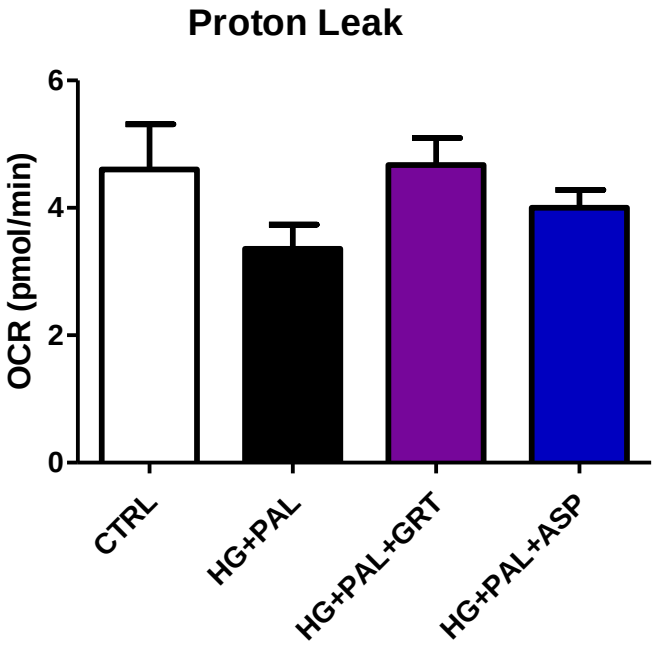

Supplementary Figure A3.1: Proton leak. Changes in proton leak in response to high glucose and palmitate media (HG+PAL) and treatment with AfriplexGRT™ (GRT) or Aspalathin (ASP). Three independent experiments were conducted with n=3 biological repeats each and a one-way ANOVA was performed.